TECHNICAL REPORT STANDARD TITLE PAGE

1. Report No.	2. Government Accession No.	3. Recipient's Catalog No.
FHWA/TX-83/ +343-1		

4. Title and Subtitle	5. Report Date
A Study of the Soil-Structure Interaction Behavior of Highway Guardrail Posts	July 1983
	6. Performing Organization Code

7. Author(s)	8. Performing Organization Report No.
James F. Dewey, Jr., Jey K. Jeyapalan, T. J. Hirsch, and Hayes E. Ross, Jr.	Research Report 343-1

9. Performing Organization Name and Address	10. Work Unit No.
Texas Transportation Institute The Texas A&M University System College Station, Texas 77843	11. Contract or Grant No. Study No. 2-18-83-343
	13. Type of Report and Period Covered Interim - September 1982 July 1983
12. Sponsoring Agency Name and Address Texas State Department of Highways and Public Transportation; Transportation Planning Division P. O. Box 5051 Austin, Texas 78763	14. Sponsoring Agency Code

15. Supplementary Notes

Research performed in cooperation with DOT,FHWA.
Research Study Title: Improved Design of Lightpoles, Guardrails, and Other Appurtenances.

16. Abstract

The Texas State Department of Highways and Public Transportation (SDHPT) currently uses two types of guardrail posts: (1) a circular wood post and (2) a steel W6x8.5 post. The current specifications require the steel post to be placed in a concrete footing. However, the concrete footing is not required for the wood post. Because of this requirement, the steel post guardrail systems are considered not as economical as the wood post guardrail systems. This research study was conducted to determine whether the concrete footings are required for the steel guardrail posts to perform satisfactorily as a traffic barrier system.

An analytical model was developed to model the guardrail post as a laterally loaded drilled shaft. The model captures the nonlinearity of the soil response and includes all components of soil resistance, lateral normal stresses, and all shear stresses acting on the shaft. The lateral earth pressures developed against the shaft are related to the fundamental earth pressure theory of Coulomb to avoid unnecessary assumptions or empiricism. This model represents the realistic behavior of drilled shafts under lateral loading conditions adequately, while being simple enough for use in day-to-day design of these shafts.

A series of static load tests and dynamic impact tests were conducted to determine whether the steel guardrail post performs satisfactorily. The results of these test indicate that the steel guardrail post, embedded without the concrete footing, performs similar to the timber post. The results of these field tests were also used to verify the analytical model, and the agreement with the (on back)

17. Key Words	18. Distribution Statement
Steel Guardrail Post, Traffic Barrier System, Lateral Loading, Analytical Model.	No restrictions. This document is available to the public through the National Technical Information Service, 5285 Port Royal Road, Springfield, Virginia 22161.

19 Security Classif. (of this report)	20. Security Classif. (of this page)	21. No. of Pages	22. Price
Unclassified	Unclassified	261	

Form DOT F 1700.7 (8-69)

theoretical predictions was found to be good.

It should be emphasized however, that the above results and statements are based on limited number of tests performed in the field on the steel and timber posts. Due to the limited time and the resources available to the authors, repeatability of the test results was never verified. Therefore, it is recommended that another series of tests be performed in the future to check the repeatability of the above results.

A STUDY OF THE SOIL-STRUCTURE INTERACTION BEHAVIOR OF HIGHWAY GUARDRAIL POSTS

by

James F. Dewey, Jr.
Research Assistant

Jey K. Jeyapalan
Assistant Research Engineer

T. J. Hirsch
Research Engineer

and

Hayes E. Ross, Jr.
Research Engineer

Research Report No. 343-1

Improved Design of Lightpoles, Guardrails, and Other Appurtenances

Research Study Number 2-18-83-343

Sponsored by
State Department of Highways and Public Transportation
in Cooperation with the
U. S. Department of Transportation
Federal Highway Administration

July 1983

TEXAS TRANSPORTATION INSTITUTE
Texas A&M University
College Station, Texas

ABSTRACT

The Texas State Department of Highways and Public Transportation (SDHPT) currently uses two types of guardrail posts: (1) a circular wood post and (2) a steel w6x8.5 post. The current specifications require the steel post to be placed in a concrete footing. However, the concrete footing is not required for the wood post. Because of this requirement, the steel post guardrail systems are considered not as economical as the wood post guardrail systems. This research study was conducted to determine whether the concrete footings are required for the steel guardrail posts to perform satisfactorily as a traffic barrier system.

An analytical model was developed to model the guardrail post as a laterally loaded drilled shaft. The model captures the nonlinearity of the soil response and includes all components of soil resistance, lateral normal stresses, and all shear stresses acting on the shaft. The lateral earth pressures developed against the shaft are related to the fundamental earth pressure theory of Coulomb to avoid unnecessary assumptions or empiricism. This model represents the realistic behavior of drilled shafts under lateral loading conditions adequately, while being simple enough for use in day-to-day design of these shafts.

A series of static load tests and dynamic impact tests were conducted to determine whether the steel guardrail post performs satisfactorily. The results of these tests indicate that the steel guardrail post, embedded without the concrete footing, performs similar to the timber post. The results of these field tests were also used to verify the analytical model, and the agreement with the theoretical predictions was found to be good.

It should be emphasized however, that the above results and statements are based on limited number of tests performed in the field on the steel and timber posts. Due to the limited time and the resources available to the authors, repeatability of the test results was never verified. Therefore, it is recommended that another series of tests be performed in the future to check the repeatability of the above results.

ACKNOWLEDGEMENTS

Funding for this research study was made possible through the sponsorship of the Texas State Department of Highways and Public Transportation. The support provided by this agency is gratefully acknowledged.

Sincere appreciation is expressed to all persons who participated in or contributed to this research. Special thanks are due to Harold Cooner and Ralph Banks, the contact representatives for the State Department of Highways and Public Transportation. Gratitude is also expressed to Don Cangelose and the personnel of the TTI research support group who constructed the loading facility and prepared the test sites. Don Rokohl, Mark Lamborn, Mark Gardner, and Dale Brown rendered invaluable assistance in conducting the field tests. Finally, special thanks are given to Pam Vernon for typing this report.

TABLE OF CONTENTS

LIST OF TABLES

LIST OF FIGURES

INTRODUCTION

Uses and Applications of Highway Guardrails

As traffic barrier systems located along highways, the primary function of guardrails and median barriers is to safely redirect errant vehicles. Guardrail installations on shoulders prevent vehicle access to steep embankments or fixed objects, whereas median barriers are used between the roadways of divided highways to prevent "across-the-median" collisions with opposing traffic. Properly designed installations accomplish the redirection of errant vehicles in such a manner as to minimize the vulnerability of vehicle occupants as well as the involvement of following and adjacent traffic. Other desirable guardrail and barrier system characteristics include minimal damage to vehicles and barrier systems; economy in construction, installation and maintenance; enhancement of highway aesthetics; and performance as headlight glare screens or highway delineators.

When a vehicle in motion collides with a guardrail, a substantial portion of the energy of the vehicle is absorbed by the guardrail. The lateral forces carried by the guardrail are transmitted to the ground through the guardrail posts. Because the resistance and the subsequent energy loss are provided by the soil

surrounding the guardrail posts, the soil properties at the site will determine the behavior of the guardrail posts. Although extensive research has been done on the efficiency of various types of guardrail systems as highway barriers, very little work has been done on the influence of soil properties on the performance of guardrail posts.

Types of Guardrail Posts

The State Department of Highways and Public Transportation currently uses two types of guardrail posts: (1) a circular wood post and (2) a steel W6 x 8.5 post. The current specifications require the wood post to have a minimum diameter of 7 inches, a minimum overall length of 69 inches, and a minimum embedment depth of 38 inches with the top of the wood post domed. A minimum overall length of 66 inches is required if the top of the wood post is beveled. The specifications do not require the wood post to be placed in a concrete footing.

The current specifications for the steel W6 x 8.5 guardrail post are the same as that for the beveled wood post with one exception, that the steel post must be placed in a concrete footing. Because of this requirement for a concrete footing, the steel post guardrail systems are not as economical as the wood post guardrail systems. To date, no experimental work has

been performed to determine whether the concrete footing is required in order for the steel post guardrail systems to perform satisfactorily as a traffic barrier.

Scope of the Study

The State Department of Highways and Public Transportation considers the wood post guardrail systems to perform adequately as a traffic barrier. These systems properly redirect errant vehicles while minimizing the vulnerability of the vehicle occupants and other adjacent vehicles. Any guardrail system which performed similarly to the system using wood posts would be considered as performing satisfactorily. With this in mind, this study was conducted to determine whether concrete footings are required for the steel guardrail posts to perform satisfactorily. The procedure used in conducting this study was:

1. A computer model for laterally loaded guardrail posts was developed in which the guardrail post was modeled as a laterally loaded drilled shaft or pile.
2. Static field load tests were performed on steel and timber guardrail posts in two different soils.
3. The results from these static tests were used to compare the static behavior of the two types of

posts. The results were also compared with the results generated from the computer model.

4. Dynamic field tests were performed on steel and timber guardrail posts in the soils used for the static tests.
5. The results from these dynamic tests were used to compare the dynamic response of the two types of posts. These results were also compared to the results predicted by the computer model.

Organization of the Report

The prime objective of this research study was to determine if concrete footings are required for the steel guardrail posts to perform satisfactorily. The studies undertaken to achieve this objective are described in subsequent chapters.

Chapter 2 contains a review of the available literature and previous work on the analysis of laterally loaded drilled shafts or piles.

Chapter 3 contains a discussion on the development of a new theoretical model to analyze the behavior of drilled shafts or guardrail posts subjected to lateral loads.

Chapter 4 describes a series of static laterally loaded guardrail post tests that were performed to determine whether the steel guardrail posts perform

satisfactorily under static loading.

Chapter 5 describes a series of dynamic laterally loaded guardrail post tests that were conducted to determine whether the steel guardrail posts perform satisfactorily under dynamic loading.

Chapter 6 contains conclusions of this study and recommendations for further research.

SUMMARY OF PREVIOUS WORK

Field Tests on Guardrail Posts

Many crash tests have been performed on guardrail systems to determine the efficiency of these systems as highway barriers. Typically, these tests have concentrated on the damage to the rail and the vehicle, the redirection response of the vehicle, and the energy dissipation capability of the guardrail system. The vehicle redirection response and the energy dissipation characteritics of the system are significantly influenced by the soil conditions.However, the post-soil interaction behavior has been rarely mentioned or studied in these tests.

In 1970, Southwest Research Institute (28) conducted a study of the post-soil interaction behavior of highway guardrail posts. In order to evaluate the effects of soil conditions and embedment geometry, a total of 72 tests were performed in two types of soils, with four embedment depths and three post widths. The results of these showed the following:

1. The dynamic resistance force (peak and average) and the kinetic energy absorbed by noncohesive soils are significantly related to the shear strength of the soil.
2. The dynamic resistance force (peak and average)

and the kinetic energy absorbed by the soil are directly related to the post width.

3. The dynamic resistance force (peak and average) and the kinetic energy absorbed by the soil are significantly affected by and directly related to the post embedment depth. The embedment depth has a more pronounced influence on post-soil system properties for soils with higher shear strengths.
4. The dynamic resistance force (peak and average) and the kinetic energy absorbed by the soil are greater than the static resistance force (peak and average) and the energy absorbed by the soil.

This study clearly shows that the performance of a highway guardrail system is significantly influenced by the post-soil interaction characteristics of the system.

Theoretical Analysis of Laterally Loaded Shafts or Piles

The soil-structure interaction behavior of guardrail posts can be analyzed by considering the guardrail post to behave as a laterally loaded pile. Various methods of analysis are currently used for laterally loaded pile design. Some methods permit the pile foundation to reach some percentage of its ultimate capacity at the maximum foundation load. Other methods assume elastic foundation

behavior up to the ultimate load. Other methods limit soil pressures as determined from elastic analysis to allowable values, while still other methods design to certain deflection and/or rotation criteria at various load levels. Regardless of the design method used, the pile must be safe against both structural collapse and soil failure (excessive pile deflection and/or rotation).

These approaches used in pile design can be classified into three categories:

1. Ultimate lateral capacity models
2. Linear load-deflection models
3. Nonlinear load-deflection models

Ultimate Lateral Capacity Models

The ultimate lateral capacity models assume that the soil surrounding the pile is in a state of plastic equilibrium and that the pile is sufficiently strong such that flexural displacements or plastic hinges do not develop. Because the soil is considered to be fully plastic, little or no additional load is required to produce additional deflection. Thus, only the ultimate capacity of the loaded pile is calculated.

Most of the ultimate capacity models are based on the assumption that the interaction between the pile and the soil can be represented by net lateral soil pressures acting on the pile. All other forces associated with the

stresses on the base and the vertical shearing stresses on the perimeter of the pile are neglected. Thus, once a distribution of ultimate lateral earth pressures has been determined, the ultimate lateral capacity may be calculated using horizontal force and moment equilibrium for a rigid body. As shown in Fig. 1, the ultimate lateral capacity is associated with rigid body rotation about some point below the ground surface. The depth to this point of rotation can be determined from the two equilibrium equations.

Several previous researchers have proposed lateral pressure distributions to be used in this type of analysis. In 1932, Seiler (41) presented the soil pressure distribution shown in Fig. 2 which was developed empirically from field test data. Seiler used the distribution to develop design charts for the embedment depth of standard timber poles.

Ivey and Hawkins (22) proposed a procedure to analyze drilled shafts to support highway sign structures. They used Rankine's passive earth pressure theory (5) with the soil distribution presented by Seiler. The Rankine theory is based on an infinitely long frictionless wall moving horizontally into the soil. In reality, the rotation of a cylindrical pile is resisted by friction or shear stresses on the sides of the pile as well as shear stresses on the base. The

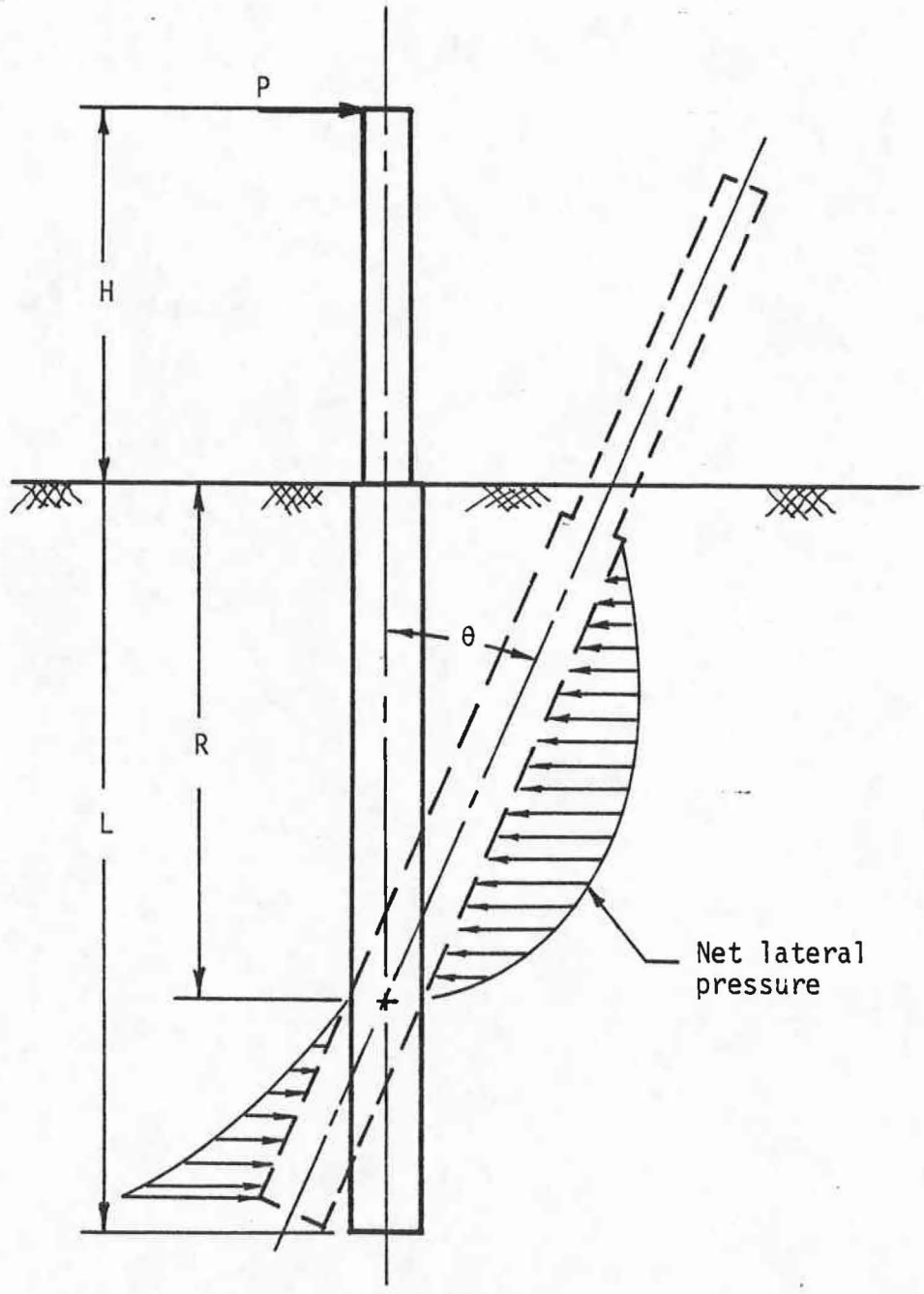

FIG. 1.-Laterally Loaded Drilled Shaft

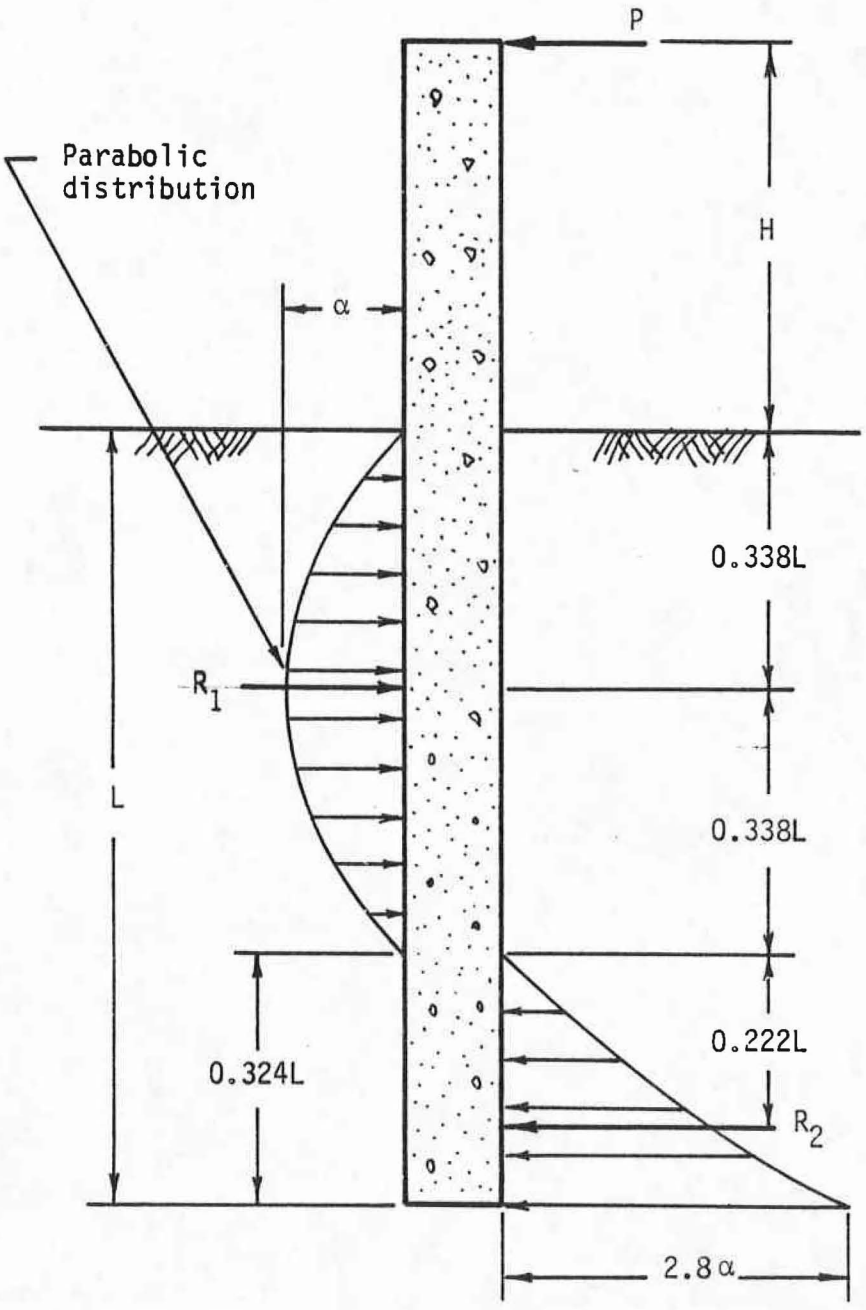

FIG. 2.-Soil Pressure Distribution Proposed by Seiler

presence of shear stresses along the face of the pile and the nonfulfillment of the plastic equilibrium state results in a very conservative solution.

Ivey (21) later developed an analysis procedure for computing the ultimate lateral capacity of circular rigid drilled shafts which takes into account all the shear stresses acting on a drilled shaft. These stresses include the shear stress in the horizontal direction along the sides of the shaft, the shear stresses in the vertical direction along the face of the shaft, and the shear stresses in the horizontal direction developed on the base of the shaft. Consequently, the solution is a three-dimensional analysis of the laterally loaded drilled shaft problem.

Ivey originally used the Rankine earth pressure theory in this analysis. As a result of the model tests Ivey (23) conducted, a modifying factor for the Rankine earth pressure coefficients was introduced. For purely cohesive soils, the factor was less than one. For typical sands, however, the factor ranged from 3.5 to 4.5. This new semi-empirical method proposed by Ivey proved to be slightly unconservative by overpredicting the ultimate loads.

Broms (6,7) presented a design procedure for short, rigid piles based on two soil pressure distributions he developed. For cohesive soils, Broms uses the

distribution shown in Fig. 3 in which the ultimate soil pressure is a function of the undrained shear strength, c and the pile diameter, B. For cohesionless soils, Broms utilizes the ultimate pressure distribution shown in Fig. 4 where γ is the effective unit weight of the soil, D is the embedment depth of the pile, B is the pile diameter, and K_p is the Rankine passive earth pressure coefficient (5). For short, rigid piles, the base of the pier moves toward the applied lateral load, and high lateral earth pressures are developed near the base of the pile. This high lateral soil reaction is represented by a lateral concentrated load acting at the base of the pile. The concentrated force can be calculated using moment equilibrium, and then the lateral capacity can be determined using horizontal force-equilibrium. These lateral pressure distributions developed by Broms are widely used in practice to predict ultimate lateral capacity of piles.

Brinch Hansen (18) proposed the lateral earth pressure distributions shown in Figs. 5 and 6, which accounts for the change in earth pressures with depth. The ultimate lateral pressure, p_{ult}, at a given depth is given by the equation:

$$p_{ult} = q'K_q + cK_c \quad \ldots\ldots\ldots\ldots\ldots\ldots\ldots\ldots\ldots\ldots \quad (1)$$

where q' is the effective overburden pressure at the depth

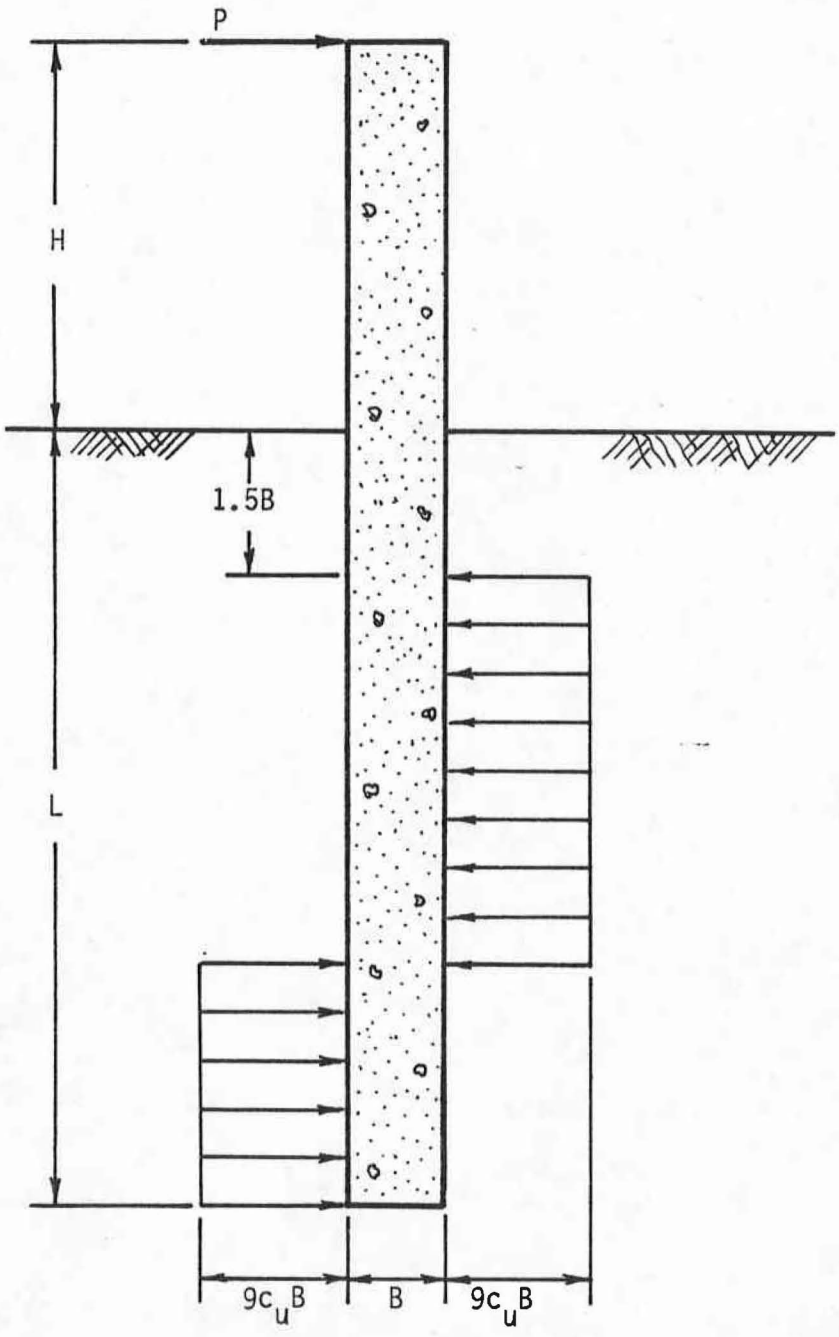

FIG. 3.-Brom's Ultimate Lateral Soil Resistance for Cohesive Soils

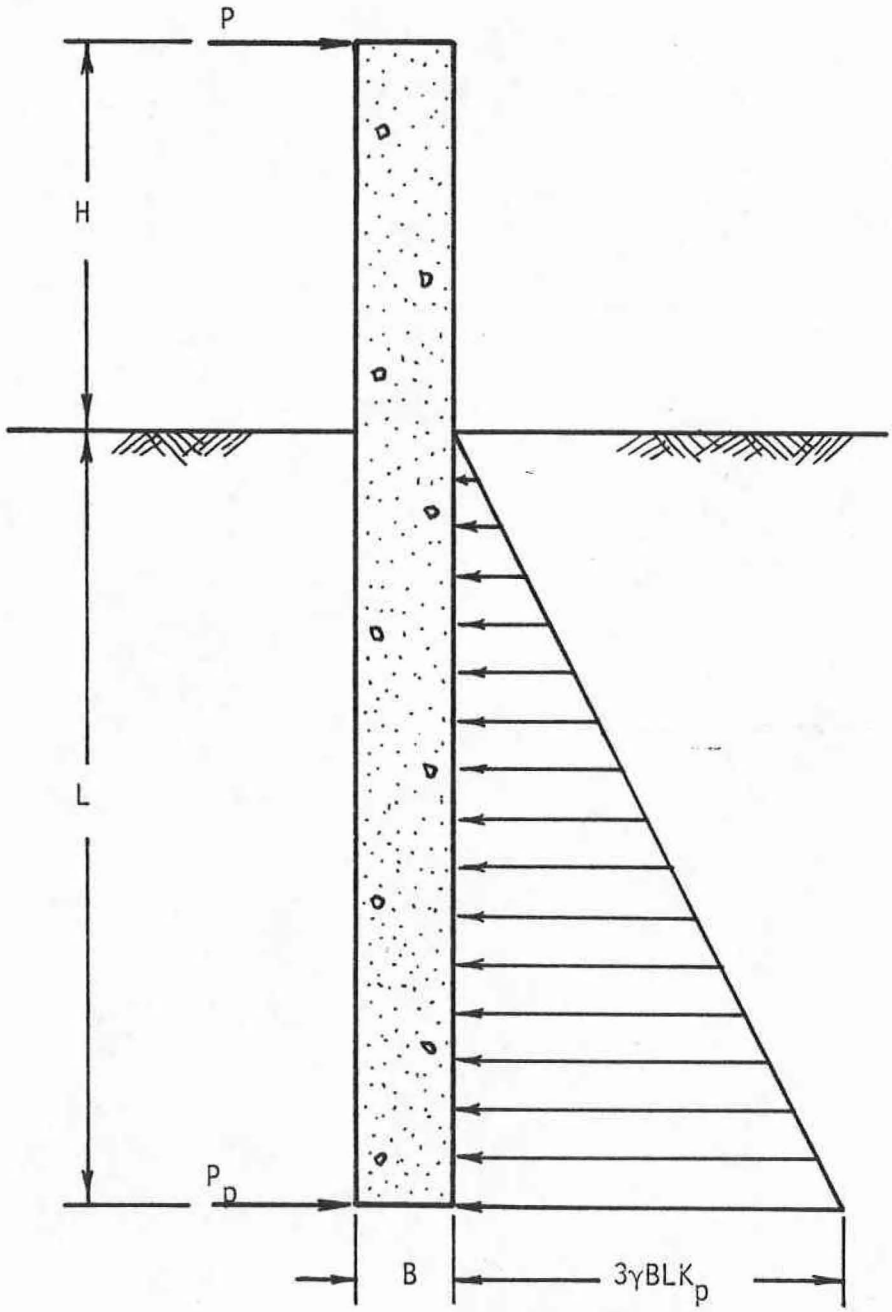

FIG. 4.-Brom's Ultimate Lateral Soil Resistance for Cohesionless Soils

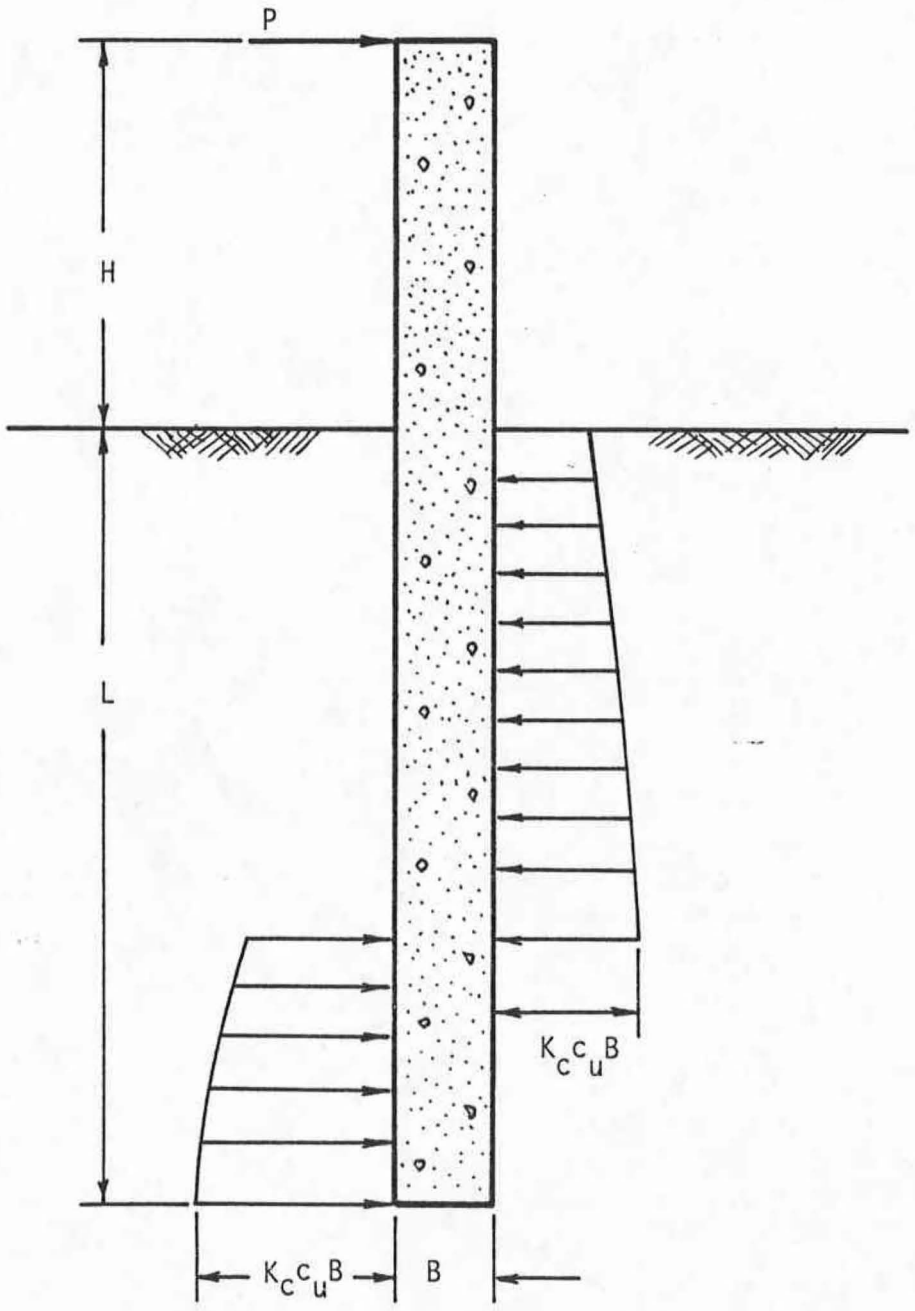

FIG. 5.-Hansen's Ultimate Lateral Soil Resistance for Cohesive Soils

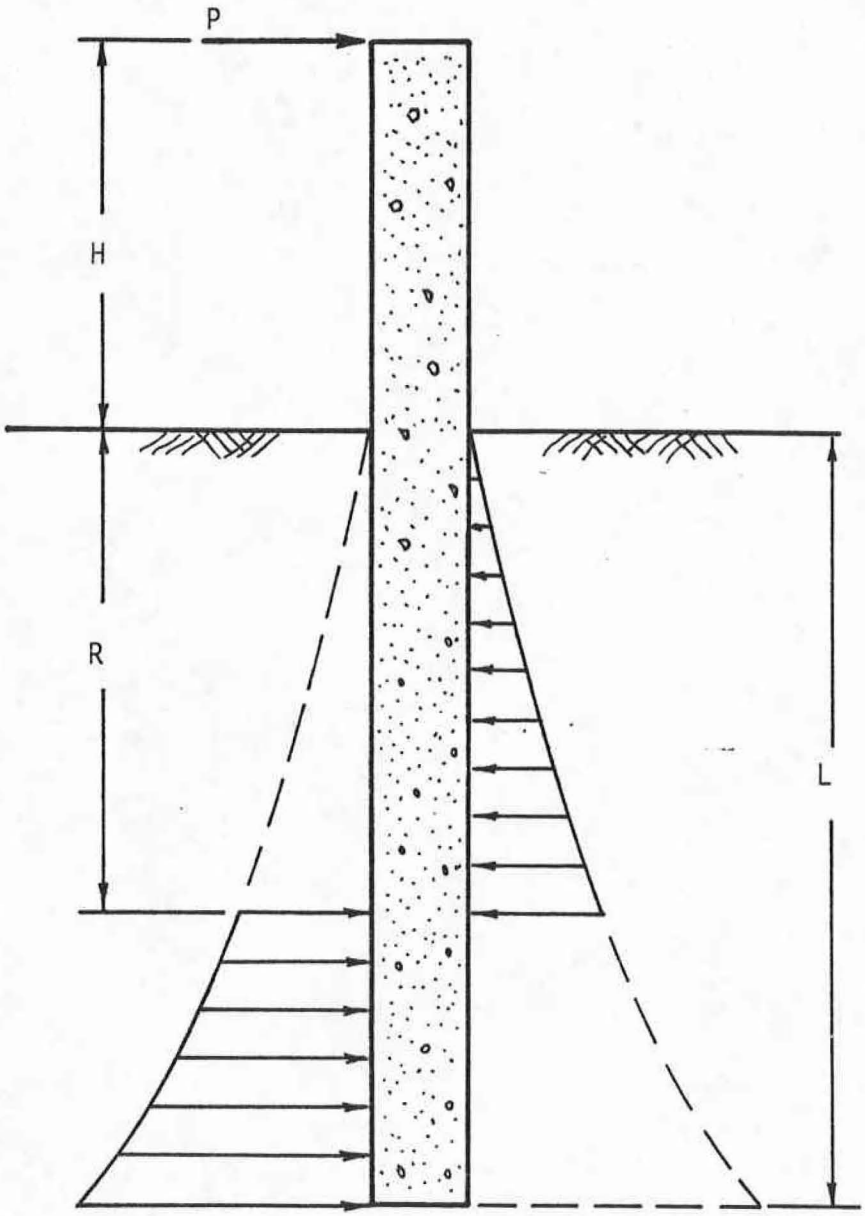

FIG. 6.-Hansen's Ultimate Lateral Soil Resistance for Cohesionless Soils

in question, c is cohesion, K_q is an earth pressure coefficient for overburden pressure, and K_c is an earth pressure coefficient for cohesion. The earth pressure coefficients, K_q and K_c, are functions of the internal angle of friction of the soil and the depth to pier diameter ratio at the point in question. Brinch Hansen presented some charts for these earth pressure coefficients. Unlike Broms' distributions, Brinch Hansen's pressure distributions are directly applicable to multi-layered soil profiles.

Reese (35) proposed equations for the ultimate lateral pressure for a purely cohesive soil. The ultimate lateral pressure is given by the equation:

$$p_{ult} = cK_c \quad \ldots\ldots\ldots\ldots\ldots\ldots\ldots\ldots\ldots\ldots \quad (2)$$

The value of K_c Reese calculated varies from 2 at the ground surface to 12 at depths in excess of approximately three pile diameters. Thompson (45) utilized the method used by Reese for computing ultimate lateral pressures with the additional assumption that the soil and pile separate on the side of the pile away from the direction of movement. Based on this, Thompson calculated a value of 8 for K_c for depths in excess of 1.5 pile diameters. This compares favorably with the value of 8.14 determined by Brinch Hansen (18) for great depth.

For soft cohesive soils, Matlock (26) presented the

following equation for the ultimate lateral pressure, p_{ult} (force/length):

$$p_{ult} = 3cB + q'B + 0.5zc \leq 9cB \quad \ldots\ldots\ldots\ldots\ldots\ldots (3)$$

where z is the depth in question. The limiting lateral soil pressure, 9cB, proposed by Matlock is identical to the ultimate lateral pressure proposed by Broms for cohesive soils.

Parker and Reese (32) developed the following equations for the ultimate lateral soil pressure, p_{ult} (force/length), for clean sands:

$$p_{ult} = \gamma' z \left[B(K_p - K_a) + zK_p(\tan \bar{\alpha} \tan \bar{\beta}) + zK_o \tan \bar{\beta}(\tan \phi - \tan \bar{\alpha})\right] \quad \ldots\ldots\ldots\ldots (4)$$

$$p_{ult} = \gamma' z\, B \left[K_p^3 + 2K_p^2 K_o \tan \phi - K_a + 2K_o \tan \phi\right] \quad \ldots\ldots\ldots (5)$$

where

γ' = average effective unit weight of soil above point in question

B = pile diameter

K_p = Rankine passive earth pressure coefficient

K_a = Rankine active earth pressure coefficient

K_o = at rest earth pressure coefficient

ϕ = internal angle of shearing resistance for the sand

$\bar{\alpha},\bar{\beta}$ = angles which define the geometry of the failure mechanism

The smaller of the two pressures determined from Eqs. 4 and 5 is used as the ultimate lateral pressure.

Menard and his coworkers [see Gambin (16)] developed a procedure for estimating the ultimate lateral soil pressure from the pressuremeter limit pressure p_1. The ultimate lateral pressure, p_{ult}, was used for depths greater than the critical depth, h_c. At depths less than the critical depth, the ultimate lateral pressure is computed as follows:

$$p_{ult} = 0.5\, p_1 \left(1 + \frac{z}{h_c}\right) \quad \ldots\ldots\ldots\ldots\ldots\ldots\ldots\ldots\ldots\ldots (6)$$

where z is the depth in question. The value for the critical depth, h_c, is a function of the soil classification and the pile diameter.

Roscoe and Schofield (40) developed an ultimate capacity analysis for stubby rectangular piles embedded in sand and constrained to rotate about the ground line. This procedure includes base shear stresses, as well as classical active and passive pressures for rough walls.

Comparitive Study of Ultimate Lateral Capacity Models

A study was conducted by Electric Power Research

Institue (EPRI) (11) to compare the most commonly used ultimate capacity analysis procedures. In this study EPRI used the methods proposed by Brinch Hansen, Broms, and Reese, where Reese's method includes the ultimate pressure formulations by Matlock (26) for soft clay, Parker and Reese (32) for sands, and Reese (35) for purely cohesive soils. Ultimate lateral capacity values were calculated for rigid shafts with diameters of 1, 3, and 6 feet, and depth-to-diameter ratios (D/B) of 3, 6, and 10 embedded in the following soil profiles:

1. Uniform soft clay (c_u = 500 psf)
2. Uniform stiff clay (c_u = 2000 psf)
3. Loose sand (ϕ = 30)
4. Dense sand (ϕ = 40)

The results of this study are presented in Table 1. From these results, EPRI concluded that the three theories gave similar results, with the following exceptions:

1. In cohesive soils with D/B less than 4, Broms' method significantly underpredicts the ultimate capacity value as obtained by either Brinch Hansen or Reese because the top 1.5 pier diameters of depth is neglected.
2. In cohesionless soils with D/B less than 3, Reese's method underpredicts the ultimate capacity value when compared to that

Table 1. Comparison Study of Existing Ultimate Capacity Methods (From EPRI (11))

B (ft)	D/B	Soft Clay	Stiff Clay	Loose Sand	Dense Sand
1	3	B+(0.47)*	B (0.47)	R (0.68)	R (0.74)
		R (0.84)	R (0.80)	BH (1.00)	BH (1.00)
		BH (1.00)	BH (1.00)	B (2.30)	B (1.58)
1	6	R (0.91)	R (0.84)	R (0.86)	R (0.98)
		B (0.94)	B (0.94)	BH (1.00)	BH (1.00)
		BH (1.00)	BH (1.00)	B (2.01)	B (1.31)
1	10	BH (1.00)	R (0.94)	R (1.05)	BH (1.00)
		R (1.03)	BH (1.00)	BH (1.00)	B (1.11)
		B (1.13)	B (1.13)	B (1.79)	R (1.23)
3	3	B (0.49)	B (0.49)	R (0.73)	R (0.77)
		R (0.98)	R (0.85)	BH (1.00)	BH (1.00)
		BH (1.00)	BH (1.00)	B (2.45)	B (1.65)
3	6	BH (1.00)	R (0.93)	R (0.92)	BH (1.00)
		B (1.00)	BH (1.00)	BH (1.00)	R (1.05)
		R (1.15)	B (1.00)	B (2.19)	B (1.43)
3	10	BH (1.00)	BH (1.00)	BH (1.00)	BH (1.00)
		B (1.25)	R (1.09)	R (1.15)	B (1.27)
		R (1.25)	B (1.25)	B (2.04)	R (1.34)
6	3	B (0.52)	B (0.52)	B (0.78)	R (0.81)
		BH (1.00)	R (0.93)	BH (1.00)	BH (1.00)
		R (1.19)	BH (1.00)	B (2.61)	B (1.76)
6	6	BH (1.00)	BH (1.00)	BH (1.00)	BH (1.00)
		B (1.10)	R (1.09)	R (1.02)	R (1.16)
		R (1.39(	B (1.10)	B (2.45)	B (1.60)
6	10	BH (1.00)	BH (1.00)	BH (1.00)	BH (1.00)
		B (1.44)	R (1.32)	R (1.37)	B (1.50)
		R (1.56)	B (1.44)	B (2.41)	R (1.60)

*( ) = $\frac{\text{Ultimate Capacity by Method in Question}}{\text{Ultimate Capacity by Brinch Hansen's Method}}$

B = Broms' Method, R = Reese's Method, BH = Brinch Hansen's Method

obtained by Brinch Hansen's or Broms' methods.

3. In cohesionless soils, Broms' method significantly overpredicts the ultimate capacity values in comparison to that by Brinch Hansen's or Reese's methods. This overprediction is more significant in loose sands than in dense sands.

Linear Load-Deflection Models

The linear load-deflection method approximates the behavior of drilled shafts under lateral loading conditions. This method of analysis predicts deflections of laterally loaded drilled shafts, and thus an entire load-deflection relationship may be determined. The linear load-deflection approach assumes that the deflections at low load levels are influenced by the stress-strain characteristics of the shaft and the stress-strain characteristics of the soil. The soil is modeled using a linear relationship between lateral deflection and lateral pressure (subgrade modulus approach), or by assuming a linear relationship between stress and strain (elastic continuum approach).

Subgrade Modulus Models. In the subgrade modulus approach, the soil is represented by a series of independent springs in a manner similar to the beam on elastic foundation problems addressed by Hetenyi (19). In this approach the lateral pressure at any given depth

can be related to the lateral pier deflection at that depth through the subgrade modulus as follows:

$$p = k_h \delta \quad \ldots\ldots\ldots\ldots\ldots\ldots\ldots\ldots\ldots\ldots \quad (7)$$

where

δ = shaft deflection (length)

p = lateral soil pressure (force/length^2)

k_h = subgrade modulus (force/length^3)

The relationship given in Eq. 7 is an approximation, since the lateral pressure is a function of not only the deflection at the point in question but also dependent on the deflection and the rotation at every point along the length of the shaft. In this regard, it is noted that the subgrade modulus is not solely a property of the soil, since it is also a function of the shaft geometry and the relative flexibility of the shaft-soil system.

The beam on the elastic foundation or subgrade modulus approach has received considerable attention in the engineering literature. Numerous solutions have been presented for flexible shafts supported by elastic foundations whose subgrade modulus variation with depth can be described by mathematical equations. Some of the most commonly used subgrade modulus variations are given in Table 2, which was adapted from Woodward, Gardner, and Greer (48). Matlock and Reese (27) have presented

Table 2. Beam on Elastic Foundation Solutions (Subgrade Modulus Approach) (From EPRI (11))

Modulus Variation with Depth	Solution Reference
Constant	Grandholm (17), Hetenyi (18)
Linear increase	Reese and Matlock (38), Hetenyi (18)
Power function increase	Palmer and Thomson (31), Matlock and Reese (27), Davisson and Prakash (13)
Polynomial function of increase	Matlock and Reese (27)
Two-layer system with the subgrade modulus constant in each layer	Davisson and Gill (12)

generalized solutions in a graphical form for both rigid and flexible shafts.

The accuracy of the subgrade modulus approach is completely dependent on the value of the subgrade modulus used in the analysis. Many methods have been proposed for computing the subgrade modulus. Terzaghi (44) proposed numerical values of the subgrade modulus for laterally loaded piles embedded in clays or sands. For piles embedded in stiff clay, the lateral subgrade modulus can be calculated from plate load tests (one foot square) on the surface of the clay as follows:

$$k_h = \frac{k_{s1}}{1.5\ B} \quad \dots\dots\dots\dots \quad (8)$$

where

k_h = lateral subgrade modulus

k_{s1} = subgrade modulus for a one-foot square plate

B = shaft width

For stiff to hard clays where plate load tests are not available, Terzaghi (44) recommended approximate values for k_{s1} as shown in Table 3.

For piles embedded in sand, Terzaghi (44) presented the following empirical equation for the subgrade modulus:

$$k_h = \frac{A\gamma' z}{1.35\ B} = \frac{n_h\ z}{B} \quad \dots\dots\dots\dots \quad (9)$$

Table 3. Values of the Subgrade Modulus (k_{si}) for One Foot Square Plates Resting on Precompressed Clay (44)

Consistency of Clay	Stiff	Very Stiff	Hard
Unconfined Compressive Strength q_u (tsf)	1-2	2-4	4
Range for $\bar{k}_{si}$ (tcf)	50-100	100-200	200
Proposed Values for $\bar{k}_{si}$ (tcf)	75	150	300

Note: 1 tsf = 95.76 kPa
1 tcf = 3.20×10^4 kg/m^3
1 ft = 0.3048 m

where

k_h = lateral subgrade modulus

z = depth below ground surface

B = width of the pile

γ' = effective unit weight of the sand

n_h = constant of horizontal subgrade reaction

A = empirical coefficient which is a function of the relative density of the sand

Values of n_h and A proposed by Terzaghi are shown in Table 4.

Terzaghi also proposed a relationship between the lateral subgrade modulus and the modulus of elasticity of the soil. This relationship is based on an elastic solution for the settlement of a uniformly loaded plate resting on an elastic half-space. This relationship is given by the following equation:

$$k_h = \frac{E_s}{1.35\ B} \quad \ldots\ldots\ldots\ldots\ldots\ldots\ldots\ldots\ldots\ldots\ldots\ldots \quad (10)$$

where

E_s = modulus of elasticity of the soil

Broms (6) presented the following equation for the subgrade modulus for piers embedded in cohesive soils:

$$\frac{k_h\ B}{E_s} = \frac{1}{m\ (1 - \nu^2)}\ (B/D)^{\frac{1}{2}} \quad \ldots\ldots\ldots\ldots\ldots\ldots\ldots\ldots\ldots\ldots \quad (11)$$

Table 4.- Previously Proposed Values of the Constant of Horizontal Subgrade Reaction, n_h (44)

Relative Density of Sand	Loose	Medium	Dense
Range of values of A	100-300	300-1000	100-2000
Proposed value of A	200	600	1500
Dry or moist sand, value of n_h(tcf)	7	21	56
Submerged sand, value of n_h (tcf)	4	14	34

Note: 1 tcf = 3.2×10^4 kg/m^3

where

m = influence factor which is a function of D/B (see Table 5)

ν = Poisson's ratio of the soil

Grandholm (17) developed the following equation for the lateral subgrade modulus based on Boussinesq's formula for the mean deflection of a beam resting on the surface of an elastic half-space:

$$\frac{k_h B}{E_s} = \frac{2\pi}{(1-\nu)(1+2\ln\frac{2\pi D}{B})} \quad \ldots\ldots\ldots\ldots\ldots\ldots (12)$$

Vesic (46) developed an equation for the subgrade modulus which gives a best-fit approximation to a continuum solution for an infinitely long beam resting on an elastic half-space and subjected to either a concentrated load or moment. This solution is the limiting value of the subgrade modulus as D/B approaches infinity. This equation indicates that the subgrade modulus is relatively insensitive to pier flexibility for long piers, and is given by

$$\frac{k_h B}{E_s} = \frac{0.65}{(1-\nu^2)} \sqrt[12]{\frac{E_s B^4}{EI_p}} \quad \ldots\ldots\ldots\ldots\ldots\ldots (13)$$

where

EI_p = effective flexural stiffness on the beam

Table 5. Numerical Values of the Influence Factor m (6)

D/B	1.0	1.5	2	3	5	10	100
m	0.95	0.94	0.92	0.88	0.82	0.71	0.37

Baguilin, Frank, and Said (2) developed equations for subgrade modulus by combining two-dimensional continuum solutions for a rigid circular disk translating in a finite elastic medium with three-dimensional solutions for a slender flexible vertical rod. The equations are as follows:

$$\frac{k_h B}{E_s} = \frac{1}{0.573 + 0.239 \ln \left(\frac{R}{15B} \right)} \quad (\text{for } \nu = 0.5) \; . \; . \; . \; . \; . \; . \; . \; (14)$$

$$\frac{k_h B}{E_s} = \frac{1}{0.808 + 0.265 \ln \left(\frac{R}{15B} \right)} \quad (\text{for } \nu = 0.33) \; . \; . \; . \; . \; . \; . \; . \; (15)$$

where

R = radius of effective soil boundary (see Table 6)

Davidson and Donovan (10) developed a semi-empirical subgrade modulus equation for drilled piers. The form of this equation was based on the analytical work of Douglas and Davis (15). However, the coefficient of the equation was adjusted to match the results from two field load tests. The resulting equation is as follows:

$$\frac{k_h B}{E_p} = 6 \left(\frac{B}{B_o} \right)^{1/4} \left(\frac{D}{B} \right)^{-1/2} \; . \; . \; . \; . \; . \; . \; . \; . \; . \; . \; . \; . \; . \; . \; . \; . \; . \; . \; . \; (16)$$

Table 6. Radius of Effective Soil Boundary (2)

Loading Condition	D/ℓ_o*	R = Radius of Effective Soil Boundary	
		$\nu = 0.5$	$\nu = 0.33$
Lateral shear, no moment	>2.4	$R = 7\ell_o$*	$R = 3.5\ell_o$
	<2.4 (rigid)	$R = 3D$	$R = 1.5D$
Moment, no lateral shear	>2.4	$R = 3\ell_o$	$R = 1.5\ell_o$
	<2.4 (rigid)	$R = 1.5D$	$R = 0.75D$

*$\ell_o = \sqrt[4]{\frac{4EI_p}{k_h B}}$

where

E_p = modulus of elasticity of the soil as obtained from the pressuremeter test

B_o = reference diameter of one foot

Another semi-empirical formulation for the subgrade modulus based on the modulus of elasticity determined from a pressuremeter tests was developed by Menard (3). The value of the subgrade modulus developed by Menard as follows:

$$\frac{k_h B}{E_p} = \frac{3}{\frac{2}{3}\left[\frac{B_o}{B}\right]\left[\frac{B}{B_o}(2.65)^{\alpha} + \frac{\alpha}{2}\right]} \quad \text{(for } B > 0.6 \text{ meters)} \quad \ldots \quad (17)$$

$$\frac{k_h B}{E_p} = \frac{18}{4\,(2.65)^{\alpha} + 3\alpha} \quad \text{(for } B < 0.6 \text{ meters)} \quad \ldots \ldots \quad (18)$$

where

B_o = reference diameter of 0.6 meters

α = rheological coefficient as given in Table 7.

A critical depth, z_c, has been defined below in which Eqs. 17 and 18 are valid. At shallower depths, the recommended subgrade modulus becomes $\lambda_z k_h$, where λ_z is a reduction coefficient defined by:

$$\lambda_z = \frac{1 + z/z_c}{2} \quad \ldots \quad (19)$$

where z_c is on the order of 2B for cohesive soils and 4B for granular soils.

Table 7. Rheological Coefficient α (16)

Type of Material	Peat E_p/pl	Peat α	Clay E_p/pl	Clay α	Silt E_p/pl	Silt α	Sand E_p/pl	Sand α	Sand and Gravel E_p/pl	Sand and Gravel α
Over consolidated	-	-	16	1	14	2/3	12	1/2	10	1/3
Normally consolidated	-	1	9/16	2/3	8-14	1/2	7-12	1/3	6-10	1/4
Weathered or altered soil	-	-	7-9	1/2	-	1/2	-	1/2	-	1/4

a = 1/2 for extensively fractured rock
a = 1/2 for normal rock
a = 2/3 for rock only slightly fractured or decomposed rock
p_1 = limit pressure from pressuremeter testing

Continuum Models. The continuum solutions for laterally loaded drilled shafts or piles are based on Mindlin's (29) elastic solution for a horizontal point load in a homogeneous elastic half-space. Poulos (33) presented solutions for the displacement and the rotation of a flexible vertical strip embedded in a uniform elastic half-space and subjected to a horizontal load or moment applied to its upper edge. This solution assumes that no slip or separation occurs between the strip and the surrounding soil.

A similar procedure for determining the displacement and the rotation of a thin, rigid vertical plate embedded in a homogeneous elastic half-space and subjected to a horizontal load or a moment applied to its upper edge was proposed by Douglas and Davis (14). Similar to the solution by Poulos (32), this solution assures no separation or slip between the plate and the soil.

Comparitive Study of Linear Load Deflection Models

The Electric Power Research Institute (EPRI) (11) conducted a comparative study of the linear load-deflection models. This study was conducted to investigate the relative magnitude of the deflection predictions of the most commonly used linear load-deflection models. This study addressed rigid piers with a diameter of 5 feet and with depth-to-diameter ratios of

3, 6, and 10. The following soil profiles were used in the study.

1. Uniform soft clay (E_s = 0.3 ksi)
2. Uniform stiff clay (E_s = 1.5 ksi)
3. Loose granular soil with linearly increasing modulus of elasticity (E_s = 0.714 ksi at a depth of 1 foot)
4. Dense granular soil with linearly increasing modulus of elasticity (E_s = 1.428 ksi at a depth of 1 foot)

Ground-line deflections for an applied moment (no applied shear) were predicted using the following methods:

1. Terzaghi 1 (Eq. 8 for stiff clay and Eq. 9 for sands)
2. Terzaghi 2 (Eq. 10)
3. Broms (Eq. 11) (Cohesive soils only)
4. Davidson and Donovan (GAI) (Eq. 16)
5. Menard (Eq. 17 and 18)
6. Baguelin (Eq. 15)
7. Douglas and Davis (14) (Cohesive soils only)
8. Poulos (32) (cohesive soils only)

These methods were ranked from softest prediction (greatest deflection) to stiffest prediction (least deflection). In addition, the ratio of the deflection obtained by Terzaghi's subgrade modulus equation (Eq. 10)

versus the deflection obtained by the theory in question was presented in order to determine the differences between the various theories. Table 8 presents the ranking of various solutions for the cases studied.

From Table 8, EPRI made the following observations:

1. The methods by Baguelin, Douglas, and Davis, and Poulos predict nearly identical deflections.
2. The least deflection is typically given by GAI's method or Menard's method.
3. Deflections predicted by the linear models can differ by a factor of 7.
4. Excluding Menard's model, the differences between the various theories decrease with increasing depth-to-diameter ratio.

Nonlinear Load-Deflection Models

A more sophisticated approach is the nonlinear load-deflection method based on the concept of p-y curves. Stress-strain behavior of soil is nonlinear, thus the lateral resistance of the soil, p, is nonlinearly related to the lateral deflection of the pier, y. This approach yields predictions that better approximate the behavior of piers under lateral loads. In this procedure, the resisting forces of the soil at the base of the shaft and the shear stresses at the perimeter of the shaft are neglected even though these components of soil resistance

Table 8. Comparitive Study for Rigid Piers Using Existing Linear Load-Deflection Methods+ (From EPRI (11))

D/B	Soft Clay (E_s = 0.3 ksi)	Stiff Clay (E_s = 1.5 ksi)	Loose Sand (E_s = 0.714z ksi)*	Dense Sand (E_s = 1.428z ksi)*
3	GAI (0.14)** Baguelin (0.23) D&D (0.25) Menard (0.31) Terzaghi 2 (1.0) Broms (1.0)	GAI (0.14) Baguelin (0.23) D&D (0.25) Menard (0.56) Terzaghi 2 (1.0) Broms (1.0) Terzaghi 1 (1.7)	GAI (0.14) Menard (0.16) Baguelin (0.23) Terzaghi 2 (1.0) Terzaghi 1 (5.0)	GAI (0.14) Menard (0.22) Baguelin (0.23) Terzaghi 2 (1.0) Terzaghi 1 (1.4)
6	GAI (0.20) Menard (0.31) Baguelin (0.37) D&D (0.37) Terzaghi 2 (1.0) Broms (1.2)	GAI (0.20) Baguelin (0.36) D&D (0.37) Menard (0.56) Terzaghi 2 (1.0) Broms (1.2) Terzaghi 1 (1.7)	Menard (0.16) GAI (0.20) Baguelin (0.36) Terzaghi 2 (1.0) Terzaghi 1 (5.0)	GAI (0.20) Menard (0.23) Baguelin (0.36) Terzaghi 2 (1.0) Terzaghi 1 (1.4)
10	Menard (0.31) GAI (0.33) D&D (0.45) Baguelin (0.45) Poulos (0.48) Terzaghi 2 (1.0) Broms (1.4)	GAI (0.33) Menard (0.56) D&D (0.45) Baguelin (0.45) Poulos (0.48) Terzaghi 2 (1.0) Broms (1.4) Terzaghi 1 (1.7)	Menard (0.16) GAI (0.33) Baguelin (0.45) Terzaghi 2 (1.0) Terzaghi 1 (5.0)	Menard (0.22) GAI (0.33) Baguelin (0.45) Terzaghi 2 (1.0) Terzaghi 1 (1.4)

+ Pier diameter equals 5 feet (1.5 m)

**() = $\frac{\text{Deflection at Ground Line by Method in Question}}{\text{Deflection at Ground Line by Terzaghi's Equation (Eq. 10)}}$

*z in feet

can significantly influence the response of laterally loaded drilled shafts. However, the p-y curve approach has gained popularity, and consequently many p-y curves for various soil types have been proposed.

Matlock (26) has proposed the following equation for soft clays:

$$\frac{p}{p_{ult}} = 0.5 \left(\frac{y}{y_{50}}\right)^{\frac{1}{3}} \quad \ldots\ldots\ldots\ldots\ldots\ldots\ldots\ldots \quad (20)$$

where

p = soil reaction pressure (force/unit length)

p_{ult} = ultimate soil reaction pressure (force/unit length)

y = pier deflection

y_{50} = pier deflection at one-half of the ultimate lateral pressure

Reese and Welch (39) have proposed the following equation for stiff clays:

$$\frac{p}{p_{ult}} = 0.5 \left(\frac{y}{y_{50}}\right)^{\frac{1}{4}} \quad \ldots\ldots\ldots\ldots\ldots\ldots\ldots\ldots \quad (21)$$

Both Eqs. 20 and 21 are defined once the ultimate lateral soil pressure, p_{ult}, and the deflection required to develop one-half of this ultimate pressure, y_{50}, are known. Matlock (26) has proposed Eq. 3 for calculating p_{ult} and has suggested that y_{50} can be computed using the

following equation:

$$y_{50} = 2.5\,\varepsilon_{50}\,B \quad \ldots\ldots\ldots\ldots\ldots\ldots\ldots\ldots \quad (22)$$

where

B = pier diameter

ε_{50} = strain corresponding to one-half of the maximum principal stress difference determined from an unconsolidated, undrained triaxial compression test.

Typical values for ε_{50} suggested by Skempton [see Welch and Reese (47)] are given in Table 9.

Parker and Reese (32) have proposed the following equation for sands:

$$\frac{p}{p_{ult}} = \tanh\left(\frac{E_{si}\,y}{p_{ult}}\right) \quad \ldots\ldots\ldots\ldots\ldots\ldots\ldots \quad (23)$$

where

p_{ult} = ultimate soil pressure as defined in Eqs. 4 and 5

$E_{si} = \frac{E_m}{1.35}$ = initial slope of the p-y curve

E_m = initial slope of the soil stress-strain curve

The stress-strain curve of the soil could be obtained, for example, from a consolidated, drained triaxial compression test. If such a test is not conducted, E_m can be approximated as follows:

Table 9. Typical Values for y_{50}

Consistency of Clay	y_{50}
Soft	0.020
Medium	0.010
Stiff	0.005

$$E_m = A\gamma' z \quad \ldots \quad (24)$$

where

γ' = effective unit weight of the soil

z = depth below ground surface

A = coefficient recommended by Terzaghi (44) for computing the lateral subgrade modulus as shown in Table 4

Reese and Allen (37) have proposed more refined techniques for developing p-y curves for both sands and clays to include strain softening.

Conclusions

It is clear from the preceding discussion that the laterally loaded drilled shaft problem requires further investigation. The ultimate lateral load capacity models only predict the ultimate load the drilled shaft will withstand without failure in the soil. The linear load deflection models represent the soil as a linear elastic material in spite of the fact that the soil is highly nonlinear. The nonlinear load deflection approach better approximates the nonlinear behavior of shafts under lateral loading conditions. However, the resisting forces and moments of the soil at the base of the shaft, and the shear stresses on the perimeter of the shaft, are neglected.

Development of an analysis procedure which captures

the nonlinearity of the soil response and includes all components of soil resistance, lateral normal stresses, and the shear stresses is necessary if the behavior of guardrail posts is to be accurately predicted. Furthermore, the lateral earth pressures developed against the shaft need to be related to the fundamental earth pressure theories of Coulomb (5) to avoid unnecessary assumptions or empiricism.

ANALYTICAL MODEL DEVELOPMENT

General

One of the principal goals of this research study was to develop an improved methodology for the analysis and design of drilled shafts or highway guardrail posts subject to lateral loads and overturning moments. This section describes the development of an analytical model for laterally loaded drilled shafts. The model is adequate to capture the realistic behavior of drilled shafts under lateral loading conditions while being simple enough for use in day-to-day design of these shafts. The analytical model development followed the steps noted below:

1. Definition of the problem.
2. Development of equations to characterize the nonlinear lateral stress-displacement response of the soil.
3. Development of an equation to calculate the horizontal shear stresses around the shaft.
4. Development of equations to calculate the vertical shear stresses acting on the perimeter of the shaft.
5. Development of equations to compute the shear stress and the compressive force acting on the

base of the shaft.

6. Development of an iterative solution to solve the lateral force and overturning moment equilibrium equations simultaneously.

The remainder of the chapter provides more details on the development of the analytical model.

Definition of the Problem

The soil-structure interaction analysis for a laterally loaded drilled shaft involves a complex distribution of normal and shear stresses at the shaft-soil interface. The analysis of these stresses is further complicated by the nonlinearity of the stress-strain behavior of the soil and the nonlinearity induced by the slip and separation at the shaft-soil interface. However, if the laterally loaded drilled shaft problem is to be properly analyzed, these complexities cannot be neglected.

In the development of this analytical model, the shaft is considered to be divided into a finite number of segments. The displacements of the segment are computed and based on this, the stresses on the segment can be calculated. Once the stresses are calculated for every segment, these stresses can be resolved into forces and added vectorially to satisfy equilibrium conditions.

The displacements of the shaft segments and the

forces acting on the shaft are shown in Figs. 7 and 8, respectively. Both the applied and the resisting forces are shown in Fig. 8. The applied forces acting on the shaft are:

1. Lateral load or ground-line shear, P_L
2. Overturning moment or ground-line moment, $M = P_L H$
3. Vertical or axial load, P_A
4. Effective weight of the shaft, W

The forces acting to resist the motion of the shaft are:

1. Lateral force resultant acting on segment i, P_i. This resultant is composed of the lateral earth pressure resultant, the resultant of the horizontal shear stress, and the drag force.
2. Vertical shear force acting on segment i, V_i.
3. Base shear force, V_B.
4. Vertical compressive force acting on the base of the shaft, F_B.

These forces acting on the drilled shaft must satisfy moment and force equilibrium. Referring to Fig. 8, the equations for the drilled shaft corresponding to moment equilibrium summed about the ground-line, lateral force equilibrium, and the vertical force equilibrium, respectively are as follows:

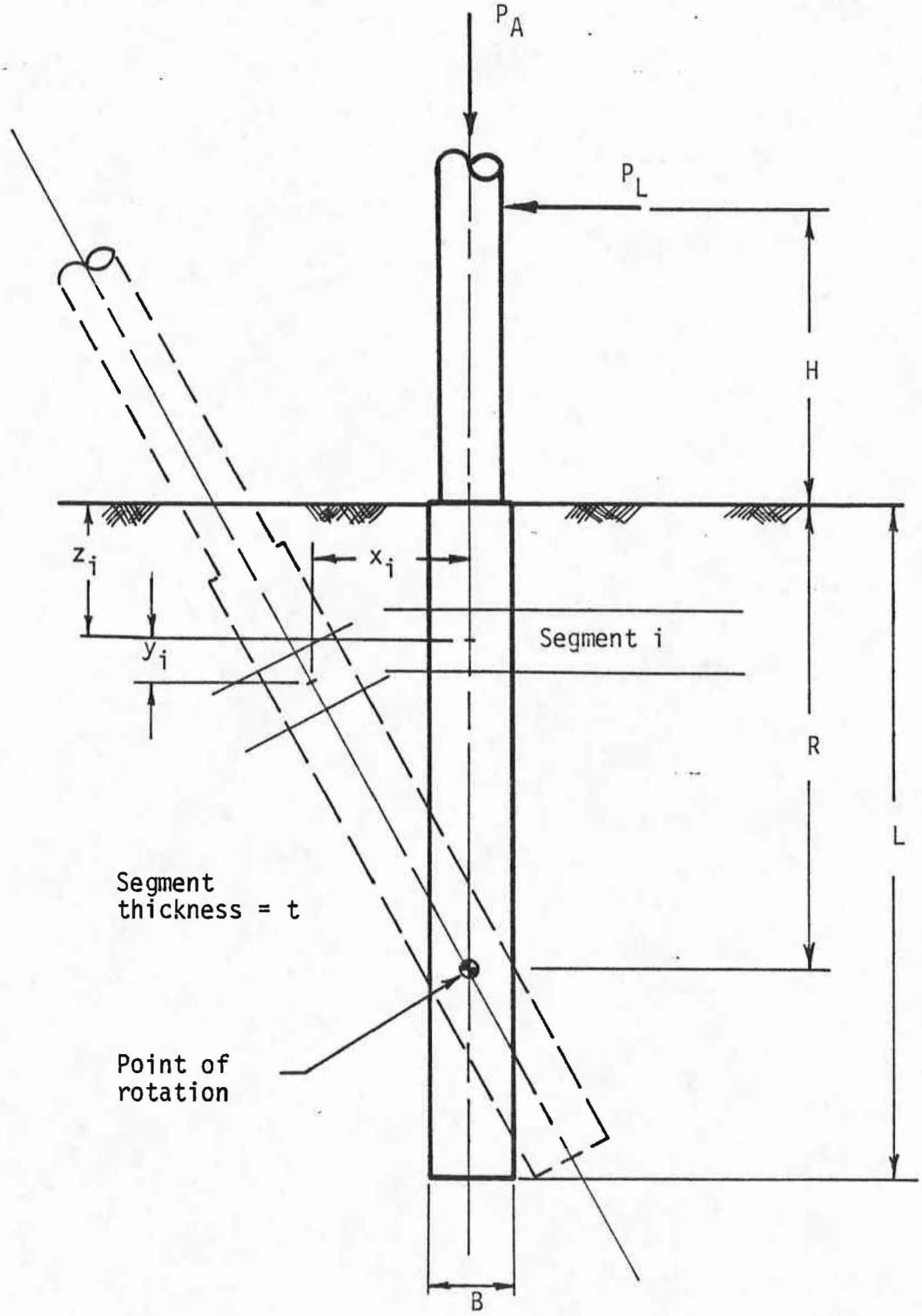

FIG. 7.-Details of the Model: Shaft Displacements

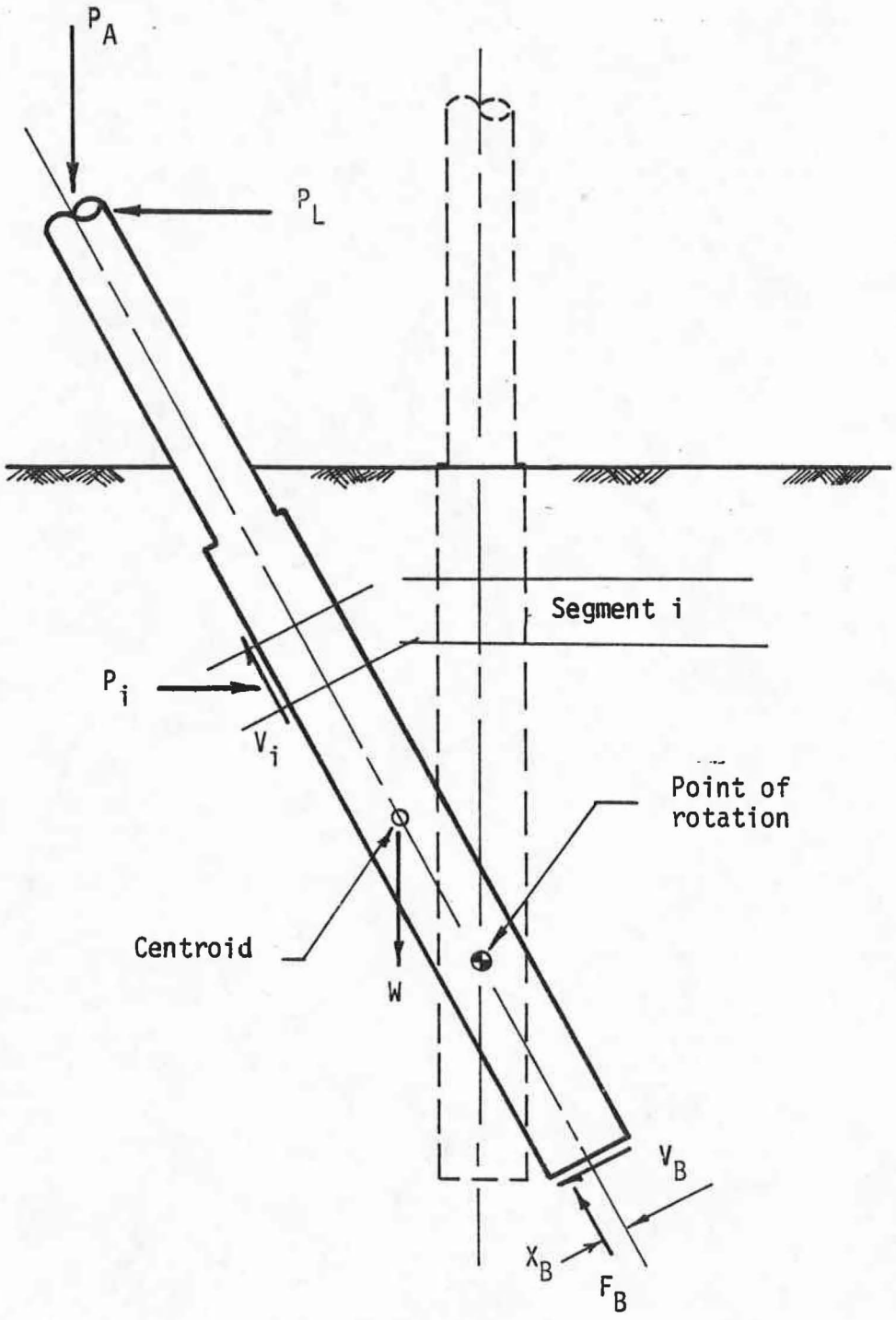

FIG. 8.-Details of the Model: Forces on the Shaft

$$M = P_L H + I\alpha = \sum_{i=1}^{n} P_i z_i \text{ (for } z_i < R) - \sum_{i=1}^{m} P_i z_i \text{ (for } z_i > R) - \sum_{i=1}^{n+m} V_i \bar{x}_i - V_B - F_B x_B \quad (25)$$

$$P_L = \sum_{i=1}^{n} P_i \text{ (for } z_i < R) - \sum_{i=1}^{m} P_i \text{ (for } z_i > R) - V_B \quad (26)$$

$$P_A = \sum_{i=1}^{n} V_i \text{ (for } z_i < R) - \sum_{i=1}^{m} V_i \text{ (for } z_i > R) + F_B - W \quad (27)$$

where:

H = Height above the ground-line to the point of application of the lateral load

L = Embedment depth of the shaft

R = Depth to the point of no lateral displacement or rotation point

z_i = Depth to the center of shaft segment i

n = Number of shaft segments above the point of rotation

m = Number of shaft segments below the point of rotation

P_i = Lateral force acting on shaft segment i including the lateral earth pressure resultant and the resultant of the horizontal shear stress

V_i = Vertical shear force acting on shaft segment i

V_B = Shear force acting on the base of the shaft

F_B = Vertical compressive force acting on the base of the shaft

W = Effective weight of the shaft

$\bar{x}_i$ = entricity of the vertical shear force relative to the shaft centerline for shaft segment i

x_B = Eccentricity of the vertical compressive force on the base relative to the centerline of the shaft

I = Moment of inertia of the shaft and soil about the ground surface

α = angular acceleration

The difficulty in analyzing the laterally loaded drilled shaft problem lies in the calculation of the resisting stresses acting on the shaft. These stresses are functions of the geometry of the shaft, the displacement or movement of the shaft relative to the soil, and the properties of the soil surrounding the shaft. Calculation of these stresses is presented in the following sections of this chapter.

Lateral Force

The lateral force, P_i, acting on segment i of the shaft is composed of three components: the resultant of the lateral earth pressure, the resultant of the

horizontal shear stress around the perimeter of the shaft, and the drag force exerted by the soil as the shaft segment rapidly moves through the soil. Analysis procedures for the computation of these stresses and the resultants are considered in the following sections.

Lateral Earth Pressure

The stress-strain behavior of soils is highly nonlinear. Thus, relating lateral earth pressures to the movement of the shaft is not a simple task. This relation between the movement and the lateral earth pressures is shown qualitatively in Fig. 9.

Referring to Fig. 9, the active state is the state of shear failure achieved by moving away from the soil mass until the lateral earth pressure has reached a minimum. The ratio of the lateral earth pressure at the active state to the overburden pressure is called the coefficient of active earth pressure and is given the symbol K_a. The passive state is the state of shear failure achieved by moving into the soil mass until the lateral earth pressure has reached a maximum. The ratio of the lateral earth pressure at the passive state to the overburden pressure is called the coefficient of passive earth pressure and is given the symbol K_p. The ratio of the lateral stress to the overburden stress, when no movement has occurred, is called the coefficient of at-

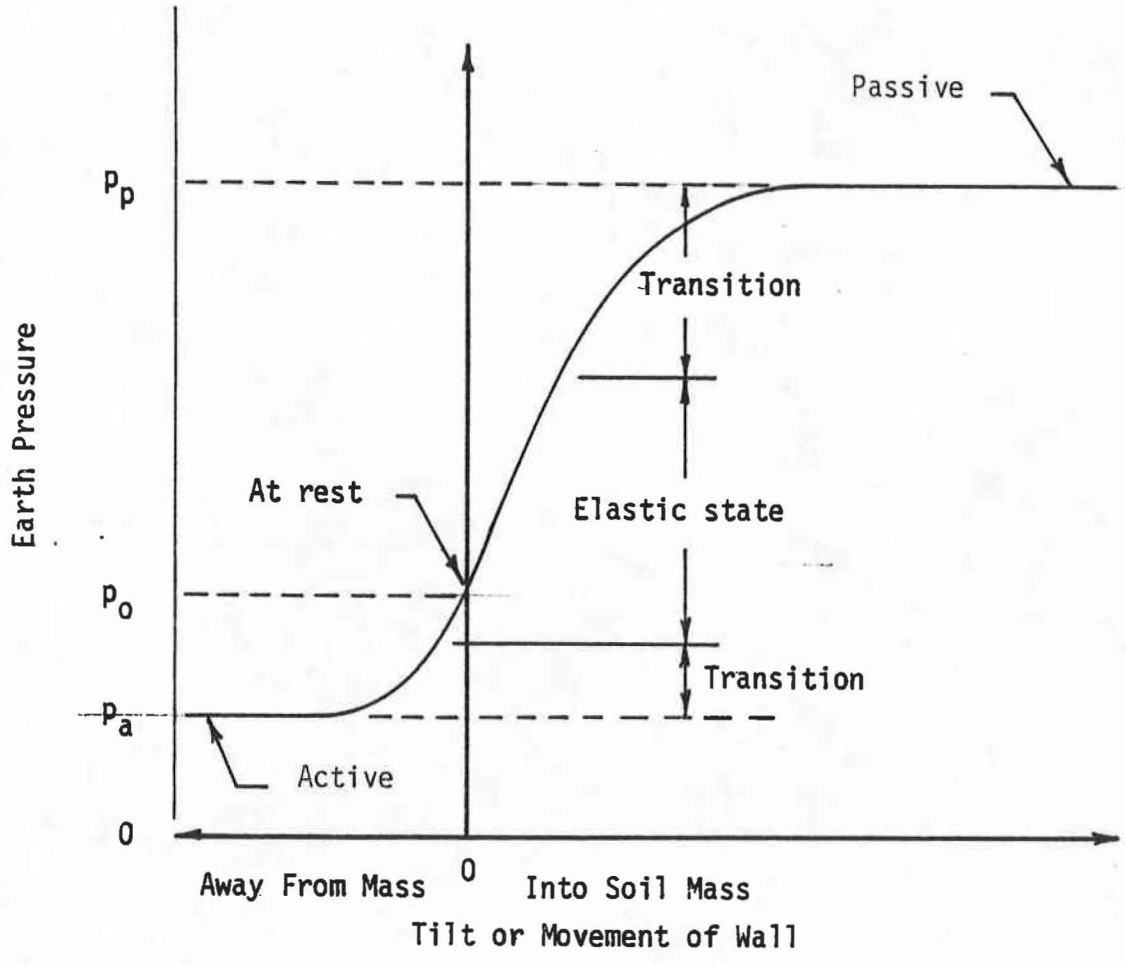

FIG. 9.-Effect of Wall Movement or Tilt on Magnitude of Resultant of Earth Pressure

rest earth pressure and is given the symbol K_o.

For both the active and passive states of shear failure, the lateral earth pressure can be calculated using the classical earth pressure theory by Coulomb (5). However, for states of stress in between these two states, the lateral earth pressure is not as easily calculated. Earth pressure theories to calculate the lateral earth pressure at a state of stress in between the active and passive states have not been developed. Thus, in order to calculate these lateral earth pressures the curve shown in Fig. 9 must be completely defined. The relation between the lateral pressures and the movement used in the development of this model is shown in Fig. 10.

Referring to Fig. 10, the lateral earth pressures developed when the movement of the shaft is into the surrounding soil mass are described by curve 1. The lateral earth pressures developed when the movement of the shaft is away from the soil mass are described by curve 2. These curves are defined by the equations,

Curve 1:

$$\sigma_p = \left[(K_p - K_o)\sigma'_v + 2c\sqrt{K_p}\right] \tanh\left[\frac{2x}{X_p}\right] + K_o\sigma'_v \quad \ldots\ldots \quad (28)$$

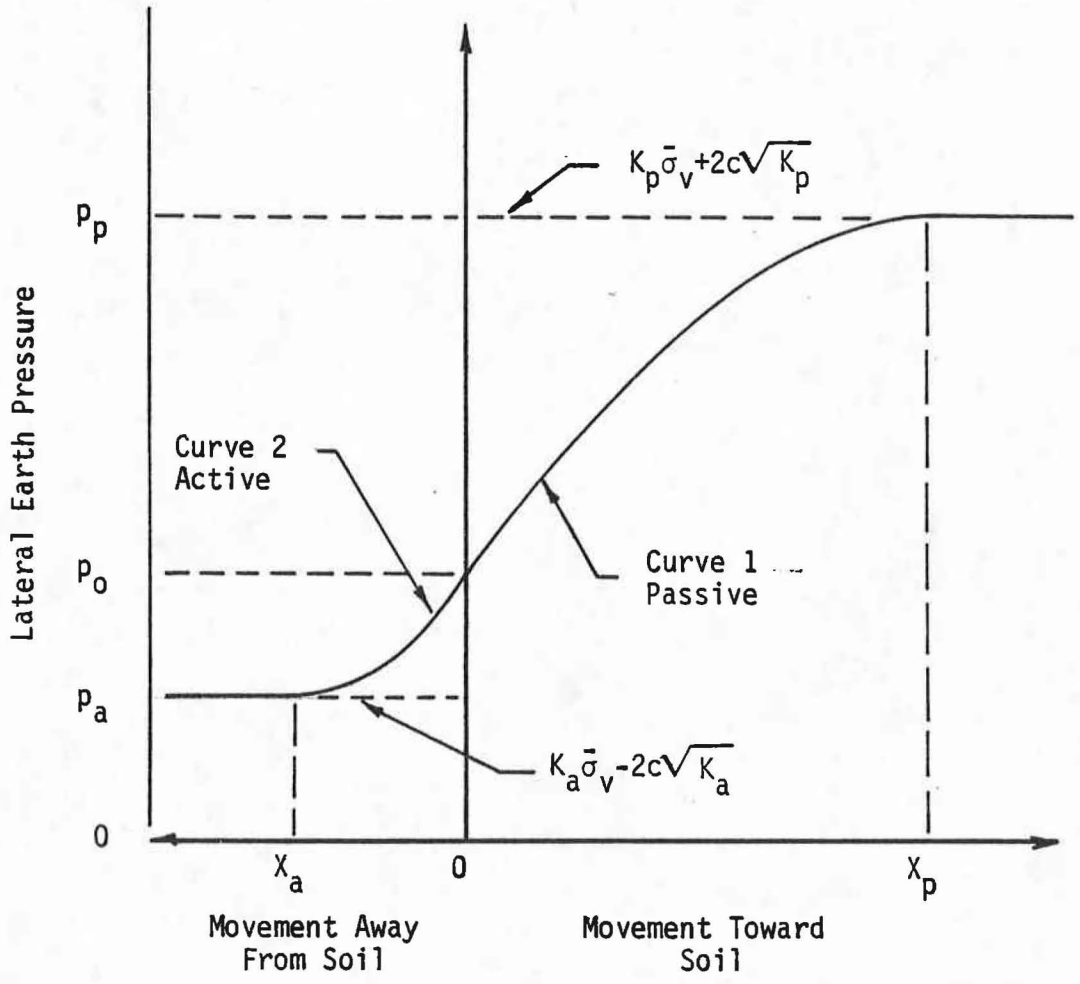

FIG. 10.-Variation of Lateral Earth Pressures With Shaft Movement

Curve 2:

$$\sigma_a = \left[(K_o - K_a)\sigma_v' + 2c\sqrt{K_a}\right] \tanh\left[\frac{-2x}{X_a}\right] + K_o\sigma_v' \quad \ldots\ldots (29)$$

where

σ_p = lateral passive earth pressure

σ_a = lateral active earth pressure

K_p = Coulomb's coefficient of passive earth pressure

K_a = Coulomb's coefficient of active earth pressure

K_o = coefficient of at-rest earth pressure

σ_v' = effective overburden pressure

c = soil cohesion

x = movement of shaft

X_p = movement required to develop ultimate passive pressure or passive state of shear failure

X_a = movement required to develop the active state of shear failure

The coefficient of passive earth pressure, K_p , as given by Coulomb is calculated as follows:

$$K_p = \frac{\sin^2(\psi - \phi)}{\sin^2\psi \, \sin(\psi + \delta) \left[1 - \sqrt{\frac{\sin(\phi + \delta)\, \sin(\phi + \beta)}{\sin(\psi + \delta)\, \sin(\psi + \beta)}}\right]^2} \quad (30)$$

where

ϕ = angle of internal shearing resistance of the soil

δ = angle of shearing resistance between the shaft and the soil

ψ = the angle of inclination of the shaft from the horizontal

β = ground slope

The coefficient of active earth pressure, K_a, as given by Coulomb is calculated similarly as follows:

$$K_a = \frac{\sin^2(\psi + \phi)}{\sin^2\psi \sin(\psi - \delta)\left[1 + \sqrt{\frac{\sin(\phi + \delta)\sin(\phi - \beta)}{\sin(\psi - \delta)\sin(\psi + \beta)}}\right]^2} \quad (31)$$

The coefficient of at-rest earth pressure, K_o, for cohesionless soils, and normally consolidated clays can be calculated as follows:

$$K_o = 1 - \sin\phi' \quad (32)$$

where

ϕ' = effective angle of internal shearing resistance.

For over-consolidated clays, the value of K_o is a function of the plasticity index and the over consolidation ratio of the soil. Correlations have been developed by Brooker and Ireland (8) to determine the value of K_o for over-consolidated soils.

The shear strength parameters ϕ and c can be measured in the laboratory by performing triaxial compression tests on soil samples. Measurement of the wall friction angle δ is much more difficult, however extensive research has been performed to correlate these values with soil types. Wall friction values for several structural materials are presented in Table 10.

The amount of movement of any point on the shaft necessary to produce either the active or passive state is proportional to the width of the shear zone adjacent to the point. As shown in Fig. 11, the minimum movement consists of rotating about some point beneath the ground surface. Typical values of the minimum tilt required to develop active and passive states have been suggested by Sowers (43) and are listed below in Table 11.

The lateral earth pressures given in Eqs. 28 and 29 are the maximum pressures developed for a given depth and the horizontal movement. These pressures would be developed if the shaft had an infinite width. Since the shaft is not infinite in width, a complex stress distribution develops around the perimeter of the shaft cross-section. This distribution will vary with the geometry of the shaft.

For circular shafts, the distribution shown in Fig. 12 is assumed to develop. As horizontal movement of the shaft segment takes place, the stresses increase on the

Table 10. Friction Angles δ Between Various Foundation Materials and Soil or Rock*

Interface Materials	Friction angle, δ, degrees**
Mass concrete or masonry on the following:	
Clean sound rock	35
Clean gravel, gravel-sand mixtures, coarse sand	29-31
Clean fine to medium sand, silty medium to coarse sand, silty or clayey gravel	24-29
Clean fine sand, silty or clayey fine to medium sand	19-24
Fine sandy silt, nonplastic silt	17-19
Very stiff and hard residual or preconsolidated clay	22-26
Medium stiff and stiff clay and silty clay	17-19
Steel sheet piles against:	
Clean gravel, gravel-sand mixture, well-graded rock fill with spalls	22
Clean sand, silty sand-gravel mixture, single-size hard rock fill	17
Silty sand, gravel or sand mixed with silt or clay	14
Fine sandy silt, nonplastic silt	11
Formed concrete or concrete sheetpiling against:	
Clean gravel, gravel-sand mixtures, well-graded rock fill with spalls	22-26
Clean sand, silty sand-gravel mixture, single size hard rock fill	17-22
Silty sand, gravel or sand mixed with silt or clay	17
Fine sandy silt, nonplastic silt	14
Various structural materials:	
Masonry on masonry, igneous and metamorphic rocks:	
Dressed soft rock on dressed soft rock	35
Dressed hard rock on dressed soft rock	33
Dressed hard rock on dressed hard rock	29
Masonry on wood (cross grain)	26
Steel on steel at sheet-pile interlocks	17
Wood on soil	14-16***

*Based in part on NAFAC (1971)
**Single values $\pm 2^{o}$. Alternate for concrete on soil is $\delta = \phi$
***May be higher in dense sand or if sand penetrates wood.

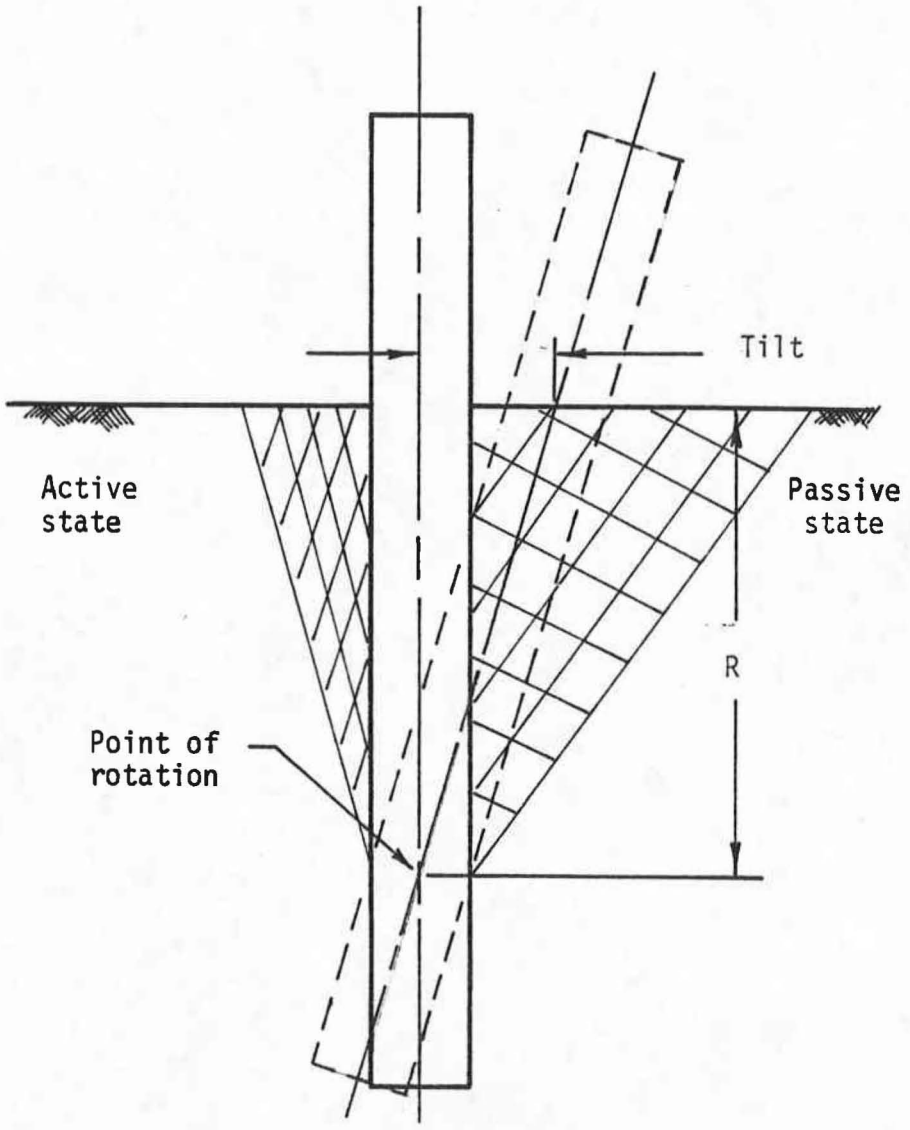

FIG. 11.-Tilt Necessary for Active and Passive States

Table 11. Typical Minimum Tilt Necessary for Active and Passive States

Soil	Active	Passive
Dense Cohesionless	0.0005R*	0.005R
Loose Cohesionless	0.002R	0.01R
Stiff Cohesive	0.01R	0.02R
Soft Cohesive	0.02R	0.04R

*R = Depth to the point of rotation.

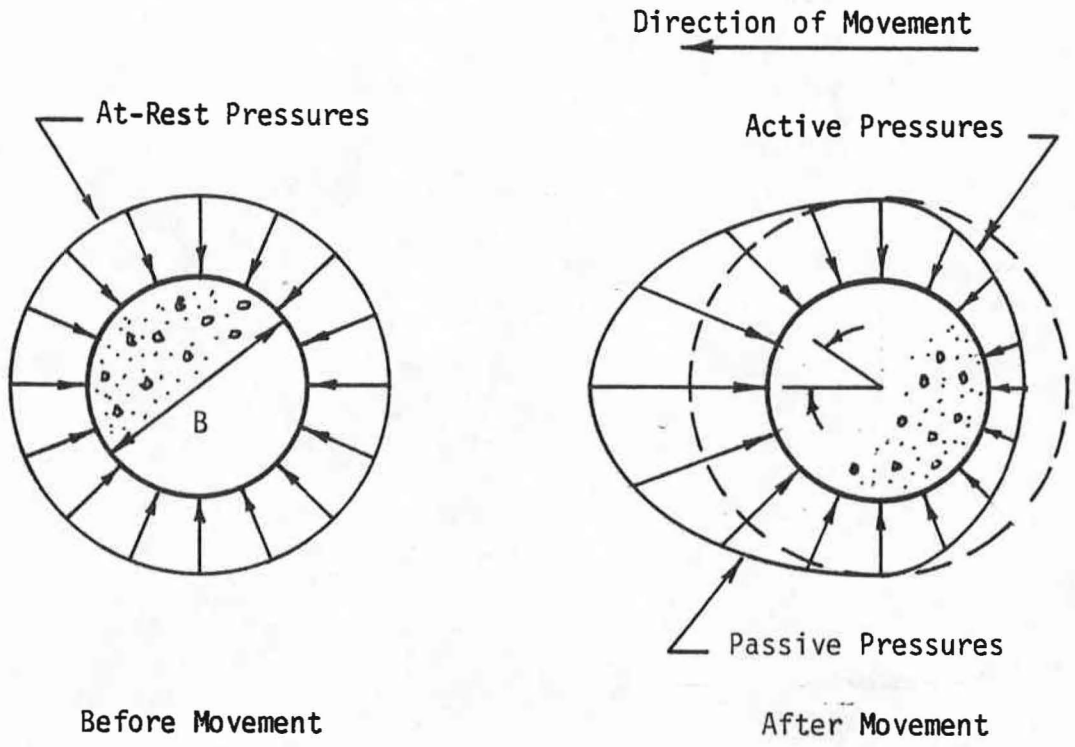

FIG. 12.-Distribution of Lateral Pressures Around a Circular Shaft

advancing surface and are reduced on the receding surface. The maximum value of stress, given in Eq. 28, is developed on the portion of the advancing surface at the point $\theta = 0$. This maximum pressure decreases to a value of the original at-rest pressure at $\theta = \pi/2$ and $\theta = -\pi/2$ as shown in Fig. 12. The pressure on the receding surface is rapidly reduced to a minimum value, as given in Eq. 29, on the portion of the surface at the point $\theta = \pi$. For cohesive soils, the active pressure as computed by Eq. 29 may be negative or tensile. However, the footing usually loses contact with the soil, and therefore tensile stresses do not act on the shaft.

A cosine distribution of pressure along the advancing perimeter of the shaft will be used to decrease the pressure from its maximum value. Thus the radial pressure on the advancing face of the shaft is written as:

$$\sigma_{rp} = \left(\left[(K_p - K_o)\sigma'_v + 2c\sqrt{K_p} \right] \tanh \frac{2x}{X_p} \right) \cos\theta + K_o\sigma'_v \quad (\text{for } -\pi/2 \leq \theta \leq \pi/2) \quad . \quad . \quad . \quad (33)$$

where:

σ_{rp} = radial stress on the advancing face of the shaft

The radial pressure on the receding face of the

shaft is similarly written as:

$$\sigma_{ra} = \left(\left[(K_o - K_a)\sigma'_v + 2c\sqrt{K_a} \right] \tanh \left[\frac{-2x}{X_a} \right] \right) \cos\theta + K_o\sigma'_v \quad (\text{for } \pi/2 \leq \theta \leq 3\pi/2) \quad . \quad . \quad . \quad (34)$$

where

σ_{ra} = radial stress on the receding face of the shaft.

This distribution of lateral pressures has been previously used in the solution of elasticity problems. Since the plastic flow concept allows the development of additional stresses in areas adjacent to the point of maximum stress, this cosine distribution may be slightly conservative.

Once the radial stresses are completely described, the resultant lateral force on a shaft segment of length, t, can be calculated as follows:

$$F_{lp} = 2 \int_0^{\pi/2} \sigma_{rp} \cos\theta \, \frac{B}{2} t \, d\theta - 2 \int_0^{\pi/2} \sigma_{ra} \cos\theta \, \frac{B}{2} t \, d\theta \quad (35)$$

where

F_{lp} = lateral earth pressure resultant force on a shaft segment

B = shaft diameter

t = shaft segment thickness

Substitution of Eqs. 33 and 34 into Eq. 35 and

rearranging yields

$$F_{lp} = Bt \int_0^{\pi/2} \left\{ \left(\left[(K_p - K_o)\sigma'_v + 2c\sqrt{K_p} \right] \tanh \left[\frac{2x}{X_p} \right] \right) \cos\theta - \left(\left[(K_o - K_a)\sigma'_v + 2c\sqrt{K_a} \right] \tanh \left[\frac{-2x}{X_a} \right] \right) \cos\theta \right\} \cos\theta \, d\theta \quad (36)$$

after integration, Eq. 36 can be written as

$$F_{lp} = Bt \frac{\pi}{4} \left(\left[(K_p - K_o)\sigma'_v + 2c\sqrt{K_p} \right] \tanh \left[\frac{2x}{X_p} \right] - \left[(K_o - K_a)\sigma'_v + 2c\sqrt{K_a} \right] \tanh \left[\frac{-2x}{X_a} \right] \right) \quad (37)$$

For noncircular shafts, the distribution of lateral earth pressures is more complex than that for the circular shafts. For rectangular cross-sections, the distributions shown in Fig. 13 are used to describe lateral stresses on the shaft. These assumed distributions were derived from contact pressure distributions beneath rigid footings. As in the case of circular shafts, once a distribution is known, the resultant lateral force acting on a shaft segment is calculated by integrating the lateral stresses over the area on which they act. The lateral force acting on the shaft segment can be written as:

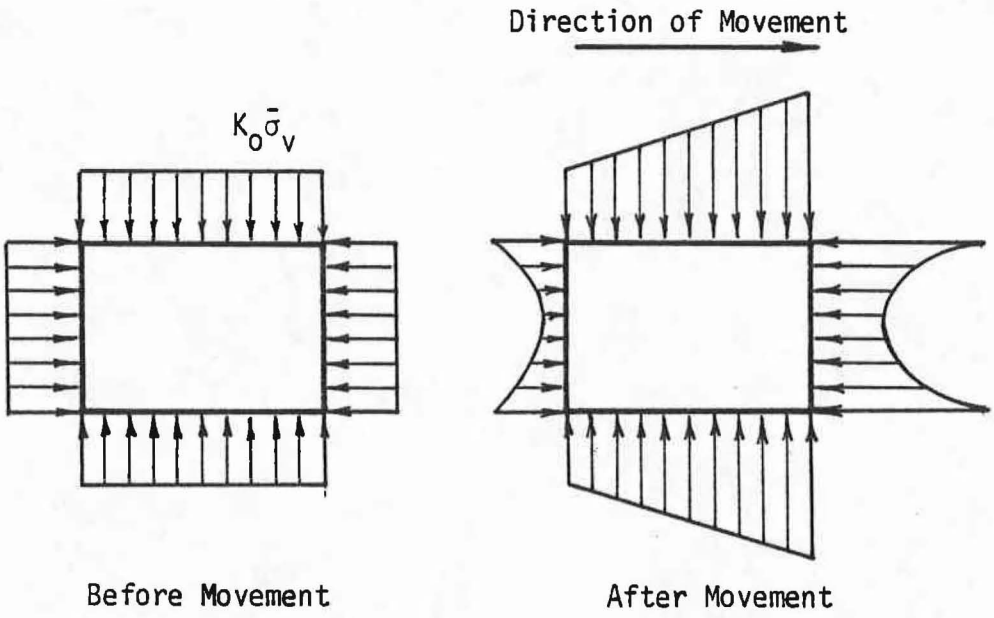

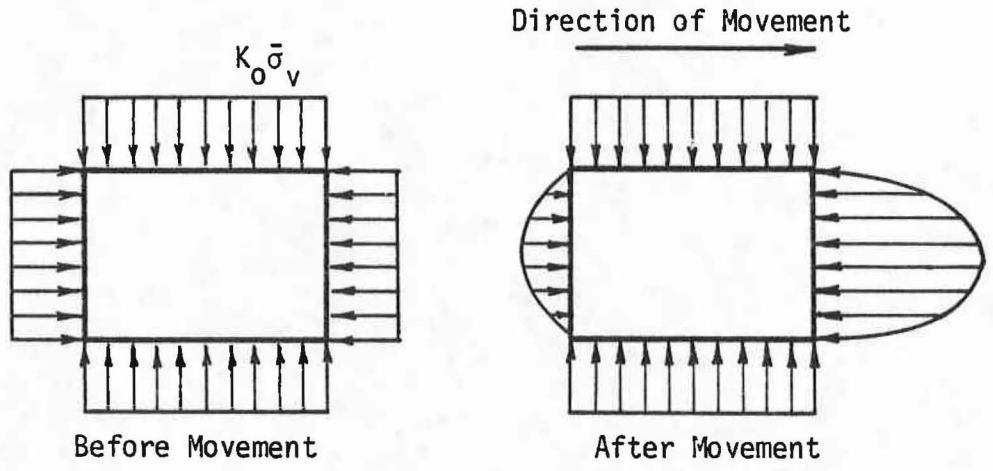

FIG. 13.-Distribution of Lateral Pressures Around a Rectangular Shaft

$$F_{lp} = Bt\, S_f \left(\left[(K_p - K_o)\sigma'_v + 2c\sqrt{K_p} \right] \tanh \left[\frac{2x}{X_p} \right] - \left[(K_o - K_a)\sigma'_v + 2c\sqrt{K_a} \right] \tanh \left[\frac{-2x}{X_a} \right] \right) \quad . . . . (38)$$

where

S_f = shape factor

B = shaft width

The shape factor, S_f, is a function of the geometry of the shaft. For circular shafts, the value of the shape factor is $\pi/4$ as shown in Eq. 38. For noncircular shafts, the value of S_f varies between 2/3 and 1.0 depending on the type of soil.

Horizontal Shear Stress

Considering the shear stresses developed by the movement of a circular shaft, it is apparent that the greatest tendency for the development of horizontal shear stresses acting around the perimeter of the shaft is at $\theta = \pi/2$ and $\theta = -\pi/2$ as shown in Fig. 12. As with the lateral earth pressures, a distribution to describe the horizontal shear stresses must be assumed in order to compute the resultant lateral force. It is seen that a sine function of θ, could be used to describe this distribution.

Since the maximum shear stress the soil can develop at the shaft-soil interface is

$$\tau_m = -\alpha_r (\sigma_r \tan \phi + c) \quad \ldots\ldots\ldots\ldots\ldots\ldots\ldots \quad (39)$$

where

τ_m = maximum shear stress

α_r = strength reduction factor

σ_r = normal stress on the plane

the distribution of the horizontal shear stress between $\theta = 0$ and $\theta = \pi/2$ is assumed as

$$\tau_{r\theta} = \alpha_r (\sigma_r \tan \phi + c) \sin \theta \quad \ldots\ldots\ldots\ldots\ldots\ldots \quad (40)$$

The strength reduction factor, α_r, is less than or equal to 1.0 and may reflect, for example, soil disturbance associated with the construction process.

Significant horizontal shear stresses at the shaft-soil interface are assumed to develop only on the advancing face of the shaft. Thus, the resultant lateral force of the horizontal shear stresses acting on a shaft segment is calculated as follows:

$$F_{ls} = 2\int_0^{\pi/2} \left[\alpha_r (\sigma_r \tan \phi + c) \sin \theta\right] \sin \theta \ \frac{B}{2} t \ d\theta \quad \ldots \quad (41)$$

where

F_{ls} = lateral force resultant of the horizontal shear stresses on a shaft segment

σ_r = radial stress on the advancing face of the shaft as given in Eq. (31)

Substituting Eq. 33 into Eq. 41 and integrating gives the following:

$$F_{ls} = Bt\left(\frac{\tan\phi}{3}\left[(K_p - K_o)\sigma'_v + 2c\sqrt{K_p}\right]\tanh\left[\frac{2x}{X_p}\right] + \frac{\pi}{4}(K_o\sigma'_v\tan\phi) + \frac{\pi}{4}c\right) \quad (42)$$

Equation 42 is an expression for the lateral force resultant of the horizontal shear stresses acting on the advancing face of a circular shaft segment. This expression is not valid for noncircular shafts. However, for rectangular shafts, the lateral force resultant of the horizontal shear stresses can also be calculated.

Horizontal shear stresses are developed only on the sides of rectangular shafts. The normal stress distribution for rectangular shafts is shown in Fig. 13. Since the normal stress is a constant over the side of a rectangular shaft segment, the resultant lateral force is easily calculated as follows:

$$F_{ls} = 2B_w t\alpha_r (K_o\sigma'_v \tan\phi + c) \quad (43)$$

where

B_w = length of the rectangular shaft segment

Drag Force

As the shaft rapidly rotates through the soil, a drag force is exerted on the shaft by the soil. This drag force will be analyzed assuming that the soil is a viscous medium flowing around the shaft. Thus, the drag force on shaft segment i is calculated as follows:

$$F_{1d} = C_D A_i \rho \frac{v_i^2}{2} \quad \ldots\ldots\ldots\ldots\ldots\ldots\ldots\ldots\ldots\ldots (44)$$

where

F_{1d} = drag force or shaft segment

C_D = drag coefficient

A_i = projected area of the body on a plane normal to the flow

ρ = mass density of the soil

v_i = velocity of the soil or shaft

The drag coefficient, C_D, is a function of the shaft geometry and the Reynolds Number. The drag coefficient curves for both circular and square shafts are given in Fig. 14.

Total Lateral Force

The total lateral force acting on segment i of the shaft, P_i, is the sum of the lateral earth pressure resultant, the resultant of the horizontal shear stress,

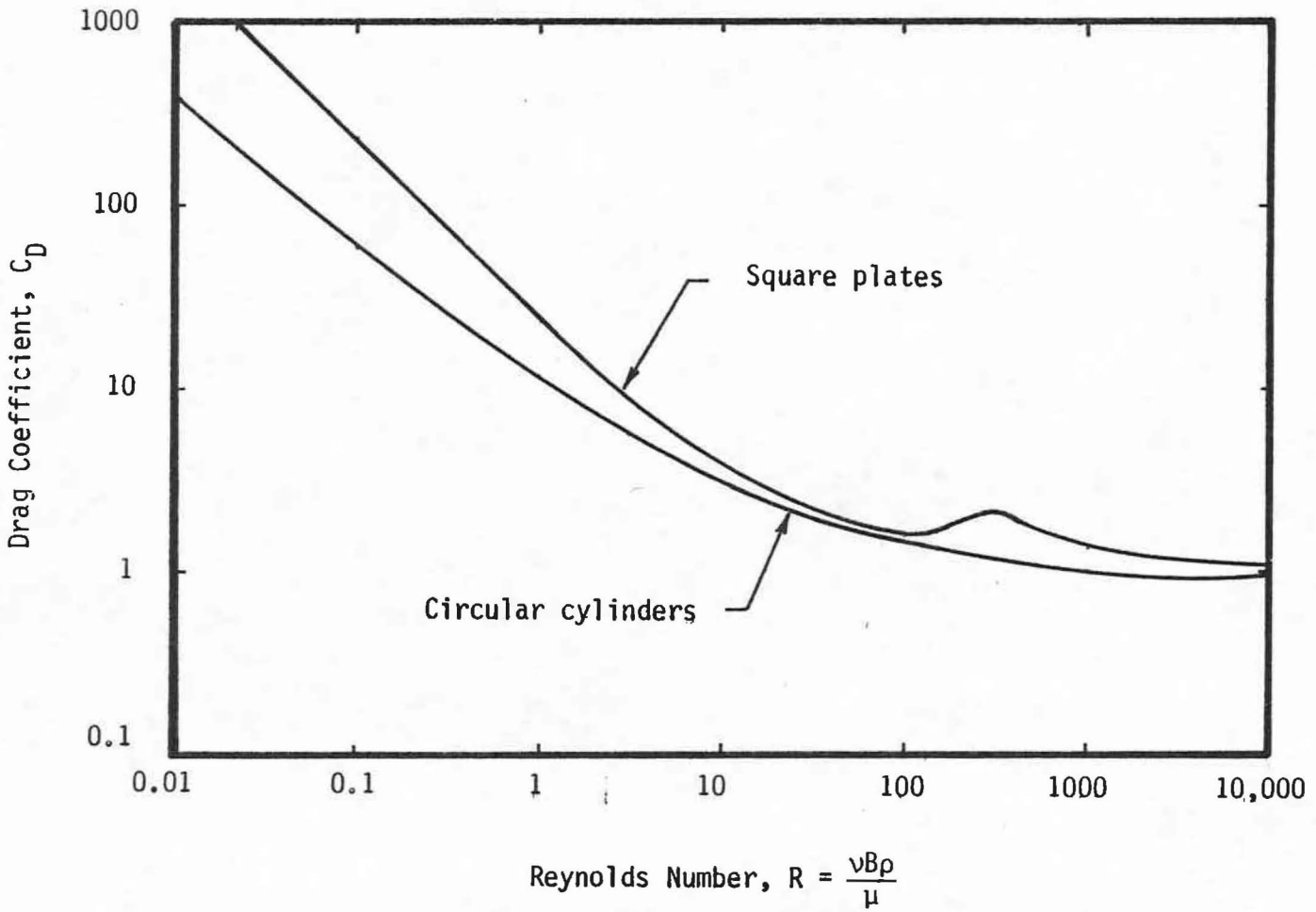

FIG. 14.-Drag Coefficients for Square Plates and Circular Cylinders

and the drag force. Thus, the total lateral resisting force on segment i is computed as follows:

$$P_i = F_{lp} + F_{ls} + F_{ld} \quad \ldots\ldots\ldots\ldots\ldots\ldots \quad (45)$$

where F_{lp}, F_{ls}, and F_{ld} were defined in Eqs. 37 or 38, 42 or 43, and 44.

Vertical Force

As a drilled shaft rotates under an applied overturning moment and ground-line shear, each point along the shaft moves horizontally and vertically. The vertical movement of a segment of the shaft causes vertical shear stresses to develop on the advancing face of the shaft. These shear stresses resist the rotation of the shaft.

Referring to Eq. 39, the ultimate shearing strength at the shaft-soil interface is:

$$\tau_m = \alpha_r (\sigma_r \tan \phi + c) \quad \ldots\ldots\ldots\ldots\ldots\ldots \quad (39)$$

Since the magnitude of the resultant of the horizontal shear stress $\tau_{r\theta}$ and the vertical shear stress τ_{zm} must be equal τ_m, the following distribution is assumed for the maximum vertical shear stress on a circular shaft:

$$\tau_{zm} = \alpha_r (\sigma_r \tan \phi + c) \cos \theta \quad \ldots\ldots\ldots\ldots\ldots\ldots \quad (46)$$

where

τ_{zm} = maximum vertical shear stress on shaft-soil interface

The vertical shear stress, however, is a function of the vertical movement of the shaft segment, as well as the horizontal movement of the shaft. Thus, the vertical shear stress on the shaft-soil interface is calculated as follows:

$$\tau_{rz} = \tau_{zm} \tanh\left[\frac{2y}{Q}\right] \quad \ldots\ldots\ldots\ldots\ldots\ldots\ldots \quad (47)$$

where

τ_{rz} = vertical shear stress

y = vertical movement of shaft segment

Q = vertical movement of shaft segment required to develop maximum vertical shear stress, sometimes called quake

The vertical force resultant of the vertical shear stress on a circular shaft segment is calculated by integrating the vertical shear stresses over the area of the advancing face of the segment on which it acts, and this is given by:

$$V_i = 2\int_0^{\pi/2} \tau_{rz} \frac{B}{2} t \, d\theta \quad \ldots\ldots\ldots\ldots\ldots\ldots\ldots \quad (48)$$

Substitution of Eq. 47 into Eq. 48 followed by integration yields:

$$V_i = Bt\,\alpha_r \left\{ \frac{\pi}{4} \left(\left[(K_p - K_o)\sigma'_v + 2c\ K_p \right] \tanh\left[\frac{2x}{X_p} \right] \right) \tan\phi + K_o\sigma'_v \tan\phi + c \right\} \tanh\left[\frac{2y}{Q} \right] \quad \ldots\ldots\ldots (49)$$

where

V_i = vertical resultant force acting on shaft segment i

For noncircular shafts a different distribution of vertical shear stress must be assumed. Vertical shear stresses are assumed to develop only on the advancing face of rectangular shafts. The normal stress distributions on rectangular shafts are shown in Fig. 13.

The vertical resultant force due to the vertical shear stress on a rectangular shaft segment is calculated as follows:

$$V_i = Bt\,\alpha_r \left\{ S_f \left(\left[(K_p - K_o)\sigma'_v + 2c\ K_p \right] \tanh\left[\frac{2x}{X_p} \right] + K_o\sigma'_v \right) \tan\phi + c \right\} \tanh\left[\frac{2y}{Q} \right] \quad \ldots\ldots\ldots (50)$$

where

S_f = shape factor

B = pile width

Base Compressive Force

As the shaft rotates under an applied lateral load,

a vertical normal force develops on the base of the shaft. This vertical normal force can be determined directly from the vertical equilibrium equation given by:

$$F_B = P_A + W - \sum_{i=1}^{n} V_i \text{ (for } z_i < R) + \sum_{i=1}^{m} V_i \text{ (for } z_i > R) \quad . . (27)$$

This base normal force is usually compressive, however, if Eq. 27 yields a negative or tensile value, the base normal force is set equal to zero. This implies that tension is not allowed to develop on the base of the shaft.

Base Shear Force

As the base of the shaft translates horizontally, a shear force is developed on the base. To determine this shear force, it is assumed that one-half of the shaft base maintains contact with the soil. It is further assumed that the normal stress on the base of the shaft increases linearly from the base centerline. Therefore, the base area in contact with the soil is:

$$\bar{A}_b = \frac{\pi B^2}{8} \quad \text{(circular shaft)} \quad . . . . . (51a)$$

$$\bar{A}_b = \frac{B_w B}{2} \quad \text{(rectangular shaft)} \quad . . . . . (51b)$$

where

$\bar{A}_b$ = area of base in contact with soil

B = pile width or diameter

B_w = shaft cross-section length for rectangular shafts

and the effective moment arm of the resultant base vertical compressive force from the centroidal axis of the shaft is:

$$\bar{x}_b = 0.30\ B \quad \ldots\ldots\ldots\ldots\ldots\ldots\ldots\ldots\ldots\ldots \quad (52)$$

Thus, the resisting moment acting on the base of the shaft is calculated as follows:

$$M_b = 0.3\ B\ F_B \quad \ldots\ldots\ldots\ldots\ldots\ldots\ldots\ldots\ldots\ldots \quad (53)$$

where

M_b = moment or base of shaft

The base shear force is calcualted as:

$$V_B = \alpha_r\ (c\bar{A}_b + F_B \tan \phi\ ) \quad \ldots\ldots\ldots\ldots\ldots\ldots\ldots\ldots \quad (54)$$

where

V_B = base shear force

c = cohesion of soil beneath the base

ϕ = angle of internal shearing resistance of the soil beneath the base.

Calculation of the Moment of Inertia

In order to calculate the moment of inertia, I, of the shaft-soil system, the amount of soil within the failure zone is related to the movement of the shaft. As the movement or rotation of the shaft increases, the amount of soil within the failure zone increases. Thus, several assumptions must be made in order to evaluate the moment of inertia.

The assumed shape of the shear failure zone when the soil has completely failed is shown in Figs. 15 and 16. The failure zone for circular shafts is shown in Fig. 15, and the failure zone for rectangular shafts is shown in Fig. 16. These failure zones are developed when sufficient movement has occurred to develop the ultimate passive pressures. For movements less than that required to develop passive pressures, the size of the failure zone is assumed to be proportionately smaller.

Iterative Solution

The moment equilibrium and the lateral force equilibrium Eqs. 25 and 26 can be solved iteratively to determine the lateral force, P_L, and the ground-line moment, M, assuming that the height to the lateral load, H, is known and is constant. If the shaft is assumed to be rigid, a convenient approach to solving these equations is outlined as follows:

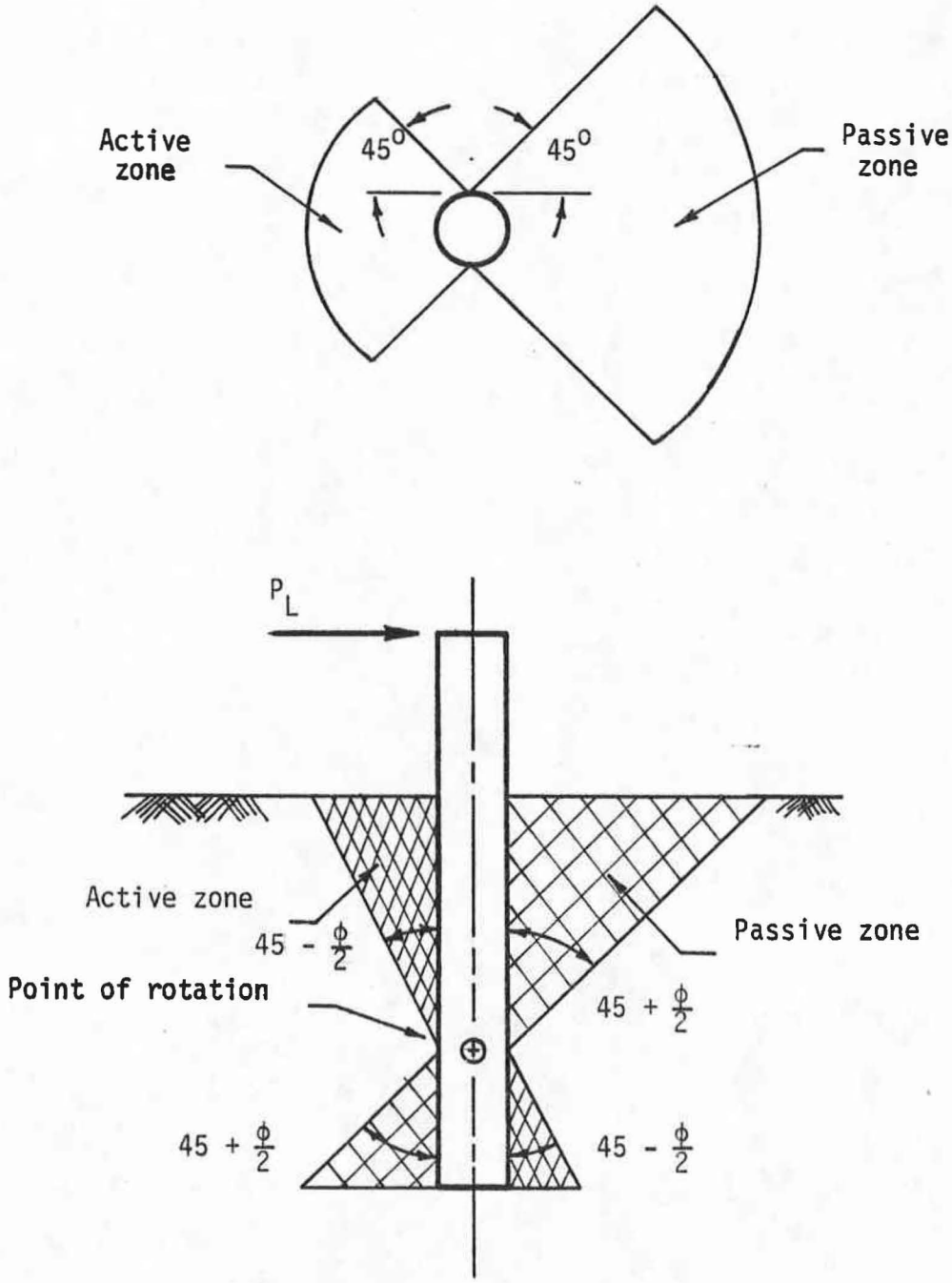

FIG. 15.-Failure Zone for Laterally Loaded Circular Shaft

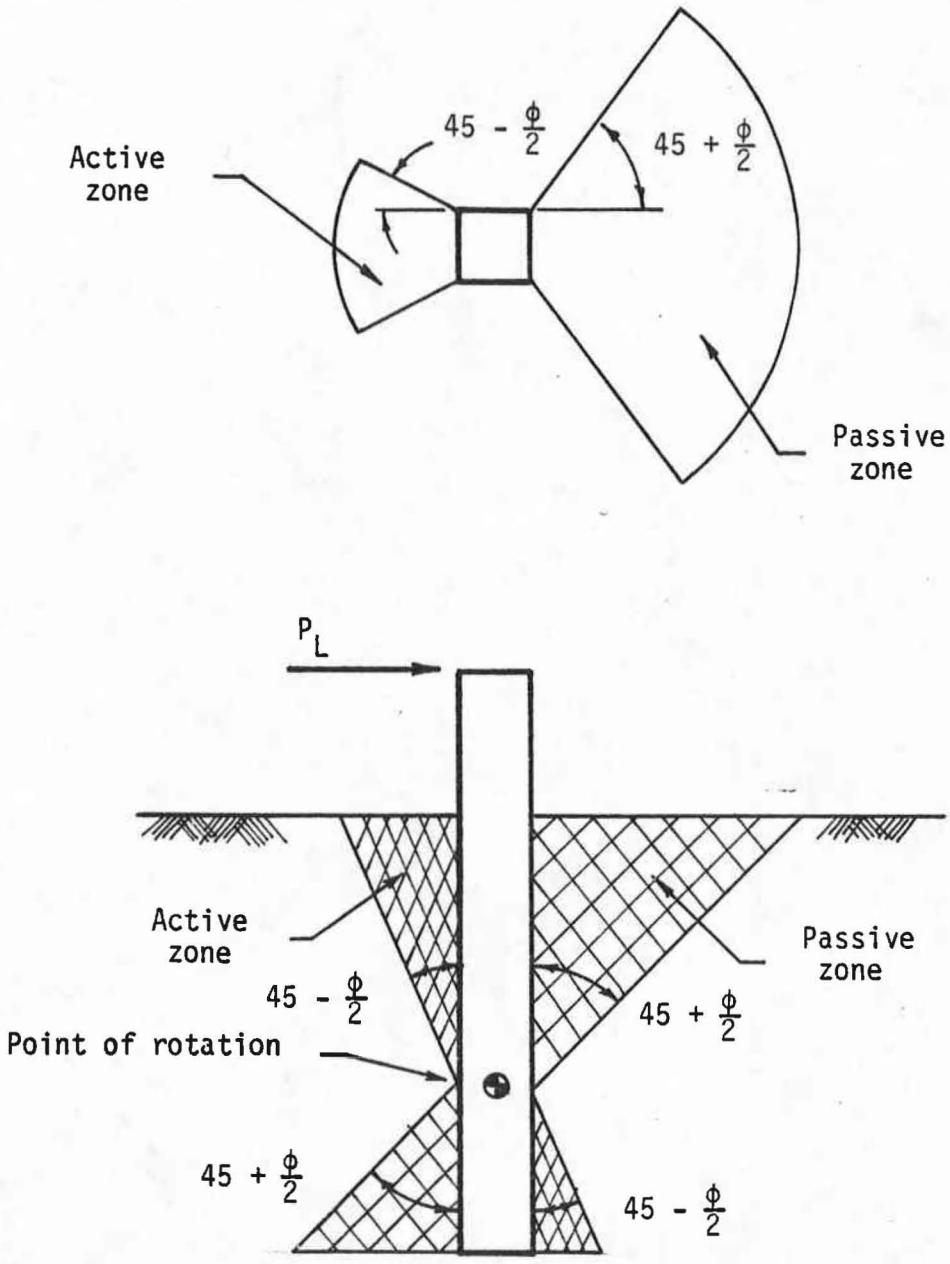

FIG. 16.-Failure Zone for Laterally Loaded Rectangular Shaft

Step 1: Assume a depth to the center of rotation, R, and an angle of rotation.

Step 2: Compute the moment about the point of application of the lateral load.

Step 3: If the moment calculated in Step 2 is non-zero, assume a new depth to the center of rotation and repeat Step 2.

Step 4: Once the moment calculated in Step 2 is within some tolerance, calculate the lateral load using the lateral force equilibrium equation.

However, if the shaft is not rigid, the iterative scheme is significantly more involved. The displacements of each segment of the shaft are not interrelated by some angle of rotation. A relaxation approach is used to solve for the flexible shaft solution. The iterative scheme used to solve the moment and lateral force equilibrium equations for an elastic shaft is outlined as follows:

Step 1: Assume a value for the ground-line displacement of the shaft.

Step 2: Assume the shaft to be rigid and solve for the rigid iterative solution using the above procedure.

Step 3: Apply all the forces from the rigid solution as loads on the elastic shaft. Use the rigid angle of rotation for the ground-line slope of the

shaft.

Step 4: Calculate the deflections of every segment of the shaft.

Step 5: From the deflections calculated in Step 4, compute the resisting forces acting on the shaft.

Step 6: Check moment equilibrium at the point of application of the lateral load. If this moment is within some specified tolerance, go to Step 9.

Step 7: Use the forces used in Step 3 as loads or the shaft. Assume a new ground-line slope.

Step 8: Repeat steps 4 thru 7 until the resisting forces calculated are in moment equilibrium.

Step 9: Check to see if the computed deflected shape matches the assumed deflected shape. If the deflected shapes agree within some specified tolerance, go to Step 12.

Step 10: If the computed deflected shape does not agree with the assumed deflected shape, average the resisting forces calculated in Step 5 with the forces used in Step 3. These averaged forces will be the loads applied on the elastic shaft in Step 3 for the next iteration.

Step 11: Repeat Steps 4 thru 10 until the solution converges to the flexible configuration of the

shaft.

Step 12: The computed deflected shape and the corresponding resisting forces are used to calculate the lateral load and ground-line moment of the flexible shaft.

The iterative scheme outlined above is easily coded into a computer program. This computer program LATPIL was written to solve for the lateral load and the overturning moment for a particular ground-line displacement using the theory and the iterative scheme as outlined in this chapter. A listing of the program and the input guide for LATPIL are given in Appendix III.

Comparison of Computer Predictions With Published Field Observatons

In this section, the theoretical model previously described is used to predict the load-deflection curves for a number of published field load tests.

Texas A&M University Tests

The Texas State Department of Highways and Public Transportation conducted lateral load tests on 3 drilled piers. The results of these tests are contained in the research reports by Coyle, et al (8, 20, 24). All three piers were constructed in similar subsurface conditons consisting of slightly overconsolidated clay. The details of the piers used in these tests are presented in

Table 12. The soil properties at the site, utilized for the predictions in this report, are presented in Tables 13 and 14.

The load test results and the predictions from the analytical model for the three piers are presented in Figs. 17 to 19. For each of the load tests, four predictions were made using the program LATPIL, varying the type of earth pressures used in the analysis. For all these tests, the test results and the analytical predictions compare favorably.

Southern California Edison Tests

Southern California Edison Company (SCE) conducted lateral load tests on 12 drilled piers. The results of these tests are contained in a paper by Bhushan, Haley, and Fong (7). All piers were constructed in similar subsurface conditions consisting of hard, heavily overconsolidated clay. The details of the piers are given in Table 15, and the soil conditions for each test are presented in Table 16.

The load test results and the predictions generated using the program LATPIL are presented in Figs. 20 to 22. The predictions for pier no. 2 and pier no. 4 compare favorably with the load test results. The prediction for pier no. 7 under-predicts the load test results. Reasons

Table 12. Pier Details

Pier No.	Pier Diameter (ft)	Embedment Length (ft)	Height of Load (ft)
1	3	20	2.6
2	3	15	2.6
3	2.5	15	2.6

Table 13. Soil Properties for Coyle's Test Shaft No. 1

Depth (ft)	ϕ deg.	δ deg.	c_u (ksf)	Unit Weight (pcf)	$\frac{X_p}{R}$	$\frac{X_a}{R}$	K_o	α
0 - 4	--	22	2.4	126	0.02	0.01	1.1	1.0
4 - 8	--	22	2.4	131	0.02	0.01	1.1	1.0
8 - 12	--	22	2.4	128	0.02	0.01	1.1	1.0
12 - 16	--	22	2.4	121	0.02	0.01	1.1	1.0
16 - 20	--	22	2.4	120	0.02	0.01	1.1	1.0

Table 14. Soil Properties for Coyle's Test Shafts No. 2 and No. 3

Depth (ft)	ϕ deg.	δ deg.	c_u (ksf)	Unit Weight (pcf)	$\frac{X_p}{R}$	$\frac{X_a}{R}$	K_o	α
0 - 3	--	22	2.2	127	0.02	0.01	1.1	1.0
3 - 6	--	22	2.2	127	0.02	0.01	1.1	1.0
6 - 9	--	22	2.4	124	0.02	0.01	1.1	1.0
9 - 12	--	22	2.8	128	0.02	0.01	1.1	1.0
9 - 15	--	22	3.2	125	0.02	0.01	1.1	1.0

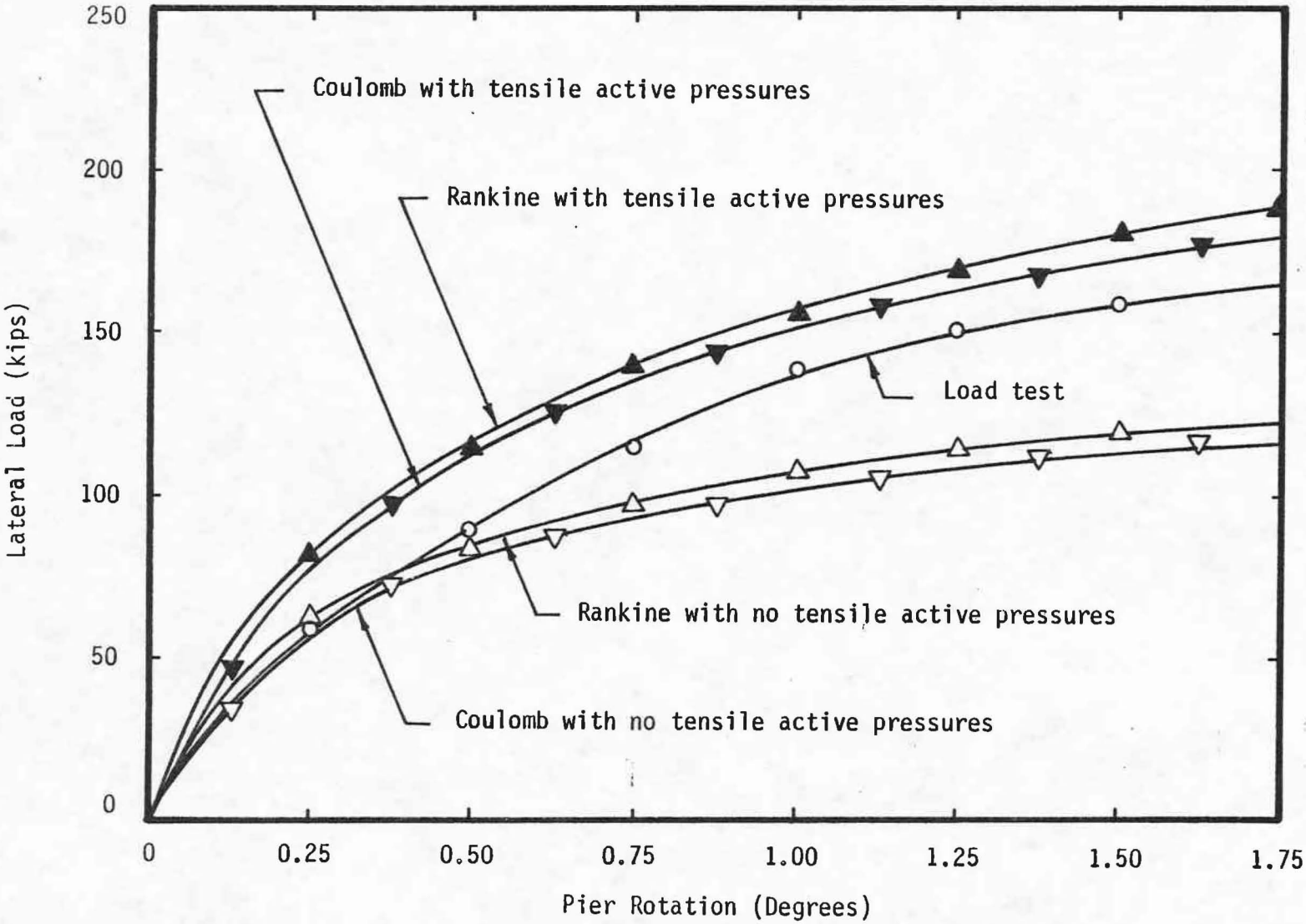

FIG. 17.-Lateral Load Vs. Pier Rotation for Coyle's Test Shaft No. 1 (1977)

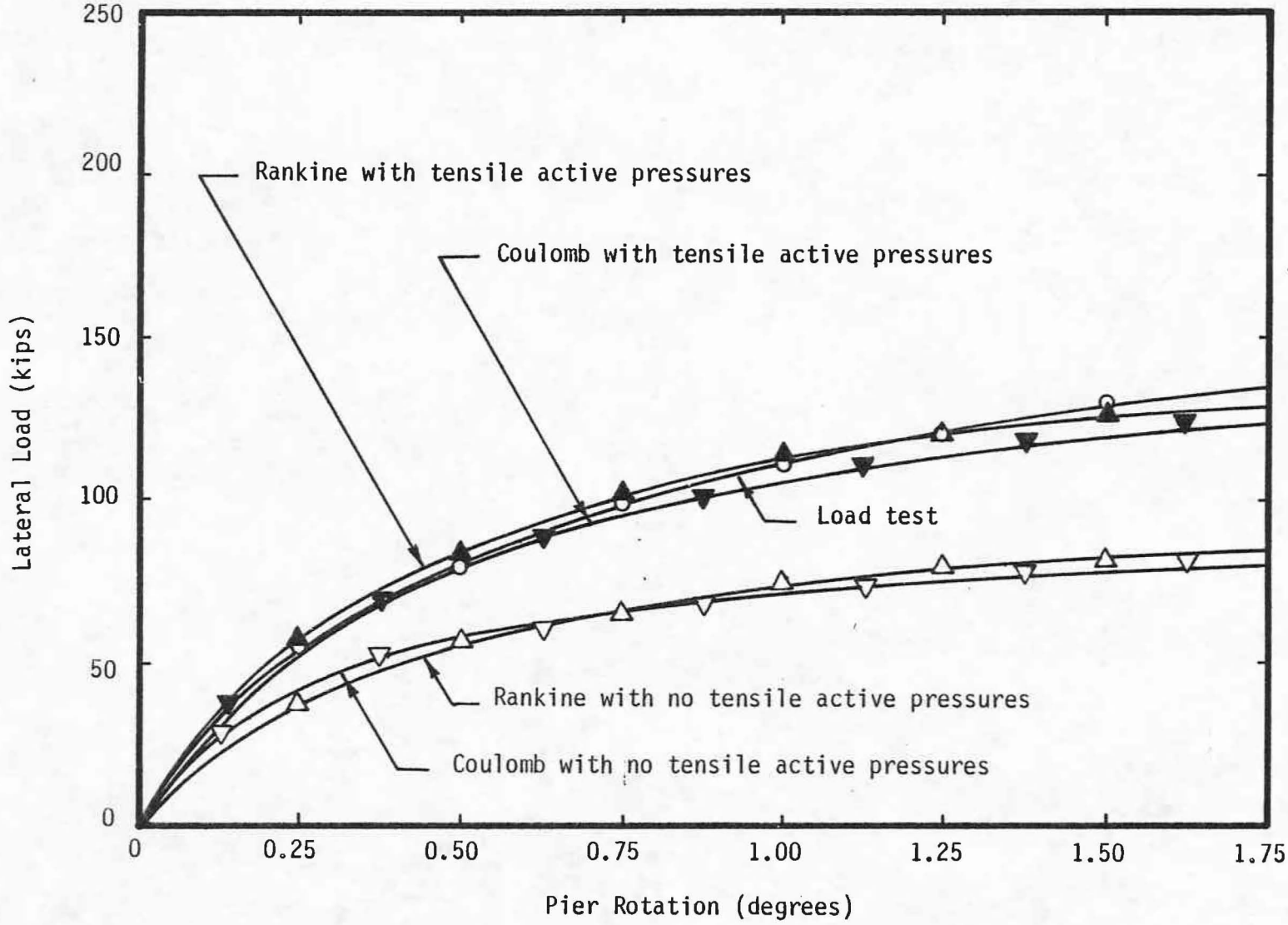

FIG. 18.-Lateral Load Vs. Pier Rotation for Coyle's Test Shaft No. 2 (1978)

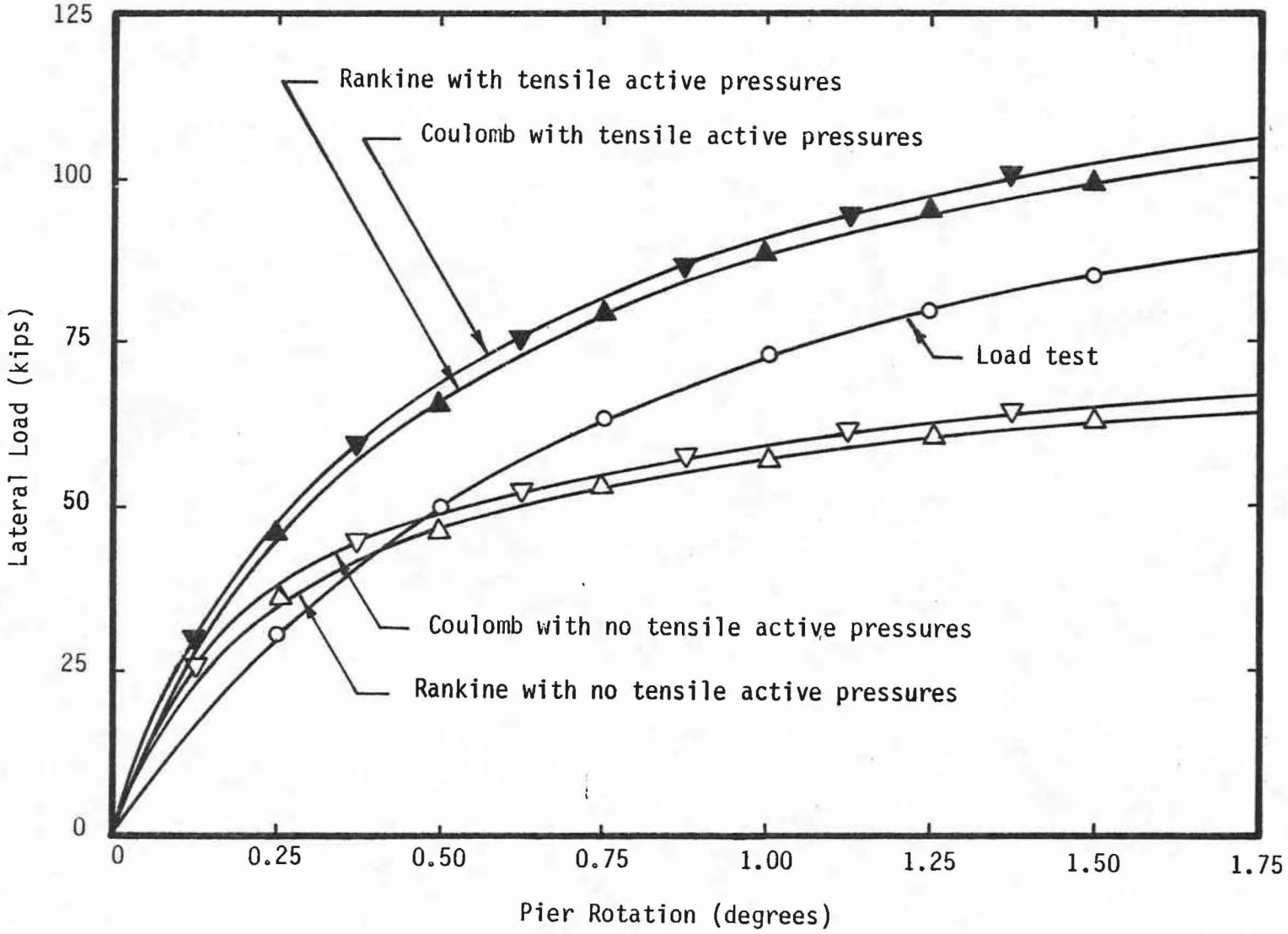

FIG. 19.-Lateral Load Vs. Pier Rotation for Coyle's Test Shaft No. 3 (1979)

Table 15. Pier Details

Pier No.	Pier Diameter (ft)	Embedment Length (ft)	Flexural Stiffness (k-in.)
2	4.0	15.0	8.19x10
4	4.0	12.5	8.19x10
7	2.0	9.0	5.08x10

Table 16. Soil Properties for SCE Tests.

Pier Test	Soil Type	Depth (ft)	Unit Weight (pcf)	C_u (psf)
2	Sandy Clay	0.9	130	5,500
4	Sandy Clay	0.16	130	4,750
7	Sandy Clay	0.16	130	4,750

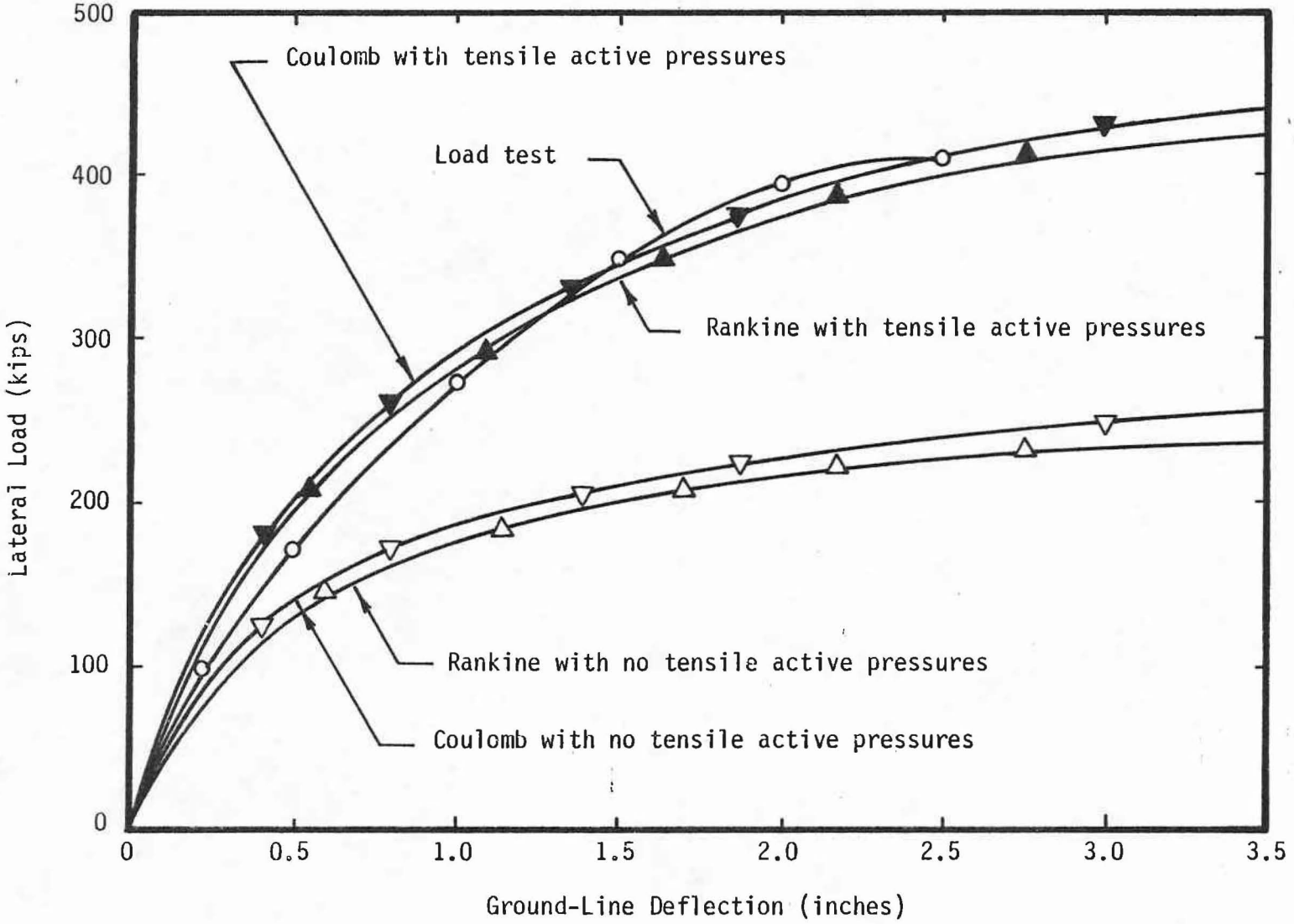

FIG. 20.-Lateral Load Vs. Ground-Line Deflection for Bushan Shaft No. 2

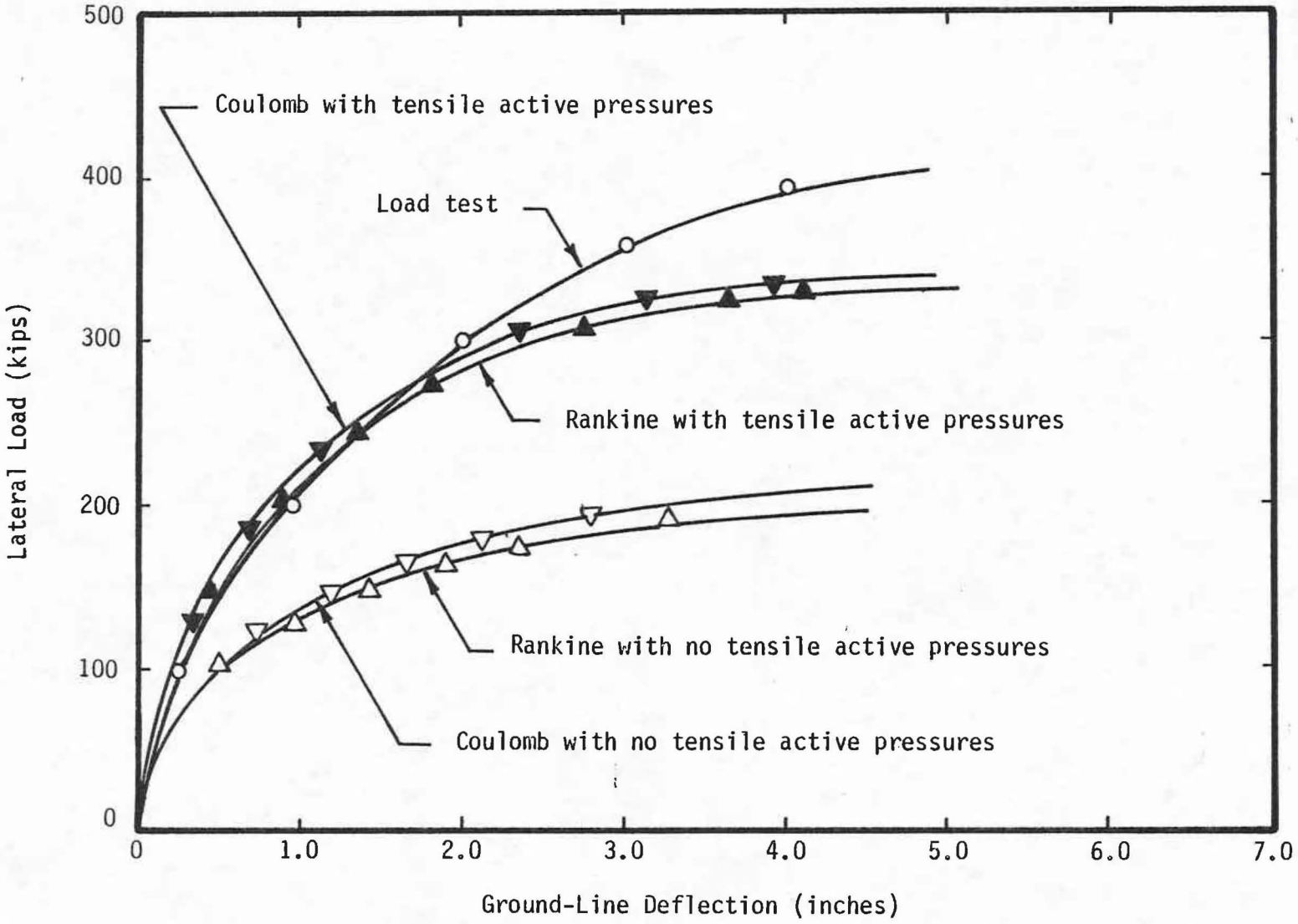

FIG. 21.-Lateral Load Vs. Ground-Line Deflection for Bushan Shaft No. 4

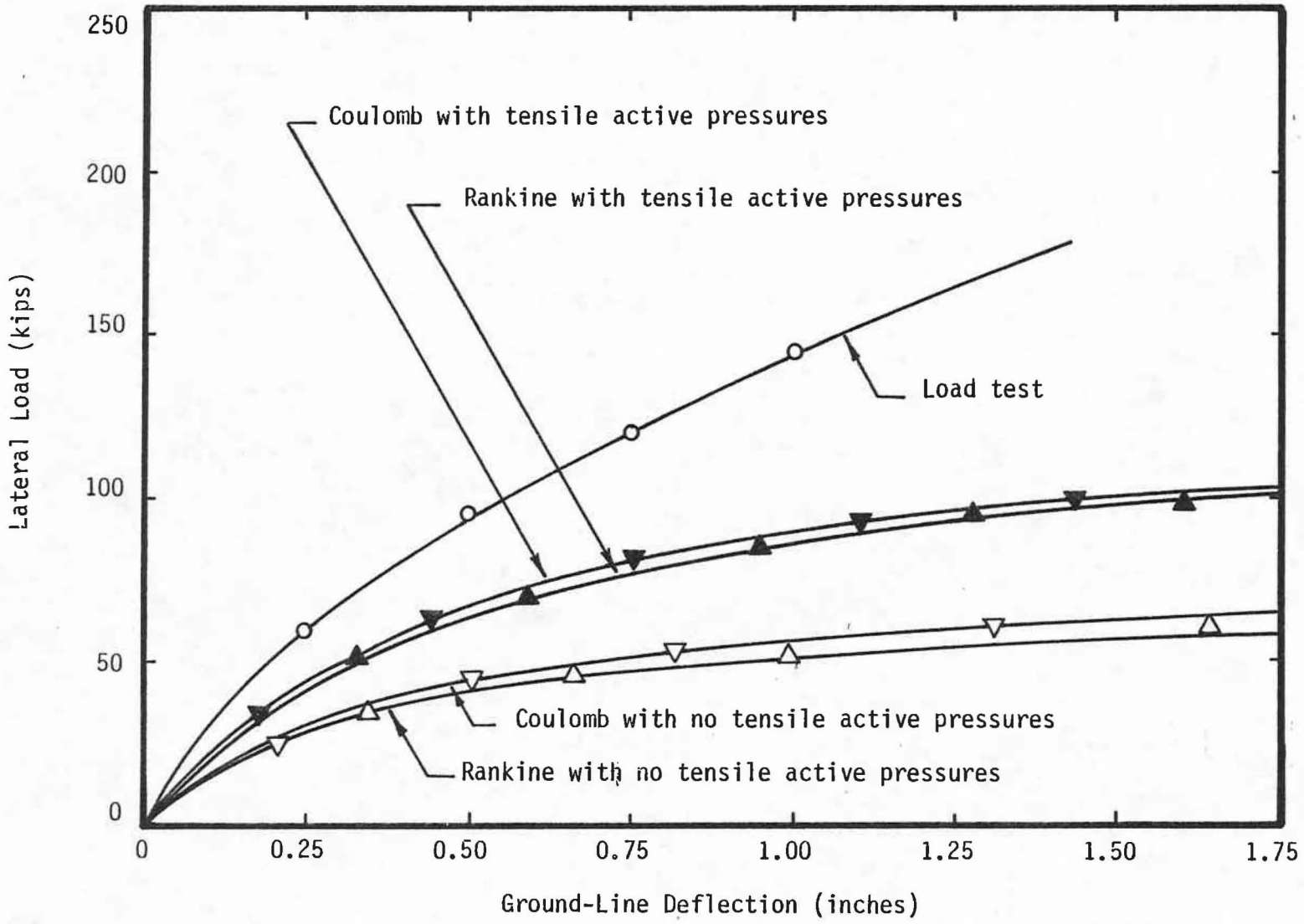

FIG. 22.-Lateral Load Vs. Ground-Line Deflection for Bushan Shaft No. 7

for this conservtive prediction are most likely due to errors in the measurement of the soil properties.

Electric Power Research Institute Tests

The Electric Power Research Institute (10) conducted lateral load tests on 14 drilled piers. The piers tested were designed as foundations for large electric transmission poles. The height of the applied lateral load above the ground surface used in the tests was 81 feet. The test results and the analytical predictions are pesented for the piers listed in Table 17.

The soil conditions at the test sites were thoroughly investigated, and many laboratory tests were performed on soil samples. The soil properties for each test site, obtained from the subsurface investigation and the laboratory testing, are presented in Tables 18 to 23.

The load test results and the predictions using the program LATPIL are shown in Figs. 23 to 28. The predicted load settlement curves for pier no. 1 compare favorably to the load test results. Test pier no. 1 is the only pier embedded in clay. For the other five piers, the predictions using Rankine earth pressures ($\delta = 0$, $\psi = 90$) significantly underpredict the results from the load tests. The predictions using Coulomb earth pressures, with values of δ selected from Table 10, overpredict the results from the load tests. Thus, the

Table 17
Pier Detail for ERRI Tests

Test No.	Pier Diameter (ft)	Embedment Length (ft)	Flexural Stiffness (k-in)
1	4.5	14.0	1.5x10
3	5.0	21.0	2.24x10
5	5.0	15.9	2.29x10
8	5.3	16.2	2.34x10
10	4.82	16.0	1.72x10
11	5.0	20.3	2.60x10

Table 18. Soil Properties for EPRI Test No. 1.

Depth (ft)	ϕ deg.	δ deg.	c_u (ksf)	Unit Weight (pcf)	$\frac{X_p}{R}$	$\frac{X_a}{R}$	K_o	α
0 - 5	0	20	1.9	132	0.02	0.01	0.6	1.0
5 - 6.5	0	20	0.7	132	0.02	0.01	0.6	1.0
6.5 - 8.5	35	25	0	126	0.005	0.0005	0.426	1.0
8.5 - 11.5	35	25	0	123	0.005	0.0005	0.426	1.0
11.5 - 14	35	25	0	123	0.005	0.0005	0.426	1.0

Table 19. Soil Properties for EPRI Test No. 3.

Depth (ft)	ϕ deg.	δ deg.	c_u (ksf)	Unit Weight (pcf)	$\frac{X_p}{R}$	$\frac{X_a}{R}$	K_o	α
0 - 2	28	25	0	110	0.01	0.002	0.531	1.0
2 - 9.5	29	25	0	110	0.01	0.002	0.515	1.0
9.5 - 11	30	25	0	110	0.005	0.0005	0.5	1.0
11 - 18	30	25	0	125	0.005	0.0005	0.5	1.0
18 - 21	28	25	0	125	0.01	0.002	0.531	1.0

Table 20. Soil Properties for EPRI Test No. 5.

Depth (ft)	ϕ deg.	δ deg.	c_u (ksf)	Unit Weight (pcf)	$\frac{X_p}{R}$	$\frac{X_a}{R}$	K_o	α
0 - 1.5	45	30	0	140	0.005	0.0005	0.293	1.0
1.5 - 5	0	18	0.7	135	0.01	0.01	0.6	1.0
5 - 10.5	46	25	0	132	0.005	0.0005	0.281	1.0
10.5 - 12	42	25	0	132	0.005	0.0005	0.331	1.0
112 - 15.8	37	25	0	132	0.005	0.0005	0.371	1.0

Table 21. Soil Properties for EPRI Test No. 8.

Depth (ft)	ϕ deg.	δ deg.	c_u (ksf)	Unit Weight (pcf)	$\frac{X_p}{R}$	$\frac{X_a}{R}$	K_o	α
0 - 4.5	32	25	0	110	0.01	0.002	0.470	1.0
4.5 - 6	38	30	0	110	0.005	0.0005	0.384	1.0
6 - 12	36	30	0	110	0.005	0.0005	0.410	1.0
12 - 13.5	45	30	0	110	0.005	0.0005	0.293	1.0
13.5 - 16.2	36	30	0	110	0.005	0.0005	0.410	1.0

Table 22. Soil Properties for EPRI Test No. 10.

Depth (ft)	ϕ deg.	δ deg.	c_u (ksf)	Unit Weight (pcf)	$\frac{X_p}{R}$	$\frac{X_a}{R}$	K_o	α
0 - 3.5	30	25	0	120	0.01	0.02	0.5	1.0
3.5 - 7	32.5	25	0	120	0.005	0.0005	0.462	1.0
7 - 10	43	25	0	130	0.005	0.0005	0.318	1.0
10 - 15	38	25	0	130	0.005	0.0005	0.384	1.0
15 - 16	45	25	0	130	0.005	0.0005	0.293	1.0

Table 23. Soil Properties for EPRI Test No. 11

Depth (ft)	ϕ deg.	δ deg.	c_u (ksf)	Unit Weight (pcf)	$\frac{X_p}{R}$	$\frac{X_a}{R}$	K_o	α
0 - 6	35.5	25	0	110	0.005	0.0005	0.419	1.0
6 - 10	30	25	0	110	0.005	0.0005	0.5	1.0
10 - 12	0	18	1.7	125	0.005	0.0005	0.6	1.0
12 - 15	38	25	0	125	0.005	0.0005	0.384	1.0
15 - 20.3	35	25	0	125	0.005	0.0005	0.426	1.0

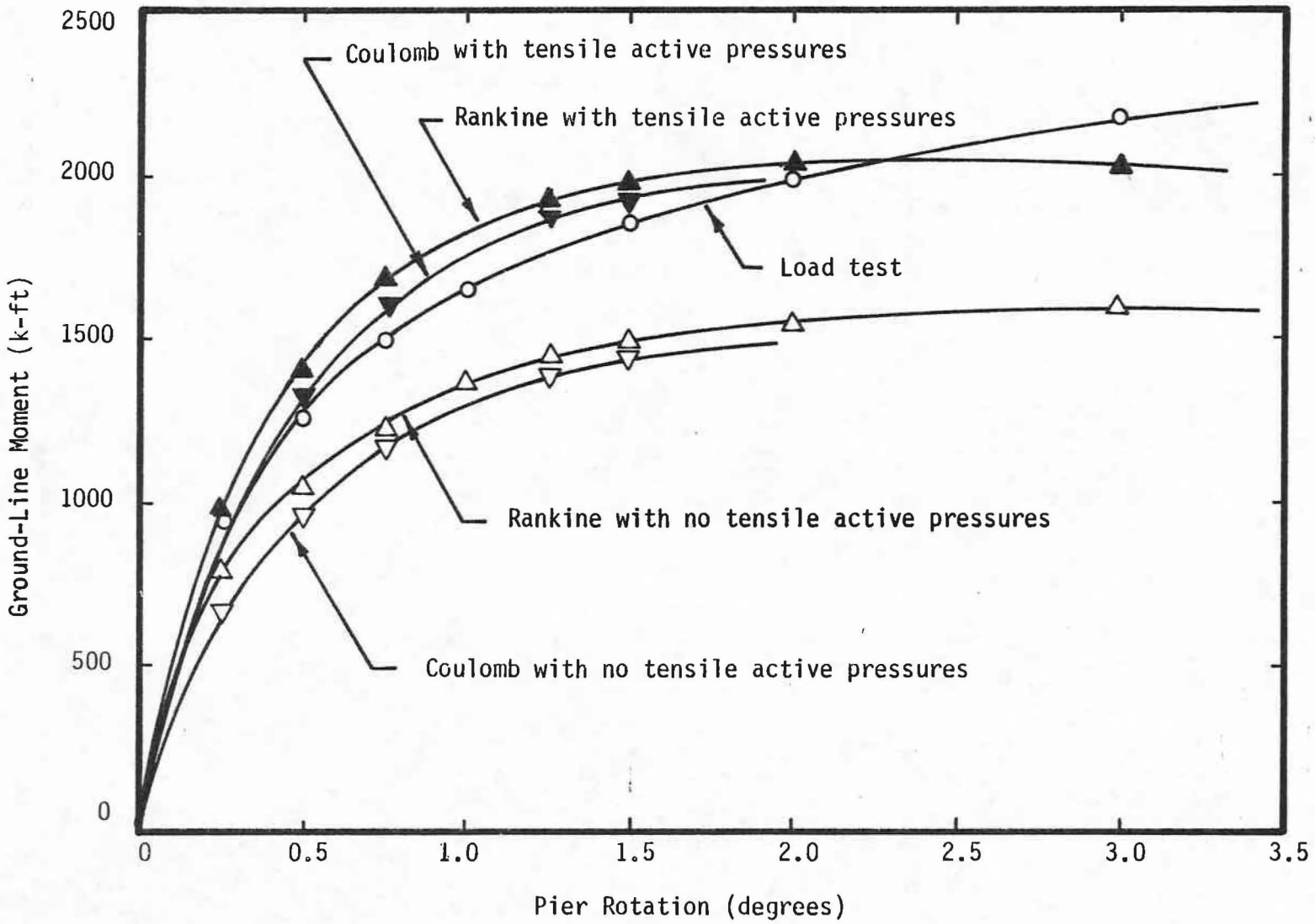

FIG. 23.-Ground-Line Moment Vs. Pier Rotation for EPRI Test Pier No. 1

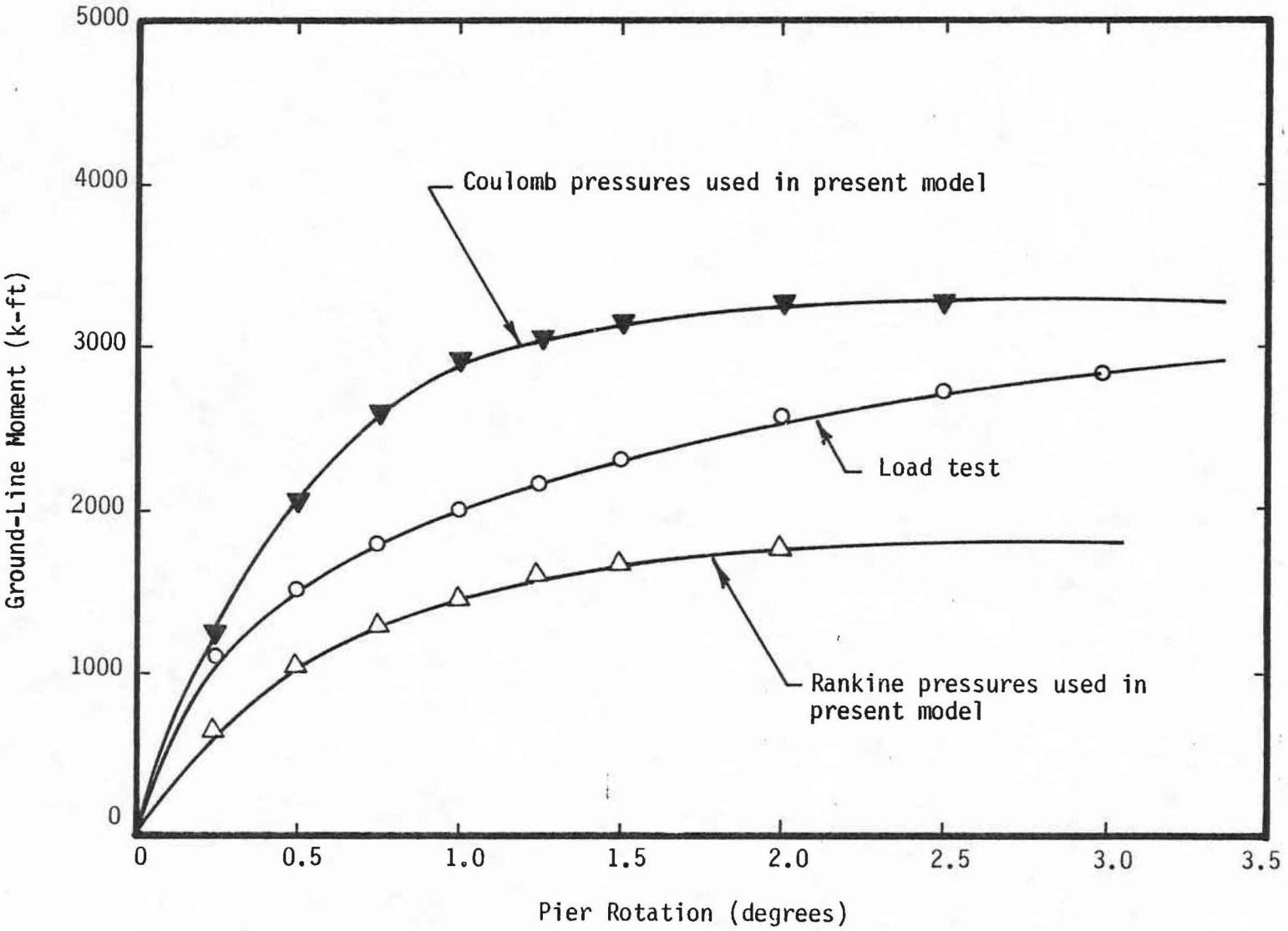

FIG. 24.-Ground-Line Moment Vs. Pier Rotation for EPRI Test Pier No. 3

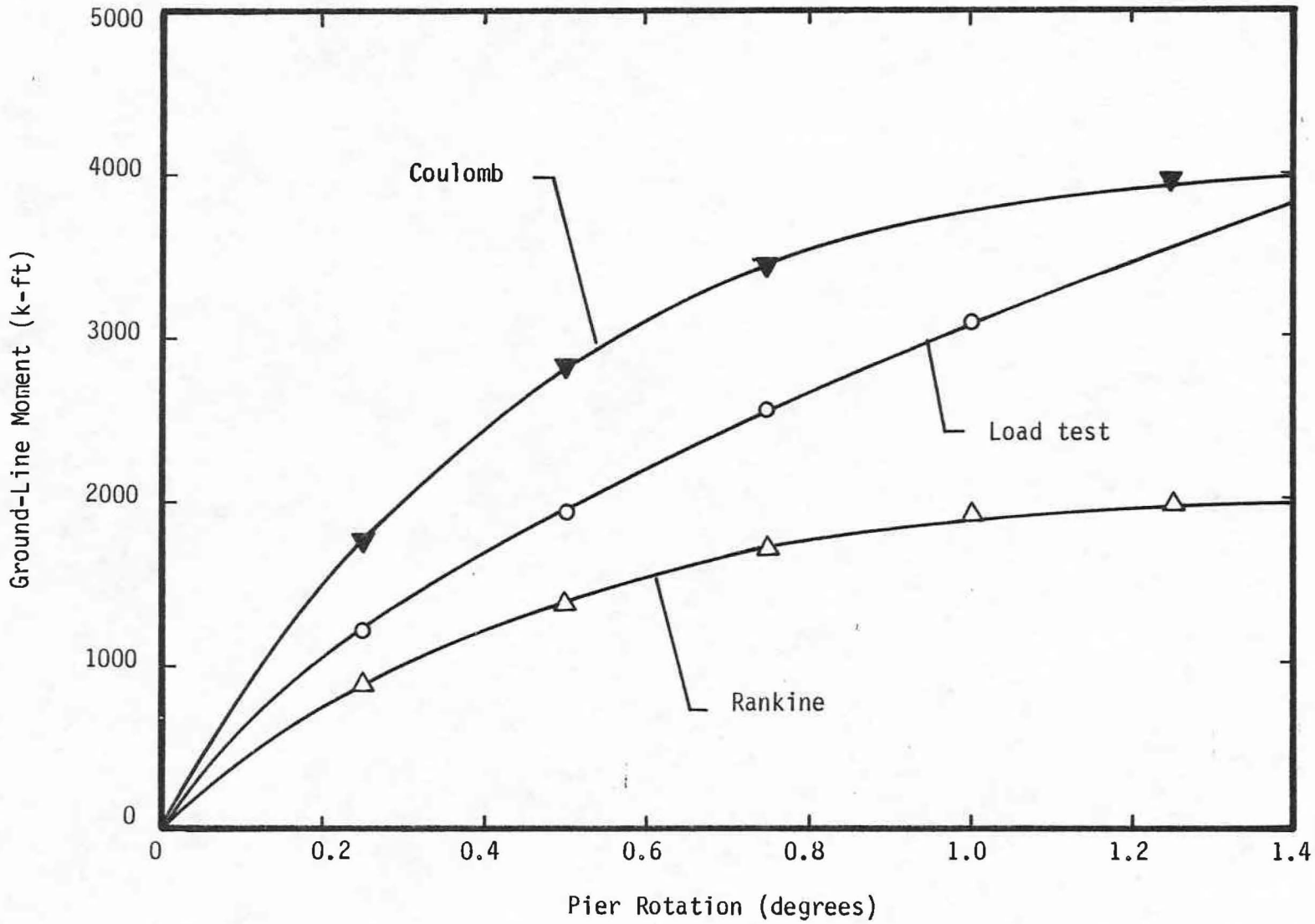

FIG. 25.-Ground-Line Moment Vs. Pier Rotation for EPRI Test Pier No. 5

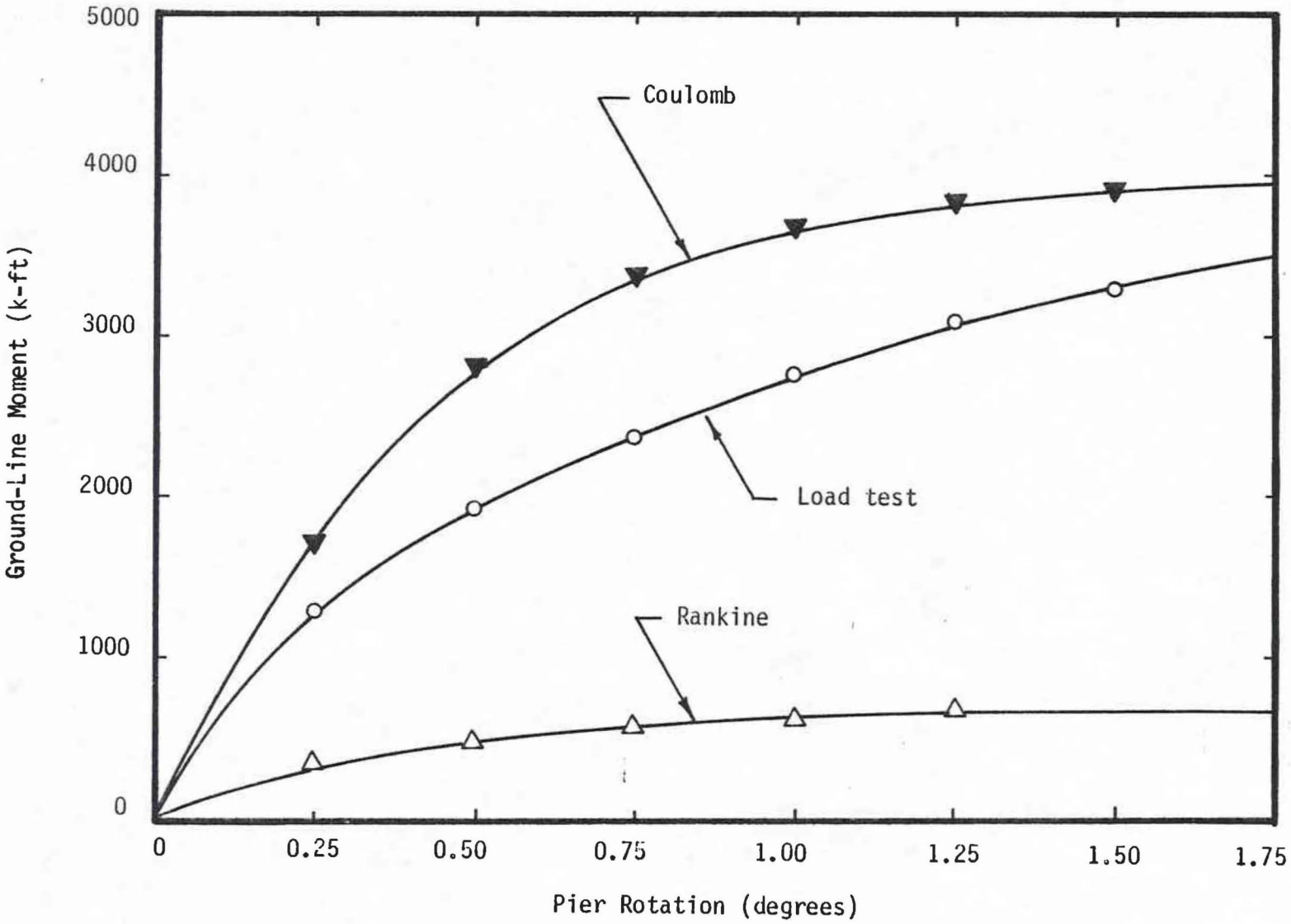

FIG. 26.-Ground-Line Moment Vs. Pier Rotation for EPRI Test Pier No. 8

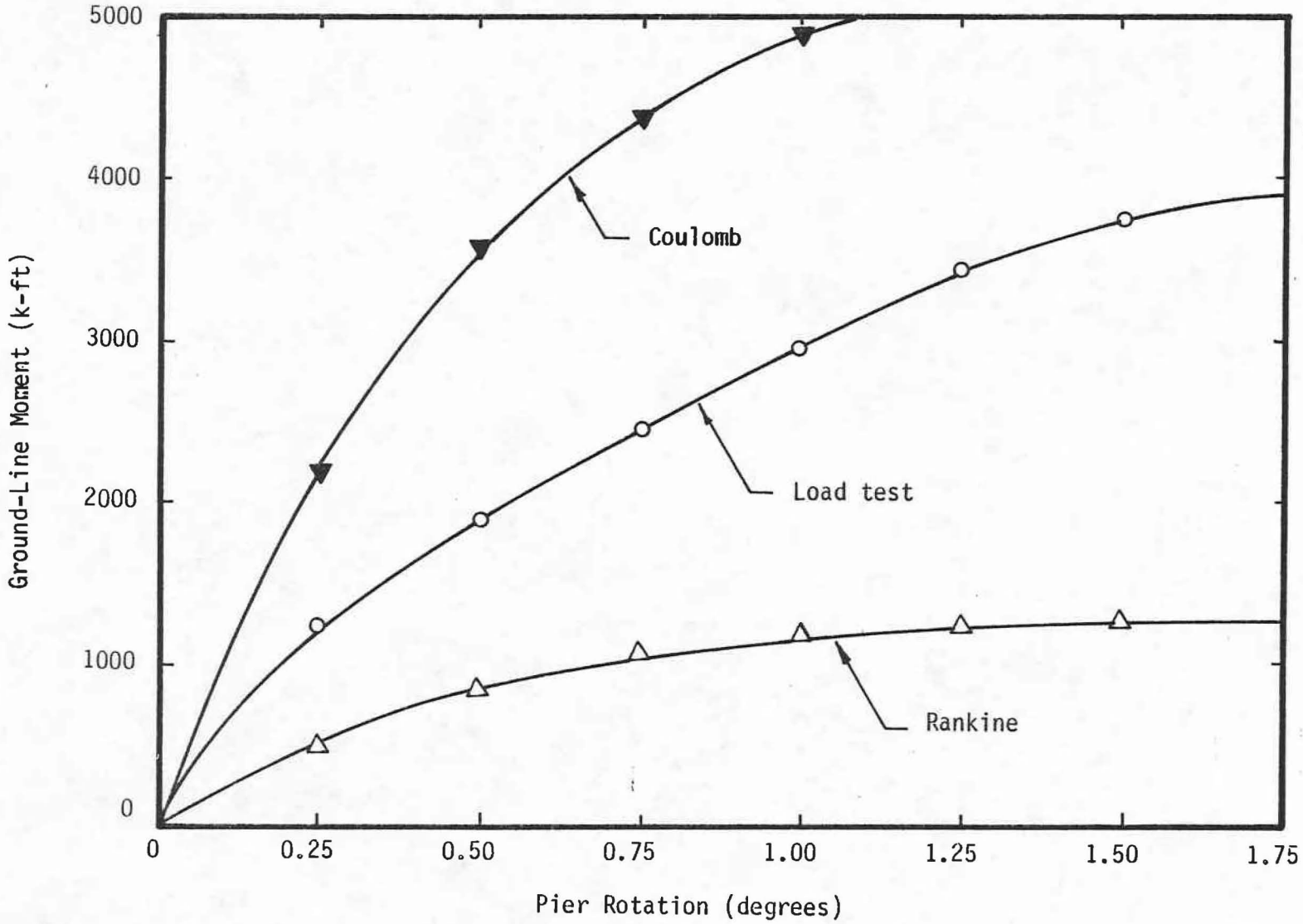

FIG. 27.-Ground-Line Moment Vs. Pier Rotation for EPRI Test Pier No. 10

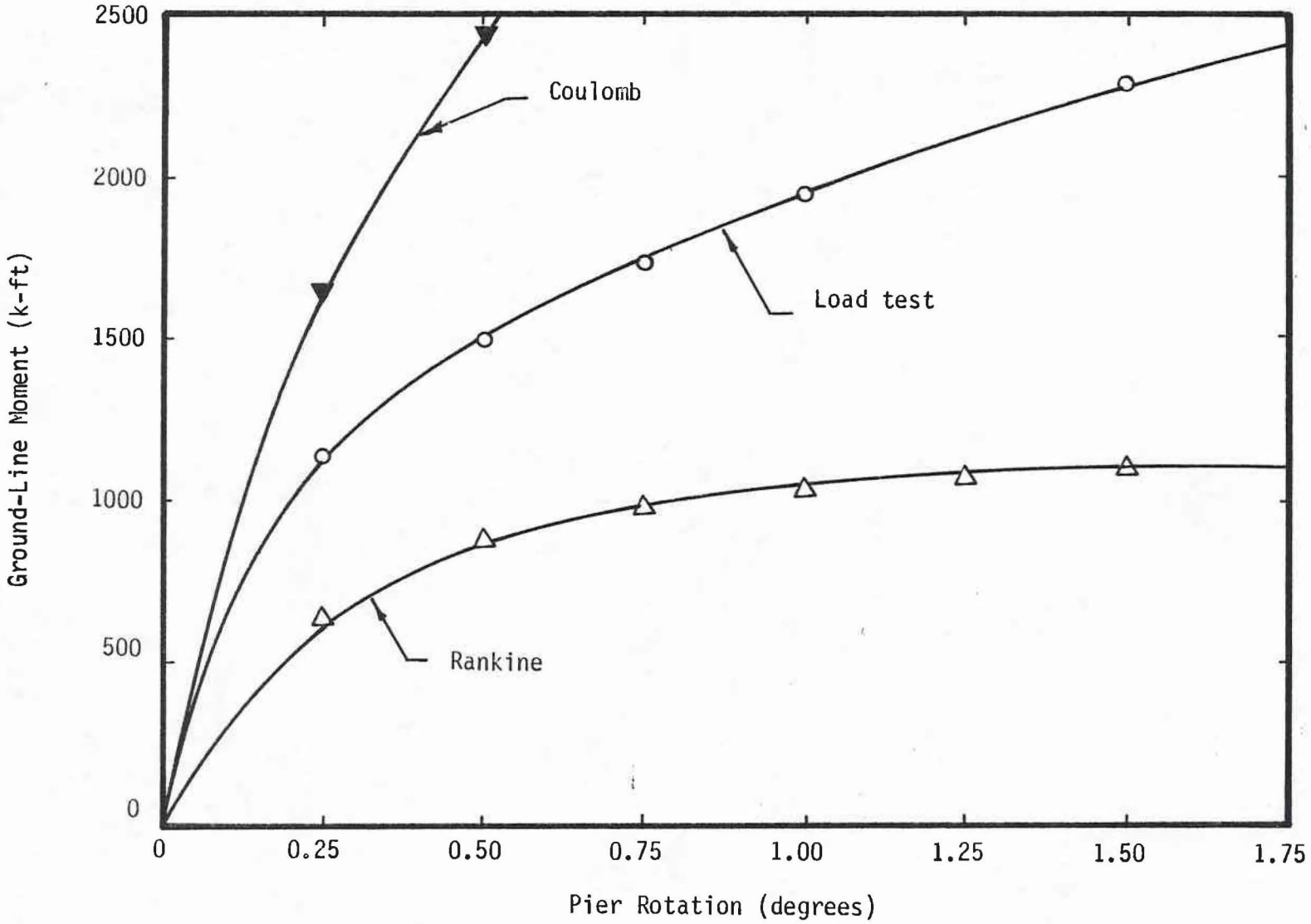

FIG. 28.-Ground-Line Moment Vs. Pier Rotation for EPRI Test Pier No. 11

actual angle of wall friction, which would cause the predicted load-deflection curve to match the field load test results, must be less than that obtained from Table 10. From these, it appears that for piers embedded in cohesionless soils the angle of friction between the pier and the soil has a significant effect on the predicted load-deflection curve.

STATIC LOAD TESTS

Introduction

One of the objectives of this research study is to perform a series of static load tests on guardrail posts. The results from these tests will aid in determining if the steel guardrail post performs satisfactorily without a concrete footing. The specifications currently require the steel (W6x8.5) post to be placed in concrete. However, if the steel post placed without a concrete footing can perform, under lateral loading, similar to the standard timber post, then the requirement of a concrete footing may be unnecessary.

To assess the effects of varying soil conditions, it was decided to perform a series of tests in two soils with different properties. A suitable test site was located at the Texas A&M University Research and Extension Center.

Testing Program

The static guardrail post tests which were conducted are summarized in Table 24. Three tests were performed in each soil type, one using a standard timber post and two using steel posts. The two tests on the steel posts were performed with different embedment depths in order to bracket the response of the timber post.

Table 24. Summary of Tests

Test No.	Post Type	Embedment Depth (in.)	Height of load (in.)	Soil Type
1	Wood	38	21	Cohesive
2	Steel	38	21	Cohesive
3	Steel	44	21	Cohesive
4	Wood	38	21	Cohesionless
5	Steel	38	21	Cohesionless
6	Steel	44	21	Cohesionless

Placement of Posts

In order to assess the effects of varying soil conditions, the tests were performed in two soils with significantly different properties. A stiff cohesive soil and a cohesionless gravel were used for this purpose. The soil at the test site is a stiff cohesive soil, thus only one soil pit had to be constructed of gravel material. The test set-up and the location of the posts are shown in Figs. 29, 30, and 31.

The posts were placed in the cohesive soil by augering and tamping the soil around the post. A 24 inch diameter auger was used, and the soil was tamped around the posts in several lifts. In a cohesionless soil however, augering is very difficult, due to the soil caving into the augered hole. Thus, after the excavation of the pit, the posts were held in place with struts, and the gravel was placed and compacted around the posts.

Soil Conditions

For the cohesive soil, soil conditions at the test site were determined using two soil borings. The boring locations, designated B-S1 and B-S2, are shown in Fig. 29. Undisturbed soil samples were taken with a 2.0 in. diameter thin-walled tube sampler. Laboratory tests on the undisturbed samples included Atterberg limits, moisture contents, unit weights, and triaxial compression

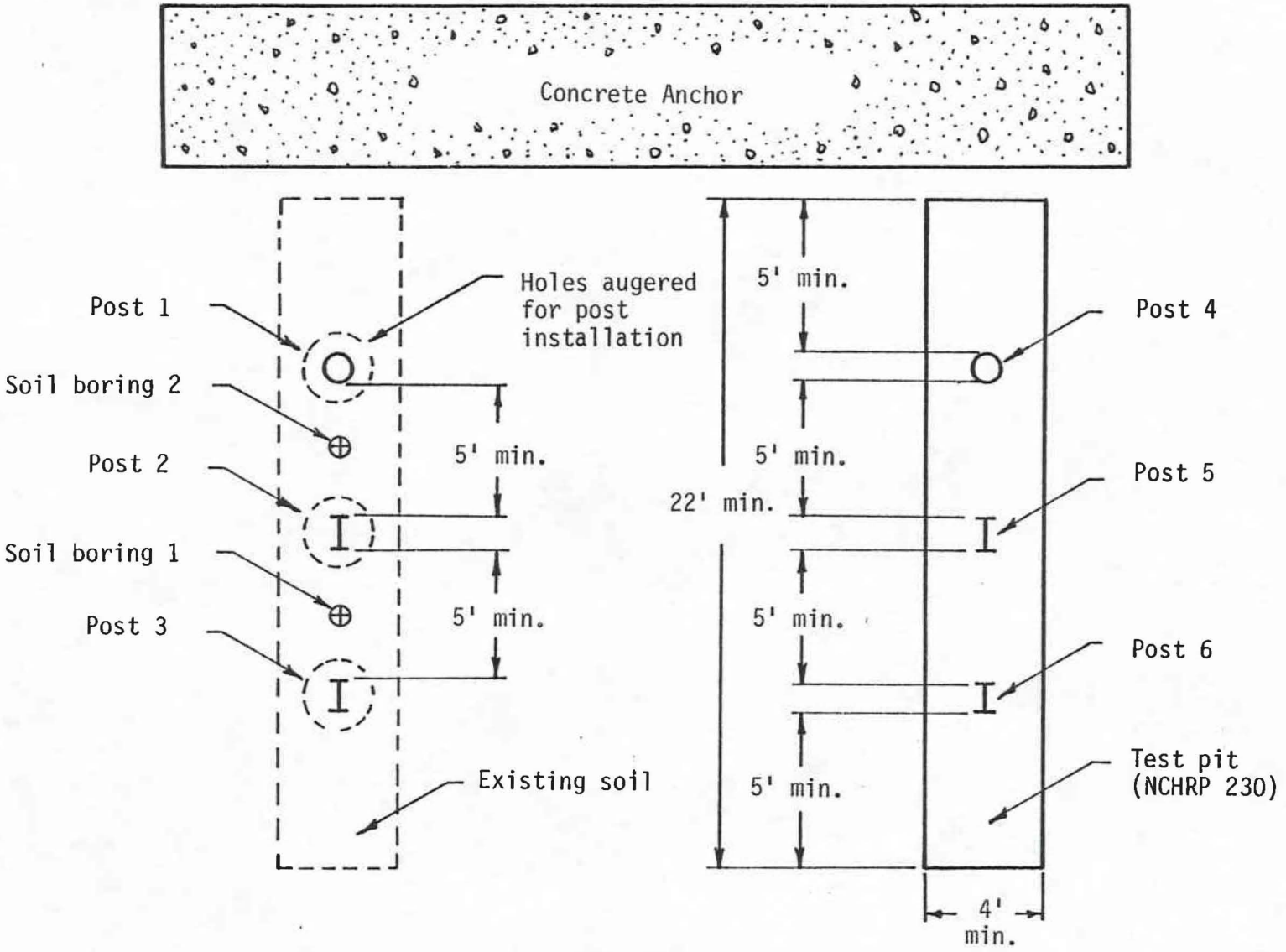

FIG. 29.-Location of Posts

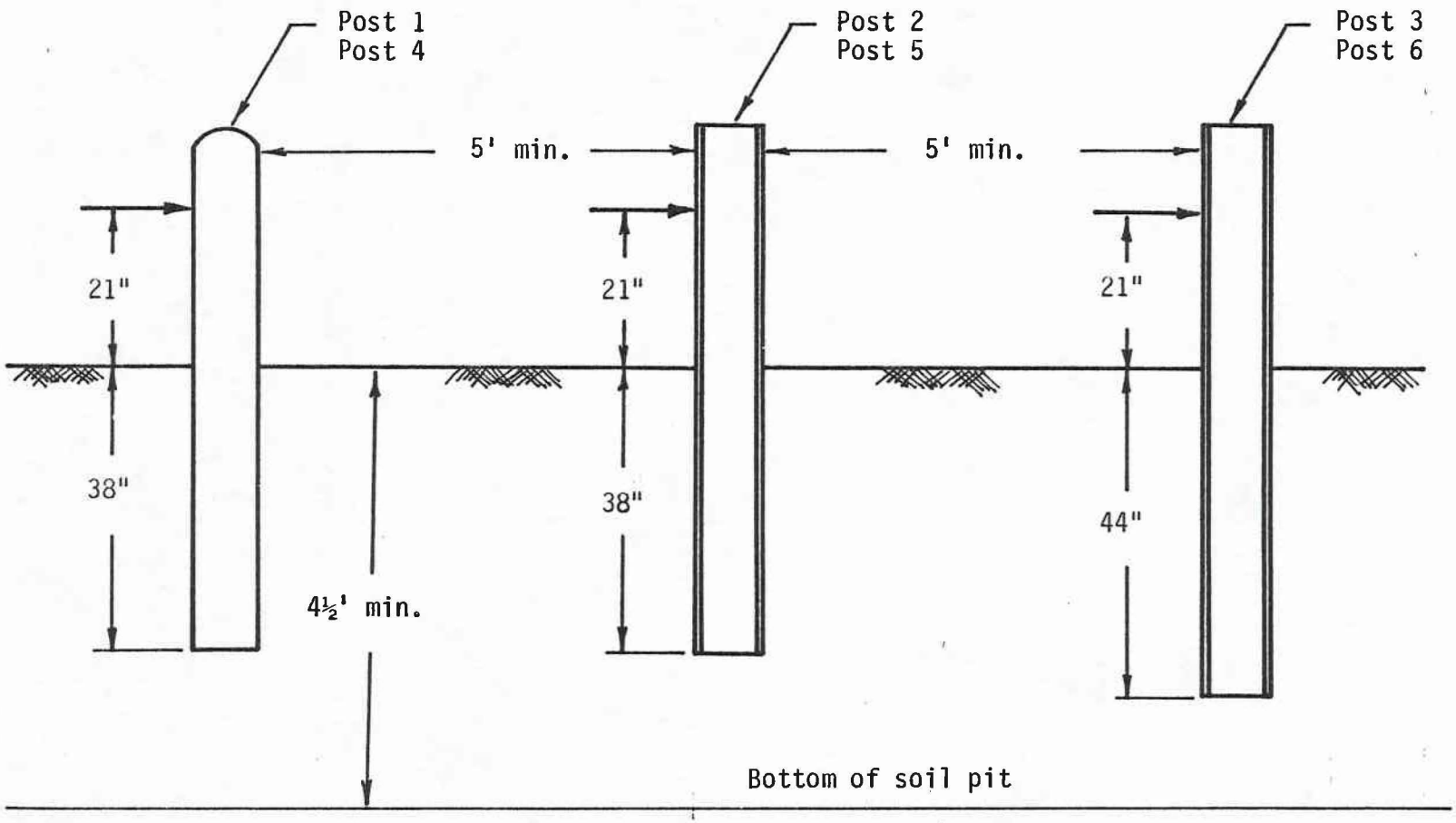

FIG. 30.-Placement of Posts

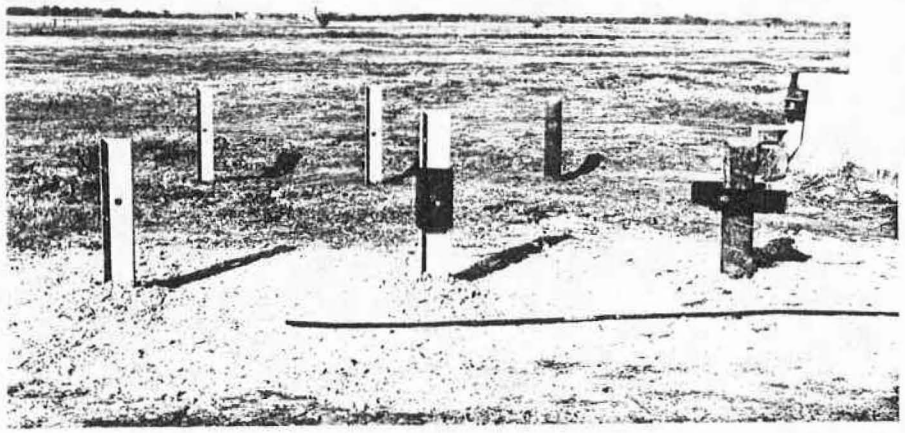

FIG. 31.-Test Site for Static Tests

tests to determine the undrained shear strength of the cohesive soil. The results of these tests are summarized in Table 25.

The test results indicate that the site consisted of stiff to very stiff clay. The shear strength of the soil increases near the surface due to a decrease in moisture content. This decrease in water content near the surface is a result of drying of the upper layer of soil.

The cohesionless soil used was crushed limestone gravel. The soil condition at the site were determined using a McGuin water pycnometer to obtain the in-site unit weight and by taking soil samples for laboratory testing. The pycnometer is shown in Fig. 32.

Laboratory testing of the samples included sieve analysis and water content determinations. The gradation curve obtained from the sieve analysis is shown in Fig. 33. The gravel was classified as a GW material by the Unified Soil Classification System. Since the maximum particle size of this material is too large to permit determination of the shear strength using a standard triaxial compression test, the angle of shearing resistance was found from correlations with the gradation curve, maximum particle size, relative density, and the overburden pressure. These correlations were developed by Leps (25) and are shown in Fig. 34. From these correlations a range of 48 to 52 degrees was chosen for

Table 25. Properties of Cohesive Soil.

Depth (ft)	Generalized Description	Unit Weight (pcf)	ϕ deg.	c_u (ksf)
0.5	Dark, grey stiff clay	126	0	3.0
1.0		125	0	2.5
1.5		123	0	1.5
2.0		123	0	1.6
3.0		125	0	1.9

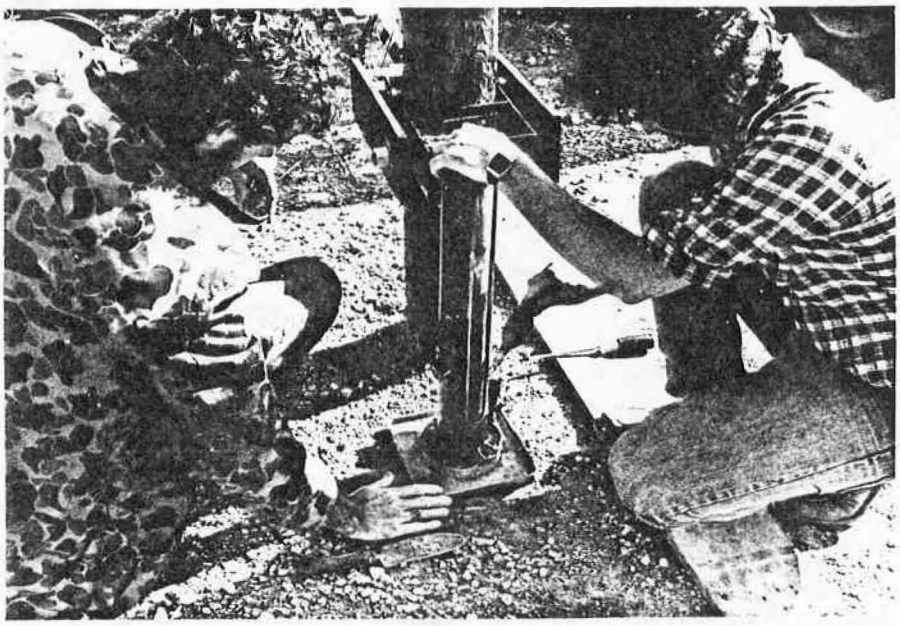

FIG. 32.-McGuin Water Pycnometer Used to Obtain In-situ Unit Weight

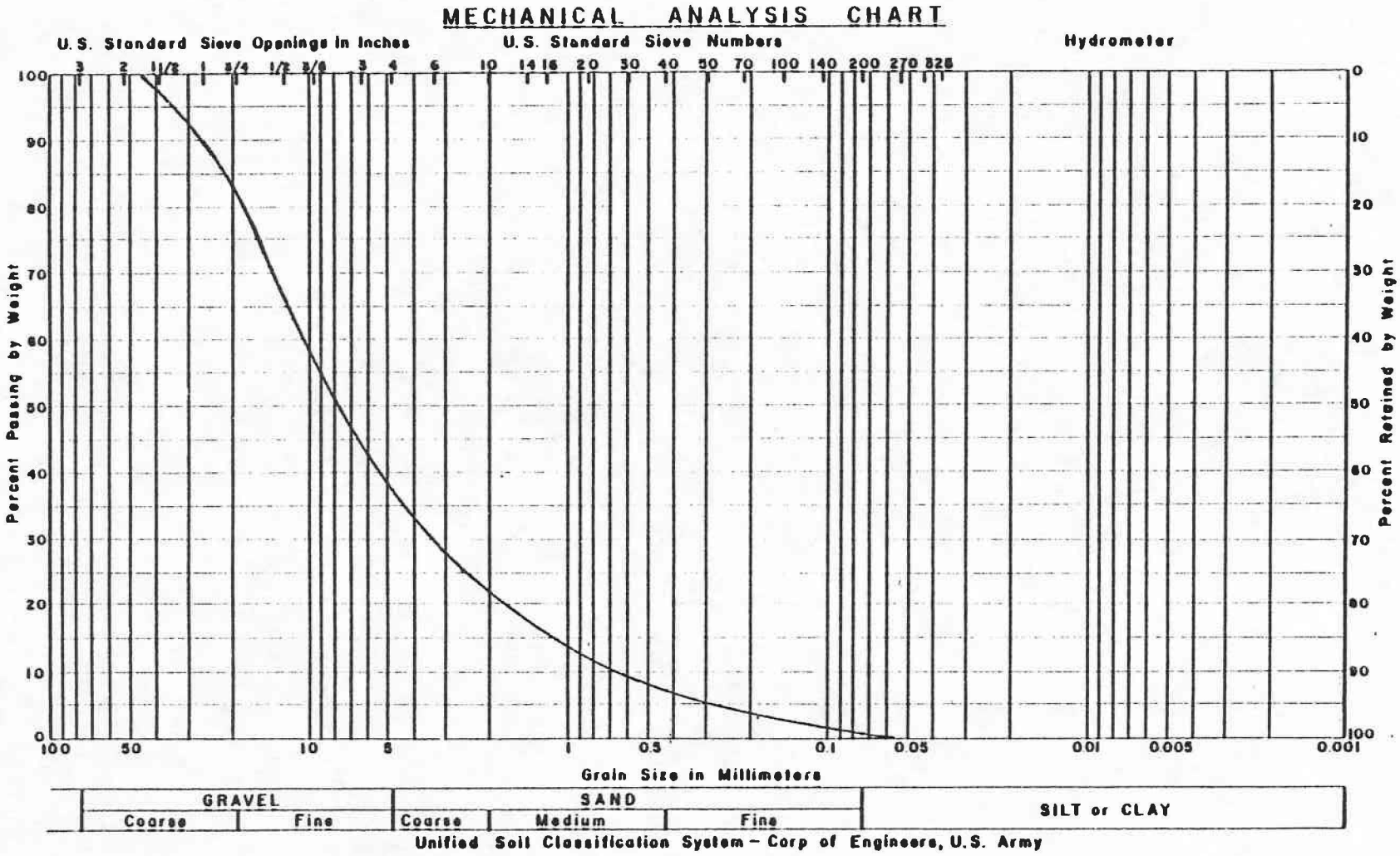

FIG. 33.-Gradation Curve for the Cohesionless Soil

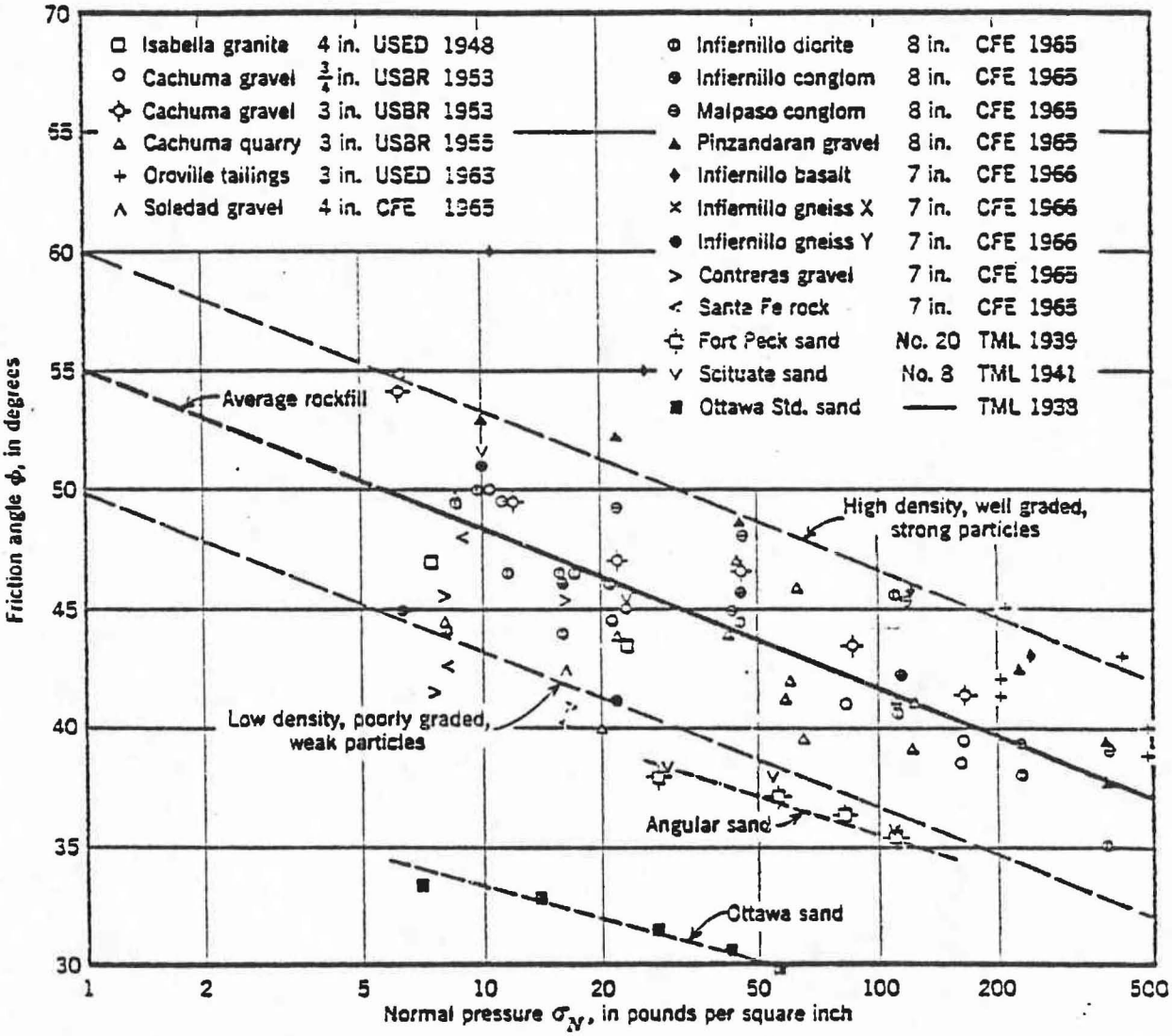

FIG. 34.-Shear Strength of Rockfill Materials from Large Triaxial Tests (after Leps (25))

the angle of internal friction. The properties of the cohesionless soil are summarized in Table 26.

Equipment and Instrumentation

In order to conduct these tests, it was necessary to develop a loading system capable of (1) applying a horizontal force on the post at a uniform displacement rate, (2) measuring the load acting on the post at known displacements, and (3) measuring the displacement of the post at the ground surface.

Loading System

A hydraulic loading device was used to apply the lateral force to the posts. The loading system is illustrated in Figs. 35 and 36. A hydraulic cylinder was attached to the concrete anchor and the post. The ram of the hydraulic cylinder was fully extended at the beginning of the test. A small hydraulic pump was used to retract the ram and to apply the load to the post.

Load Measurement

The load applied to the post was measured by means of a force transducer attached between the post and the hydraulic cylinder, as shown in Figs. 35 and 36. The transducer was calibrated up to a maximum load of 10,000 pounds. The force transducer was constructed of a metal

Table 26. Properties of Cohesionless Soil.

Depth (ft)	Generalized Description	Unit Weight (pcf)	ϕ deg.	c_u (ksf)
0.5	Well graded crushed limestone gravel.	115	48 - 52	0
1.0		115	48 - 52	0
1.5		120	48 - 52	0
2.0		120	48 - 52	0
3.0		125	48 - 52	0

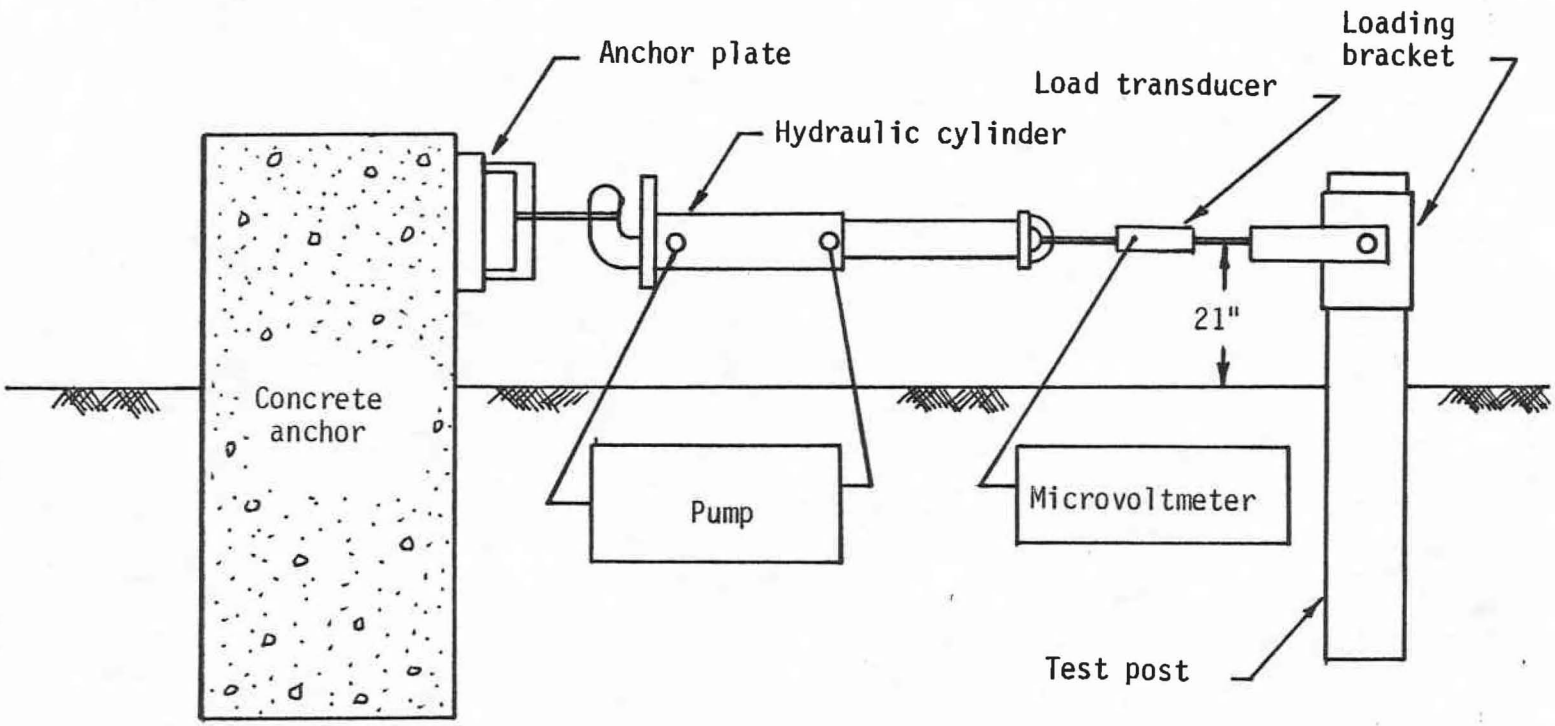

FIG. 35.-Lateral Loading System

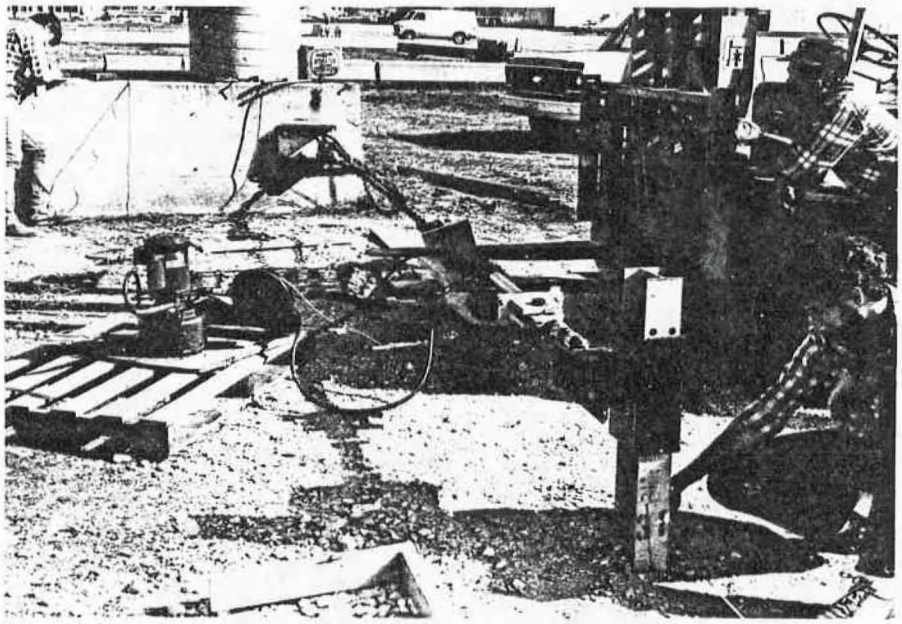

FIG. 36.-Static Testing System

bar instrumented with a full bridge of strain gages. The output from these strain gages were measured with a digital microvoltmeter calibrated to read the load directly.

Displacement Measurement

For the static load tests, the post deflection at the ground surface was measured. Since the soil around the post deforms as the post is loaded, the post displacement must be measured from a fixed point some distance away from the post. A wooden stake was driven into the ground about 15 feet away from the post. A metal tape was attached to the stake and the post displacements were measured from this fixed point as shown in Fig. 37.

Test Procedure

The procedure used in these tests is summarized below.

A specially constructed loading bracket was attached to the post at the height of 21 inches above the ground. This bracket, shown in Fig. 38, assured the pull to be horizontal and eliminated the development of stress concentrations in the post itself. The load transducer was attached to the loading bracket. The hydrualic cylinder was full extended and positioned between the

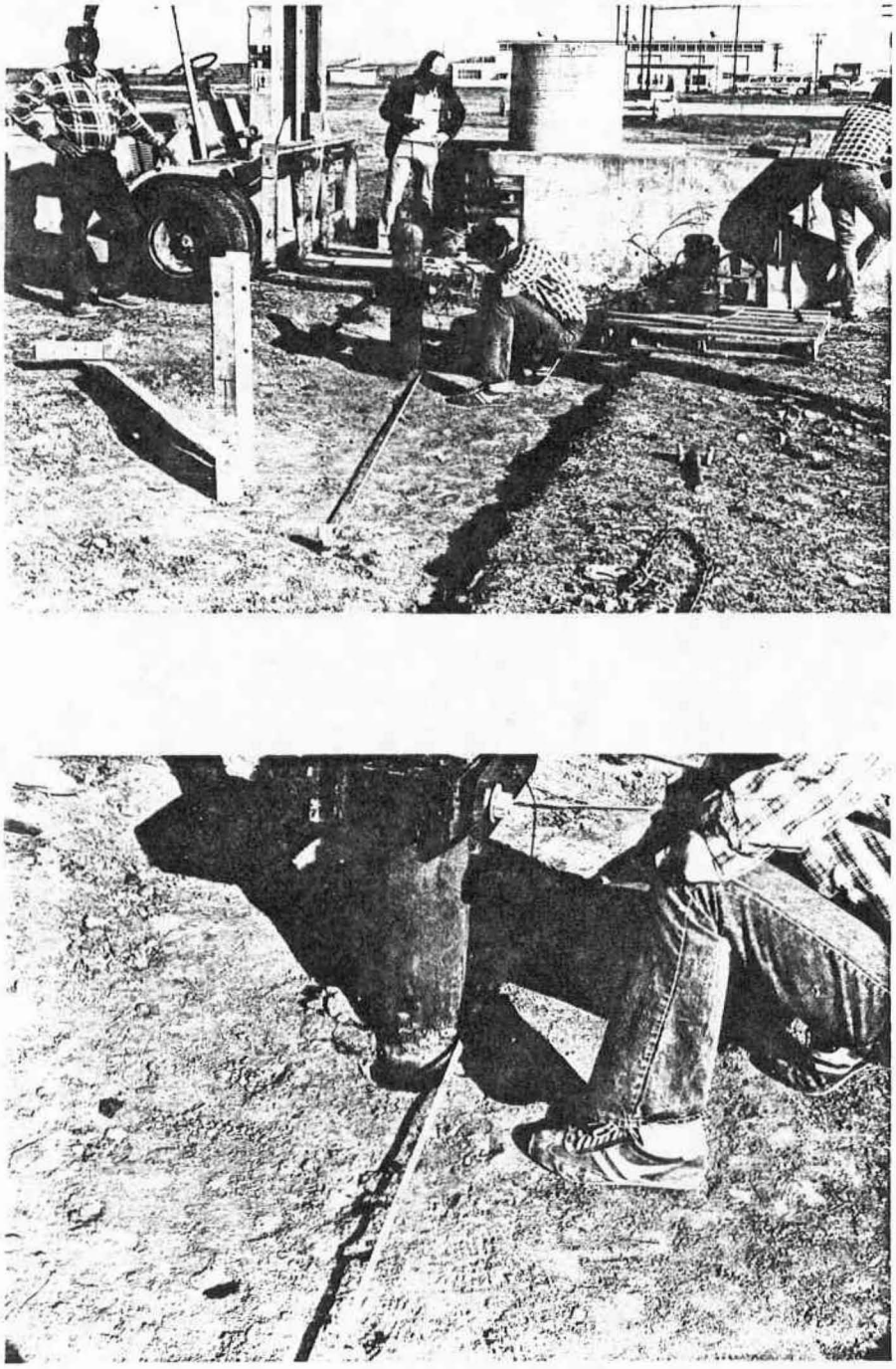

FIG. 37.-Measurement of Post Displacements

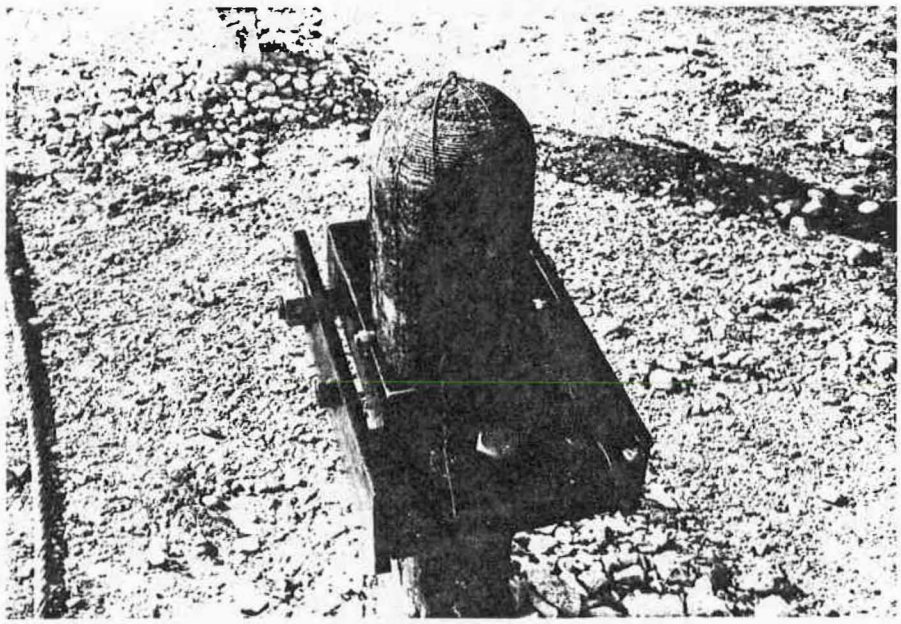

FIG. 38a.-Loading Bracket for the Circular Timber Post

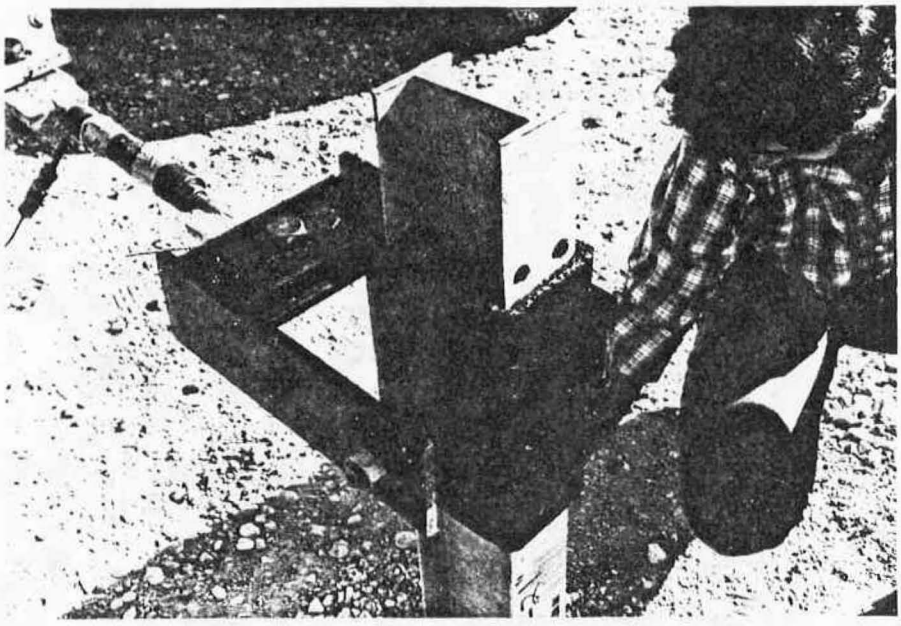

FIG. 38b.-Loading Bracket for the Steel Post

concrete anchor and the load transducer. A fork lift was used to hold the cylinder at a height of 21 inches in order to keep the weight of the equipment from applying an initial load. The load transducer was then calibrated and zeroed. The wooden stake was driven, and the tape positioned for displacement measurements. The hydraulic pump was turned on and the load was applied to the post. The load was read off the digital voltmeter at every 1/4 inch of movement of the post at the ground surface. The tests were terminated after the hydraulic cylinder had traveled the entire stroke length.

Test Results

The results of the static guardrail post tests are presented in Figs. 39 to 48 and in Table 27. The load-deflection curves for each test performed in the cohesive soil are given in Figs. 39 to 41, and the results from these three tests plotted on the same graph are shown in Figs. 42 and 43. The load-deflection curves for each test performed in the cohesionless soil are given in Figs. 44 to 46, and the results from these three tests plotted on the same graph are shown in Figs. 47 and 48. Maximum load values and dissipated energy values for all tests are presented in Table 27.

From the results of these static post tests, it is clear that the steel guardrail posts perform similar to

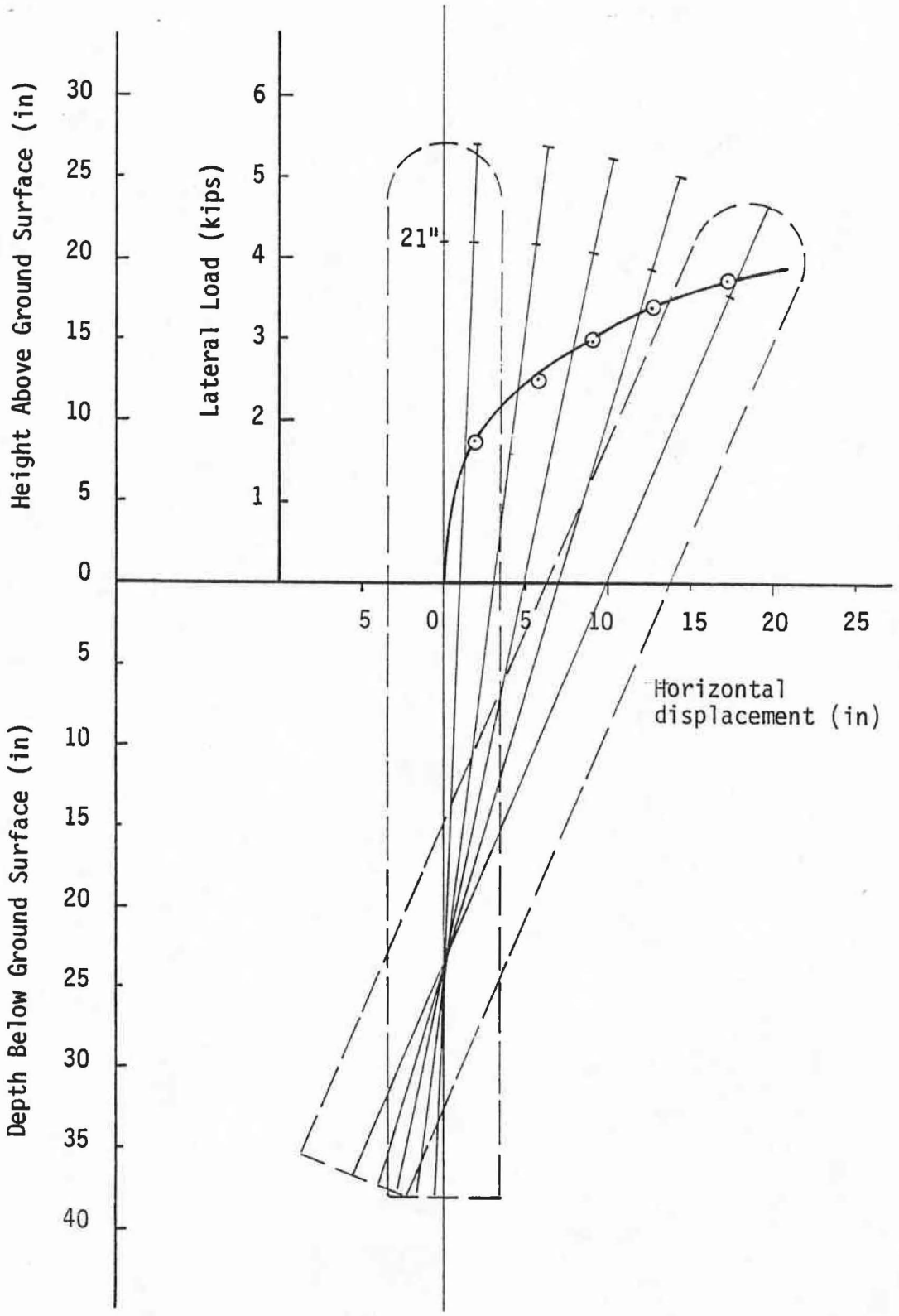

FIG. 39.-Lateral Load Versus Deflection for Post 1

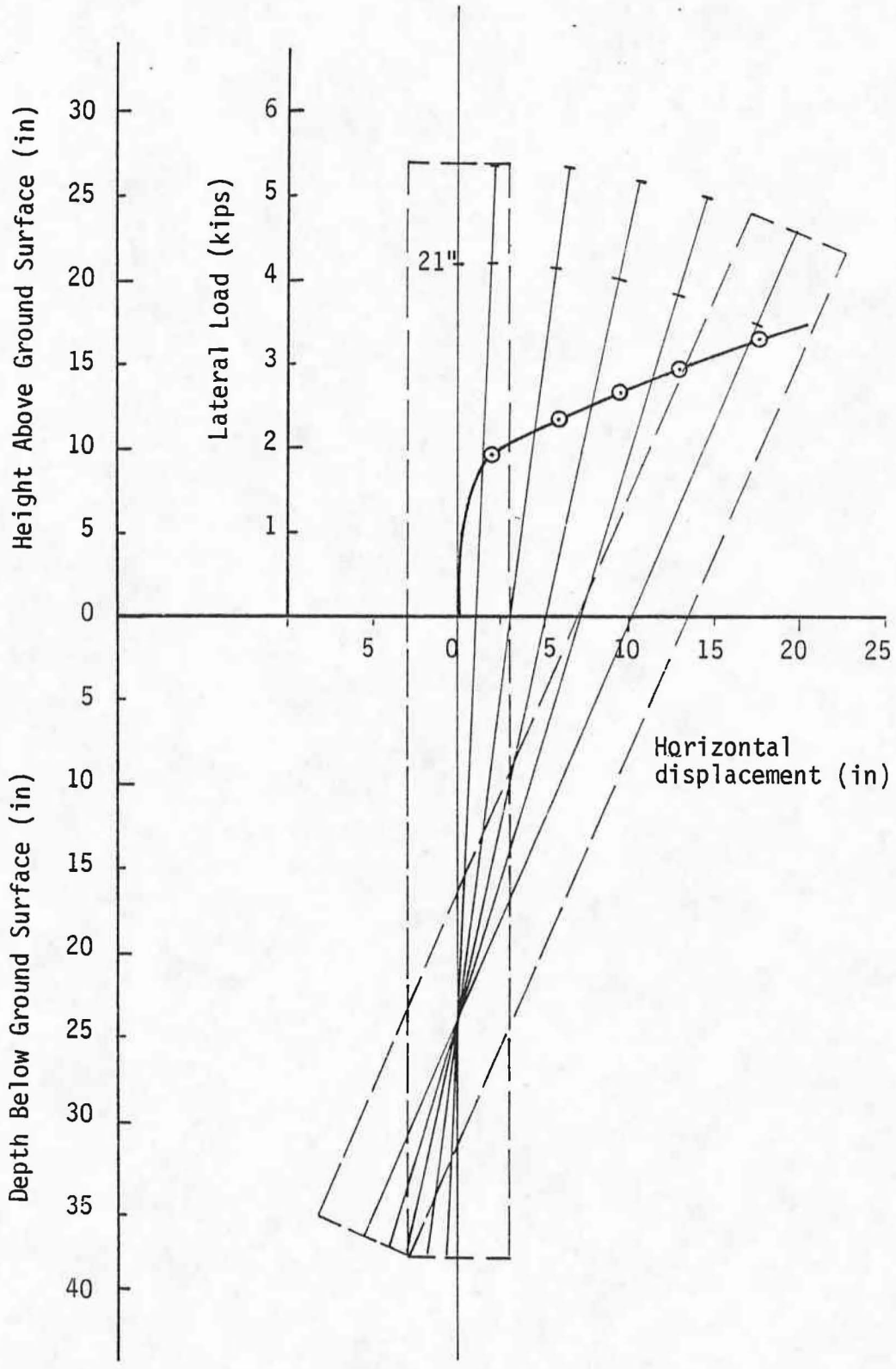

FIG. 40.-Lateral Load Versus Deflection for Post 2

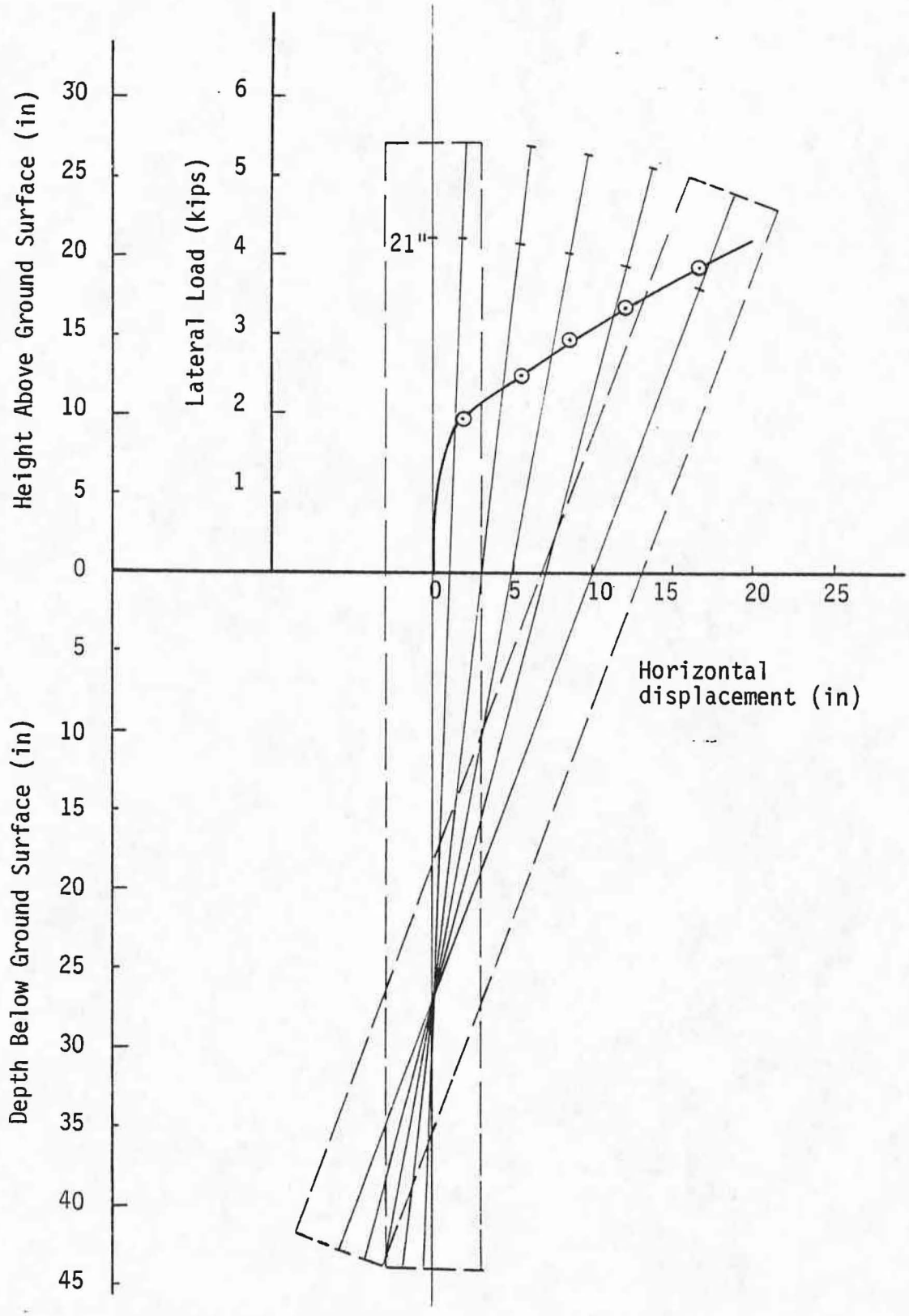

FIG. 41.-Lateral Load Versus Deflection for Post 3

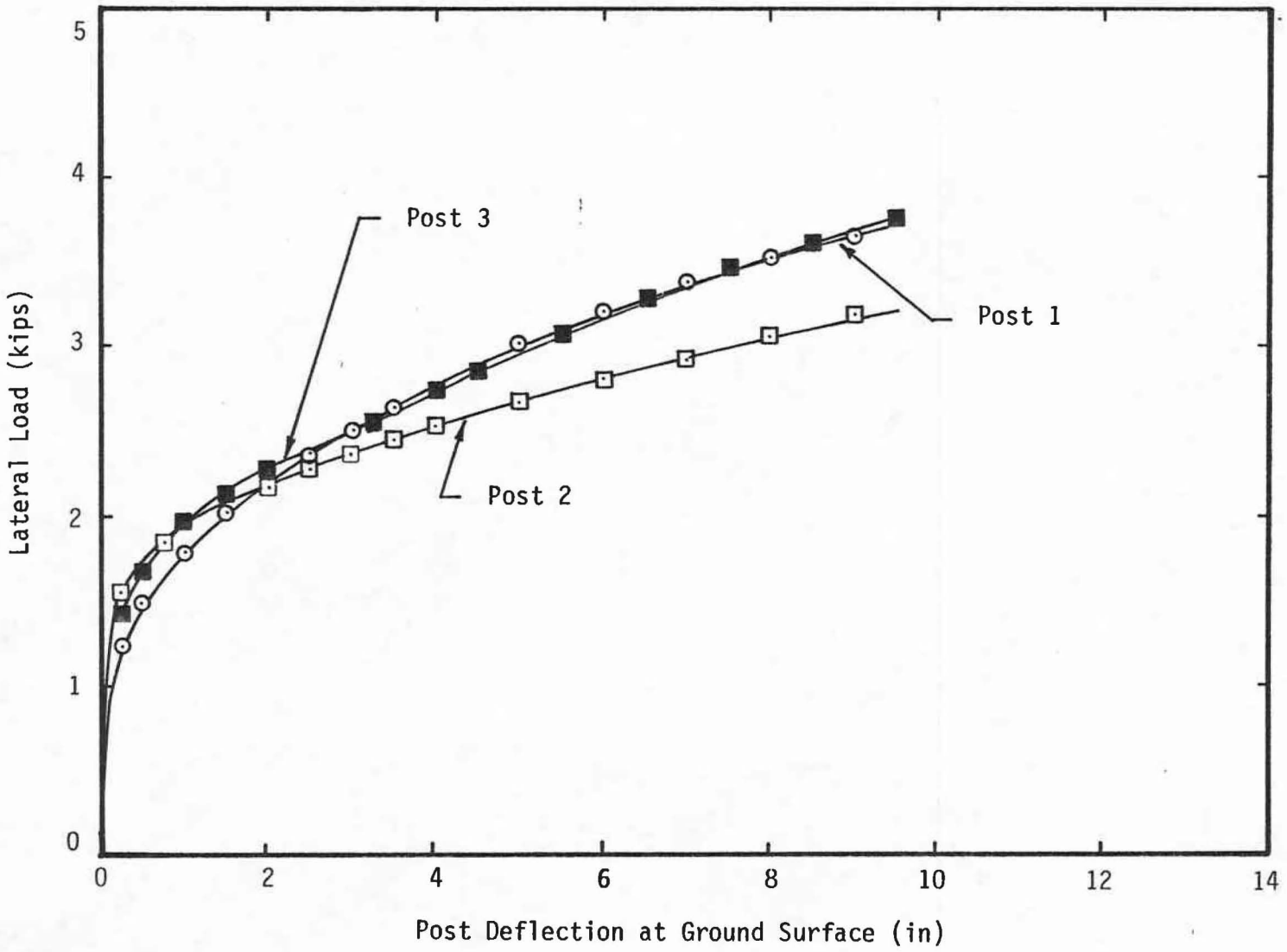

FIG. 42.-Static Test Results in the Cohesive Soil

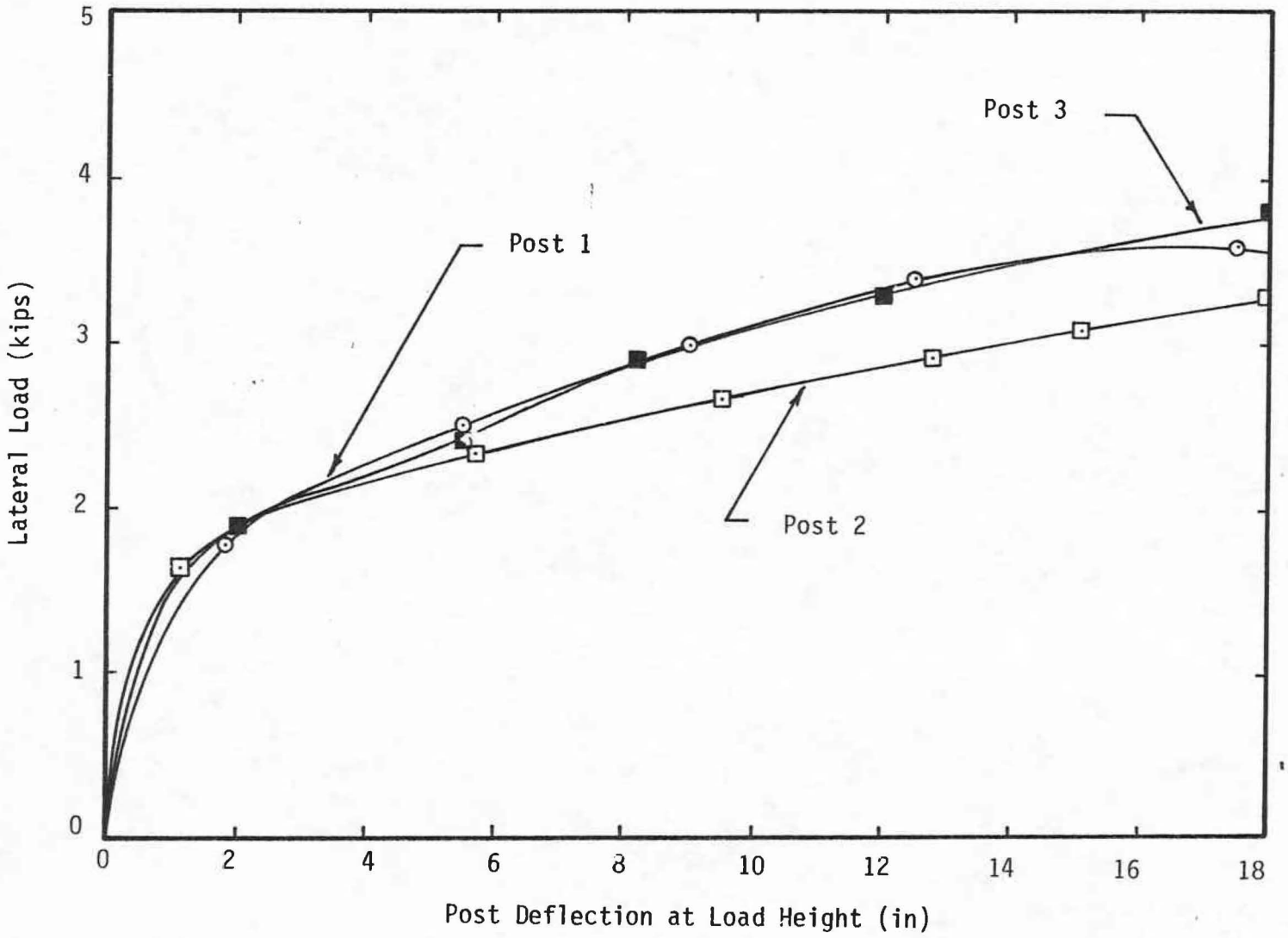

FIG. 43.-Static Test Results in the Cohesive Soil

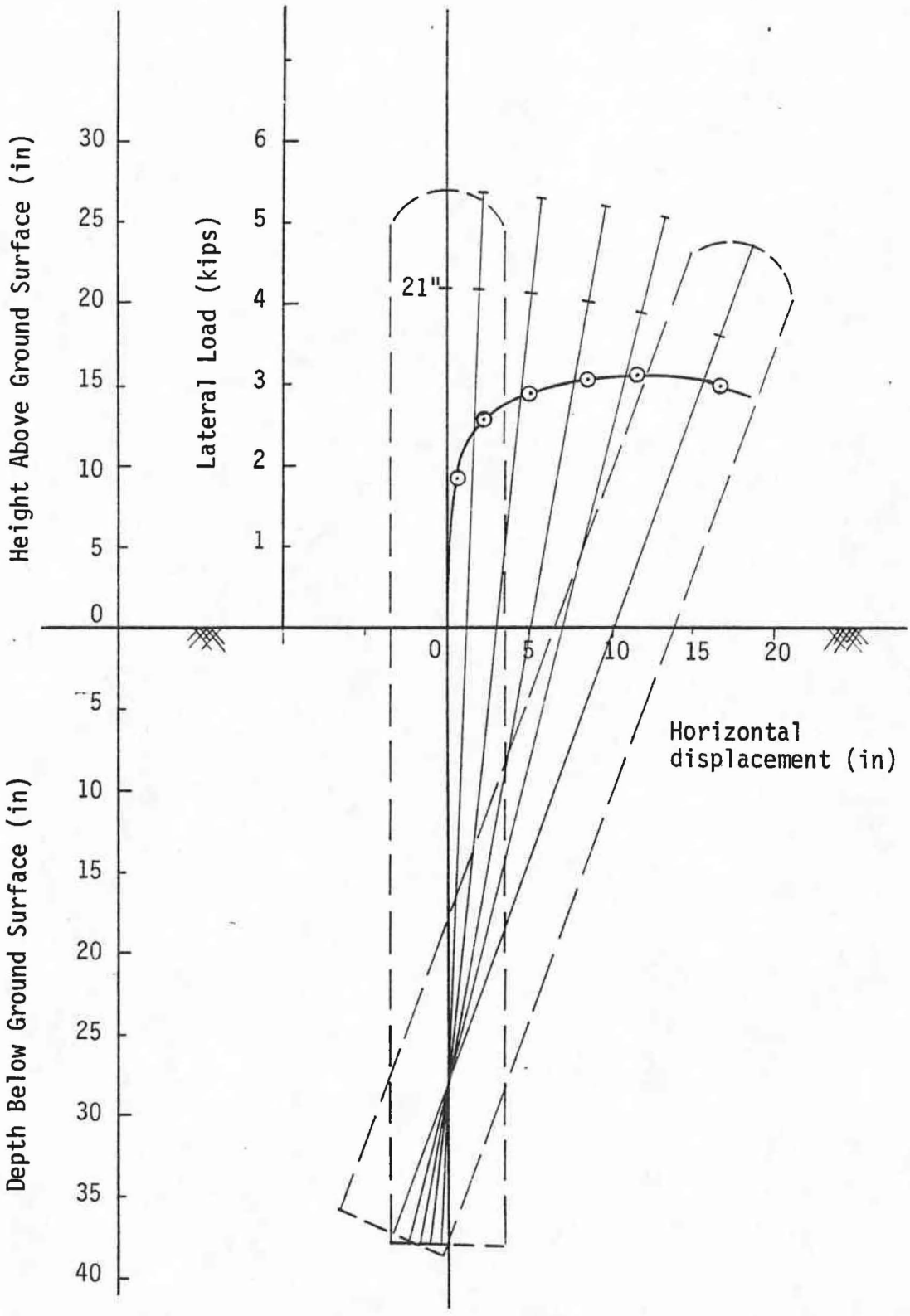

FIG. 44.-Lateral Load Versus Deflection for Post 4

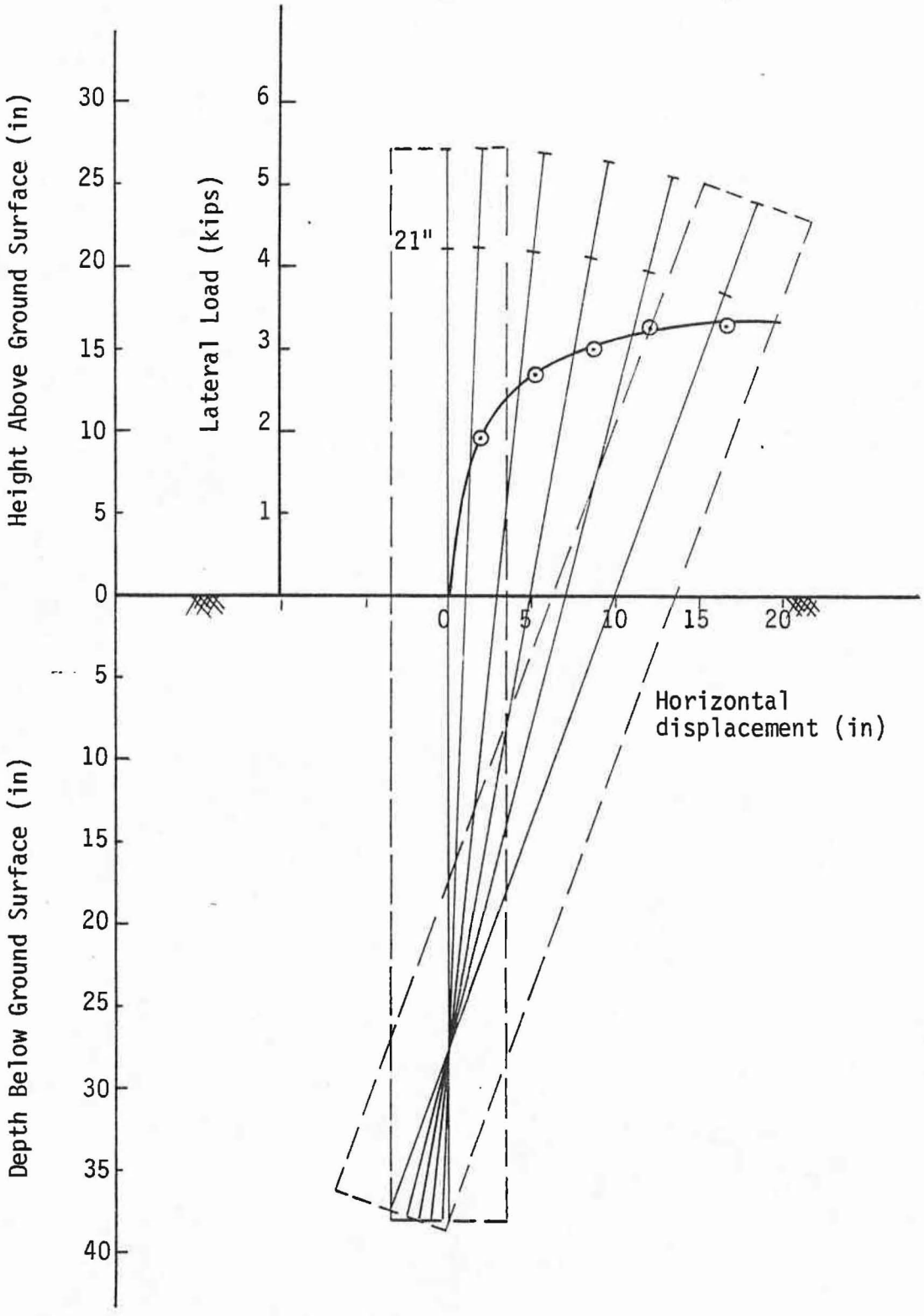

FIG. 45.-Lateral Load Versus Deflection for Post 5

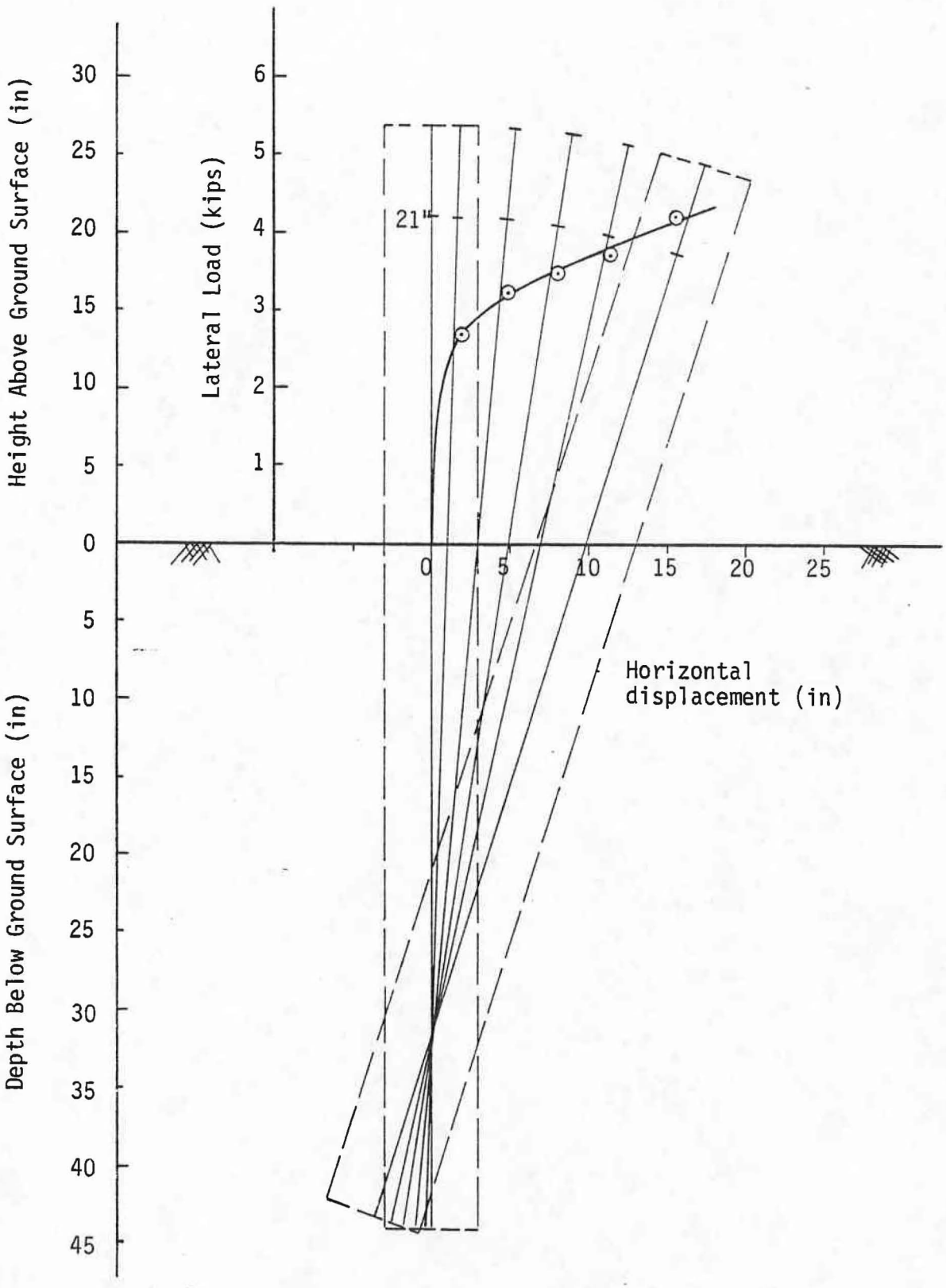

FIG. 46.-Lateral Load Versus Deflection for Post 6

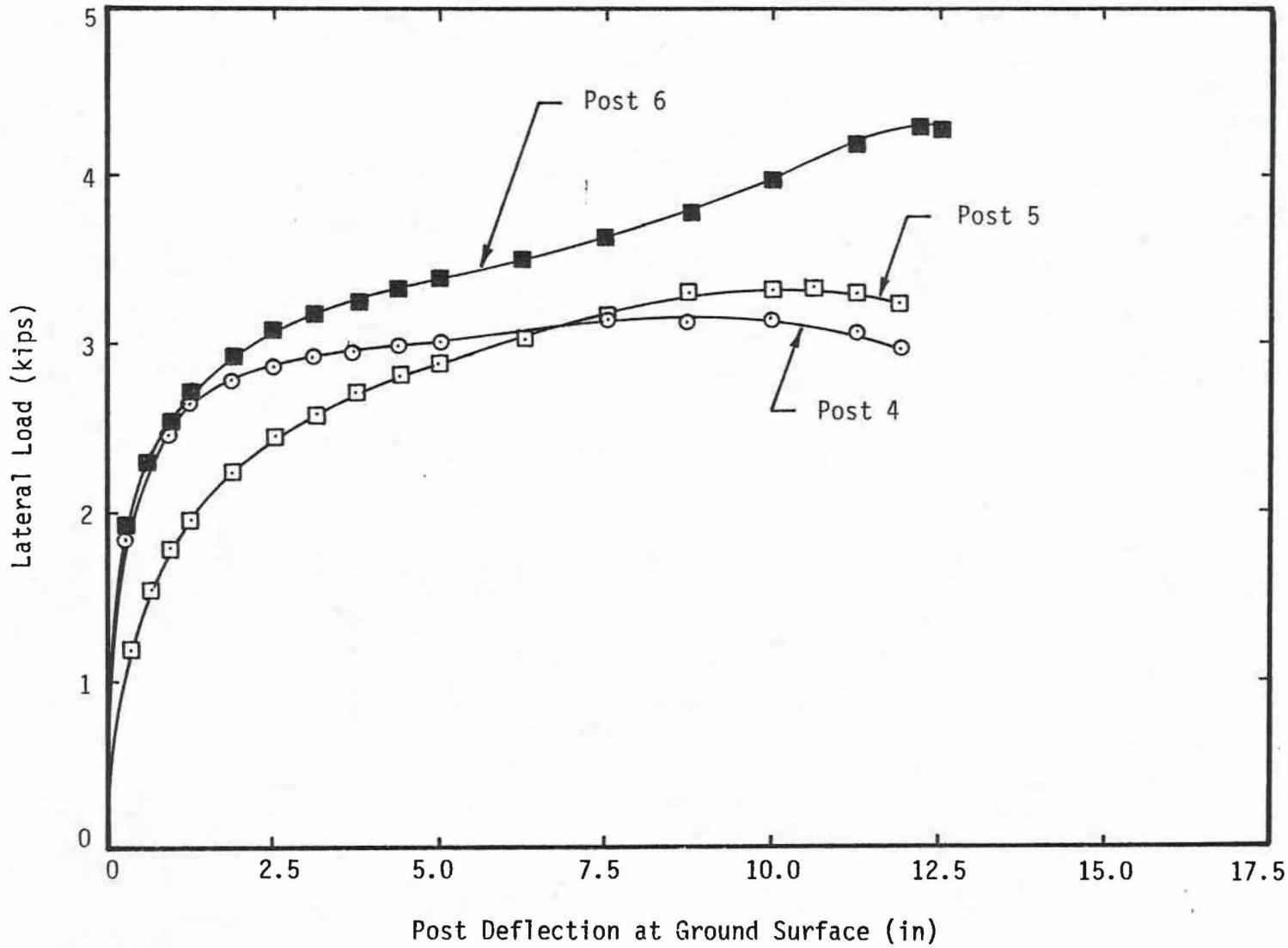

FIG. 47.-Static Tests Results in the Cohesionless Soil

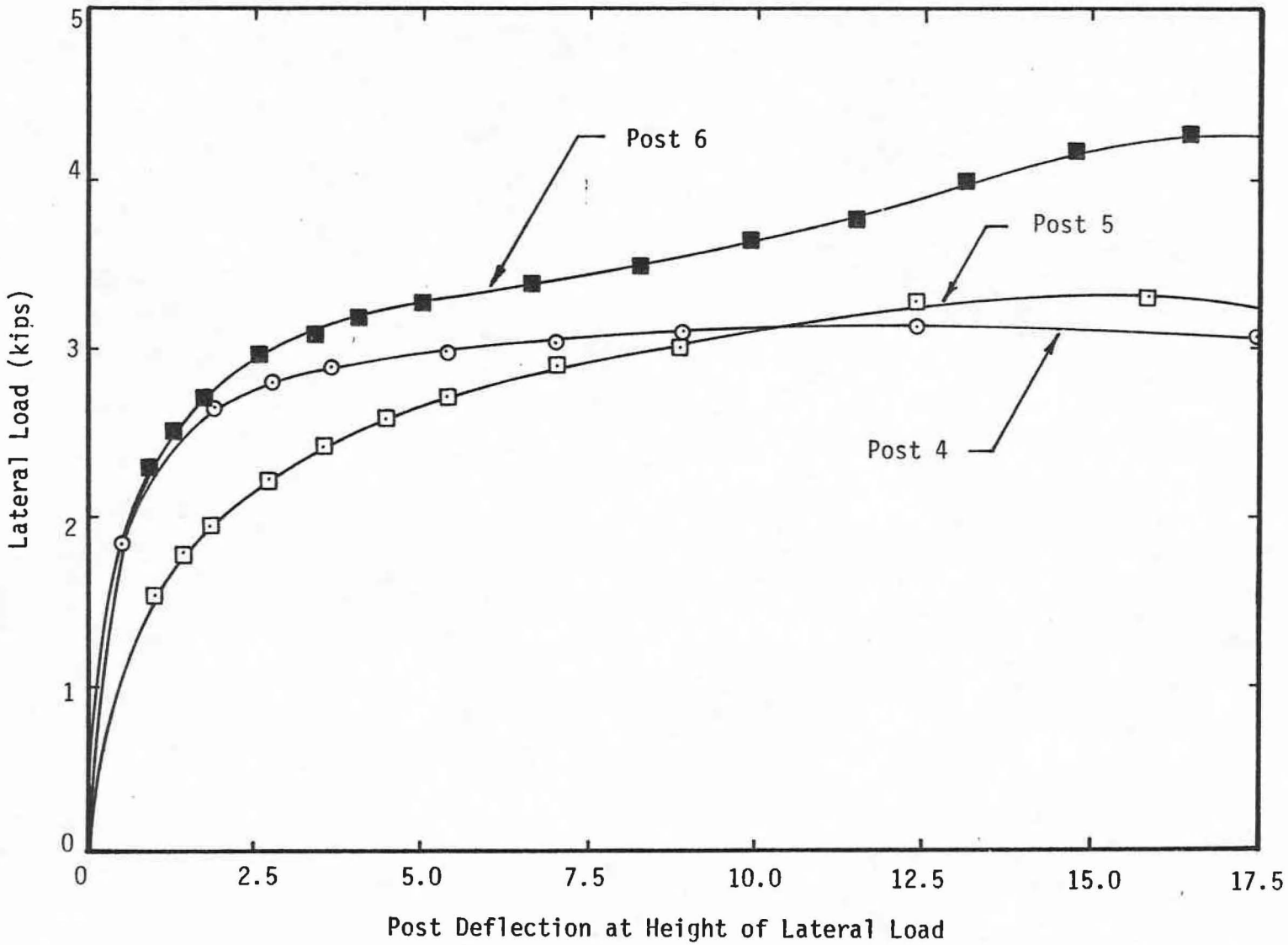

FIG. 48.-Static Test Results in the Cohesionless Soil

Table 27
SUMMARY OF RESULTS: STATIC TESTS

Test No.	Maximum Force (kips)	Force at 18 in. Movement (kips)	Energy* (ft-kips)
1	3.7	3.7	4.2
2	3.3	3.3	3.8
3	3.8	3.8	4.3
4	3.2	2.9	4.4
5	3.3	3.2	4.2
6	3.9	3.9	5.2

*Energy dissipated after 18 in. of movement.

the standard timber posts.

In the cohesive soil, the steel post embedded 44 inches performed almost exactly as the timber post embedded the minimum 38 inches. The steel post embedded 38 inches performed similar to the wood post, however there was a small decrease in both the maximum load and the energy dissipated. The decrease in the maximum lateral load was 11 percent, and the decrease in the energy dissipated was 10 percent.

In the cohesionless soil, the lateral load capacity and the energy absorbed by the steel post embedded 44 inches were greater than those of the timber post. For the steel post embedded 38 inches, the maximum load was 3 percent higher than the maximum load carried by the timber post, however the energy absorbed by the steel post was 5 percent lower than the energy absorbed by the timber post.

Comparison of Test Results With Theoretical Predictions

The parameters and the data needed for the theoretical analysis of the six tests are listed in Tables 28 to 33. The field load test results are shown in Figs. 49 to 54, with the analytical results obtained using the computer program LATPIL.

Since the angle of internal friction of the cohesionless soil could not be determined precisely by

Table 28 Input Data for Post 1.

Pile Properties

Dimensions: 7 in. diameter

Embedment = 38 in.

No. of Increments = 20

Height of Load = 1.75 ft

Flexural Stiffness = 1.483×10^6 lb-ft^2

Effective Pile Weight = 55 lbs

Soil Properties

Layer	ϕ (deg.)	δ (deg.)	c_u (ksf)	Unit Weight	Depth (ft)	$\frac{X_p}{R}$	$\frac{X_a}{R}$	K_o	α
1	0	22	3.0	115	0.5	0.07	0.01	1.0	1.0
2	0	22	2.5	115	1.0	0.07	0.01	1.0	1.0
3	0	22	1.5	115	1.5	0.07	0.01	1.0	1.0
4	0	22	1.6	115	2.0	0.07	0.01	1.0	1.0
5	0	22	1.9	115	3.167	0.07	0.01	1.0	1.0

Surface surcharge = 0.0

Tension cutoff = 1

Tolerance = 0.0001

Table 29 Input Data for Post 2.

Pile Properties

Dimensions: 3.94 in. x 5.83 in.

Embedment = 38 in.

No. of Increments = 20

Height of Load = 1.75 ft

Flexural Stiffness = 3.303×10^6 lb-ft^2

Effective Pile Weight = 70 lbs

Soil Properties

Layer	ϕ (deg.)	δ (deg.)	c_u (ksf)	Unit Weight	Depth (ft)	$\frac{X_p}{R}$	$\frac{X_a}{R}$	K_o	α
1	0	22	3.0	115	0.5	0.07	0.01	1.0	1.0
2	0	22	2.5	115	1.0	0.07	0.01	1.0	1.0
3	0	22	1.5	115	1.5	0.07	0.01	1.0	1.0
4	0	22	1.6	115	2.0	0.07	0.01	1.0	1.0
5	0	22	1.0	115	3.167	0.07	0.01	1.0	1.0

Surface surcharge = 0.0

Tension cutoff = 1

Tolerance = 0.0001

Table 30 Input Data for Post 3.

Pile Properties

Dimensions: 3.94 in. x 5.83 in.

Embedment = 44 in.

No. of Increments = 20

Height of Load = 1.75 ft

Flexural Stiffness = 3.306×10^6 lb-ft^2

Effective Pile Weight = 70 lb

Soil Properties

Layer	ϕ (deg.)	δ (deg.)	c_u (ksf)	Unit Weight	Depth (ft)	$\frac{X_p}{R}$	$\frac{X_a}{R}$	K_o	α
1	0	22	3.0	115	0.5	0.07	0.01	1.0	1.0
2	0	22	2.5	115	1.0	0.07	0.01	1.0	1.0
3	0	22	1.5	115	1.5	0.07	0.01	1.0	1.0
4	0	22	1.6	115	2.0	0.07	0.01	1.0	1.0
5	0	22	1.9	115	3.67	0.07	0.01	1.0	1.0

Surface surcharge = 0.0

Tension cutoff = 1

Tolerance = 0.0001

Table 31 Input Data for Post 4.

Pile Properties

Dimensions: 3.94 in. x 5.83 in.

Embedment = 38 in.

No. of Increments = 20

Height of Load = 1.75 ft

Flexural Stiffness = 1.483×10^6 lb-ft^2

Effective Pile Weight = 55 lbs

Soil Properties

Layer	ϕ (deg.)	δ (deg.)	c_u (ksf)	Unit Weight	Depth (ft)	$\frac{X_p}{R}$	$\frac{X_a}{R}$	K_o	α
1	52	22	0	115	0.5	0.01	0.0005	0.257	1.0
2	52	22	0	115	1.0	0.01	0.0005	0.257	1.0
3	51.4	22	0	115	1.5	0.01	0.0005	0.264	1.0
4	50.5	22	0	115	2.0	0.01	0.0005	0.275	1.0
5	49.3	22	0	115	3.167	0.01	0.0005	0.289	1.0

Surface surcharge = 0

Tension cutoff = 1

Tolerance = 0.0001

Table 32 Input Data for Post 5.

Pile Properties

Dimensions: 3.94 in. x 5.83 in.

Embedment = 38 in.

No. of Increments = 20

Height of Load = 1.75 ft.

Flexural Stiffness = 3.303×10^6 lb-ft^2

Effective Pile Weight = 70 lbs

Soil Properties

Layer	ϕ (deg.)	δ (deg.)	c_u (ksf)	Unit Weight	Depth (ft)	$\frac{X_p}{R}$	$\frac{X_a}{R}$	K_o	α
1	52	22	0	115	0.5	0.01	0.0005	0.257	1.0
2	52	22	0	115	1.0	0.01	0.0005	0.275	1.0
3	51.4	22	0	115	1.5	0.01	0.0005	0.264	1.0
4	50.5	22	0	115	2.0	0.01	0.0005	0.275	1.0
5	49.3	22	0	115	3.167	0.01	0.0005	0.289	1.0

Surface surcharge = 0

Tension cutoff = 1

Tolerance = 0.0001

Table 33 Input Data for Post 6.

Pile Properties

Dimensions: 3.92 in. x 5.83 in.

Embedment = 44 in.

No. of Increments = 20

Height of Load = 1.75 ft

Flexural Stiffness = 3.303×10^6 lb-ft^2

Effective Pile Weight = 70 lbs

Soil Properties

Layer	ϕ (deg.)	δ (deg.)	c_u (ksf)	Unit Weight	Depth (ft)	$\frac{X_p}{R}$	$\frac{X_a}{R}$	K_o	α
1	52	22	0	115	0.5	0.01	0.0005	0.257	1.0
2	52	22	0	115	1.0	0.01	0.0005	0.257	1.0
3	51.4	22	0	115	1.5	0.01	0.0005	0.264	1.0
4	50.5	22	0	115	2.0	0.01	0.0005	0.275	1.0
5	49.3	22	0	115	3.67	0.01	0.0005	0.289	1.0

Surface surcharge = 0

Tension cutoff = 1

Tolerance = 0.0001

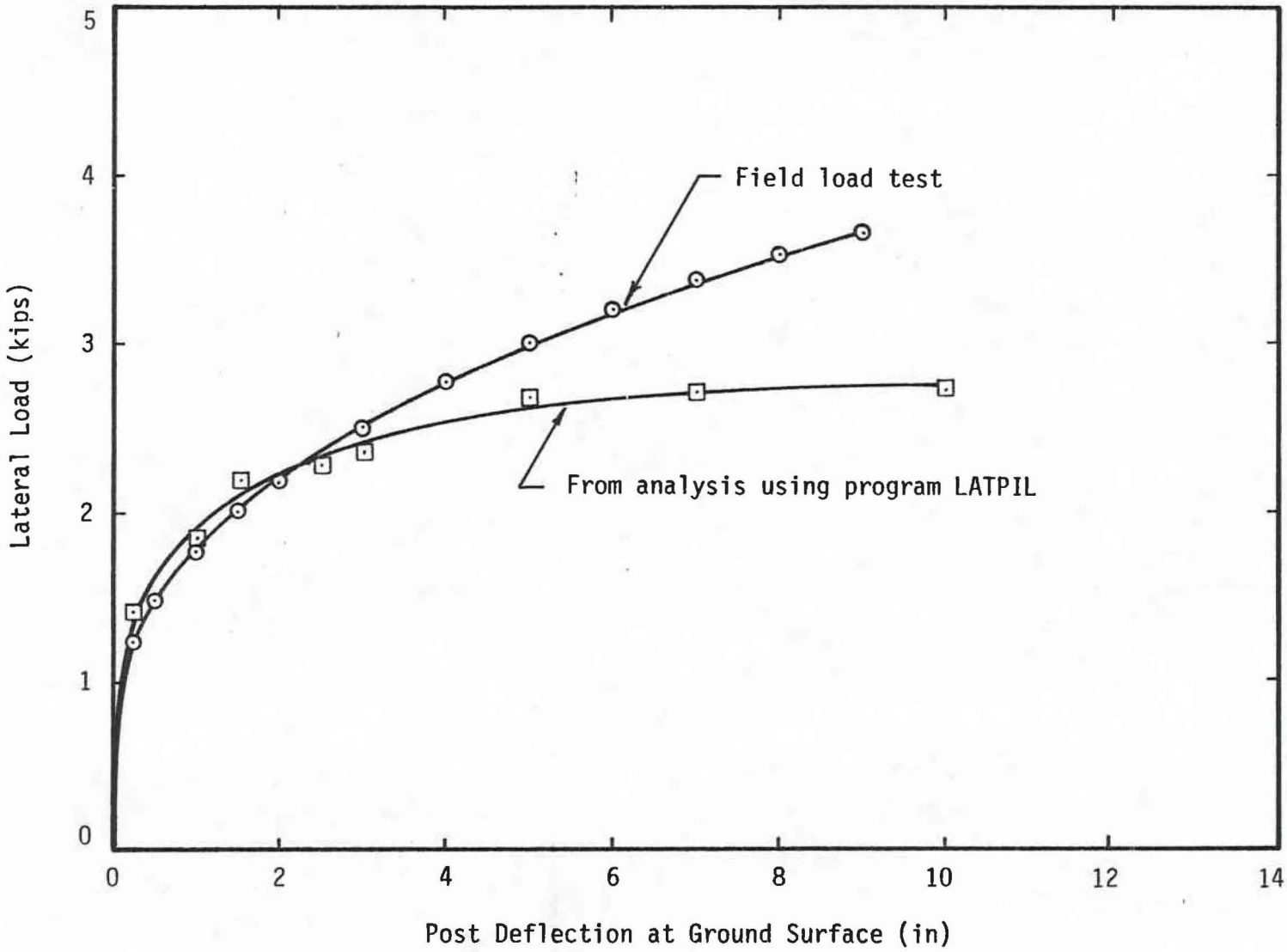

FIG. 49.-Comparison of Analysis and Field Load Test for Post 1

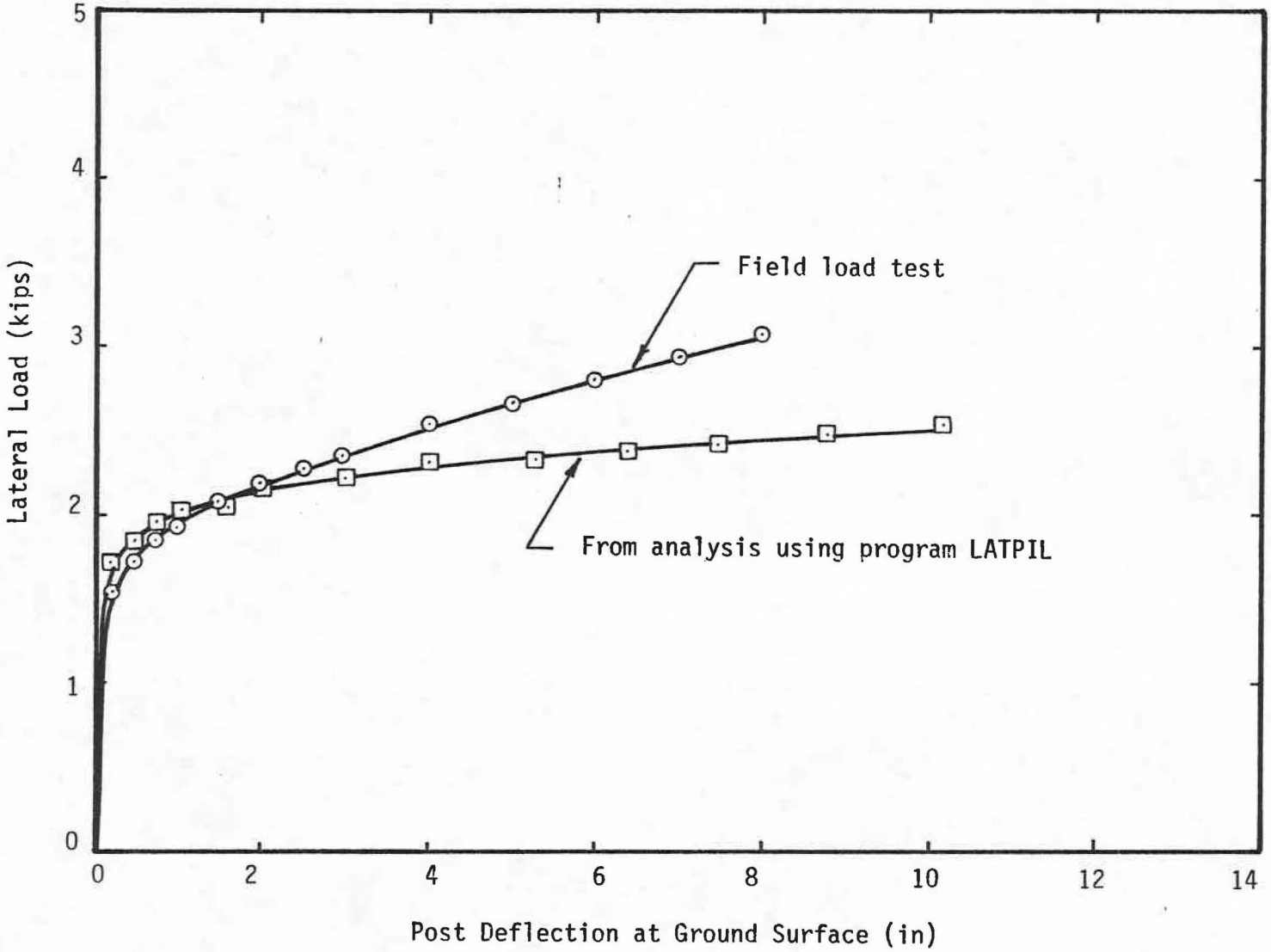

FIG. 50.-Comparison of Analysis and Field Load Test for Post 2

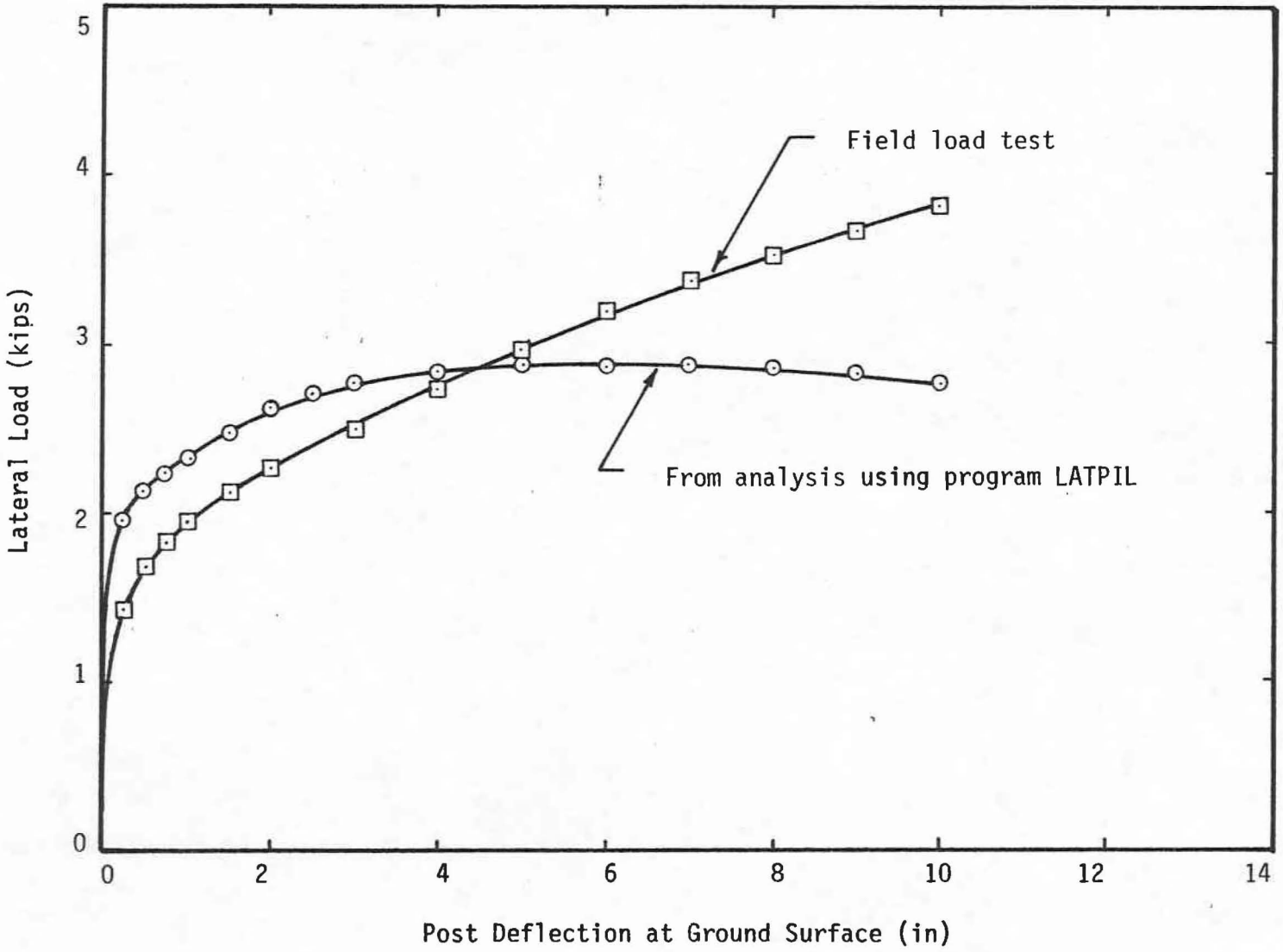

FIG. 51.-Comparison of Analysis and Field Load Test for Post 3

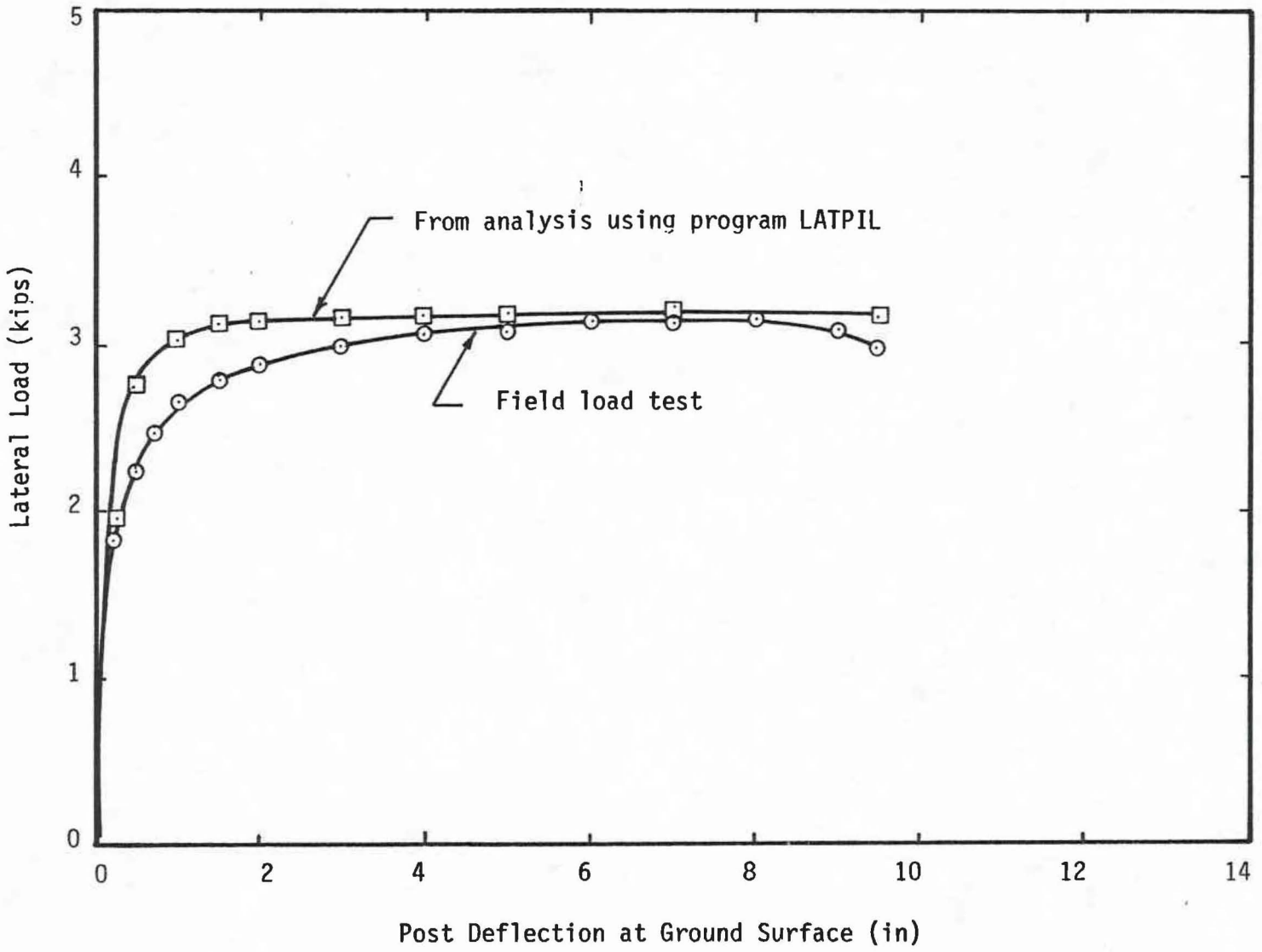

FIG. 52.-Comparison of Analysis and Field Load Test for Post 4

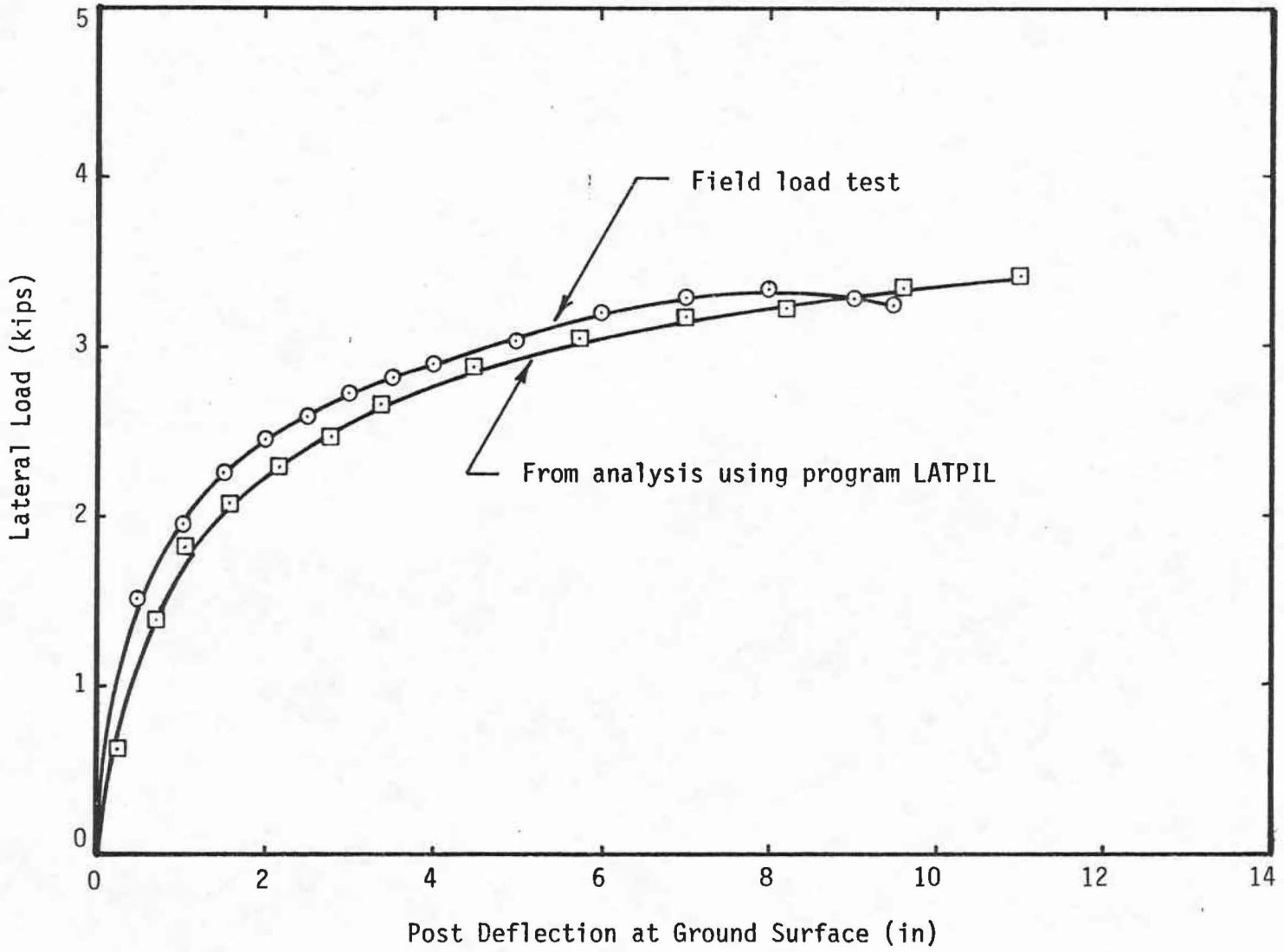

FIG. 53.-Comparison of Analysis and Field Load Test for Post 5

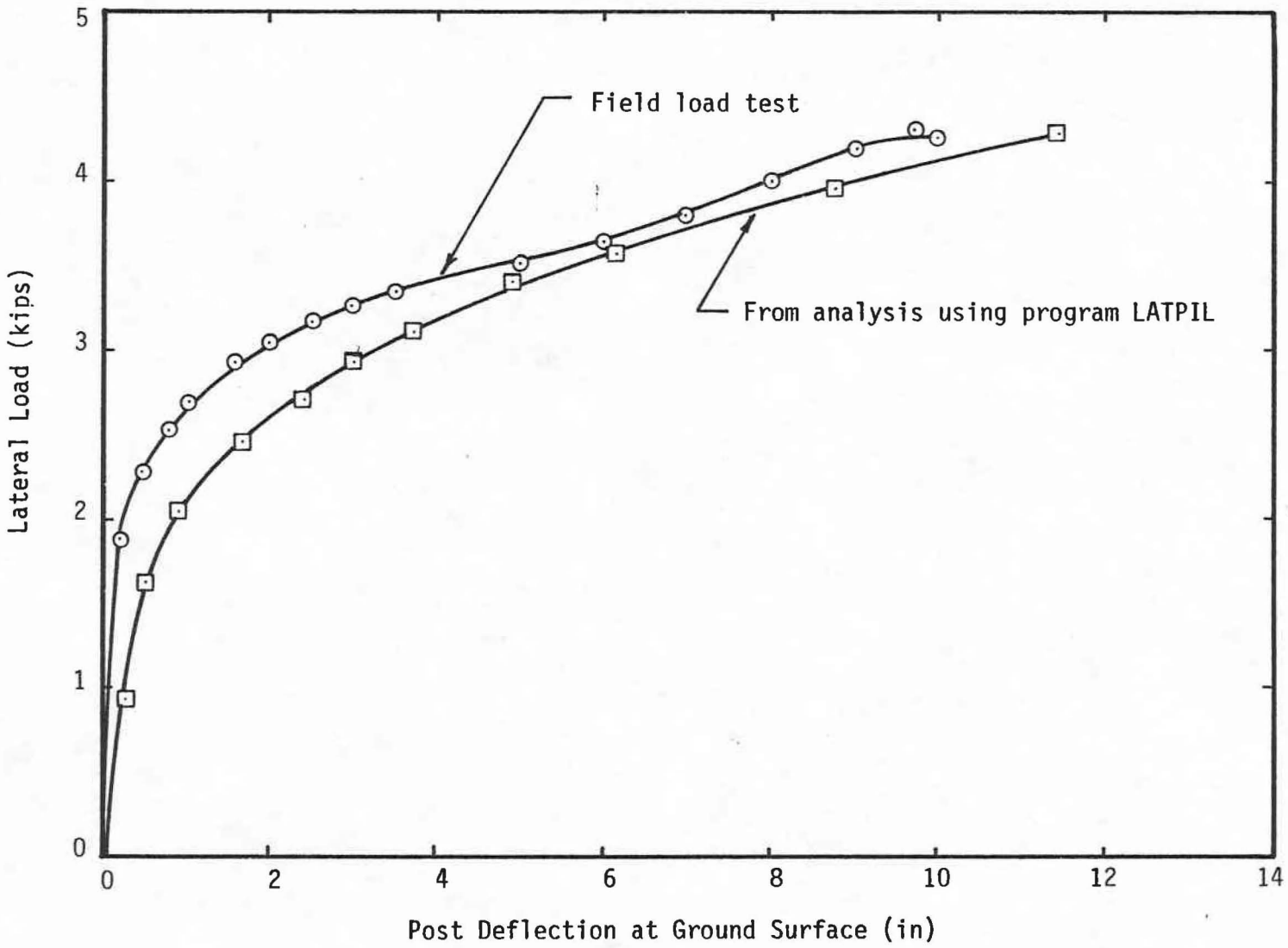

FIG. 54.-Comparison of Analysis and Field Load Test for Post 6

laboratory tests, the ranges of values selected from the correlations, as previously discussed, were used.

The agreement between the analysis and the field load tests is good in all six tests. In the cohesive soil, the analytical results and the field test results match very well at ground-line displacements less than 4 inches. A post displacement of 4 inches at the ground surface corresponds to a post rotation of about 10 degrees. For displacements in excess of 4 inches, the post rotates a significant amount and the applied load tends to pull the post out of the ground. This axial pull on the post induces vertical shear stresses along the perimeter of the post which tend to increase the lateral capacity of the post. For this reason, the theoretical analysis underpredicts the lateral load for post displacements greater than 4 inches.

In the cohesionless soil, the theoretical predictions agreed well with the field load tests. Both the shapes of the load-deflection curves and the maximum load values are predicted well by the model. The wood post in the cohesionless soil reached its maximum lateral capacity at 4 inches of ground surface movement, and the lateral load remained fairly constant for ground surface displacements in excess of 4 inches. However, the steel posts continued to gain lateral capacity throughout the entire test.

DYNAMIC LOAD TESTS

Introduction

The response of the guardrail posts to static loads was used to evaluate the lateral load capacity and the energy absorption capacity of the two types of guardrail posts. However, the response of the guardrail posts when hit by a moving vehicle is a better measure of the performance of the post-soil system. Thus, one of the objectives of this research study was to perform a series of dynamic load tests on the two types of guardrail posts. The results from these tests, and from the static load tests, will determine whether the steel guardrail post can perform satisfactorily without the concrete footing.

Testing Program

The dynamic load tests that were conducted are summarized in Table 34.

From the results of the static load tests, it was decided that dynamic load tests on the steel guardrail posts embedded 44 inches were not necessary. Both the static lateral load capacity and the energy dissipation capacity of the steel posts embedded 44 inches exceeded the capacities for the wood posts embedded 38 inches. Although the dynamic behavior of the guardrail posts is

Table 34. Summary of Dynamic Tests

Test No.	Post Type	Embedment Depth (in.)	Height of Rail (in.)	Soil Type
C1	Wood	38	21	Cohesionless
C2	Steel	38	21	Cohesionless
C3	Wood	38	21	Cohesive
C4	Steel	38	21	Cohesive

quite different from the static behavior, the results of the static tests give a good indication of the relative performance of these posts.

Equipment and Instrumentation

Dynamic load testing of the guardrail posts require systems capable of (1) dynamic load application, (2) dynamic load measurement, and (3) measurement of post deflection.

Loading System

The dynamic testing program was accomplished using a cart of known mass to simulate an automobile. This cart, shown in Fig. 55, was used because of the extreme rigidity of the cart. Consequently, very little energy is dissipated in deforming or crushing of the cart itself.

The cart was positioned about 100 feet away from the posts. A cable was attached to the cart, placed around the pulley, as shown in Fig. 56, and connected to a truck which pulled the cart into the post. A cable release mechanism was placed directly ahead of the pulley to detach the cable from the cart. Since the cart has no means of steering two concrete barriers, as shown in Fig. 57, were used to guide the cart toward the post.

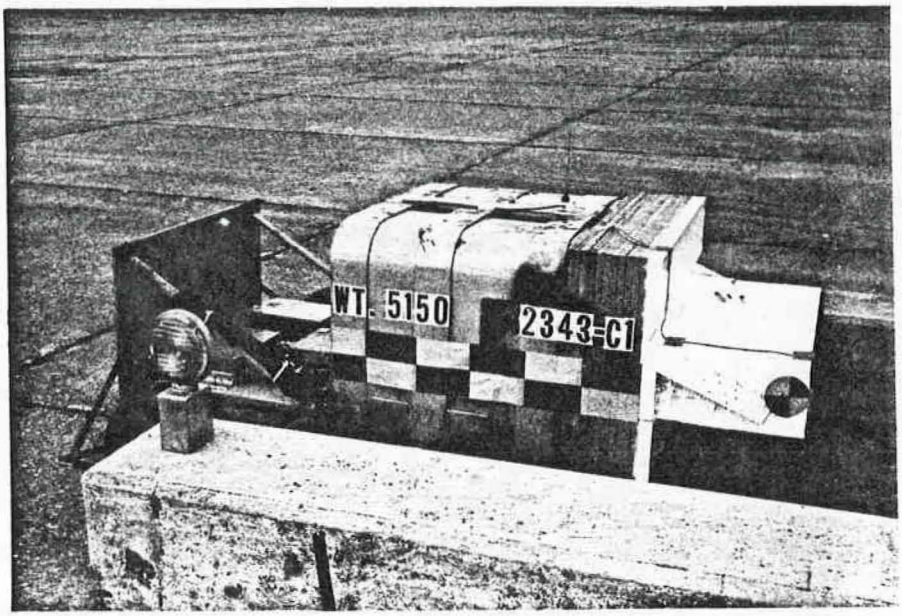

FIG. 55.-Automobile Simulation Cart

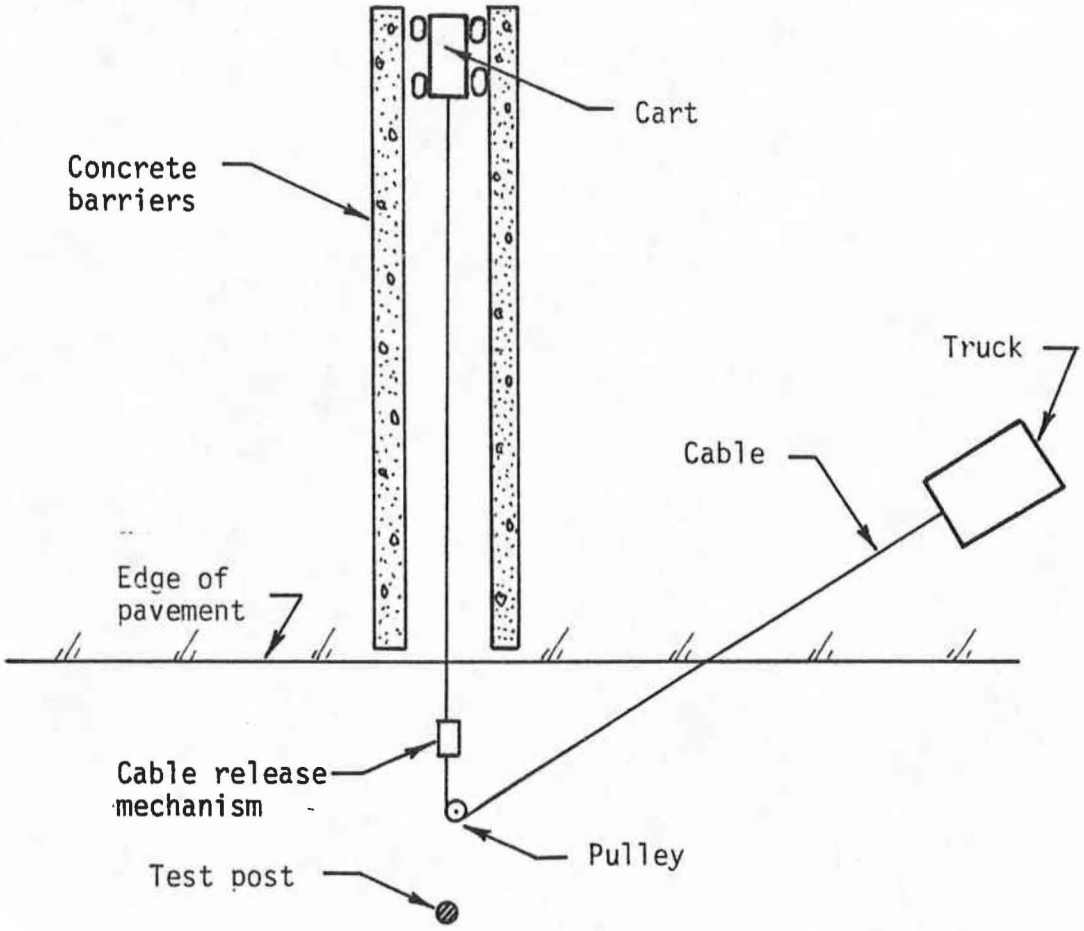

FIG. 56.-Schematic of Test Layout

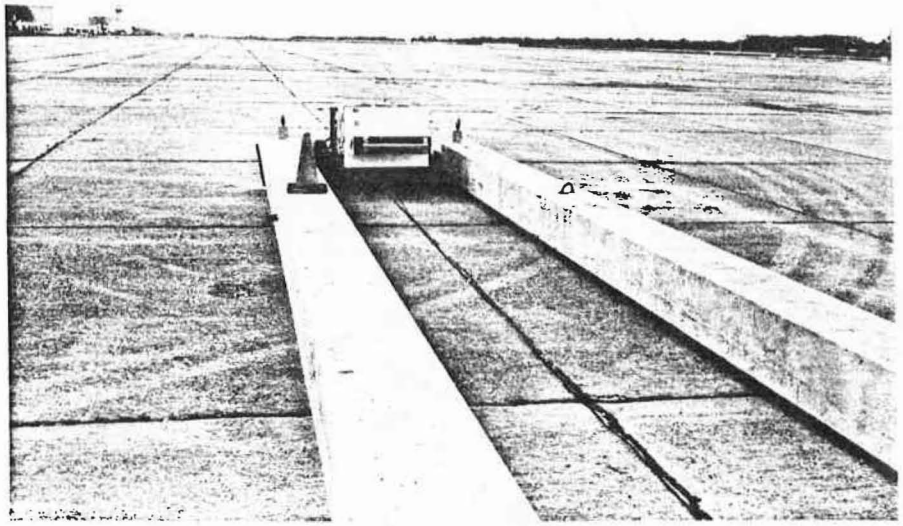

FIG. 57.-Concrete Guide Barriers

Dynamic Load Measurement

The cart was instrumented with an accelerometer as shown in Fig. 58 to measure the lateral deceleration during impact with the post. By knowing the mass of the cart, the lateral force applied to the guardrail post can be calculated using the product of the cart mass and the cart deceleration. The accelerometer data was recorded by a computer every 0.0003 seconds, and an output of force was obtained directly from this computer.

Post Displacement Measurement

Since the duration of the impact test is only a fraction of a second, direct measurement of the post displacement during the test is very difficult. However, the post displacement can be obtained indirectly by two methods. In the first method, each test was photographed with a high speed camera at a speed of 408 frames per second. The displacements of the post were scaled off the high speed film. In the second method, the post displacement can be calculated from the accelerometer data by integrating the deceleration time curve twice. The cart velocity at the point of impact must be known for the second method and this was obtained from the high speed film.

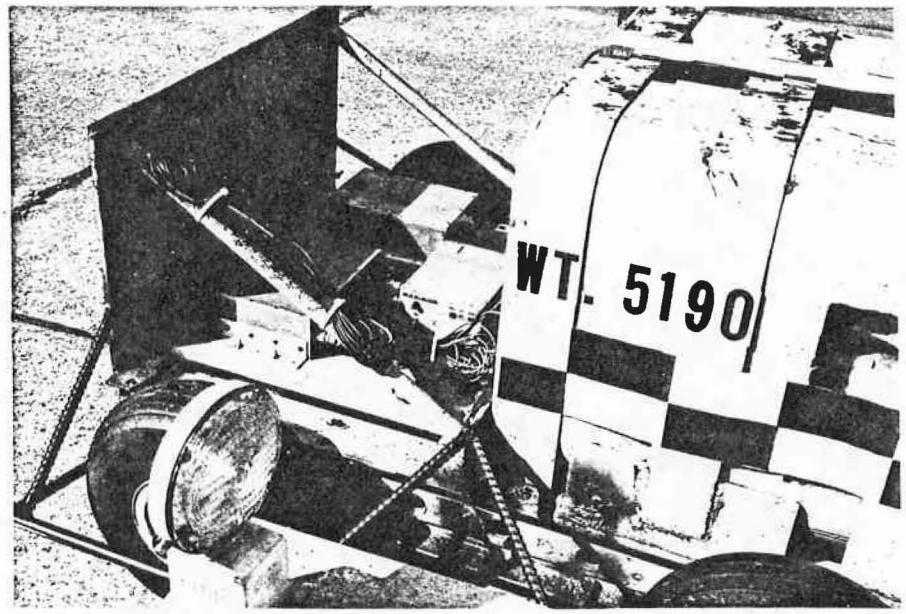

FIG. 58.-Cart With Electronic Equipment

Placement of the Posts

The dynamic tests were performed in the same two soils used in the static tests. However, a test site located near the pavement at the Texas A&M University Research and Extension Center was used instead of the site for the static tests. This site was chosen because the posts needed to be installed near the edge of the runway so the cart could be easily pulled toward the post. The procedure used for installing the posts was the same as that used for the static tests.

Soil Conditions

The properties of the cohesive soil were determined by performing laboratory tests on samples obtained with a 2.0 in. diameter thin-walled tube samples. As for the static tests, the laboratory tests on the soil samples included Atterberg limits, moisture content, unit weight, and triaxial compression tests to determine the undrained shear strength of the cohesive soil. The results of these tests are shown in Tables 35 and 36. The test results show the properties to be very similar to the properties of the cohesive soil used in the static tests.

The crushed limestone gravel used in the static tests was also used for the impact tests. Thus, the properties are the same as previously determined for the static tests.

Table 35 Soil Properties for Test C3.

Depth (ft)	Generalized Description	Unit Weight (pcf)	ϕ_u (deg.)	c_u (ksf)
0.5	Dark Grey Stiff Clay	125	0	3.2
1.0		126	0	2.5
1.5		124	0	1.4
2.0		123	0	1.6
3.0		125	0	2.0

Table 36 Soil Properties for Test C4.

Depth	Generalized Description	Unit Weight (pcf)	ϕ_u (deg.)	c_u (ksf)
0.5	Dark Grey Stiff Clay	125	0	2.0
1.0		124	0	1.6
1.5		124	0	1.4
2.0		124	0	1.5
3.167		125	0	1.6

Test Results

The results of the four impact tests are shown in Table 37 and Figs. 59-74. For each test the results obtained include the deceleration-time curve, velocity-time curve, displacement-time curve, and the load-deflection curve. Table 37 presents a comparison of the ultimate lateral load, dissipated energy and the impact velocity for all four tests. Sequential photographs of each test are presented in Appendix IV.

The wood post in test C1 broke upon impact with the cart. The post, however, had no visible signs of defects or cracks before the test. The maximum lateral load carried by the post was 13.3 kips. However, the wood post used in test C3 carried a lateral laod of 16.3 kips without breaking. Thus, due to the nonhomogenity of wood, the strength of the timber posts varies significantly. Since the post in test C1 broke during impact, a comparison of the steel and timber post in the cohesionless soil is not possible.

In the cohesive soil, the steel post (test C4) performed similar to the timber post (test C3). The maximum lateral load carried by the steel post was 4% higher than the maximum lateral load carried by the timber post. The total energy dissipated by the steel post also exceeded the total energy dissipated by the wood post by 10%. Thus, based on the lateral load

Table 37. Summary of Results: Dynamic Tests

Test No.	Impact Velocity (ft/sec)	Maximum Force (kips)	Energy After 18 in. (ft-kip)	Total Energy (ft-kip)
C1**	26.6	13.3	-	1.3
C2	26.1	22.4	22.4	29.2
C3	22.7	16.3	19.2	27.2
C4	24.1	17.0	17.1	29.9

** Post broke during impact.

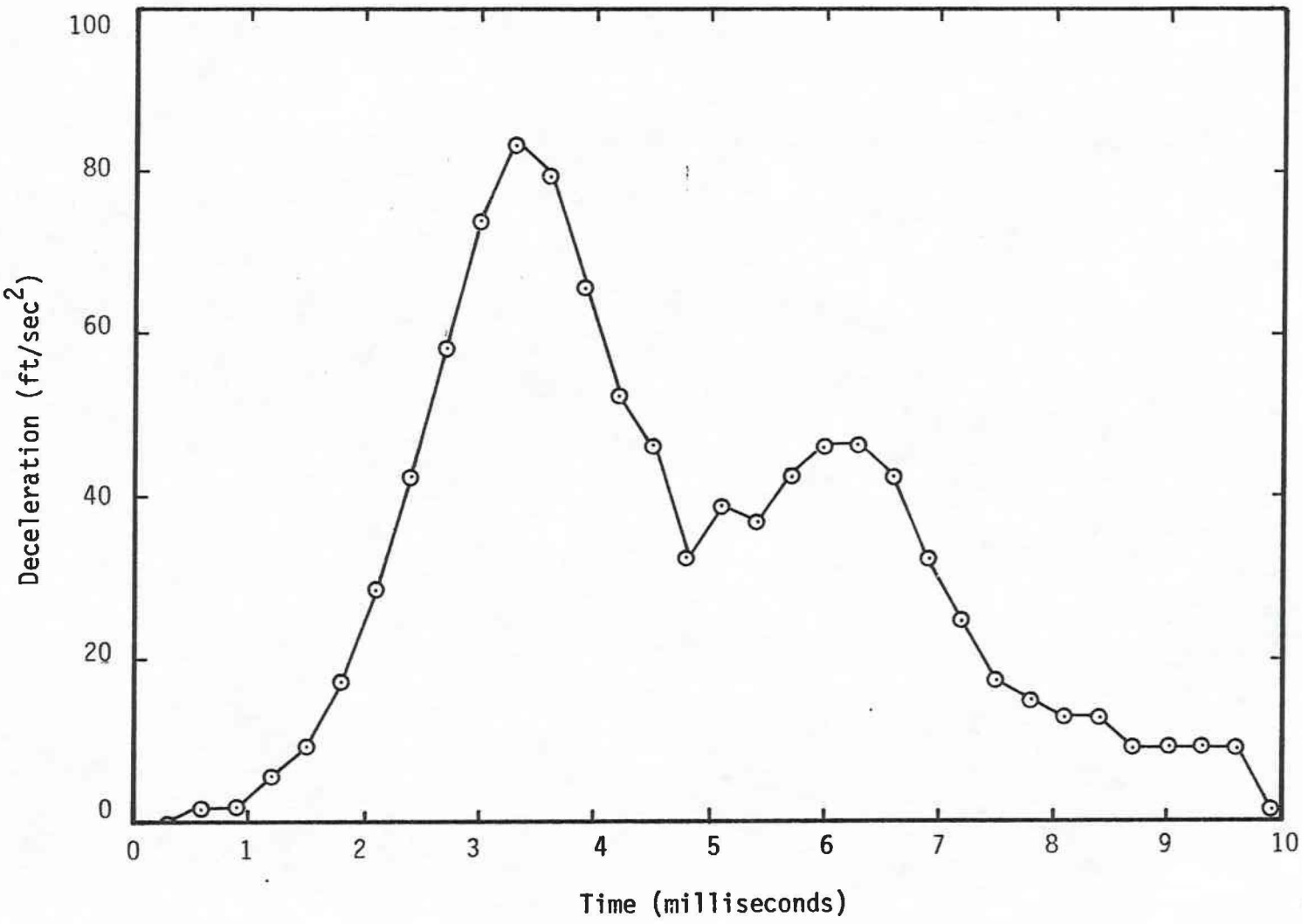

FIG. 59.-Cart Deceleration Versus Time for Test C1

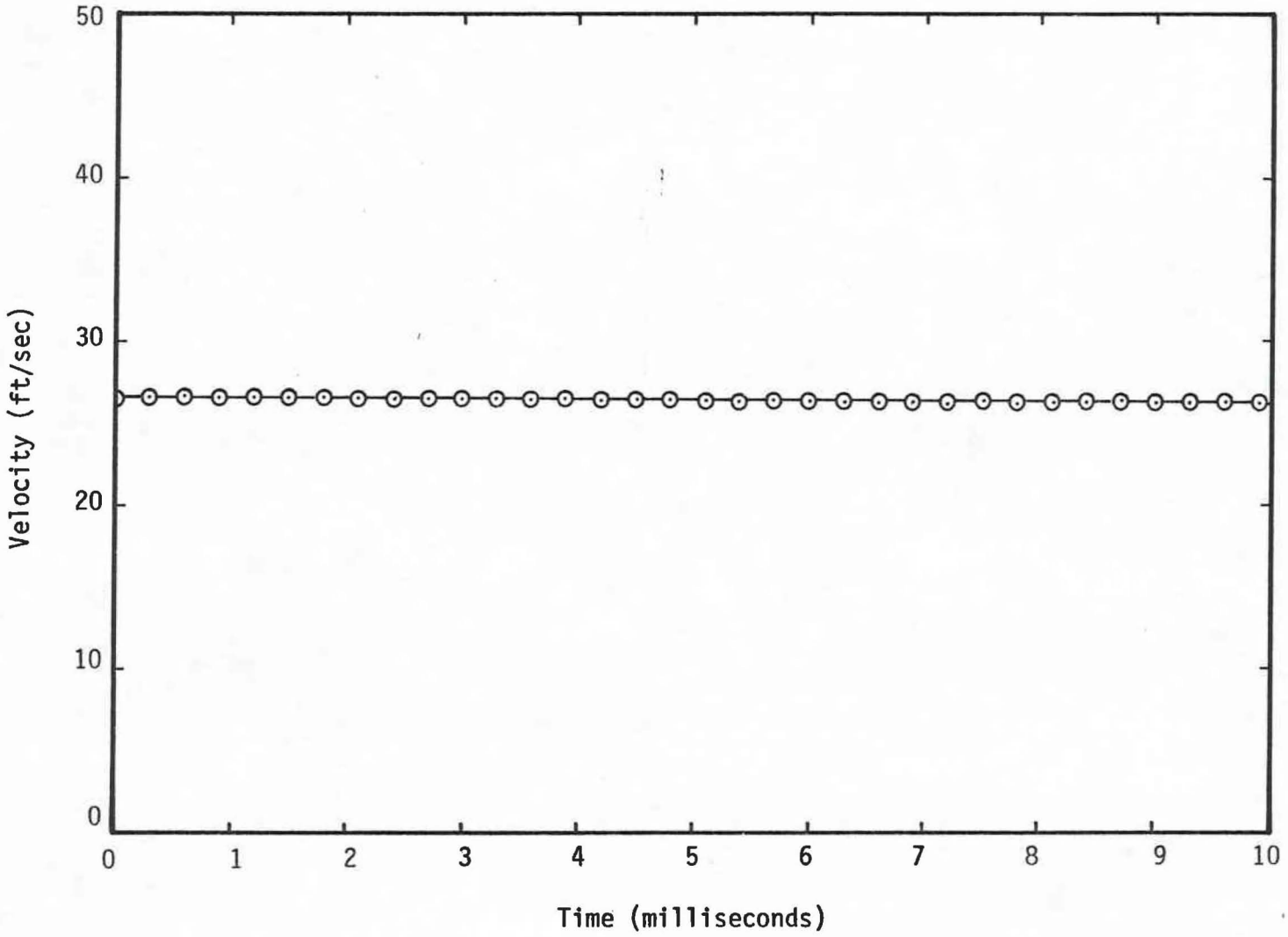

FIG. 60.-Cart Velocity Versus Time for Test C1

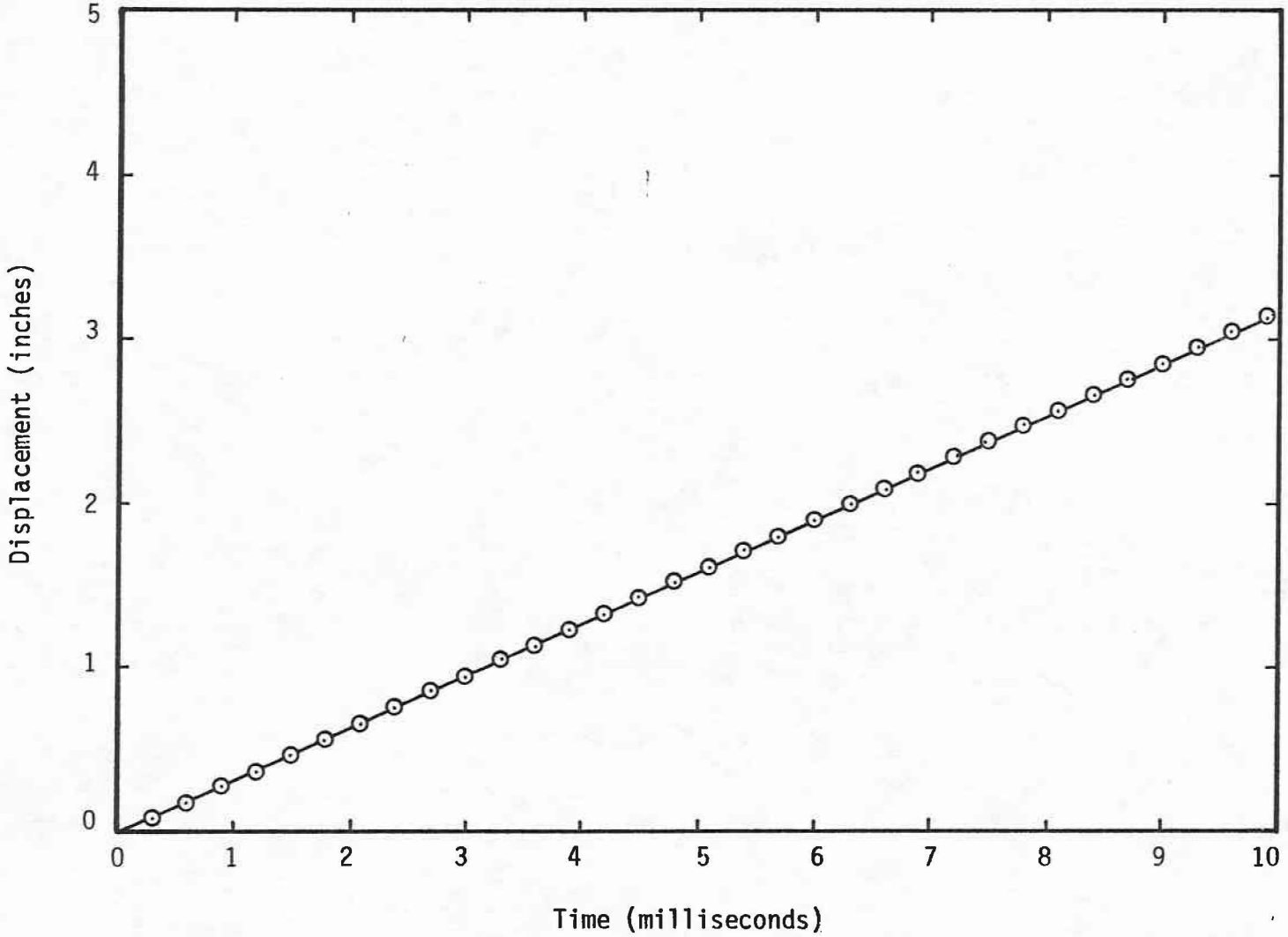

FIG. 61.-Cart Displacement Versus Time for Test C1

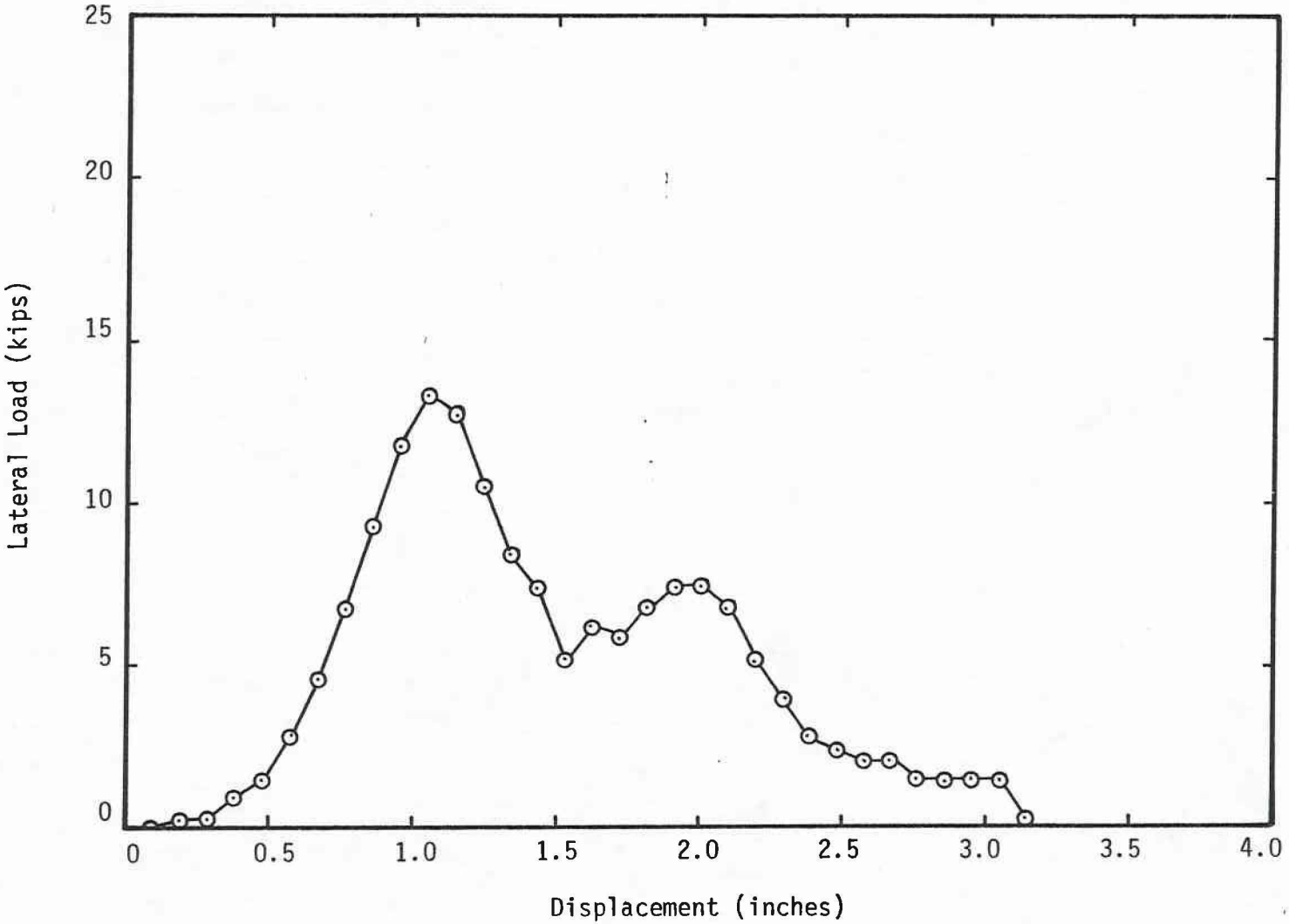

FIG. 62.-Lateral Load Versus Post Displacement for Test C1

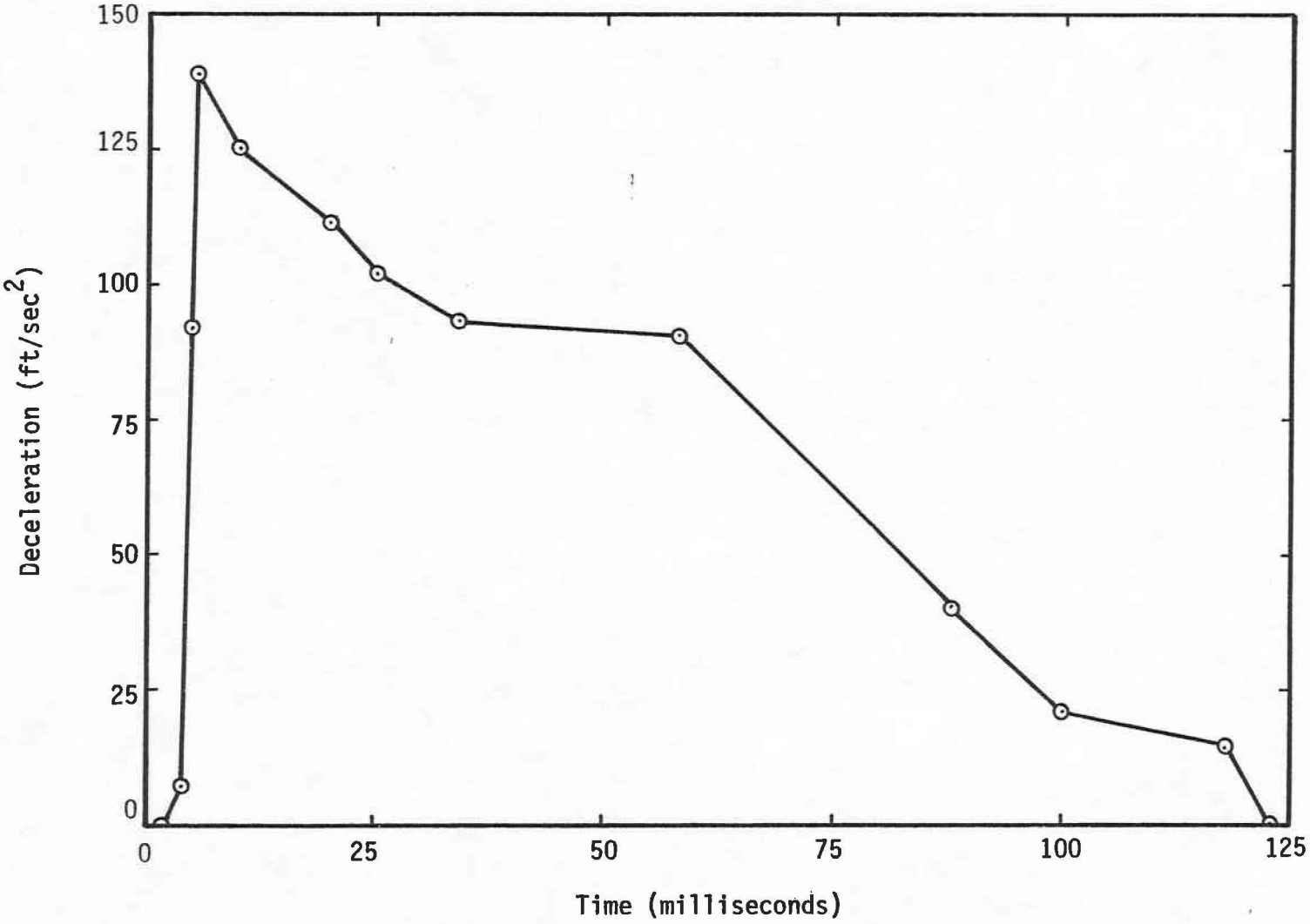

FIG. 63.-Cart Deceleration Versus Time for Test C2

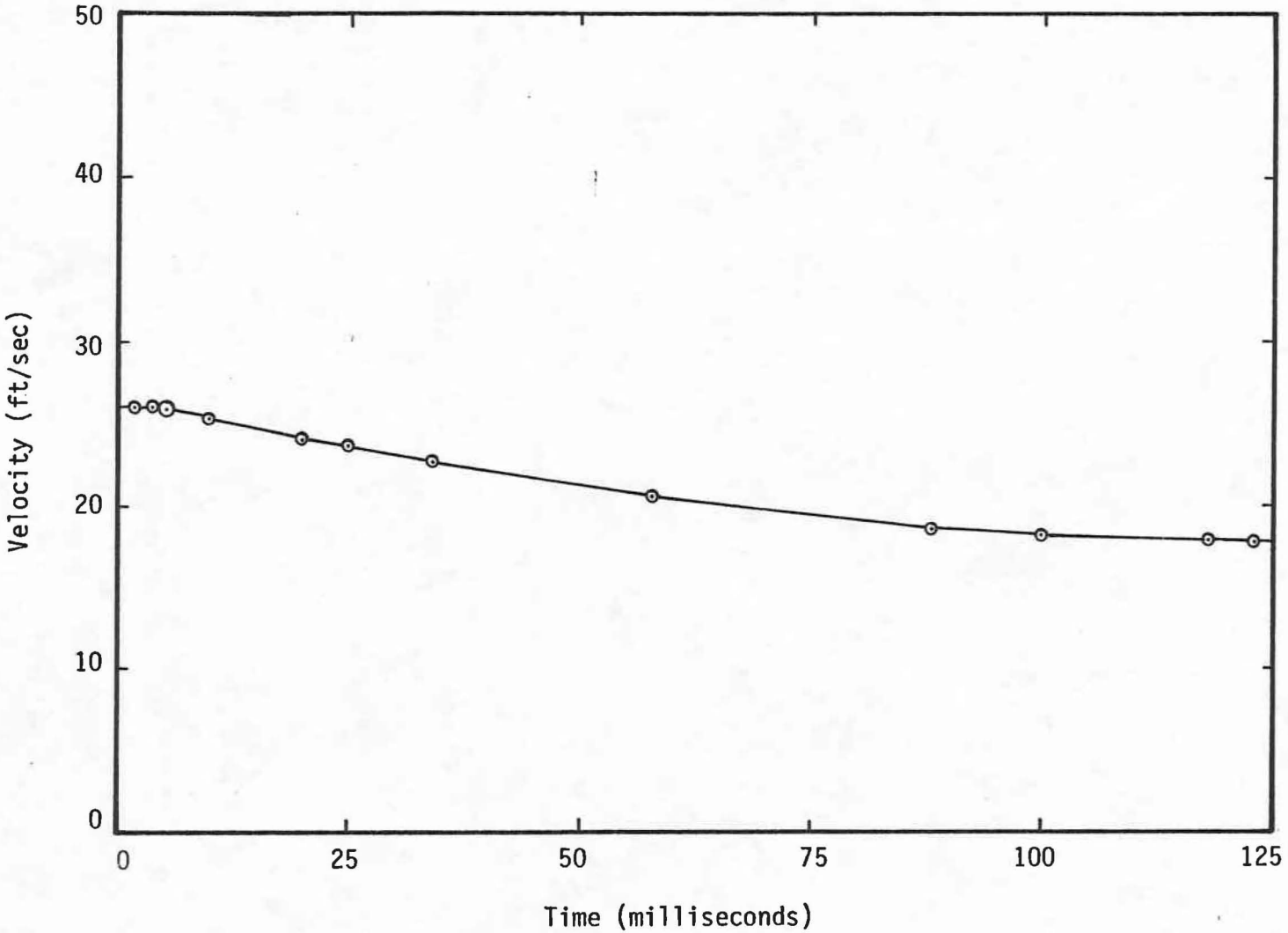

FIG. 64-Cart Velocity Versus Time for Test C2

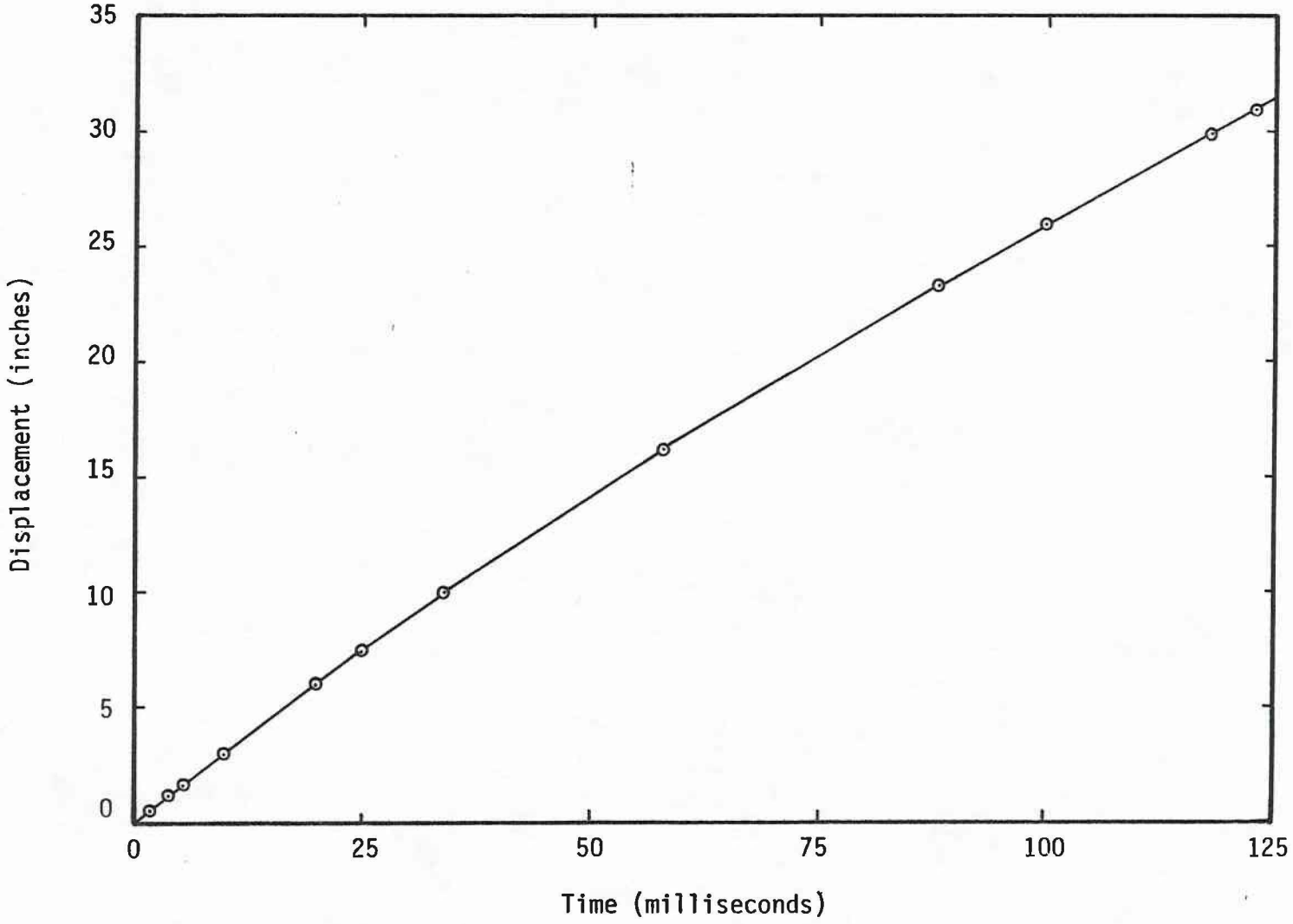

FIG. 65.-Cart Displacement Versus Time for Test C2

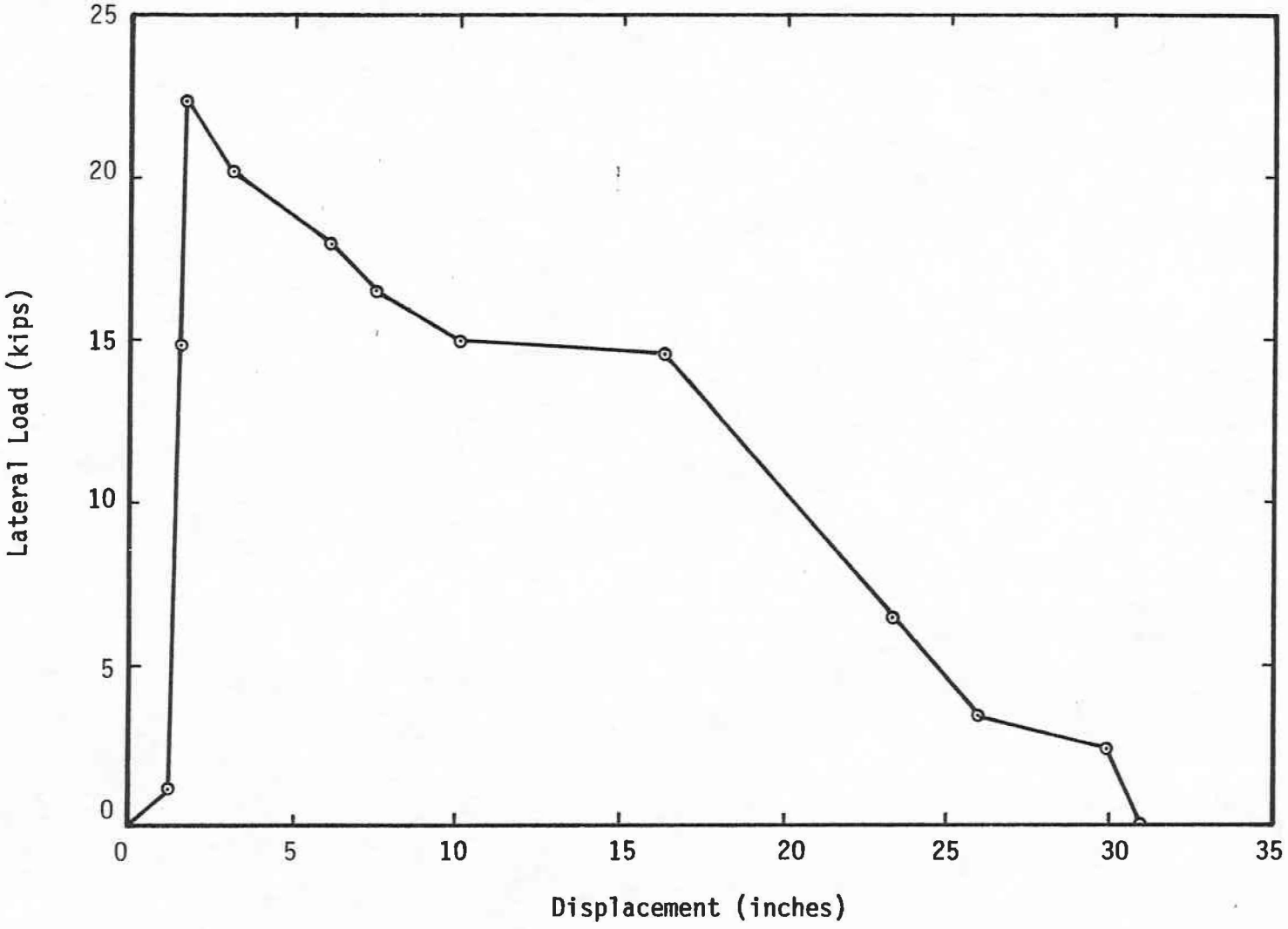

FIG. 66.-Lateral Load Versus Post Displacement for Test C2

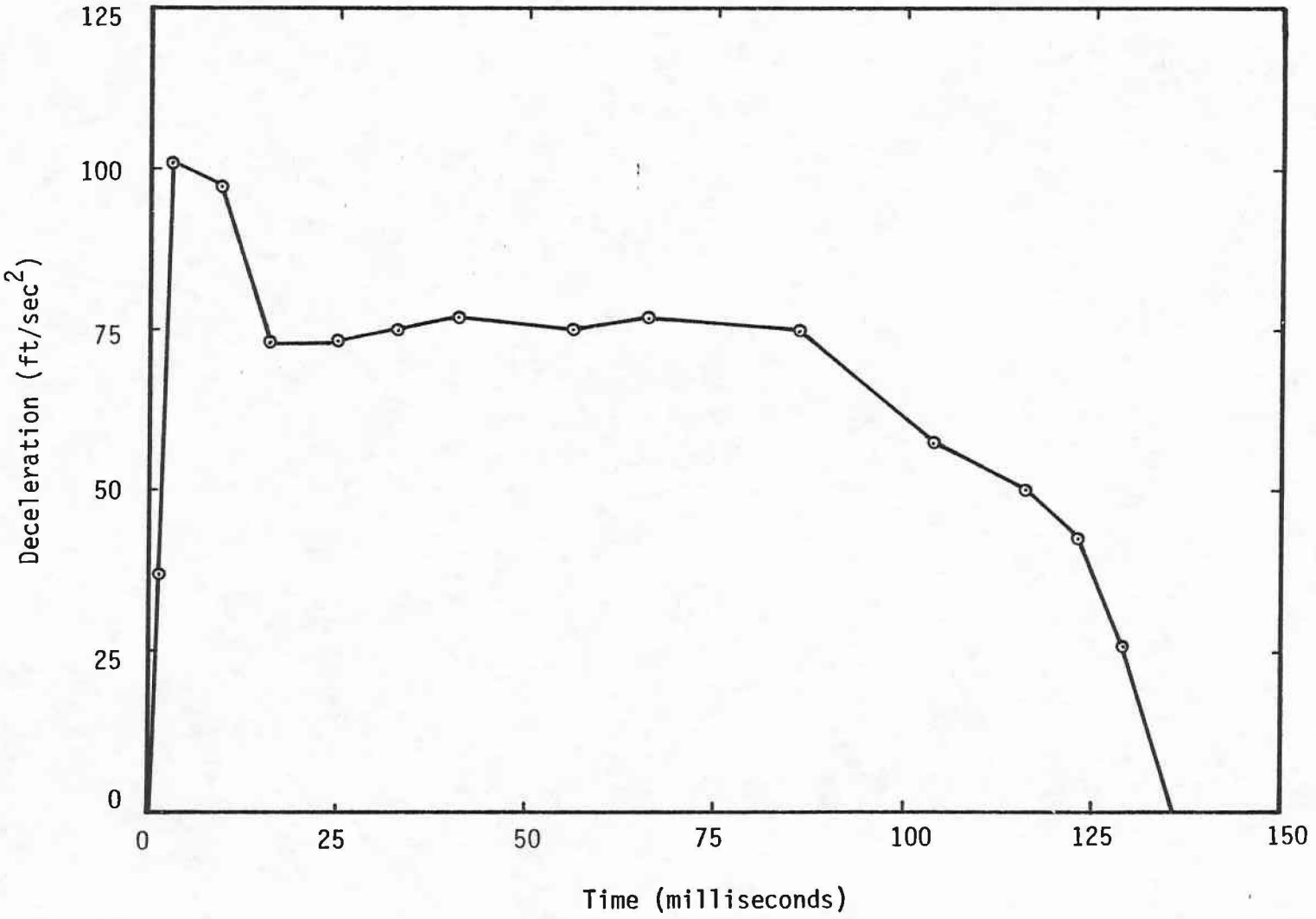

FIG. 67.-Cart Deceleration Versus Time for Test C3

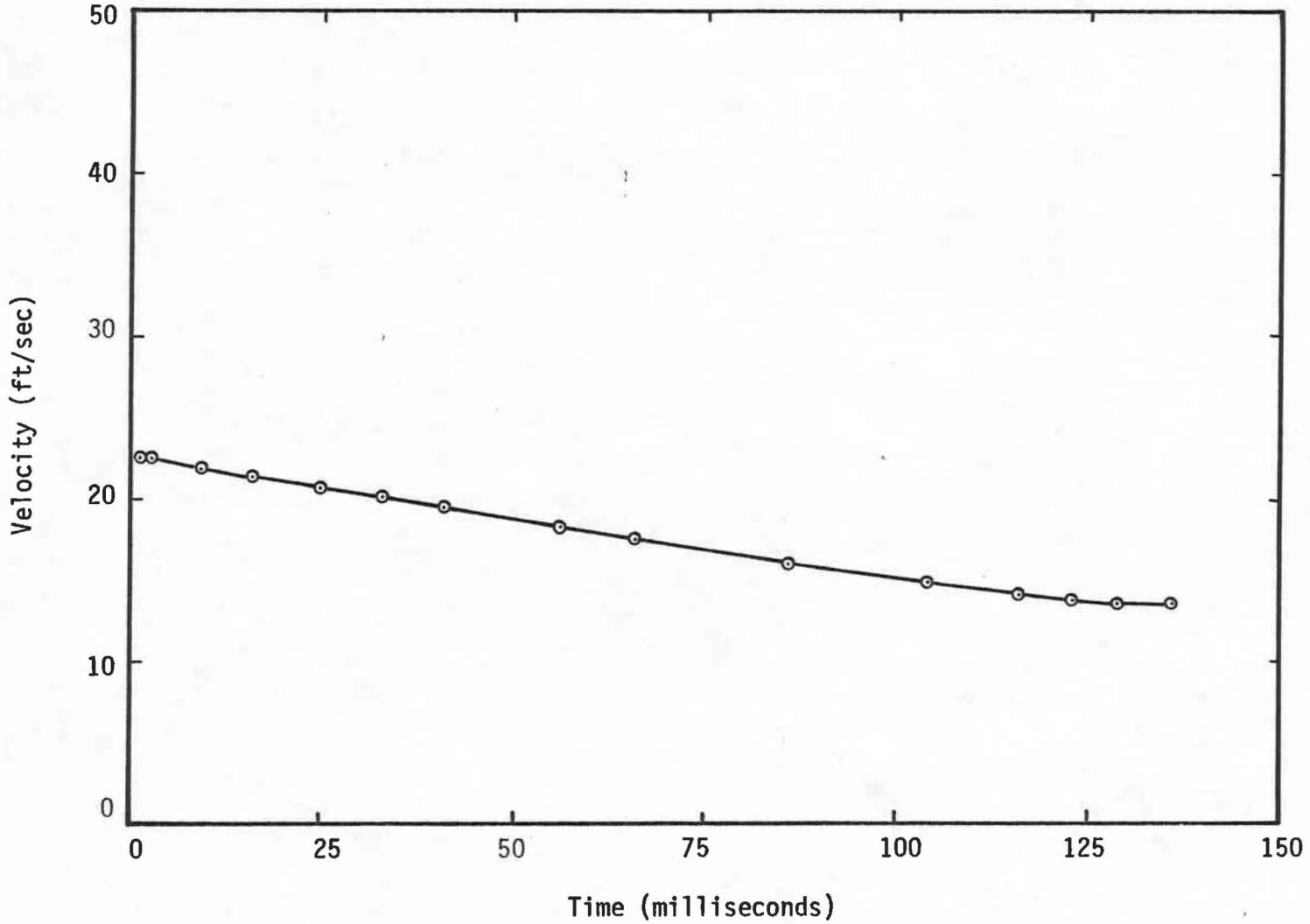

FIG. 68.-Cart Velocity Versus Time for Test C3

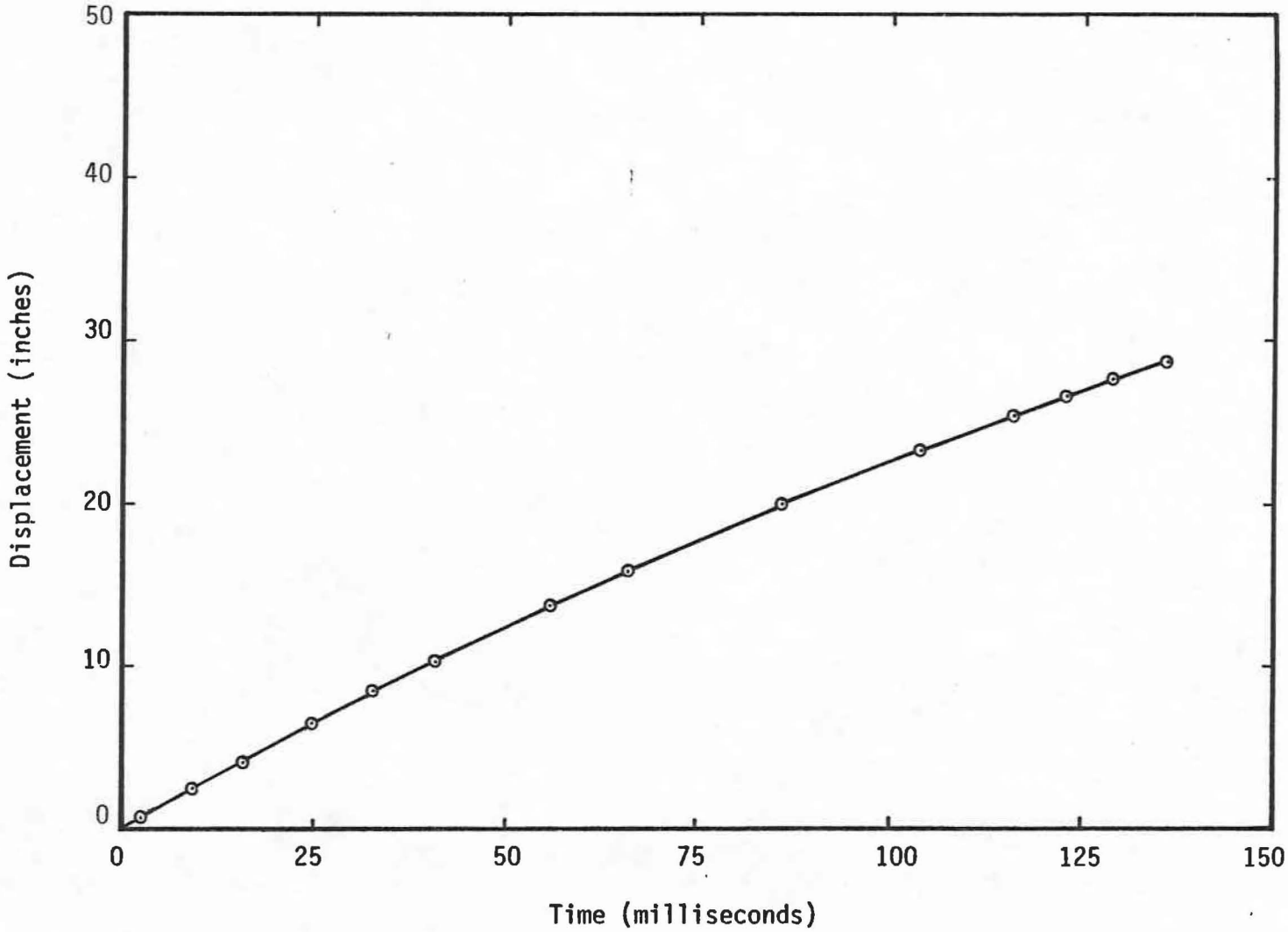

FIG. 69.-Cart Displacement Versus Time for Test C3

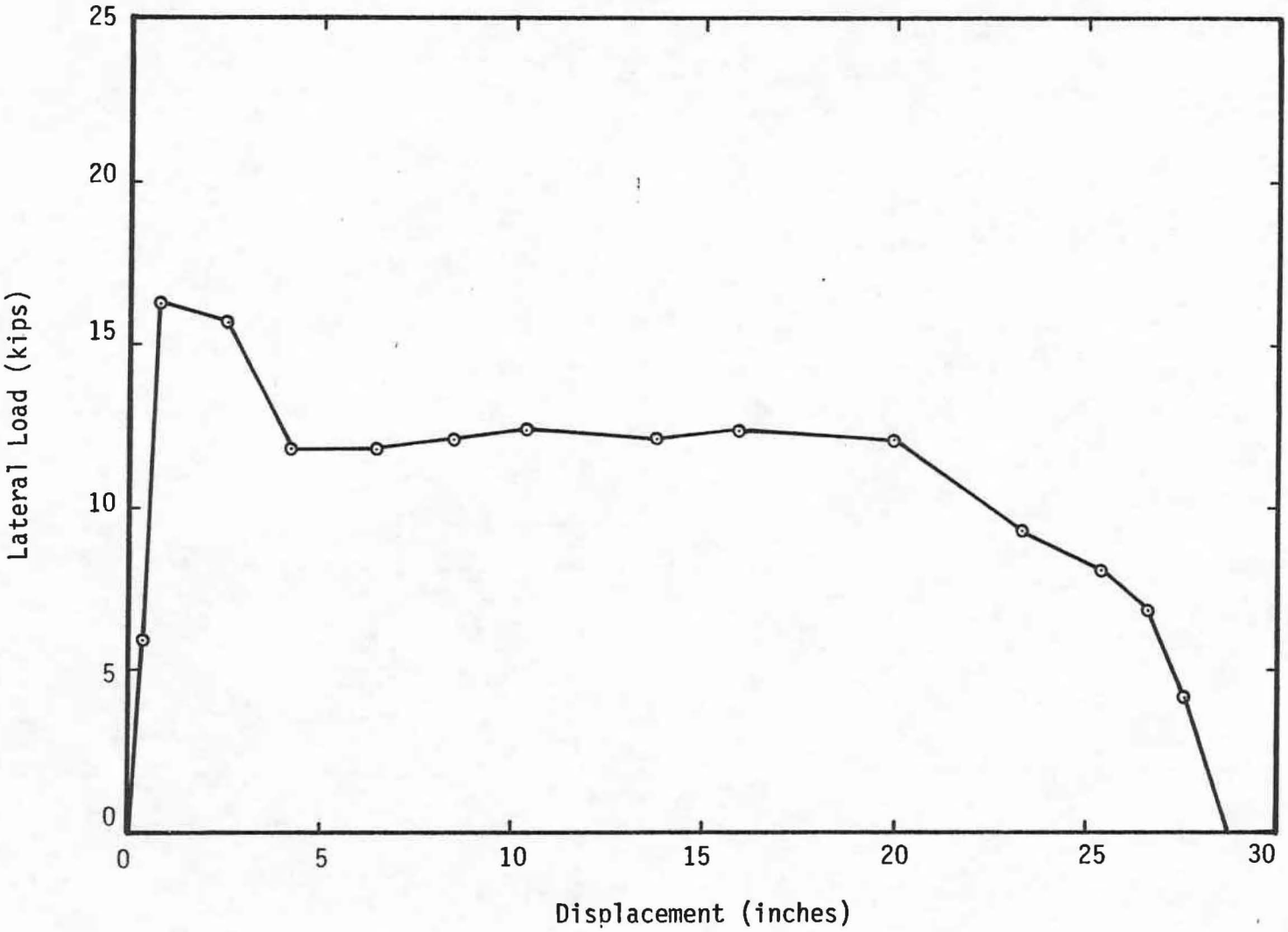

FIG. 70.-Lateral Load Versus Post Displacement for Test C3

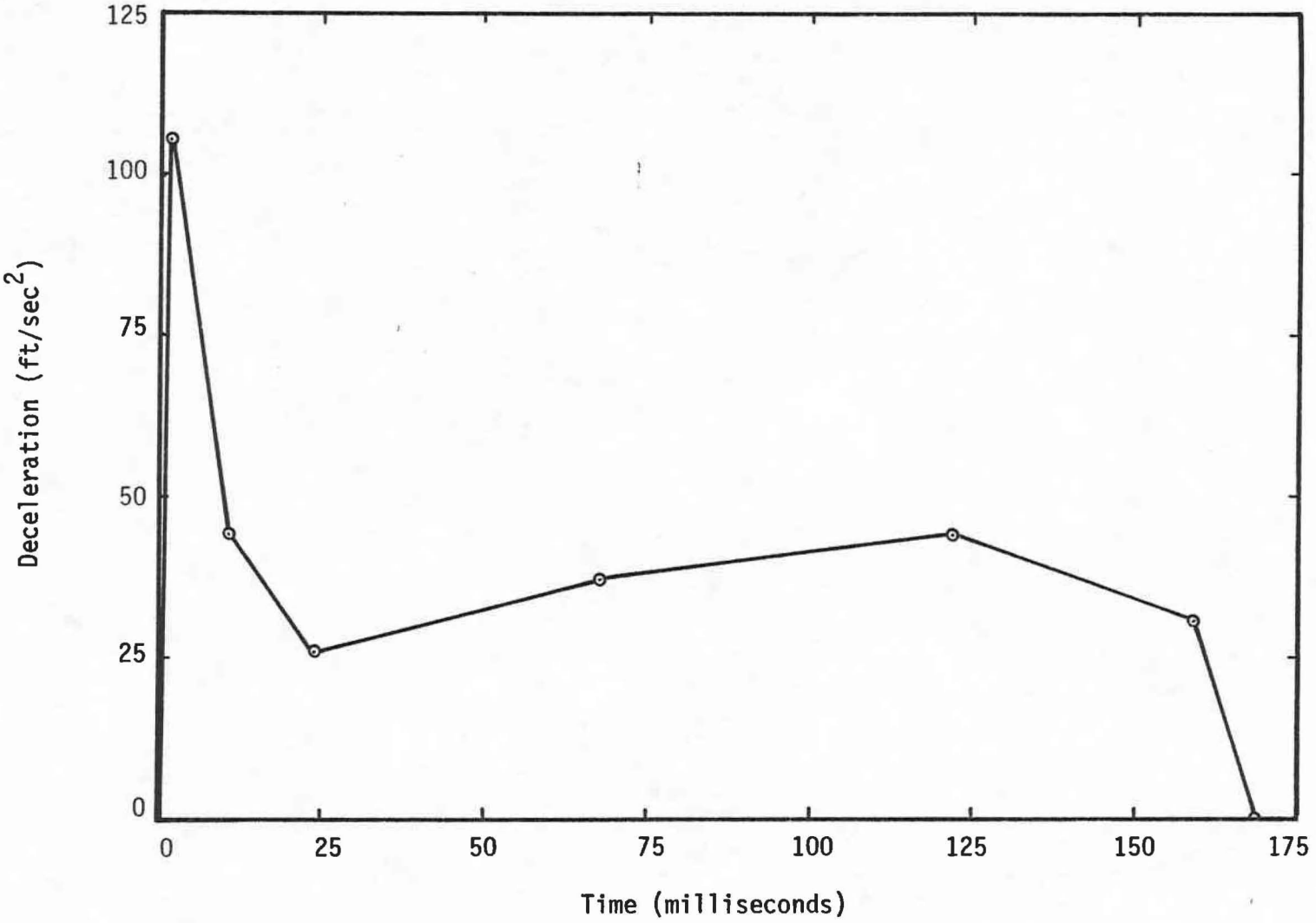

FIG. 71.-Cart Deceleration Versus Time for Test C4

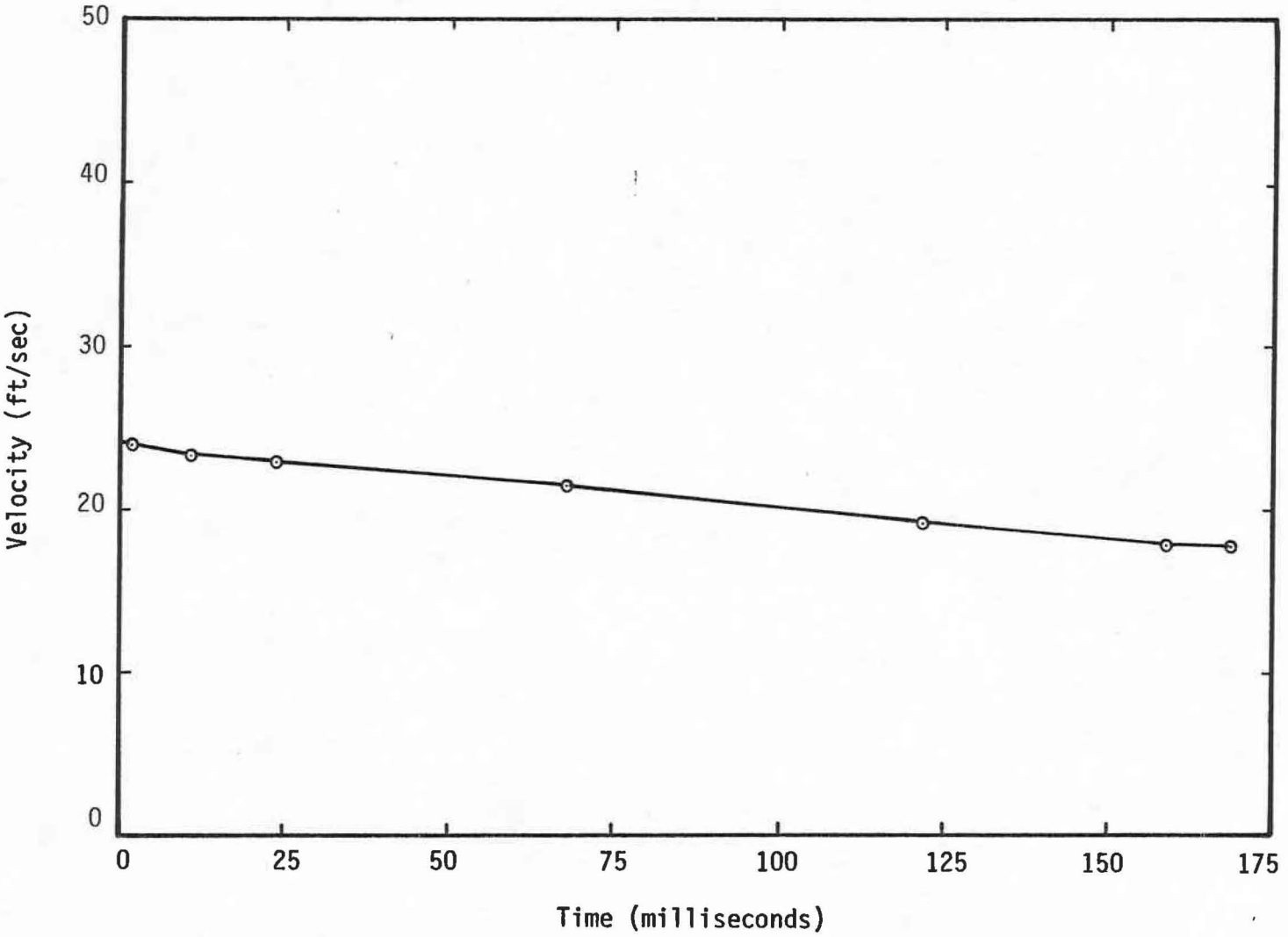

FIG. 72.-Cart Velocity Versus Time for Test C4

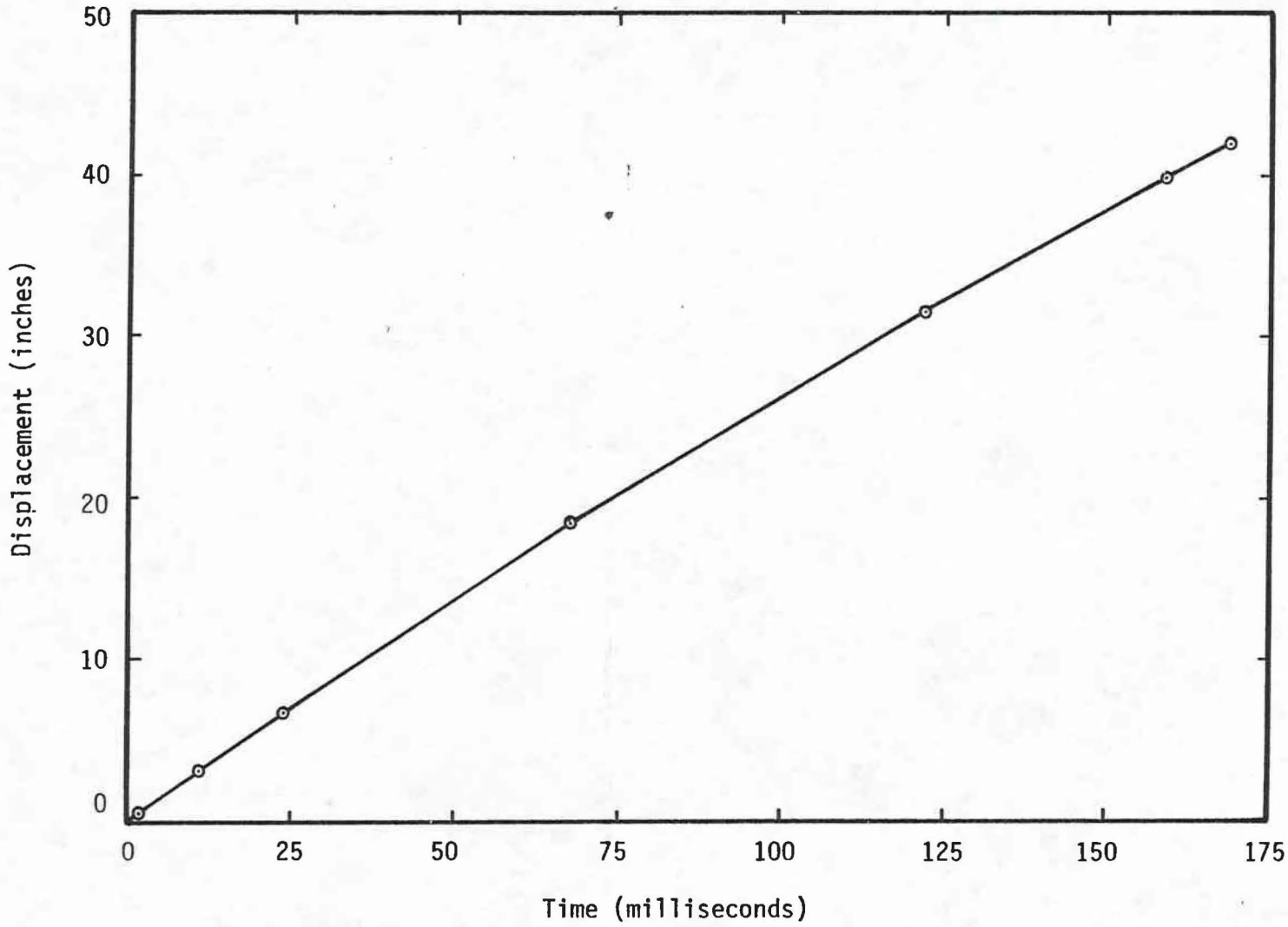

FIG. 73.-Cart Displacement Versus Time for Test C4

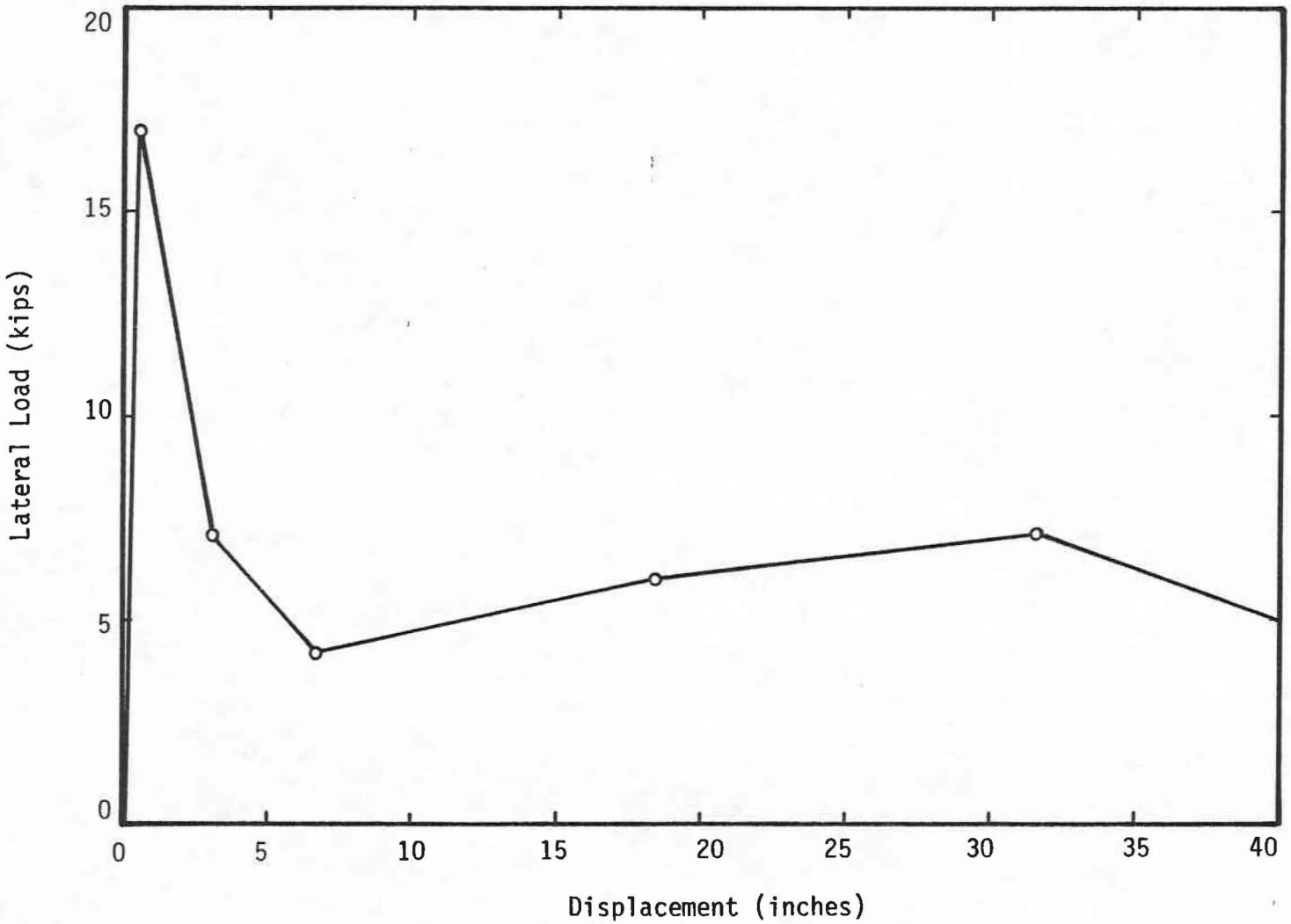

FIG. 74.-Lateral Load Versus Post Displacement for Test C4

capacity and the total dissipated energy, the performance of the steel guardrail post actually exceeded the performance of the timber post.

Comparison of Test Results With Theoretical Predictions

The parameters and the data needed for the theoretical analysis of the impact tests are listed in Tables 38 to 40. Since the wood post broke during impact in test C1, a theoretical analysis was not performed. The analytical predictions obtained using the computer program LATPIL are shown in Figs. 75 to 77 with the field load test results.

Since the viscosity of the soil cannot be determined easily, a range of values were used to obtain the analytical predictions. The range of viscosity values used for each of the tests was selected in order to bracket the field load test results.

As shown in Fig. 75, for test C2 the predicted load-deflection curves closely follow the field load test results. However, for the tests performed in the cohesive soil the analytical predictions do not compare well with the results from the field load test.

For test C3, the shape of the predicted load deflection curves closely resemble the shape of the load-deflection curve from the field load test, but the analysis underpredicts the lateral load capacity. For

Table 38 Input Data for Post C2.

Pile Properties

Dimensions: 3.74 in. x 5.83 in.

Embedment = 38 in.

No. of Increments = 20

Height of Load = 1.75 ft

Flexural Stiffness = 3.303×10^6 lb-ft^2

Effective Pile Weight = 70 lbs

Soil Properties

Layer	ϕ (deg.)	δ (deg.)	c_u (ksf)	Unit Weight (pcf)	Depth (ft)	$\frac{X_p}{R}$	$\frac{X_a}{R}$	K_o	α	μ $\frac{\text{(lb-sec)}}{\text{ft}^2}$
1	52	22	0	115	0.5	0.01	0.0005	0.257	1.0	50-150
2	52	22	0	115	1.0	0.01	0.0005	0.257	1.0	50-150
3	51.4	22	0	115	1.5	0.01	0.0005	0.264	1.0	50-150
4	50.5	22	0	115	2.0	0.01	0.0005	0.275	1.0	50-150
5	49.3	22	0	115	3.167	0.01	0.0005	0.289	1.0	50-150

Surface surcharge = 0.0

Tension cutoff = 1

Tolerance = 0.001

Table 39 Input Data for Post C3.

Pile Properties

Dimensions: 7 in. diameter

Embedment = 38 in.

No. of Increments = 20

Height of Load = 1.75 ft

Flexural Stiffness = 3.303×10^6 lb-ft^2

Effective Pile Weight = 55 lbs

Soil Properties

Layer	ϕ (deg.)	δ (deg.)	c_u (ksf)	Unit Weight (pcf)	Depth (ft)	$\frac{X_p}{R}$	$\frac{X_a}{R}$	K_o	α	μ $\left(\frac{\text{lb-sec}}{\text{ft}^2}\right)$
1	-	22	3200	120	0.5	0.07	0.01	1.0	1.0	100-1000
2	-	22	2500	120	1.0	0.07	0.01	1.0	1.0	100-1000
3	-	22	1400	120	1.5	0.07	0.01	1.0	1.0	100-1000
4	-	22	1600	120	2.0	0.07	0.01	1.0	1.0	100-1000
5	-	22	2000	120	3.167	0.07	0.01	1.0	1.0	100-1000

Surface surcharge = 0.0

Tension cutoff = 1

Tolerance = 0.001

Table 40 Input Data for Post C4.

Pile Properties

Dimensions: 3.94 in. x 5.83 in.

Embedment = 38 in.

No. of Increments = 20

Height of Load = 1.75 ft

Flexural Stiffness = 3.303×10^6 lb-ft^2

Effective Pile Weight = 70 lbs

Soil Properties

Layer	ϕ (deg.)	δ (deg.)	c_u (ksf)	Unit Weight (pcf)	Depth (ft)	$\frac{X_p}{R}$	$\frac{X_a}{R}$	K_o	α	μ $\frac{\text{(lb-sec)}}{\text{ft}^2}$
1	-	22	2000	120	0.5	0.07	0.01	1.0	1.0	50-125
2	-	22	1600	120	1.0	0.07	0.01	1.0	1.0	50-125
3	-	22	1400	120	1.5	0.07	0.01	1.0	1.0	50-125
4	-	22	1500	120	2.0	0.07	0.01	1.0	1.0	50-125
5	-	22	1600	120	3.167	0.07	0.01	1.0	1.0	50-125

Surface surcharge = 0

Tension cutoff = 1

Tolerance = 0.001

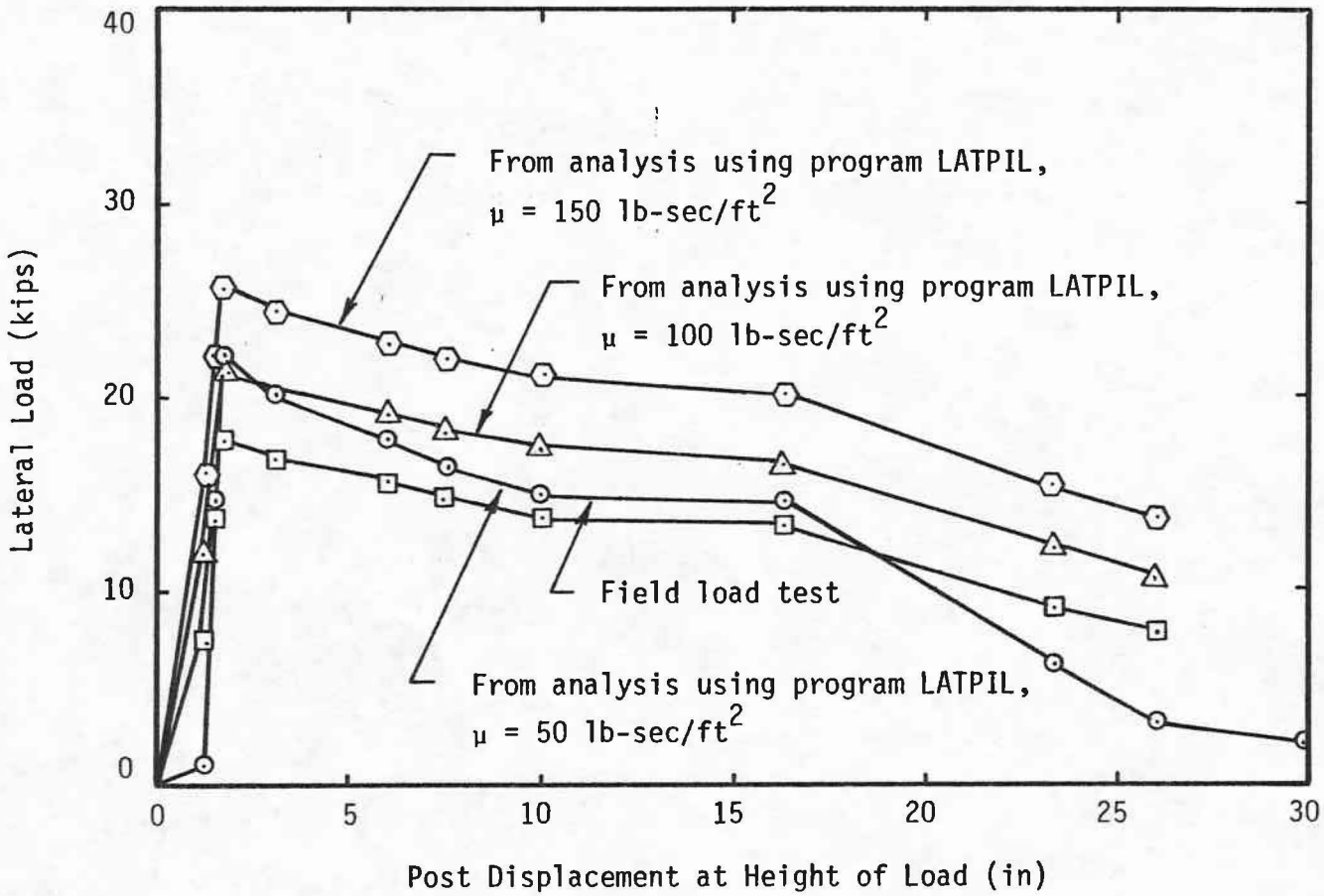

FIG. 75.-Comparison of Analysis and Field Load Test Results for Test C2

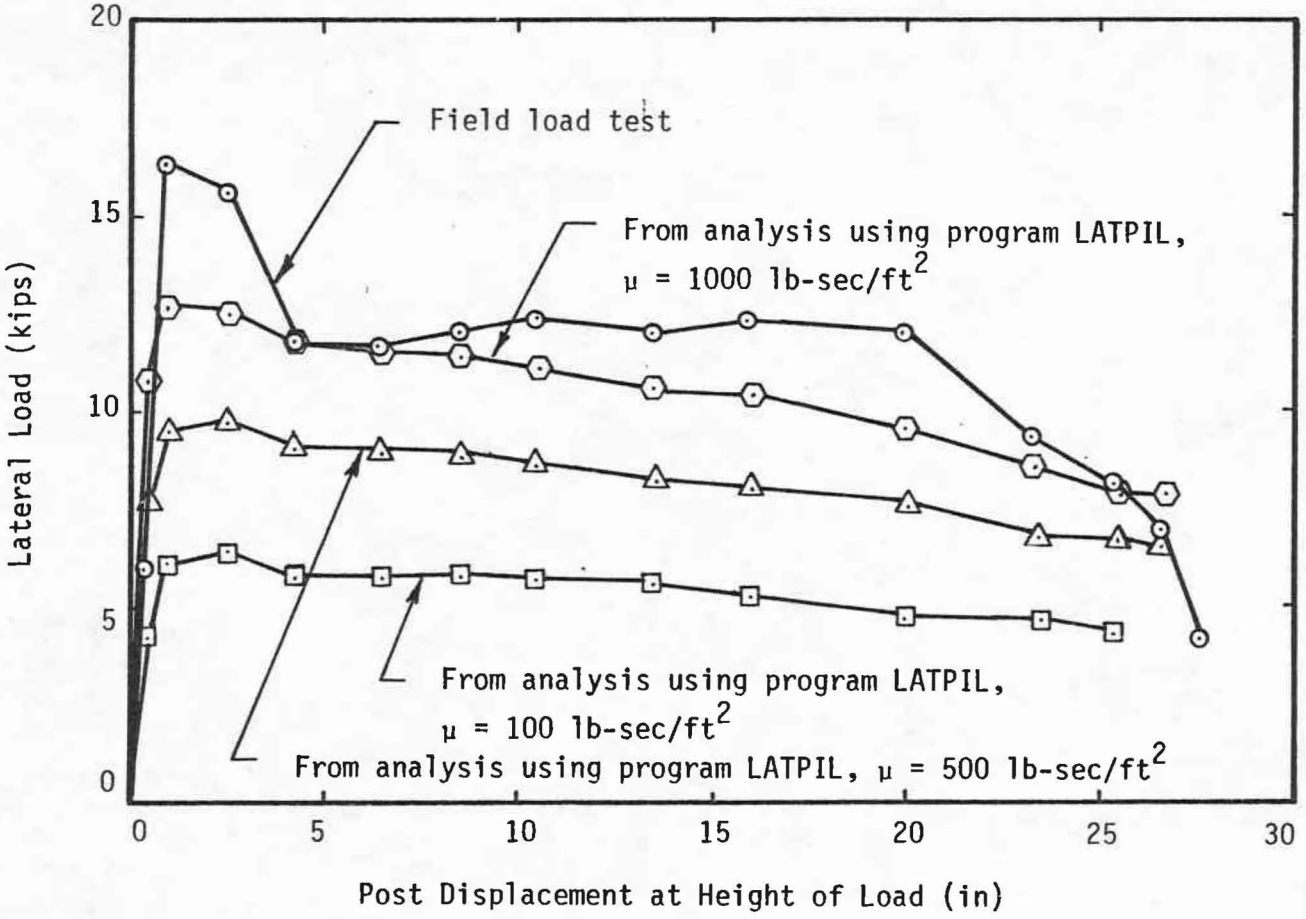

FIG. 76.-Comparison of Analysis and Field Test Results for Test C3

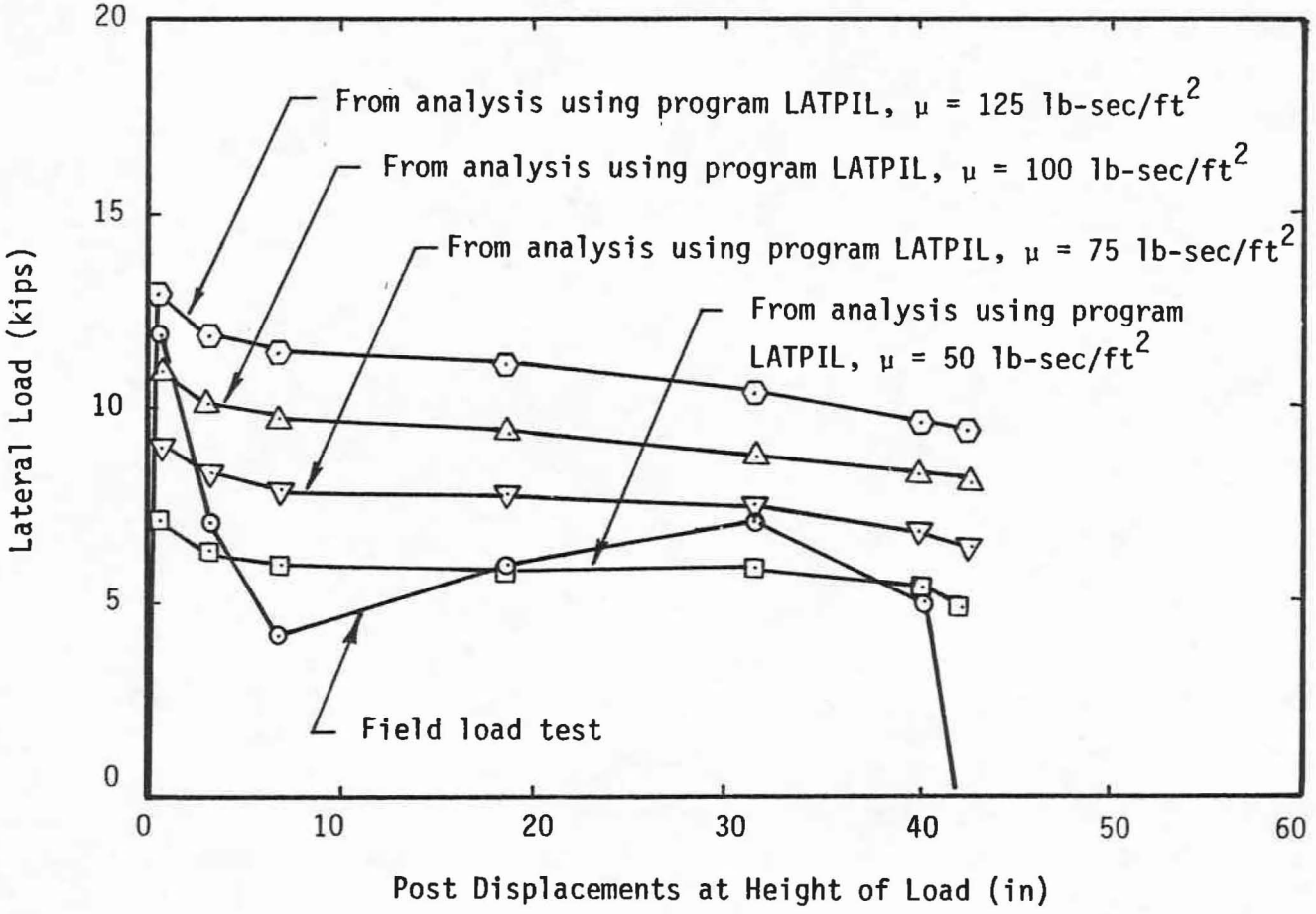

FIG. 77.-Comparison of Analysis and Field Test Results for Test C4

test C4, the shape of the predicted load-deflection curves are similar to the shape of the predicted load-deflection curves for test C3. However, the predicted load-deflection curves do not resemble the field load test curve. The predicted lateral loads agree well with the field load test results.

The results of these comparisons suggest the following reasons for the discrepancies between the analytical predictions and the field load test results for the posts in the cohesive soil:

1. Effective shear strength parameters, ϕ' and c', are required to define the failure zone as shown in Figs. 15 and 16. The shear strength parameters measured in the laboratory and used in the analysis were the undrained shear strength parameters.
2. Since the analytic1 prediction underpredicts the field test results for test C3, the drag coefficients used for the circular shafts are conservative.
3. The field test results for test C4 are not consistent with the results obtained from the other tests. The decrease in the lateral load at 7 inches of movement and the subsequent increase in the lateral load indicates that there is some error in the test results.

To determine the effect of these possible errors on the results of the analytical predictions, a parameter study was conducted by changing the value of the effective angle of friction, ϕ'. For both tests C3 and C4, the soil is assumed to be normally consolidated, thus having no effective cohesion. For each value assumed, an analytical predicton was obtained. The results of this study are shown in Figs. 78 and 79.

From the results of this parameter study, it is concluded that the analytical model is somewhat sensitive to the effective angle of internal friction. Although a wide range of values for ϕ' were used the analytical predictions for test C3 are still conservative. Thus, the drag coefficients used in the analytical model for circular piles must be conservative. For test C4, the analytical predictions were less sensitive to the angle of internal friction, because the load capacity is greater than that of test C3.

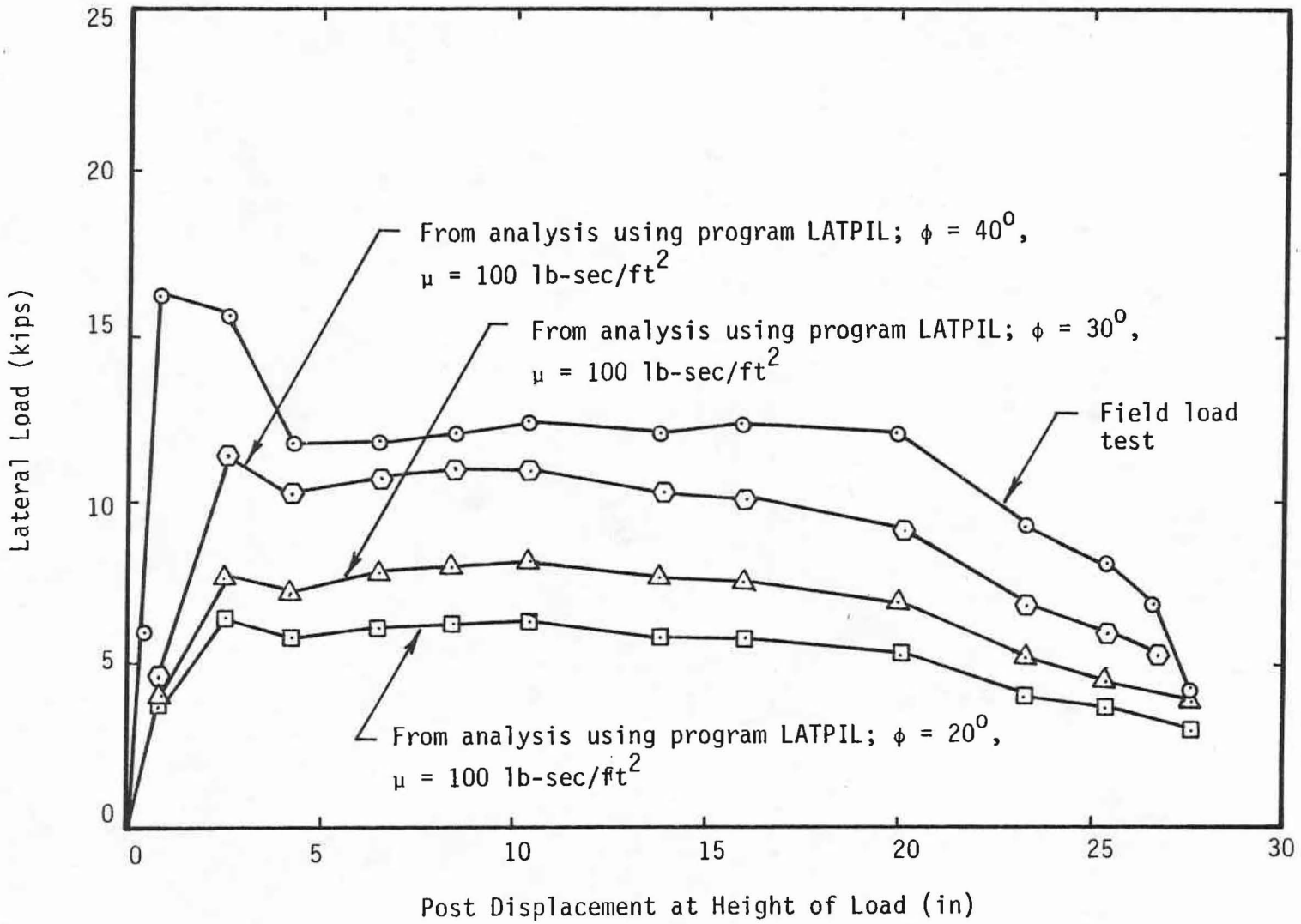

FIG. 78.-Effect of Effective Angle of Friction on Analytical Predictions for Test C3

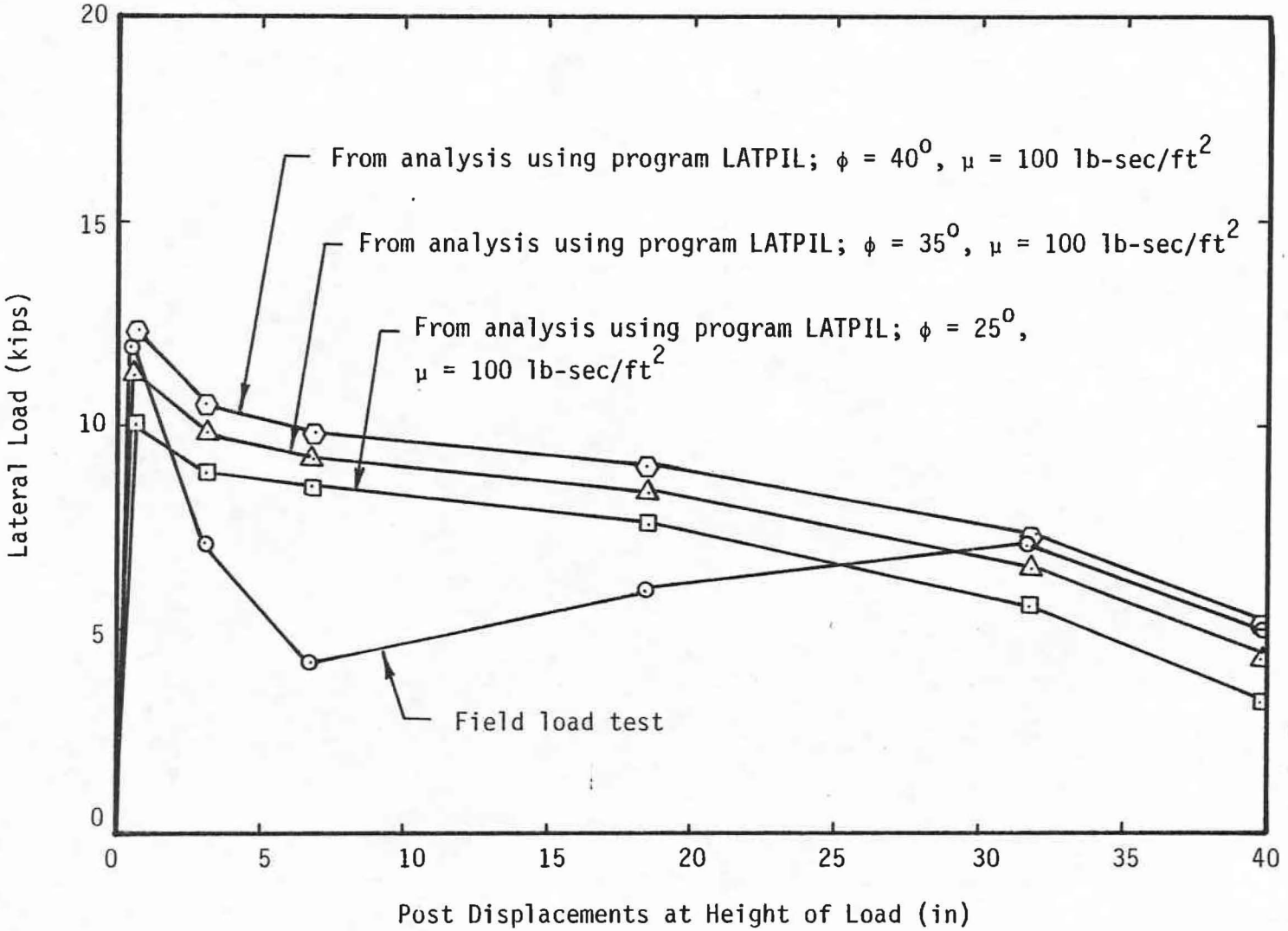

FIG. 79.-Effect of Effective Angle of Friction on Analytical Predictions for Test C4

CONCLUSIONS AND RECOMMENDATIONS

Introduction

In this chapter, the conclusions drawn from this research study are summarized, and the recommendations for further research are discussed.

Conclusions

The conclusions that can be drawn from this research study are as follows:

1. The analytical model developed during this research study can be used for the analysis of laterally loaded piles or drilled piers. The comparison of test results with the analytical predictions indicate that the analysis procedure developed are reliable for statically loaded drilled piers.
2. The static guardrail post tests conducted as part of this research study indicate that the steel guardrail posts embedded 38 inches without a concrete footing performed similar to the timber post embedded 38 inches.
3. Comparisons of the static field test results with the analytical predictions indicate that the analytical model provides a useful means for predicting the response of guardrail posts to static loads.

4. The dynamic guardrail post tests conducted as part of this research study showed that the steel guardrail post embedded 38 inches without a concrete footing performed similar to the timber post embedded 38 inches. Thus, based on the results of both the static and dynamic field tests, the steel guardrail post embedded without a concrete footing performs satisfactorily as a traffic barrier system.
5. Comparisons of the dynamic field test results with the analytical model appears to provide a useful means for predicting the response of guardrail posts to dynamic loads. However, the analytical model is sensitive to the soil viscosity.
6. It should be emphasized however, that the above results and conclusions are based on limited number of tests performed in the field on the steel and timber posts. Due to the limited time and the resources available to the authors, repeatability of the test results was never verified. Therefore, it is essential that the above statements are applied to state standards and specifications with caution and additional tests be performed in the future to check the repeatability of the above results.

Recommendations for Further Research

The following areas are recommended for further research:

1. The conclusions drawn from this research study were

based on a limited number of load tests conducted on the steel and timber guardrail posts embedded in two different soils. To further support the findings of this study, additional load tests should be conducted in various soils which are used as backfill materials around guardrail posts by the highway departments.

2. To better understand the dynamic behavior of guardrail posts under lateral loads, additional dynamic field load tests should be performed. Guardrail posts could be instrumented to measure accelerations and stress distributions along the post. The tests should be conducted in various types of backfill materials.
3. Since the dynamic behavior of the soil is significantly influenced by the viscosity of the soil, a study to develop a procedure to determine soil viscosity is also desirable.
4. In addition, the computer program LATPIL can be modified to compute the load-deflection curve without the acceleration and the velocity data as input.

APPENDIX I.-REFERENCES

APPENDIX I.-REFERENCES

1. Adams, J. I., and Radhakrishna, H. S., "The Lateral Capacity of Deep Augered Footings," Proceedings of 8th Conference on Soil Mechanics and Foundation Engineering, Moscow, 1973, ISSMFE, Vol. 2.1, pp. 1-8.
2. Baguelin, F., Frank R., and Said, Y. H., "Theoretical Study of Lateral Reaction Mechanism of Piles," Geotechnique, Vol. 27, No. 3, November 1977, pp. 405-434.
3. Baguelin, F., Jezequel, J. F., and Shields, D., The Pressuremeter and Foundation Engineering, Aedermannsdorf, Switzerland, Trans Tech Publications, 1978.
4. Bhushan, K., Haley, S. C., and Fong, P. T., "Lateral Load Tests on Drilled Piers in Stiff Clays," Journal of the Geotechnical Engineering Division, ASCE, Vol. 105, No. GT8, August 1979, pp. 969-985.
5. Bowles, J. E., Foundation Analysis and Design, 2nd Ed., McGraw-Hill Book Company, New York, 1977, pp. 543-550, 641-642.
6. Broms, B., "Lateral Resistance of Piles in Cohesive Soils," Journal of Soil Mechanics and Foundations Division, ASCE, Vol. 90, No. SM2, March 1964, pp. 27-63.

7. Broms, B., "Lateral Resistance of Piles in Cohesionless Soils," Journal of Soil Mechanics and Foundations Division, ASCE, Vol. 90, No. SM3, March 1964, pp. 123-156.

8. Brooker, Elmer W., and H. O. Ireland, "Earth Pressures at Rest Related to Stress History," Canadian Geotechnical Journal, Vol. 11, No. 1, 1965.

9. Coyle, H. M., Bierschwale, M. W., Bartoskewitz, R. E., "Field Tests and New Design Procedure for Laterally Loaded Drilled Shafts in Clay," Texas Transportation Institute, Research Report No. 211-3, January 1981.

10. Davidson, H. L., and Donovan, T. D., "Design Approach for Laterally Loaded Drilled Piers," Report to Pennsylvania Power and Light Company, December 1977.

11. Davidson, H. L., "Laterally Loaded Drilled Pier Research," GAI Report to Electric Power Research Institute (EPRI), January 1982.

12. Davisson, M. T., and Gill, H. L., "Laterally Loaded Piles in a Layered Soil System," Journal of Soil Mechanics and Foundations Division, ASCE, Vol. 89, No. 39, 1963, pp. 63-94.

13. Davisson, M. T., and Prakash, S., "A Review of Soil-Pole Behavior," published in Stresses in Soils and Layered Systems, Highway Research Record, No. 39,

1963, pp. 25-48.

14. DiGioia, A. M., Donovan, T. D., and Cortese, F. J., "A Multi-Layered/Pressuremeter Approach to Laterally Loaded Rigid Caisson Design," presented at seminar on Lateral Pressures Related to Large Diameter Pipes, Piles, Tunnels, and Caissons, Dayton, Ohio, February 1975, ASCE.

15. Douglas, D. J., and Davis, E. H., "The Movement of Buried Footings Due to Moment and Horizontal Load and the Movement of Anchor Plates," Geotechnique, Vol. 14, No. 2, June 1964, pp. 115-132.

16. Gambin, M., "Calculation of Foundations Subjected to Horizontal Forces Using Pressuremeter Data, "ols-Soils, No. 30/31, 1971, pp. 17-59.

17. Grandholm, H., "On the Elastic Stability of Piles Surrounded by a Supporting Medium," Handigar Ingeniors Vetenskaps Akademien, 1929, No. 89.

18. Hansen, Brinch J., "The Ultimate Resistance of Rigid Piles Against Transversal Forces," The Danish Geotechnical Institute Bulletin, No. 12, 1961, pp. 5-9.

19. Hetenyi, M., Beams on Elastic Foundation, The University of Michigan Press, Ann Arbor, Michigan, 1946, pp. 52-53.

20. Holloway, G. L., Coyle, H. M., Bartoskewitz, R. E., and Sarver, W. G., "Field Test and Preliminary

Design Method for Laterally Loaded Drilled Shafts in Clay," Research Report 211-2, Study No. 2-5-77-211, September 1978.

21. Ivey, D. L., "Theory, Resistance of a Drilled Shaft Footing to Overturning Loads," Texas Transportation Institute, Research Report No. 105-1, February 1968.

22. Ivey, D. L., Hawkins, L., "Signboard Footings to Resist Wind Load," Civil Engineering, Vol. 36, No. 12, December 1966, pp. 34-35.

23. Ivey, Don L., Koch, Kenneth J., and Raba, Carl F., Jr., "Resistance of a Drilled Shaft Footing to Overturning Loads, Model Tests and Correlation with Theory," Research Report 105-2, Texas Transportation Institute, Texas A&M University, July, 1968.

24. Kasch, V. R., Coyle, H. M., Bartoskewitz, R. E., and Sarver, W. G., "Lateral Load Test of a Drilled Shaft in Clay, "Texas Transportation Institute," Research Report 211-1, Research Study 2-5-77-211, November 1977.

25. Leps, Thomas M., "Review of Shearing Strength of Rockfill." Journal of the Soil Mechanics and Foundations Division, ASCE, Vol. 96, No. SM4, July 1970, pp. 1157-1170.

26. Matlock, H., "Correlations for Design of Laterally Loaded Piles in Soft Clay," Proceedings, 2nd Annual Offshore Technology Conference, Houston, 1970,

American Institute of Mining, Metalt., and Petroleum Engineering, pp. 577-594.

27. Matlock, H., and Reese, L. C., "Generalized Solutions for Laterally Loaded Piles," Journal of Soil Mechanics and Foundations Divison, ASCE, Vol. 86, No. SM5, October 1960, pp. 63-91.

28. Miche, Jarvis D., "Response of Guardrail Posts During Impact," Research Report No. 03-9051, Southwest Research Institute, October 1970.

29. Mindlin, R. D., "Force at a Point in the Interior of a Semi-Infinite Solid," Physics, Vol. 7, 1936, pp. 195-202.

30. Monahan, D. R., and Fiss, R. A., "Evaluation of Full-Scale Test Results of Transmission Pole Foundations," presented at IEEE Winter Meeting, New York, New York, January 29 - February 3, 1978.

31. Palmer, L. A., and Thompson, J. B., "The Earth Pressure and Deflection Along Embedded Lengths of Piles Subjected to Lateral Thrust," Proceedings, 2nd International Conference on Soil Mechanics and Foundation Engineering, Rotterdam, 1948, ISSMPE, Vol. 5, pp. 156-161.

32. Parker, F., Jr., and Reese, L. C., "Experimental and Analytical Studies of Behavior of Single Piles in Sand Under Lateral and Axial Loading," Research Report 117-2, Center for Highway Research, The

University of Texas at Austin, November 1970.

33. Poulos, H. G., "Behavior of Laterally Loaded Piles: I-Single Piles," Journal of Soil Mechanics and Foundations Division, ASCE, Vol. 97, No. SM5, May 1971, pp. 711-731.

34. Poulos, H. G., and Davis, E. H., Pile Foundation Analysis and Design, John Wiley and Sons, New York, 1980.

35. Reese, L. C., "Discussion of Soil Modulus for Laterally Loaded Piles, by McClelland, B., and Focht, J. A., Jr.," Transactions, ASCE, Vol. 123, 1958, pp. 1071-1074.

36. Reese, L. C., "Laterally Loaded Piles," Geotechnical Engineering Software Activity Center, University of Colorado, Boulder, Colorado, Report No. D-75-14, May 1975.

37. Reese, L. C., and Allen, J. D., "Structural Analysis and Design of Lateral Loading," published in Drilled Shaft Design and Construction Guidelines Manual, U. S. Department of Transportation, Vol. 1, July 1977.

38. Reese, L. C., and Matlock, H., "Nondimensionl Solutions for Laterally Loaded Piles with Soil Modulus Assumed Proportional to Depth," Proceedings, 8th Texas Conference on Soil Mechanics and Foundation Engineering, Austin, Texas, 1956.

39. Reese, L. C.,and Welch, R., "Lateral Loading of Deep Foundations in Stiff Clay," Journal of Geotechnical Division, ASCE, Vol. 101, No. GT7, July 1975, pp. 633-649.

40. Roscoe, K. H., nd Schofield, R. K., "The Stability of Short Pier Foundations in Sand," British Welding Journal, August 1956.

41. Seiler, J. F., "Effect of Depth of Embedment on Pole Stability," Wood Preserving News, Vol. 10, No. 11, November 1932, pp. 152-168.

42. Sogge, R. L., "Laterally Loaded Pile Design," Journal of Geotechnical Engineering Division, ASCE, Vol. 107, No. GT9, September, 1981, pp. 1179-1199.

43. Sowers, G. F., Introductory Soil Mechanics and Foundations: Geotechnical Engineering, Fourth Edition, MacMillan, New York, 1979, pp. 391.

44. Terzaghi, K., "Evaluation of Coefficients of Subgrade Reaction," Geotechnique, Vol. 5, 1955, pp. 297-326.

45. Thompson, G. R., "Application of the Finite Element Method to the Development of p-y Curves for Saturated Clays," M. S. Thesis, University of Texas at Austin, May 1960.

46. Vesic, A. B., "Bending of Beams Resting on Isotropic Elastic Solid," Journal of Engineering Mechanics

Division, ASCE, Vol. 87, No. EM-2, April 1961.

47. Welch, R. C., and Reese, L. C., "Lateral Load Behavior of Drilled Shafts," Center for Highway Research, The University of Texas at Austin, Research Report 89-10, May 1972.

48. Woodward, R. J., Gardner, W. S., and Greer, D. M., Drilled Pier Foundations, McGraw Hill, New York, 1972, p. 43.

APPENDIX II.-NOTATION

APPENDIX II.-NOTATION

The following symbols are used in this paper:

A = empirical coefficient in Terzaghi's equation for subgrade modulus;

$\bar{A}_b$ = area of the pier base in contact with the underlying soil;

A_p = projected area of shaft segment;

B = pile width or diameter;

B_o = reference diameter of 0.6 meters;

B_w = pile cross-section dimension;

c = cohesion of the soil;

C_D = drag coefficient;

c_u = undrained cohesive shear strength;

D = pier embedment depth;

EI_p = flexural stiffness of the pier;

E_m = initial slope of the soil stress-strain curve;

E_p = modulus of elasticity of the soil as obtained from the pressuremeter test;

E_s = modulus of elasticity of the soil;

E_{si} = initial slope of the p-y curve;

F_B = compressive force of the base of the pier;

F_{1d} = drag force on pier segment;

F_{1p} = lateral earth pressure resultant force on pier segment;

F_{ls} = lateral force resultant of the horizontal shear stresses or a pier segment;

H = height above the ground-line to the point of application of the lateral load;

h_c = critical depth for determining soil pressure from pressuremeter limit pressure;

I = moment of inertia of pier and soil about the ground-line

K_a = coefficient of active earth pressure;

K_c = earth pressure coefficient for cohesion;

K_o = coefficient of at-rest earth pressure;

K_p = coefficient of passive earth pressure;

K_q = earth pressure coefficient for overburden pressure;

k_h = lateral subgrade modulus;

k_{s1} = subgrade modulus for a one foot square plate;

L = embedment depth of the pier;

M_b = moment on base of shaft;

m = number of pier segments below the point of rotation;

n = number of pier segments above the point of rotation;

n_h = constant of horizontal subgrade modulus;

P_A = applied axial load to pier;

P_i = lateral force on pier segment i;

P_A = applied lateral load to pier;

p = soil reaction pressure (force/unit length);

p_{ult} = ultimate soil reaction pressure (force/unit length);

Q = movement required to develop ultimate skin friction;

R = depth to the point of rotation;

R_e = radius of effective soil boundary,

S_f = shape factor;

t = pier segment thickness;

V_B = shear force on base of the pier;

V_i = vertical shear force on the perimeter of a pier segment;

v = velocity of pier segment;

W = effective weight of the pier;

X_a = lateral movement required to develop ultimate active earth pressure;

X_p = lateral movement required to develop ultimate passive earth pressure;

x_i = lateral movement of pier segment i;

$\bar{x}_i$ = eccentricity of the vertical shear force relative to the shaft centerline for shaft segment i;

x_b = eccentricity of the vertical compressive force on the base relative to the centerline of the shaft;

y = lateral deflection;

y_v = vertical movement of shaft segment;

y_{50} = pier deflection at one-half of the ultimate lateral pressure;

z = depth below the ground surface;

z_c = critical depth for determining the lateral subgrade modulus from the pressuremeter limit pressure;

z_i = depth below the ground surface to the midpoint of shaft segment i;

α = angular acceleration of the pier;

$\bar{\alpha}$ = angle which defines the geometry of the failure mechanism;

α_r = shear strength reduction factor;

α' = rheological coefficient used in determining the lateral subgrade modulus from the pressuremeter limit pressure;

β = ground slope;

$\bar{\beta}$ = angle which defines the geometry of the failure mechanism used to cmpute the ultimate lateral soil pressure for clean sands;

δ = angle of friction between the shaft and the soil;

ε_{50} = strain corresponding to one-half of the maximum principal stress difference

determined from an unconsolidated, undrained triaxial compression test;

γ = total unit weight of the soil;

γ' = effective unit weight of the soil;

θ = angle of rotation of the shaft;

λ_c = reduction coefficient for the lateral subgrade modulus determined from the pressurementer limit pressure for depths less than z ;

μ = soil viscosity;

ν = Poisson's ratio for the soil;

ρ = mass density of the soil;

σ_a = active earth pressure;

σ_p = passive earth pressure;

σ_{ra} = radial active earth pressure;

σ_{rp} = radial passive earth pressure;

σ'_v = effective overburden pressure of the soil;

τ_m = maximum shear strength of the soil;

$\tau_{r\theta}$ = horizontal shear stress around circular shaft;

τ_{rz} = vertical shear stress;

τ_{zm} = maximum vertical shear stress;

ϕ = angle of internal friction of the soil.

APPENDIX III.-COMPUTER PROGRAM LATPIL

Input Definitions

The following symbols are used in the program input:

B = pile diameter or width, ft;

B1 = pile cross-section depth, ft;

EL = pile embedment depth, ft;

HP = height of applied lateral load above ground surface, ft;

EPILE = modulus of elasticity of pile, lb/ft ;

AIPILE = second moment of area of pile cross-section, ft^4;

N = number of pile segments;

AXP = axial load on pile, lb;

WP = effective pile weight, lb;

PHI (I) = array containing the value of the angle of internal friction of each soil layer, degrees;

DELTA (I) = array containing the value of the angle of friction between the pile and the soil for each soil layer, degrees;

C (I) = array containing the value of soil cohesion of each soil layer, lb/ft ;

GAMMT (I) = array containing the value of the total unit weight of each soil layer, lb/ft ;

D1 (I) = array containing the depth to the bottom of the soil layer, ft;

XP (I) = array containing the value of tilt required to develop passive earth pressure for each soil layer, dimensionless;

XA (I) = array containing the value of tilt required to develop active earth pressure for each soil layer, dimensionless;

EO (I) = array containing the value of the at-rest earth pressure coefficient (K) for each soil layer, dimensionless;

ALPHA (I) = array containing the value of the shear strength reduction factor for each soil layer, dimensionless;

VIS (I) = array containing the value of the soil viscosity for each soil layer, lb-sec/ft ;

VSM (I) = array containing the value of the amount of vertical movement required to develop ultimate skin friction, ft;

Q = surface surcharge, lb/ft ;

DW = depth to the water table, ft;

GH2O = unit weight of water, lb/ft ;

TOL = tolerance on solution (0.0001 is usually sufficient);

NSTOP = option code; if NSTOP = 0, computation is performed, and if NSTOP = 1 only data is printed;

NTCUT = option code; if NTCUT = 0, tensile active

pressures are allowed, and if NTCUT = 1, tensile active pressures are not allowed;

NSOL = option code; if NSOL = 0, only rigid solution is performed, and if NSOL = 1, both rigid and flexible solutions are performed;

NDISP = number of displacement values for which solutions are generated

DISP (I) = array containing the post displacements at the height of the applied load for which solutions are to be generated, in.;

V (I) = array containing the post velocities at the point of the applied load, ft/sec; and

ACCEL (I) = array containing the post accelerations at the point of the applied load, ft/sec .

Input Format

I. First Card

Item	Column	Format
B	1-10	F10.3
B1*	11-20	F10.3
EL	21-30	F10.3
HP	31-40	F10.3
N	41-45	I5

*For circular piles B1 = 0

II. Second Card

Item	Column	Format
EPILE	1-20	F20.3
AIPILE	21-40	F20.3

III. Next Series of Cards

Soil layer properties are input in sequential order beginning with the uppermost layer. There are always 5 soil layers and 10 cards in this series. For layer J the imput is as follows:

Card 1

Item	Column	Format
DELTA (J)	1-5	F5.1
PHI (J)	6-10	F5.1
C (J)	11-20	F10.3
GAMMT (J)	21-30	F10.3
D1 (J)	31-40	F10.3
XP (J)	41-50	F10.3
XA (J)	51-60	F10.3
EO (J)	61-70	F10.3
ALPHA (J)	71-80	F10.3

Card 2

Item	Column	Format
VIS (J)	1-10	F10.3
YSM (J)	11-20	F10.3

IV. Next Card

Item	Column	Format
AXP	1-10	F10.3
WP	11-20	F10.3
Q	21-30	F10.3

V. Next Card

Item	Column	Format
DW	1-10	F10.3
GH20	11-20	F10.3

VI. Next Card

Item	Column	Format
NSTOP	1-5	I5
NTCUT	5-10	I5
TOL	10-20	F10.3

VII. Next Card

Item	Column	Format
NDISP	1-5	I5

VIII. Next Series of Cards

There are as many cards in this series as there are displacement values for which solutions are desired. For displacement value number J the input is as follows:

Item	Column	Format
DISP (J)	1-10	F10.2
V (J)	11-20	F10.2
ACCEL (J)	21-30	F10.2

IX. Next Card

Item	Column	Format
NSOL	1-5	I5

```
      DIMENSION PHI(5),C(5),GAMMT(5),D1(5),XP(5),XA(5),EO(5),ALPHA(5)
      DIMENSION X(50),P1(50),PASS(50),ACT(50),PMA(50)
      DIMENSION M(50)
      DIMENSION EP(5),EA(5),EPMEO(5),EOMEA(5),DELTA(5)
      DIMENSION Z(50),ZM1(50),HSHEAR(50),VSHEAR(50)
      DIMENSION PASSP(50),ACTP(50),PMAP(50),MP(50),HSHEAP(50)
      DIMENSION VSHEAP(50),XFLEX(50),COEFS(50),SIGNX(50),ROT(50)
      DIMENSION DRAGF(50),DRAGFP(50),VIS(5),SHFC(5),YSM(5),Y(50)
      DIMENSION DISP(25),V(25),ACCEL(25)
C
C
C
C     VARIABLES USED IN THIS PROGRAM
C
C
C     INPUT DATA
C
C           PHI(5) - ANGLE OF INTERNAL FRICTION FOR THE FIVE SOIL LAYERS
C           DELTA(5) - ANGLE OF FRICTION BETWEEN PILE AND SOIL LAYER
C           C(5) - SHEAR STRENGTH OF THE SOIL LAYERS
C           GAMMT(5) - TOTAL UNIT WEIGHT OF THE SOIL LAYERS
C           D1(5) - DEPTH TO LOWER BOUNDARY OF EACH OF THE SOIL LAYERS
C           XP(5) - MOVEMENT REQUIRED TO DEVELOP PASSIVE PRESSURE
C           XA(5) - MOVEMENT REQUIRED TO DEVELOP ACTIVE PRESSURE
C           EO(5) - AT-REST EARTH PRESSURE COEFFICIENTS
C           ALPHA(5) - SHEAR STRENGTH REDUCTION FACTORS
C           VIS(5) - SOIL VISCOSITY
C           YSM(5) - MOVEMENT REQUIRED TO DEVELOP ULTIMATE SKIN FRICTION
C
C           B - PILE DIAMETER OR PILE WIDTH
C           B1 - PILE CROSS-SECTION DEPTH
C           EL - PILE EMBEDMENT LENGTH
C           H - HEIGHT OF APPLIED LATERAL LOAD
C           N - NUMBER OF PILE INCREMENTS
C
C           AXP - APPLIED AXIAL LOAD
C           WP - EFFECTIVE WEIGHT OF THE PILE
C           Q - SURCHARGE AT GROUND SURFACE
C
C           DW - DEPTH TO GROUND WATER TABLE
C           GH2O - UNIT WEIGHT OF WATER
C
C           NSTOP - SWITCH TO DETERMINE IF ONLY DATA IS TO BE PRINTED
C           TOL - TOLERANCE ON THE DEPTH OF ROTATION
C           TCUT - SWITCH FOR TENSION CUTOFF
C           NSOL - OPTION CODE: 0 - RIGID SOLUTION; 1 - FLEXIBLE SOLUTION
C
```

```
C         DISP(25) - POST DISPLACEMENTS AT HEIGHT OF LOAD FOR WHICH
C                    SOLUTIONS ARE TO BE COMPUTED
C         V(25) - POST VELOCITIES AT HEIGHT OF APPLIED LOAD
C                 (AUTOMOBILE VELOCITY)
C         ACCEL(25) - POST ACCELERATIONS AT HEIGHT OF APPLIED LOAD
C                     (AUTOMOBILE ACCELERATIONS OR DECELERATIONS)
C
C
C
C   CALCULATED QUANTITIES
C
C
C
C         X(50) - LATERAL DISPLACEMENT OF EACH PILE SEGMENT
C         Y(50) - VERTICAL DISPLACEMENT OF EACH PILE SEGMENT
C         XFLEX(50) - LATERAL DISPLACEMENT OF EACH PILE SEGMENT
C                     COMPUTED USING SINGULARITY FUNCTIONS
C         P1(50) - OVERBURDEN PRESSURE AT EACH PILE SEGMENT
C         PASS(50) - PASSIVE PRESSURE AT EACH PILE SEGMENT
C         ACT(50) - ACTIVE PRESSURE AT EACH PILE SEGMENT
C         PMA(50) - RESULTANT FORCE AT EACH PILE SEGMENT
C         M(50) - PORTION OF OVERTURNING MOMENT DUE TO EACH PILE SEGMENT
C         TOTM - TOTAL SUM OF MOMENTS
C         HSHEAR(50) - HORIZONTAL SHEAR FORCE ON PILE SEGMENT
C         VSHEAR(50) - VERTICAL SHEAR FORCE ON PILE SEGMENT
C         BSHEAR - SHEAR FORCE ON THE BASE OF THE PILE
C         PTOT - TOTAL LATERAL LOAD AT HEIGHT H ABOVE GROUND
C         GLMOM - GROUND-LINE MOMENT
C         GLDEF - GROUND-LINE DEFLECTION
C         FBASE - COMPRESSIVE FORCE ON PILE BASE
C         DRAGC - DRAG COEFFICIENT
C         DRAGF(50) - DRAG FORCE ON EACH PILE SEGMENT
C         RN - REYNOLD'S NUMBER
C         AINERT - SECOND MOMENT OF INERTIA OF PILE-SOIL SYSTEM
C                  ABOUT THE POINT OF APPLICATION OF THE LOAD
C
C
C
      READ 800,B,B1,EL,H,N
      READ 803,EPILE,AIPILE
      DO 10 I=1,5
      READ 805, DELTA(I),PHI(I),C(I),GAMMT(I),D1(I),XP(I),XA(I),EC(I),AL
     $PHA(I)
   10 READ 806,VIS(I),YSM(I)
      READ 810, AXP,WP,Q
      READ 815, DW,GH2O
      READ 820, NSTOP,NTCUT,TOL
```

```
      READ 821,NDISP
      DO 15 I=1,NDISP
   15 READ 810,DISP(I),V(I),ACCEL(I)
      READ 821,NSOL
      PRINT 830
      PRINT 840
      DO 20 I=1,5
      PRINT 845, I,PHI(I),DELTA(I),C(I),GAMMT(I),D1(I)
      PRINT 850, XP(I),XA(I),EO(I),ALPHA(I)
   20 PRINT 855, VIS(I)
      PRINT 860, DW
      PRINT 870
      PRINT 875, B,B1,EL,H,N,EPILE,AIPILE
      PRINT 880
      PRINT 885, AXP,WP,Q,GH2O,NTCUT,TOL
      IF (NSTOP.NE.0) STOP
      CALL OVERP(PHI,C,GAMMT,D1,N,P1,DW,GH2O,Q,Z,ZM1,EL)
      CALL SOILP(PHI,EP,EA,EO,EPMEO,EOMEA,DELTA,C,SHFC,B1)
      EL1=EL/N
      DO 500 K3=1,NDISP
      XH=DISP(K3)/12.
      VELH=V(K3)
      ACCH=ACCEL(K3)
      R=0.65
      I7=0
      E=0.01
      DO 106  K=1,100
      R1=R*EL+H
      THETA=ARSIN(XH/R1)
      A=THETA*180./3.14159
      LR1=INT(R*EL/EL1)
      DO 40 J=1,N
      ROT(J)=THETA
      IF (((2*J-1)*EL1*0.5).GT.(R*EL))GO TO 45
      Y(J)=(R*EL-(2*J-1)*EL1*0.5)*(1.-COS(THETA))
      X(J)=(R*EL-(2*J-1)*EL1*0.5)*SIN(THETA)
      SIGNX(J)=1.0
      GO TO 40
   45 X(J)=((2*J-1)*EL1*0.5-R*EL)*SIN(THETA)
      SIGNX(J)=-1.0
      Y(J)=((2*J-1)*EL1*0.5-R*EL)*(1.-COS(THETA))
   40 CONTINUE
      CALL MOMINT(EL,R,H,B,D1,PHI,GAMMT,WP,AINERT,X,N,XP,XA,B1)
      CALL LATPR(PHI,C,EP,EA,EO,EPMEO,EOMEA,D1,EL,N,THETA,H,PASS,ACT,PMA
     $,ALPHA,B,HSHEAR,VSHEAR,VTOTL,I7,NTCUT,R,X,XP,XA,P1,SIGNX,ROT,DRAGF
     $,GAMMT,VIS,XH,VELH,B1,SHFC,YSM,Y,ACCH,DELTA,AXP,WP,FBASE)
      CALL MOMEQ(EL,N,B,R,H,PMA,HSHEAR,VSHEAR,TOTM,FBASE,AXP,WP,VTOTL,TH
```

```
   $ETA,X,C,PHI,BSHEAR,K,M,ALPHA,XH,ROT,SIGNX,DRAGF,B1,AINERT,ACCH)
     IF (TOTM) 50,60,70
  50 IF (K.EQ.1) GO TO 80
     IF (TOTM/TOTMP) 55,56,57
  55 E=E*0.1
     GO TO 80
  56 GO TO 110
  57 GO TO 80
  60 GO TO 110
  70 IF (K.EQ.1) GO TO 90
     IF (TOTM/TOTMP) 75,76,77
  75 E=E*0.1
     GO TO 90
  76 GO TO 110
  77 GO TO 90
  80 R=R+E
     IF (E.LT.TOL) GO TO 110
     GO TO 100
  90 R=R-E
     IF (E.LT.TOL) GO TO 110
 100 DO 105 L=1,N
     PASSP(L)=PASS(L)
     ACTP(L)=ACT(L)
     PMAP(L)=PMA(L)
     MP(L)=M(L)
     HSHEAP(L)=HSHEAR(L)
     VSHEAP(L)=VSHEAR(L)
     DRAGFP(L)=DRAGF(L)
 105 CONTINUE
     BSHEAP=BSHEAR
     TOTMP=TOTM
 106 CONTINUE
 110 IF (ABS(TOTM)-ABS(TOTMP)) 120,120,140
 120 GO TO 150
 140 DO 145 I1=1,N
     PASS(I1)=PASSP(I1)
     ACT(I1)=ACTP(I1)
     PMA(I1)=PMAP(I1)
     M(I1)=MP(I1)
     HSHEAR(I1)=HSHEAP(I1)
     VSHEAR(I1)=VSHEAP(I1)
     DRAGF(I1)=DRAGFP(I1)
 145 CONTINUE
     TOTM=TOTMP
     BSHEAR=BSHEAP
 150 PTOT=0.0
     DO 200 J=1,N
```

```
      PTOT=PTOT+PMA(J)+HSHEAR(J)+DRAGF(J)
  200 CONTINUE
      PTOT=PTOT-BSHEAR
      GLMOM=PTOT*H
      GLDEF=R*EL*TAN(THETA)*12.
      PRINT 900
      R=R*EL
      PRINT 905, A,R,PTOT,GLMOM,XH
      PRINT 910
      DO 300 L1=1,N
      PRINT 920, Z(L1),X(L1)*SIGNX(L1),PASS(L1),ACT(L1),PMA(L1),HSHEAR(L
     $1),VSHEAR(L1),DRAGF(L1)
  300 CONTINUE
      PRINT 922,BSHEAR,TOTM
      IF (NSOL.EQ.0)GO TO 500
      TOLM=ABS(TOTM)
      DO 310 J=1,N
      PMAP(J)=PMA(J)
      HSHEAP(J)=HSHEAR(J)
      VSHEAP(J)=VSHEAR(J)
      DRAGFP(J)=DRAGF(J)
  310 CONTINUE
      PTOTP=PTOT
      GLMOMP=GLMOM
      ANGLE=THETA
      K8=1
  315 K7=0
      K8=K8+1
      THETAG=ANGLE
  316 A=THETAG*180./3.14159
      K7=K7+1
      THETA=THETAG
  317 CALL FLEXEQ(B,H,EL,R,PMAP,HSHEAP,PTOTP,N,XH,THETAG,EPILE,AIPILE,XF
     $LEX,GLMOMP,TOTM,VSHEAP,ROT,DRAGFP,B1)
      DO 320 K1=1,N
      X(K1)=ABS(XFLEX(K1))
      SIGNX(K1)=ABS(XFLEX(K1))/XFLEX(K1)
      Y(K1)=ABS((R*EL-(2*K1-1)*EL1*0.5))*(1.0-COS(ROT(K1)))
  320 CONTINUE
      CALL MOMINT(EL,R,H,B,D1,PHI,GAMMT,WP,AINERT,X,N,XP,XA,B1)
  324 CALL LATPR(PHI,C,EP,EA,EO,EPMEO,EOMEA,D1,EL,N,THETA,H,PASS,ACT,PMA
     $,ALPHA,B,HSHEAR,VSHEAR,VTOTL,I7,NTCUT,R,X,XP,XA,P1,SIGNX,ROT,DRAGF
     $,GAMMT,VIS,XH,VELH,B1,SHFC,YSM,Y,ACCH,DELTA,AXP,WP,FBASE)
      CALL MOMEQ(EL,N,B,R,H,PMA,HSHEAR,VSHEAR,TOTM,FBASE,AXP,WP,VTOTL,TH
     $ETA,XFLEX,C,PHI,BSHEAR,K,M,ALPHA,XH,ROT,SIGNX,DRAGF,B1,AINERT,ACCH
     $)
      PTOT=0.0
```

```
      DO 330 J=1,N
      PTOT=PTOT+PMA(J)+HSHEAR(J)+DRAGF(J)
  330 CONTINUE
      PTOT=PTOT-BSHEAR
      GLMOM=PTOT*H
      IF (R.EQ.1)GO TO 341
      I7=INT(R*N)+1
      DO 340 J=I7,N
  340 X(J)=-1.0*X(J)
  341 IF (ABS(TOTM).LT.TOLM)GO TO 348
      IF (K7.NE.1)GO TO 347
      IF (TOTM.LE.0.0)GO TO 346
      THETAP=THETAG
      THETAG=(1.+1./K8**2.)*THETAP
      TOTMP=TOTM
      GO TO 316
  346 THETAP=THETAG
      THETAG=(1.-1./K8**2.)*THETAP
      TOTMP=TOTM
      GO TO 316
  347 SLOPE=(TOTMP-TOTM)/(THETAP-THETAG)
      THETAP=THETAG
      THETAG=THETAP-TOTM/SLOPE
      TOTMP=TOTM
      GO TO 316
  348 DO 349 J=1,N
      PMAP(J)=(PMAP(J)+PMA(J))/2.
      HSHEAP(J)=(HSHEAP(J)+HSHEAR(J))/2.
      VSHEAP(J)=(VSHEAP(J)+VSHEAR(J))/2.
      DRAGFP(J)=(DRAGFP(J)+DRAGF(J))/2.
  349 CONTINUE
      PTOTP=(PTOTP+PTOT)/2.
      GLMOMP=(GLMOMP+GLMOM)/2.
  350 ERRORF=ABS(THETAG-ANGLE)
      IF (ERRORF.LE.TOL) GO TO 355
      ANGLE=(ANGLE+THETAG)/2.
      GO TO 315
  355 GLDEF=X(1)+EL1/2.*SIN(ROT(1))
      GLSLP=THETAG
      A=GLSLP*180./3.14159
      PRINT 930
      R=R*EL
      PRINT 935,A,R,PTOT,GLMOM,GLDEF
      PRINT 910
      DO 360 J=1,N
      PRINT 920,Z(J),X(J),PASS(J),ACT(J),PMA(J),HSHEAR(J),VSHEAR(J),DRAG
     $F(J)
```

```
360 CONTINUE
    PRINT 922,BSHEAR,TOTM
500 CONTINUE
    STOP
800 FORMAT (4F10.3,I5)
803 FORMAT (2F20.3)
805 FORMAT (2F5.1,7F10.3)
806 FORMAT (2F10.3)
810 FORMAT (3F10.3)
815 FORMAT (2F10.3)
820 FORMAT (2I5,F10.3)
821 FORMAT (I5)
830 FORMAT ('1',T59,'****************',/,' ',T59,'*  INPUT DATA  *',/,
   $' ',T59,'****************')
840 FORMAT ('0',T5,'SOIL PROPERTIES',/,'+',T5,'________________',//)
845 FORMAT (' ',T5,'LAYER ',I2,/,'0',T10,'ANGLE OF FRICTION = ',F5.1,/
   $,'0',T10,'FRICTION ANGLE BETWEEN PILE AND SOIL = ',F5.1,/,'0',T10,
   $'SHEAR STRENGTH = ',F6.0,/,'0',T10,'TOTAL UNIT WEIGHT = ',F5.1,/,'
   $0',T10,'DEPTH TO BOTTOM OF LAYER = ',F6.2)
850 FORMAT ('0',T10,'MOVEMENT NEEDED TO DEVELOP PASSIVE PRESSURE / PIL
   $E EMBEDMENT = ',F6.4,/,'0',T10,'MOVEMENT NEEDED TO DEVELOP ACTIVE
   $PRESSURE / PILE EMBEDMENT = ',F6.4,/,'0',T10,'AT-REST EARTH PRESSU
   $RE COEFFICIENT = ',F5.3,/,'0',T10,'SHEAR REDUCTION FACTOR =',F4.2)
855 FORMAT ('0',T10,'SOIL VISCOSITY = ',F6.2,///)
860 FORMAT (' ',T10,'DEPTH TO WATER TABLE =',F5.2,///)
870 FORMAT ('0',T5,'PILE PROPERTIES',/,'+',T5,'________________',//)
875 FORMAT(' ',T10,'PILE WIDTH =',F6.3,/,'0',T10,'PILE DEPTH =',F6.3,/
   $,'0',T10,'PILE EMBEDMENT =',F6.2,/,'0',T10,'HEIGHT OF APPLIED LATE
   $RAL LOAD =',F6.2,/,'0',T10,'NUMBER OF PILE INCREMENTS =',I5,/,'0',
   $T10,'MODULUS OF ELASTICITY =',E11.4,/,'0',T10,'MOMENT OF INERTIA =
   $',E11.4,///)
880 FORMAT ('0',T5,'OTHER INFORMATION',/,'+',T5,'_________________',//
   $)
885 FORMAT (' ',T10,'APPLIED AXIAL LOAD =',F10.2,/,'0',T10,'EFFECTIVE
   $WEIGHT OF PILE =',F10.2,/,'0',T10,'SURFACE SURCHARGE =',F6.1,/,'0'
   $,T10,'UNIT WEIGHT OF WATER =',F6.2,/,'0',T10,'TENSION CUTOFF =',I2
   $,/,'0',T10,'TOLERANCE =',F10.6)
900 FORMAT ('1',T52,'**************************',/,' ',T52,'*      R
   $IGID SOLUTION',6X,'*',/,' ',T52,'**************************',///
   $)
905 FORMAT ('0',T10,'ANGLE OF ROTATION =',F7.3,/,'0',T10,'DEPTH TO ROT
   $ATION POINT =',F10.6,/,'0',T10,'TOTAL LATERAL LOAD =',F10.2,/,'0',
   $T10,'GROUND-LINE MOMENT =',F10.1,/,'0',T10,'DEFLECTION AT TOP OF P
   $ILE =',F10.6,///)
910 FORMAT (' ',T16,'DEPTH',8X,' LAT DISP',9X,'PASS',12X,'ACT',9X,'PAS
   $S-ACT',9X,'HSHEAR',9X,'VSHEAR',8X,'DFORCE',/,'+',T16,'_____',8X,'
   $________',9X,'____',12X,'__',9X,'________',9X,'______',9X,'______
```

```
     $',8X,'_____',//)
  920 FORMAT (' ',10X,F10.6,5X,F10.6,5X,F10.2,5X,F10.2,5X,F10.2,5X,F10.2
     $,5X,F10.2,4X,F10.2)
  922 FORMAT('0',T10,'BASE SHEAR FORCE =',F10.1,/,'0',T10,'SUM OF MOMENT
     $S AT POINT OF LOAD APPLICATION = ',E10.3,/)
  930 FORMAT ('1',T52,'*************************',/,' ',T52,'*    FLE
     $XIBLE SOLUTION     *',/,' ',T52,'*************************',//)
  935 FORMAT('0',T10,'GROUND-LINE SLOPE =',F8.5,/,'0',T10,'DEPTH TO ZERO
     $ DISPLACEMENT =',F8.3,/,'0',T10,'TOTAL LATERAL LOAD =',F10.2,/,'0'
     $,T10,'GROUND-LINE MOMENT =',F10.1,/,'0',T10,'GROUND-LINE DEFLECTIO
     $N =',F10.4,///)
      END
C
C  ****************************************************************
C  *                                                              *
C  *  SUBROUTINE OVERP CALCULATES THE OVERBURDEN PRESSURE AT      *
C  *   THE MIDPOINT OF EACH PILE SEGMENT                          *
C  *                                                              *
C  ****************************************************************
C
C
      SUBROUTINE OVERP(PHI,C,GAMMT,D1,N,P1,DW,GH2O,Q,Z,ZM1,EL)
      DIMENSION PHI(5),C(5),GAMMT(5),D1(5),P1(N),Z(N),ZM1(N)
      EL1=EL/N
      DO 100 I=1,N
      P1(I)=0.0
  100 Z(I)=(I-0.5)*EL1
      L1=INT(D1(1)/EL1)
      L2=INT(D1(2)/EL1)
      L3=INT(D1(3)/EL1)
      L4=INT(D1(4)/EL1)
      L1P1=L1+1
      L2P1=L2+1
      L3P1=L3+1
      L4P1=L4+1
      ZM1(1)=EL1*0.5
      DO 200 J=2,N
  200 ZM1(J)=Z(J)-Z(J-1)
      IF (Z(1).GT.DW) GAMMT(1)=GAMMT(1)-GH2O
      P1(1)=P1(1)+ZM1(1)*GAMMT(1)+Q
      DO 210 I=2,L1
      U=0.0
      IF (Z(I).GT.DW) U=GH2O
  210 P1(I)=P1(I-1)+ZM1(I)*(GAMMT(1)-U)
      DO 220 I=L1P1,L2
      U=0.0
      IF (Z(I).GT.DW) U=GH2O
```

```
  220 P1(I)=P1(I-1)+ZM1(I)*(GAMMT(2)-U)
      DO 230 I=L2P1,L3
      U=0.0
      IF (Z(I).GT.DW) U=GH2O
  230 P1(I)=P1(I-1)+ZM1(I)*(GAMMT(3)-U)
      DO 240 I=L3P1,L4
      U=0.0
      IF (Z(I).GT.DW) U=GH2O
  240 P1(I)=P1(I-1)+ZM1(I)*(GAMMT(4)-U)
      DO 250 I=L4P1,N
      U=0.0
      IF (Z(I).GT.DW) U=GH2O
  250 P1(I)=P1(I-1)+ZM1(I)*(GAMMT(5)-U)
      RETURN
      END
C
C
C   ************************************************************
C   *                                                          *
C   *  SUBROUTINE SOILP CALCULATES THE FOLLOWING SOIL          *
C   *    PARAMETERS; (1) COULOMB PASSIVE PRESSURE COEFFI-      *
C   *                    CIENT (EP)                            *
C   *                (2) COULOMB ACTIVE PRESSURE COEFFI-       *
C   *                    CIENT (EA)                            *
C   *                (3) EP - EO                               *
C   *                (4) EO - EA                               *
C   *                                                          *
C   ************************************************************
C
C
      SUBROUTINE SOILP(PHI,EP,EA,EO,EPMEO,EOMEA,DELTA,C,SHFC,B1)
      DIMENSION PHI(5),EP(5),EA(5),EO(5),EPMEO(5),EOMEA(5),DELTA(5)
      DIMENSION C(5),SHFC(5)
      PI=3.14159
      DO 10 I=1,5
      DR=DELTA(I)*PI/180.
      PHIR=PHI(I)*PI/180.
      RAD=SQRT(SIN(DR+PHIR)*SIN(PHIR)/COS(DR))
      EP(I)=(COS(PHIR)**2)/(COS(DR)*(1.-RAD)**2)
      EA(I)=(COS(PHIR)**2)/(COS(DR)*(1.+RAD)**2)
      EPMEO(I)=EP(I)-EO(I)
      EOMEA(I)=EO(I)-EA(I)
      IF (EPMEO(I).LT.0.0)EPMEO(I)=0.0
      IF (EOMEA(I).LT.0.0)EOMEA(I)=0.0
      SHFC(I)=PI/4.
      IF(C(I).NE.0.0.AND.B1.NE.0.0)SHFC(I)=2./3.
   10 CONTINUE
```

```
      RETURN
      END
C
C
C     ****************************************************************
C     *                                                              *
C     *   SUBROUTINE LATPR CALCULATES THE FOLLOWING QUANTITIES       *
C     *   AT EACH PILE SEGMENT:                                      *
C     *                                                              *
C     *       (1) PASSIVE PRESSURE                                   *
C     *       (2) ACTIVE PRESSURE                                    *
C     *       (3) RESULTANT PRESSURE (PASS - ACT)                    *
C     *       (4) HORIZONTAL SHEAR FORCE                             *
C     *       (5) VERTICAL SHEAR FORCE                               *
C     *                                                              *
C     ****************************************************************
C
C
      SUBROUTINE LATPR(PHI,C,EP,EA,EO,EPMEO,EOMEA,D1,EL,N,THETA,H,PASS,A
     $CT,PMA,ALPHA,B,HSHEAR,VSHEAR,VTOTL,I7,NTCUT,R,X,XP,XA,P1,SIGNX,ROT
     $,DRAGF,GAMMT,VIS,XH,VELH,B1,SHFC,YSM,Y,ACCH,DELTA,AXP,WP,FBASE)
      DIMENSION EP(5),EA(5),EO(5),EPMEO(5),EOMEA(5),D1(5),PASS(N),VIS(5)
      DIMENSION ACT(N),PMA(N),X(N),ALPHA(5),VSHEAR(N),GAMMT(5),DRAGF(N)
      DIMENSION HSHEAR(N),XP(5),XA(5),P1(N),PHI(5),C(5),SIGNX(N),ROT(N)
      DIMENSION SHFC(5),YSM(5),Y(N),DELTA(5)
      VTOTL=0.0
      PI=3.14159
      EL1=EL/N
      L1=INT(D1(1)/EL1)
      L2=INT(D1(2)/EL1)
      L3=INT(D1(3)/EL1)
      L4=INT(D1(4)/EL1)
      LR1=INT(R*EL/EL1)
      DO 10 I=1,N
      IF (I.LE.L1) J=1
      IF (I.GT.L1.AND.I.LE.L2) J=2
      IF (I.GT.L2.AND.I.LE.L3) J=3
      IF (I.GT.L3.AND.I.LE.L4) J=4
      IF (I.GT.L4) J=5
      IF (VELH.EQ.0.0)GO TO 5
      VEL=VELH*X(I)/XH
      BD=SQRT(B*EL1)
      IF (B1.EQ.0.0)BD=B
      RN=VEL*BD*GAMMT(J)/(32.2*VIS(J))
      IF (RN.LE.0.0)GO TO 5
      IF (B1.NE.0.0)GOTO 6
      DRAGC=10.**(-0.650515*ALOG10(RN)+1.12764)
```

```
      GO TO 9
    6 DRAGC=10.**(-1.0*ALOG10(RN)+1.301)
    9 DRAGF(I)=DRAGC*B*EL1*VEL**2./2.*GAMMT(J)/32.2*SIGNX(I)
      GO TO 7
    5 DRAGF(I)=0.0
    7 XPASS=XP(J)*R*ABS(1-(2*I-1)*0.5*EL1/R/EL)
      XACT=XA(J)*R*ABS(1-(2*I-1)*0.5*EL1/R/EL)
      IF (XPASS.LE.0.0)XPASS=XP(J)/100.
      IF (XACT.LE.0.0)XACT=XA(J)/100.
    8 C1=EO(J)*P1(I)
      A1=(P1(I)*EPMEO(J)+2.*C(J)*SQRT(EP(J)))*TANH(2*X(I)/XPASS)
      PASS(I)=A1+C1
      ACT(I)=(P1(I)*EOMEA(J)+2.*C(J)*SQRT(EA(J)))*TANH(-2*X(I)/XACT)+C1
      IF (NTCUT.NE.1) GO TO 15
      IF (ACT(I).LT.0.0) ACT(I)=0.0
   15 PMA(I)=SIGNX(I)*(PASS(I)-ACT(I))*SHFC(J)*EL1*B*COS(ROT(I))
      IF (B1.EQ.0.0)GO TO 18
      HSHEAR(I)=ALPHA(J)*2.*B1*EL1*((PASS(I)+ACT(I))/2.*TAN(PHI(J)*PI/18
     $0.)+C(J))
      VSHEAR(I)=ALPHA(J)*EL1*B*((PASS(I)-ACT(I))*SHFC(J)*TAN(PHI(J)*PI/1
     $80.)+C(J))*TANH(2./YSM(J)*Y(I))
      GO TO 19
   18 HSHEAR(I)=ALPHA(J)*B*EL1*(TAN(PHI(J)*PI/180.)/3.*A1+PI/4.*EO(J)*P1
     $(I)*TAN(PHI(J)*PI/180.)+PI/4.*C(J))
      VSHEAR(I)=ALPHA(J)*B*EL1*(PI/4.*TAN(PHI(J)*PI/180.)*A1+EO(J)*P1(I)
     $*TAN(PHI(J)*PI/180.)+C(J))*TANH(2./YSM(J)*Y(I))
   19 HSHEAR(I)=SIGNX(I)*HSHEAR(I)*TANH(2*X(I)/YSM(J))
   10 CONTINUE
      LR1P1=LR1+1
      DO 17 I=1,N
      IF (I.GE.LR1P1)GO TO 16
      VTOTL=VTOTL+VSHEAR(I)
      GO TO 17
   16 VTOTL=VTOTL-VSHEAR(I)
   17 CONTINUE
      SVERT=(AXP+WP)*COS(THETA)-VTOTL
      IF (SVERT.LT.0.0)SVERT=0.0
      FBASE=SVERT
      RETURN
      END
C
C
C   ***************************************************************
C   *                                                             *
C   *   SUBROUTINE MOMEQ SUMS MOMENTS FOR THE ENTIRE PILE         *
C   *                                                             *
C   ***************************************************************
```

```
C
C
      SUBROUTINE MOMEQ(EL,N,B,R,H,PMA,HSHEAR,VSHEAR,TOTM,FBASE,AXP,WP,VT
     $OTL,THETA,X,C,PHI,BSHEAR,K,M,ALPHA,XH,ROT,SIGNX,DRAGF,B1,AINERT,AC
     $CH)
      DIMENSION PMA(N),HSHEAR(N),VSHEAR(N),DRAGF(N)
      DIMENSION X(N),C(5),PHI(5),M(N),ALPHA(5),ROT(N),SIGNX(N)
      PI=3.14159
      EL1=EL/N
      B2=B1
      IF (B1.EQ.0.0)B2=B
      RACC=ACCH*COS(ROT(1))/(H+R*EL)
      DO 10 I=1,N
      VMA=H*COS(ROT(1))+(2*I-1)*EL1*0.5*COS(ROT(I))
      M(I)=VMA*(PMA(I)+HSHEAR(I)+DRAGF(I))-VSHEAR(I)*B2/2.
   10 CONTINUE
   25 TOTM=0.0
      DO 30 I=1,N
   30 TOTM=TOTM+M(I)
      TOTM=TOTM+FBASE*(XH+X(N)-0.3*B2)
      BSHEAR=ALPHA(5)*(C(5)*PI*B**2/8.+FBASE*TAN(PHI(5)*PI/180.))
      IF (B1.NE.0.0)BSHEAR=ALPHA(5)*(C(5)*B*B1/2.+FBASE*TAN(PHI(5)*PI/18
     $0.))
      TOTM=TOTM-BSHEAR*(EL+H)-AINERT*RACC
      RETURN
      END
C
C
C   ****************************************************************
C   *                                                              *
C   *   SUBROUTINE FLEXEQ COMPUTES THE PILE DEFLECTIONS USING      *
C   *   THE PRESSURES CALCULATED.                                  *
C   *                                                              *
C   ****************************************************************
C
      SUBROUTINE FLEXEQ(B,H,EL,R,PMA,HSHEAR,PTOT,N,XH,THETAG,EPILE,AIPIL
     $E,XFLEX,GLMOM,TOTM,VSHEAR,ROT,DRAGF,B1)
      DIMENSION PMA(N),HSHEAR(N),XFLEX(N),COEFS(50),VSHEAR(N),ROT(N)
      DIMENSION DRAGF(N)
      EL1=EL/N
      PI=3.14159
      COEFS(1)=(PMA(1)+HSHEAR(1)+DRAGF(1))/EL1
      DO 100 I=2,N
      COEFS(I)=(PMA(I)-PMA(I-1)+HSHEAR(I)-HSHEAR(I-1)+DRAGF(I)-DRAGF(I-1
     $))/EL1
  100 CONTINUE
      CONST1=-1.*EPILE*AIPILE*THETAG
```

```
      CONST2=EPILE*AIPILE*XH
      B2=B1
      IF (B1.EQ.0.0)B2=B
      R7=R*EL
      DO 200 J=1,N
      SUM=0.0
      SUM1=0.0
      Z=(J-0.5)*EL1
      DO 150 K=1,J
      SUM=SUM-1./24.*COEFS(K)*(Z-EL1*(K-1))**4.-0.5*VSHEAR(K)*B2/2.*(Z-(
     $K-0.5)*EL1)**2.
      SUM1=SUM1-1./6.*COEFS(K)*(Z-EL1*(K-1))**3.-VSHEAR(K)*B2/2.*(Z-(K-0
     $.5)*EL1)
  150 CONTINUE
      XFLEX(J)=(1./6.*PTOT*(Z+H)**3.+SUM+CONST1*(Z+H)+CONST2)/(EPILE*AIP
     $ILE)
      ROT(J)=(PTOT/2.*(Z+H)**2.+SUM1+CONST1)/(EPILE*AIPILE)
      ROT(J)=ABS(ROT(J))
  200 CONTINUE
      DO 220 I=1,N
      IF (XFLEX(I).LE.0.)GO TO 230
  220 CONTINUE
      R=1.0
      GO TO 240
  230 R=((2*I-1)*0.5+XFLEX(I-1)/(XFLEX(I-1)-XFLEX(I)))/N
  240 RETURN
      END
C
C
C     ****************************************************************
C     *                                                              *
C     *   SUBROUTINE MOMINT CALCULATES THE MOMENT OF INERTIA OF      *
C     *   THE PILE AND SOIL INVOLVED IN THE FAILURE ABOUT THE       *
C     *   POINT OF LOAD APPLICATION                                  *
C     *                                                              *
C     ****************************************************************
C
C
      SUBROUTINE MOMINT(EL,R,H,B,D1,PHI,GAMMT,WP,AINERT,X,N,XP,XA,B1)
      DIMENSION D1(5),PHI(5),GAMMT(5),X(N),XP(5),XA(5)
      PI=3.14159
      EL1=EL/N
      L1=INT(D1(1)/EL1)
      L2=INT(D1(2)/EL1)
      L3=INT(D1(3)/EL1)
      L4=INT(D1(4)/EL1)
      AINERT=0.0
```

```
      DO 10 I=1,N
      IF (I.LE.L1) J=1
      IF (I.GT.L1.AND.I.LE.L2) J=2
      IF (I.GT.L2.AND.I.LE.L3) J=3
      IF (I.GT.L3.AND.I.LE.L4) J=4
      IF (I.GT.L4) J=5
      XPASS=XP(J)*R*ABS(1-(2*I-1)*0.5*EL1/R/EL)
      XACT=XA(J)*R*ABS(1-(2*I-1)*0.5*EL1/R/EL)
      IF (XPASS.LE.0.0)XPASS=XP(J)/100.
      IF (XACT.LE.0.0)XACT=XA(J)/100.
      DIST1=ABS((R*EL-(2*I-1)*0.5*EL1))*TAN((45.+PHI(J)/2.)*PI/180.)
      DIST1=DIST1*TANH(2.*X(I)/XPASS)
      DIST2=ABS((R*EL-(2*I-1)*0.5*EL1))*TAN((45.-PHI(J)/2.)*PI/180.)
      DIST2=DIST2*TANH(2.*X(I)/XACT)
      RADIUS=(2*I-1)*0.5*EL1+H
      TMASS=DIST1*B+DIST1**2./2.*(PHI(J)*PI/180.+PI/2.)
      TMASS=TMASS+DIST2*B+DIST2**2./2.*(PI/2.-PHI(J)*PI/180.)
      TMASS=TMASS*EL1*GAMMT(J)/32.2
      AINERT=AINERT+TMASS*RADIUS**2.
   10 CONTINUE
      IF (B1.EQ.0.0) GO TO 15
      AINERT=AINERT+WP/32.2/12.*B1**2.+WP/32.2/3.*(EL+H)**2.
      GO TO 20
   15 AINERT=AINERT+WP/32.2/16.*B**2.+WP/32.2/3.*(EL+H)**2.
   20 RETURN
      END
```

SAMPLE OUTPUT

The sample output listing shown on the following pages is for the dynamic impact test C2. The input data for the computer program LATPIL is listed below.

```
  0.3283    0.4917     3.167      1.75   20
       4176000000.          0.00079089
22.  52.        0.     115.0      0.63     0.005    0.0005    0.2569        1
 100.000     0.025
22.  52.        0.     115.0      1.26     0.005    0.0005    0.2569        1
 100.000     0.025
22. 51.4        0.     115.0      1.89     0.005    0.0005    0.2639        1
 100.000     0.025
22. 50.5        0.     115.0      2.52     0.005    0.0005    0.2746        1
 100.000     0.025
22. 49.3        0.     115.0     3.167     0.005    0.0005    0.2892        1
 100.000     0.025
     0.       70.        0.
   3.167      62.4
       1    .00100
  2
 1.2522    26.083     7.445
 1.565     26.033     92.443
  0
```

```
                                                  ****************
                                                  *  INPUT DATA  *
                                                  ****************
SOIL PROPERTIES
---------------

LAYER  1
     ANGLE OF FRICTION =  52.0
     FRICTION ANGLE BETWEEN PILE AND SOIL =  22.0
     SHEAR STRENGTH =     0.
     TOTAL UNIT WEIGHT = 115.0
     DEPTH TO BOTTOM OF LAYER =   0.63
     MOVEMENT NEEDED TO DEVELOP PASSIVE PRESSURE / PILE EMBEDMENT = 0.0050
     MOVEMENT NEEDED TO DEVELOP ACTIVE PRESSURE / PILE EMBEDMENT = 0.0005
     AT-REST EARTH PRESSURE COEFFICIENT = 0.257
     SHEAR REDUCTION FACTOR =1.00
     SOIL VISCOSITY = 100.00


LAYER  2
     ANGLE OF FRICTION =  52.0
     FRICTION ANGLE BETWEEN PILE AND SOIL =  22.0
     SHEAR STRENGTH =     0.
     TOTAL UNIT WEIGHT = 115.0
     DEPTH TO BOTTOM OF LAYER =   1.26
     MOVEMENT NEEDED TO DEVELOP PASSIVE PRESSURE / PILE EMBEDMENT = 0.0050
     MOVEMENT NEEDED TO DEVELOP ACTIVE PRESSURE / PILE EMBEDMENT = 0.0005
     AT-REST EARTH PRESSURE COEFFICIENT = 0.257
     SHEAR REDUCTION FACTOR =1.00
     SOIL VISCOSITY = 100.00


LAYER  3
     ANGLE OF FRICTION =  51.4
     FRICTION ANGLE BETWEEN PILE AND SOIL =  22.0
     SHEAR STRENGTH =     0.
     TOTAL UNIT WEIGHT = 115.0
     DEPTH TO BOTTOM OF LAYER =   1.89
     MOVEMENT NEEDED TO DEVELOP PASSIVE PRESSURE / PILE EMBEDMENT = 0.0050
     MOVEMENT NEEDED TO DEVELOP ACTIVE PRESSURE / PILE EMBEDMENT = 0.0005
     AT-REST EARTH PRESSURE COEFFICIENT = 0.264
     SHEAR REDUCTION FACTOR =1.00
     SOIL VISCOSITY = 100.00


LAYER  4
     ANGLE OF FRICTION =  50.5
     FRICTION ANGLE BETWEEN PILE AND SOIL =  22.0
     SHEAR STRENGTH =     0.
     TOTAL UNIT WEIGHT = 115.0
     DEPTH TO BOTTOM OF LAYER =   2.52
     MOVEMENT NEEDED TO DEVELOP PASSIVE PRESSURE / PILE EMBEDMENT = 0.0050
```

MOVEMENT NEEDED TO DEVELOP ACTIVE PRESSURE / PILE EMBEDMENT = 0.0005
AT-REST EARTH PRESSURE COEFFICIENT = 0.275
SHEAR REDUCTION FACTOR =1.00
SOIL VISCOSITY = 100.00

LAYER 5
ANGLE OF FRICTION = 49.3
FRICTION ANGLE BETWEEN PILE AND SOIL = 22.0
SHEAR STRENGTH = 0.
TOTAL UNIT WEIGHT = 115.0
DEPTH TO BOTTOM OF LAYER = 3.17
MOVEMENT NEEDED TO DEVELOP PASSIVE PRESSURE / PILE EMBEDMENT = 0.0050
MOVEMENT NEEDED TO DEVELOP ACTIVE PRESSURE / PILE EMBEDMENT = 0.0005
AT-REST EARTH PRESSURE COEFFICIENT = 0.289
SHEAR REDUCTION FACTOR =1.00
SOIL VISCOSITY = 100.00

DEPTH TO WATER TABLE = 3.17

PILE PROPERTIES

PILE WIDTH = 0.328
PILE DEPTH = 0.492
PILE EMBEDMENT = 3.17
HEIGHT OF APPLIED LATERAL LOAD = 1.75
NUMBER OF PILE INCREMENTS = 20
MODULUS OF ELASTICITY = 0.4176E 10
MOMENT OF INERTIA = 0.7909E-03

OTHER INFORMATION

APPLIED AXIAL LOAD = 0.00
EFFECTIVE WEIGHT OF PILE = 70.00
SURFACE SURCHARGE = 0.0
UNIT WEIGHT OF WATER = 62.40
TENSION CUTOFF = 1
TOLERANCE = 0.001000

****
* RIGID SOLUTION *
****

ANGLE OF ROTATION = 1.597

DEPTH TO ROTATION POINT = 1.994892
TOTAL LATERAL LOAD = 11923.45
GROUND-LINE MOMENT = 20866.0
DEFLECTION AT TOP OF PILE = 0.104350

DEPTH	LAT DISP	PASS	ACT	PASS-ACT	HSHEAR	VSHEA
0.079175	0.053385	402.76	1.03	16.40	40.22	1.25
0.237525	0.048973	1208.27	3.08	49.19	120.62	3.43
0.395875	0.044561	2013.78	5.13	81.98	200.87	5.21
0.554225	0.040149	2819.30	7.19	114.77	280.76	6.57
0.712575	0.035737	3624.81	9.24	147.57	359.76	7.52
0.870925	0.031325	4430.32	11.30	180.36	436.72	8.05
1.029275	0.026913	5235.83	13.35	213.15	509.05	8.17
1.187625	0.022501	5593.60	15.90	227.65	517.70	7.14
1.345975	0.018089	6339.42	18.02	258.00	554.31	6.50
1.504325	0.013677	7085.23	20.14	288.35	551.75	5.48
1.662675	0.009265	7831.04	22.26	318.71	479.48	4.09
1.821025	0.004853	7677.66	25.56	312.31	264.86	2.02
1.979375	0.000441	8345.28	27.78	339.47	22.34	0.16
2.137725	-0.003971	9012.90	30.00	-366.63	-268.21	2.02
2.296075	-0.008383	9680.52	32.23	-393.79	-541.61	4.52
2.454425	-0.012795	8998.93	36.62	-365.79	-633.48	6.12
2.612775	-0.017207	9579.50	38.99	-389.39	-767.95	8.75
2.771125	-0.021619	10160.08	41.35	-412.99	-868.04	11.64
2.929475	-0.026031	10740.65	43.71	-436.58	-946.87	14.81
3.087825	-0.030443	11321.23	46.08	-460.18	-1013.60	18.24

BASE SHEAR FORCE = 82.3
SUM OF MOMENTS AT POINT OF LOAD APPLICATION = -0.120E 03

****
* FLEXIBLE SOLUTION *
****

GROUND-LINE SLOPE = 1.95885
DEPTH TO ZERO DISPLACEMENT = 2.137
TOTAL LATERAL LOAD = 9799.14
GROUND-LINE MOMENT = 17148.5
GROUND-LINE DEFLECTION = 0.0472

DEPTH	LAT DISP	PASS	ACT	PASS-ACT	HSHEAR	VSHEA
0.079175	0.044886	402.76	1.03	16.40	40.18	1.47
0.237525	0.040341	1208.27	3.08	49.19	120.34	3.81
0.395875	0.035942	2013.78	5.13	81.98	199.92	5.45
0.554225	0.031695	2819.30	7.19	114.78	278.17	6.45
0.712575	0.027604	3624.81	9.24	147.58	353.52	6.92

0.870925	0.023667	4430.32	11.30	180.37	423.01	6.95
1.029275	0.019884	5235.83	13.35	213.17	481.40	6.63
1.187625	0.016249	5593.60	15.90	227.68	471.45	5.49
1.345975	0.012755	6339.42	18.02	258.04	477.47	4.79
1.504325	0.009394	7085.23	20.14	288.40	440.79	3.97
1.662675	0.006155	7831.04	22.26	318.77	349.37	3.06
1.821025	0.003026	7677.65	25.56	312.38	172.75	1.81
1.979375	0.000007	542.11	44.36	-20.32	-0.03	0.06
2.137725	-0.002958	9012.90	30.00	-366.71	-198.42	0.00
2.296075	-0.005840	9680.52	32.23	-393.87	-399.94	0.98
2.454425	-0.008668	8998.93	36.62	-365.87	-490.90	1.69
2.612775	-0.011453	9579.50	38.99	-389.48	-630.46	2.63
2.771125	-0.014205	10160.08	41.35	-413.08	-750.94	3.64
2.929475	-0.016933	10740.65	43.71	-436.69	-854.32	4.74
3.087825	-0.019642	11321.23	46.08	-460.30	-943.83	5.92

BASE SHEAR FORCE = 38.1
SUM OF MOMENTS AT POINT OF LOAD APPLICATION = -0.903E 00

****
* RIGID SOLUTION *
****

ANGLE OF ROTATION = 1.922
DEPTH TO ROTATION POINT = 2.138040
TOTAL LATERAL LOAD = 18189.21
GROUND-LINE MOMENT = 31831.1
DEFLECTION AT TOP OF PILE = 0.130417

DEPTH	LAT DISP	PASS	ACT	PASS-ACT	HSHEAR	VSHEA
0.079175	0.069056	402.76	1.03	16.39	40.24	1.94
0.237525	0.063744	1208.27	3.08	49.18	120.71	5.38
0.395875	0.058432	2013.78	5.13	81.97	201.16	8.22
0.554225	0.053120	2819.30	7.19	114.75	281.56	10.46
0.712575	0.047808	3624.81	9.24	147.54	361.82	12.12
0.870925	0.042496	4430.32	11.30	180.33	441.66	13.17
1.029275	0.037184	5235.83	13.35	213.11	520.43	13.63
1.187625	0.031872	5593.60	15.90	227.61	540.57	12.22
1.345975	0.026560	6339.42	18.02	257.96	602.85	11.55
1.504325	0.021248	7085.23	20.14	288.30	648.85	10.34
1.662675	0.015936	7831.04	22.26	318.65	656.51	8.59
1.821025	0.010624	7677.66	25.56	312.26	505.73	5.45
1.979375	0.005312	8345.28	27.78	339.41	322.60	2.99
2.137725	-0.000000	9012.90	30.00	366.56	7.25	0.06
2.296075	-0.005312	9680.52	32.23	-393.72	-361.14	3.33
2.454425	-0.010624	8998.93	36.62	-365.72	-561.25	6.00
2.612775	-0.015936	9579.50	38.99	-389.32	-742.28	9.61
2.771125	-0.021248	10160.08	41.35	-412.91	-862.63	13.61
2.929475	-0.026560	10740.65	43.71	-436.51	-948.18	17.99
3.087825	-0.031872	11321.23	46.08	-460.10	-1016.24	22.77

BASE SHEAR FORCE = 31.7
SUM OF MOMENTS AT POINT OF LOAD APPLICATION = 0.693E 03

****
* FLEXIBLE SOLUTION *
****

GROUND-LINE SLOPE = 2.53602
DEPTH TO ZERO DISPLACEMENT = 2.302
TOTAL LATERAL LOAD = 15180.40
GROUND-LINE MOMENT = 26565.7
GROUND-LINE DEFLECTION = 0.0571

DEPTH	LAT DISP	PASS	ACT	PASS-ACT	HSHEAR	VSHEA
0.079175	0.054199	402.76	1.03	16.39	40.23	2.47
0.237525	0.048532	1208.27	3.08	49.18	120.62	6.38
0.395875	0.043093	2013.78	5.13	81.97	200.79	9.01
0.554225	0.037894	2819.30	7.19	114.76	280.37	10.53
0.712575	0.032946	3624.81	9.24	147.55	358.46	11.12
0.870925	0.028255	4430.32	11.30	180.35	433.11	10.96
1.029275	0.023826	5235.83	13.35	213.15	500.49	10.23
1.187625	0.019661	5593.60	15.90	227.66	501.97	8.24
1.345975	0.015760	6339.42	18.02	258.03	527.85	7.00
1.504325	0.012121	7085.23	20.14	288.40	518.77	5.66
1.662675	0.008741	7831.04	22.26	318.76	462.58	4.31
1.821025	0.005614	7677.65	25.56	312.38	306.43	2.62
1.979375	0.002732	8345.27	27.78	339.55	170.16	1.62
2.137725	0.000089	5379.62	30.00	218.40	3.62	0.44
2.296075	-0.002326	9680.52	32.23	-393.90	-168.77	0.02
2.454425	-0.004520	8998.93	36.62	-365.90	-283.53	0.45
2.612775	-0.006503	9579.50	38.99	-389.51	-416.09	0.79
2.771125	-0.008281	10160.08	41.35	-413.12	-535.60	1.01
2.929475	-0.009860	10740.65	43.71	-436.74	-642.07	1.12
3.087825	-0.011244	11321.22	46.08	-460.35	-736.80	1.11

BASE SHEAR FORCE = 0.0
SUM OF MOMENTS AT POINT OF LOAD APPLICATION = 0.426E 03

APPENDIX IV.-SEQUENTIAL PHOTOGRAPHS OF IMPACT TESTS

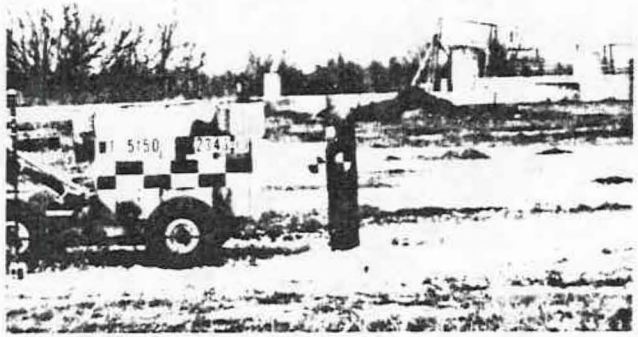

0.000 sec

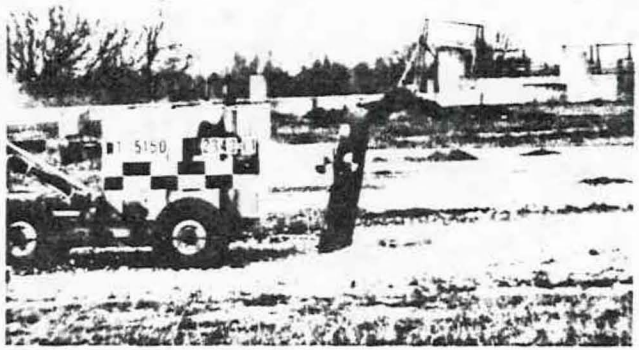

0.015 sec

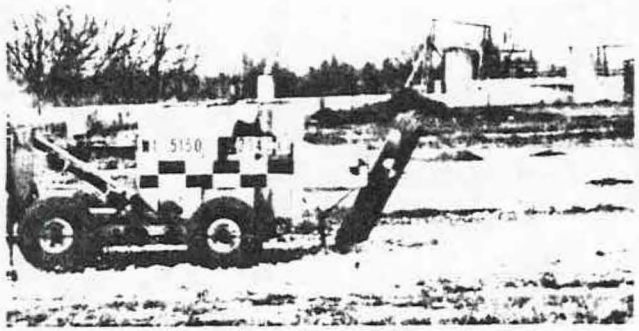

0.034 sec

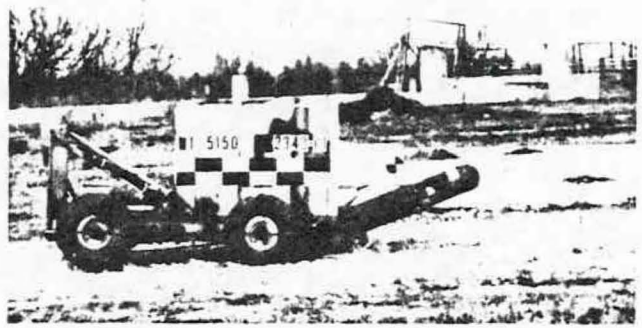

0.078 sec

FIG. 80.-Sequence Photographs for Test C1

0.000 sec

0.017 sec

0.066 sec

0.108 sec

FIG. 81a.-Sequence Photographs for Test C2

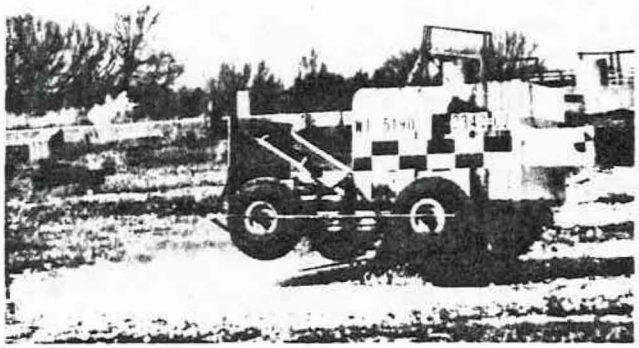

0.312 sec

0.547 sec

0.945 sec

FIG. 81b.-Sequence Photographs for Test C2

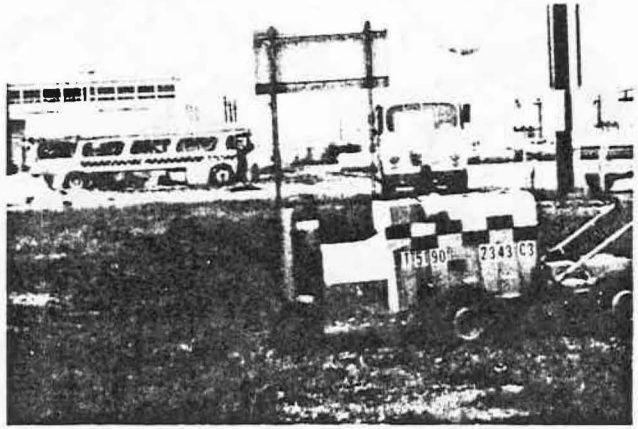

0.000 sec

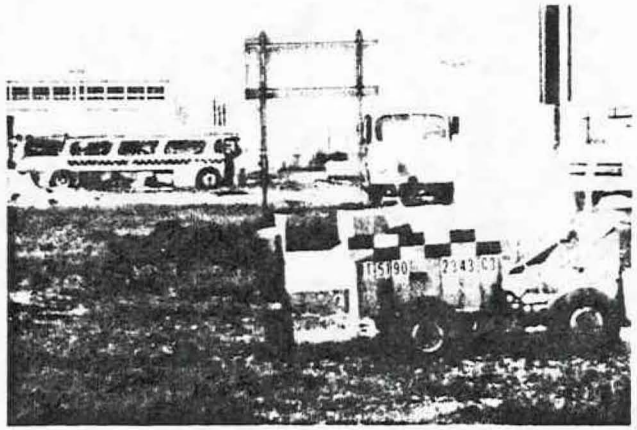

0.020 sec

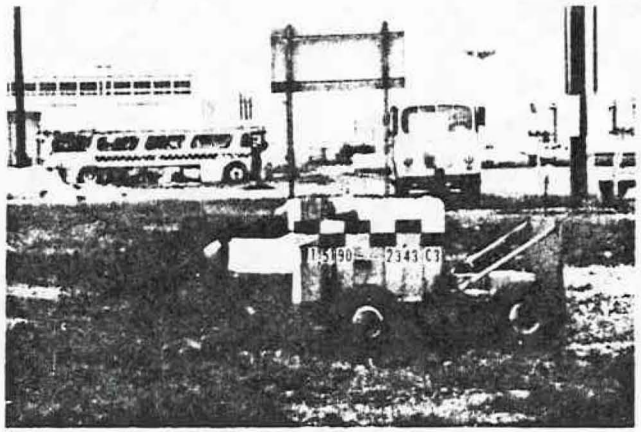

0.108 sec

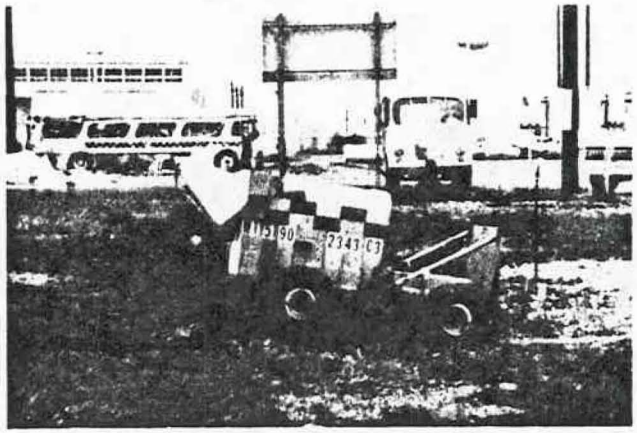

0.177 sec

FIG. 82a.-Sequence Photographs for Test C3

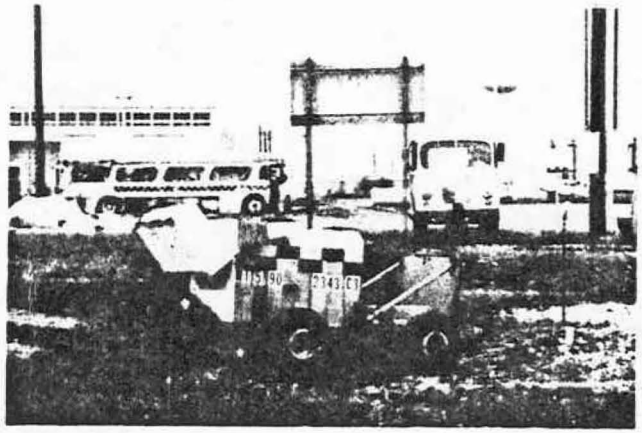

0.396 sec

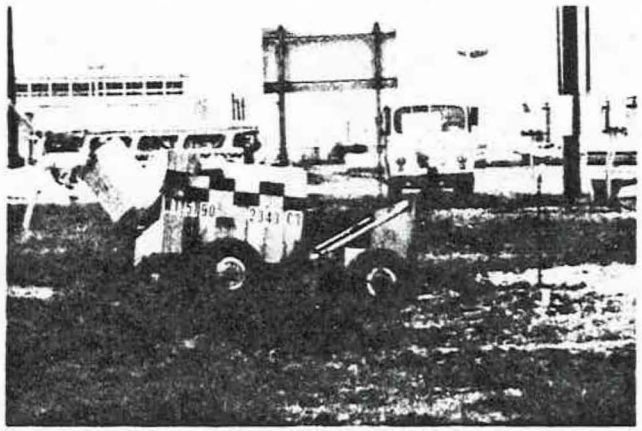

0.627 sec

1.467 sec

FIG. 82b.-Sequence Photographs for Test C3

0.000 sec

0.020 sec

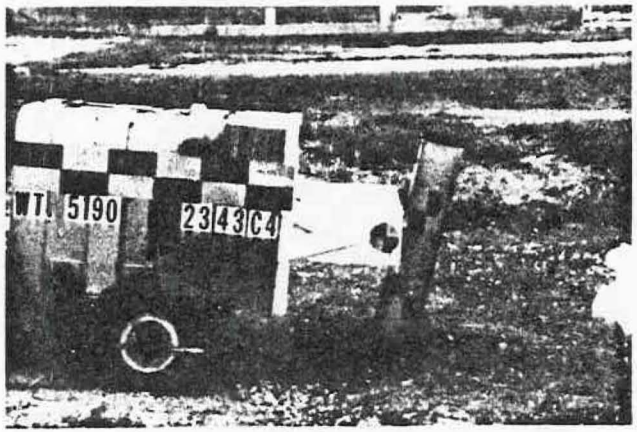

0.040 sec

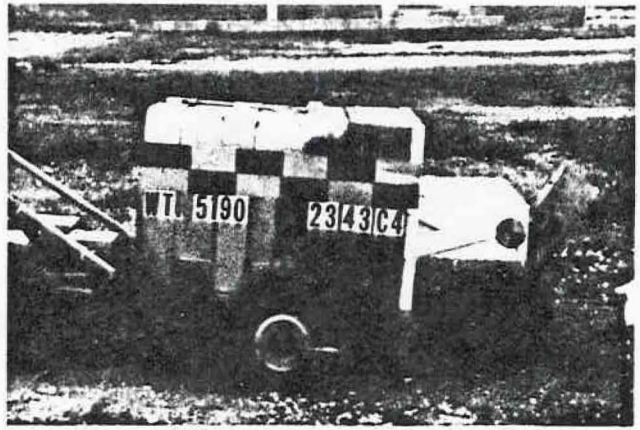

0.099 sec

FIG. 83a.-Sequence Photographs for Test C4

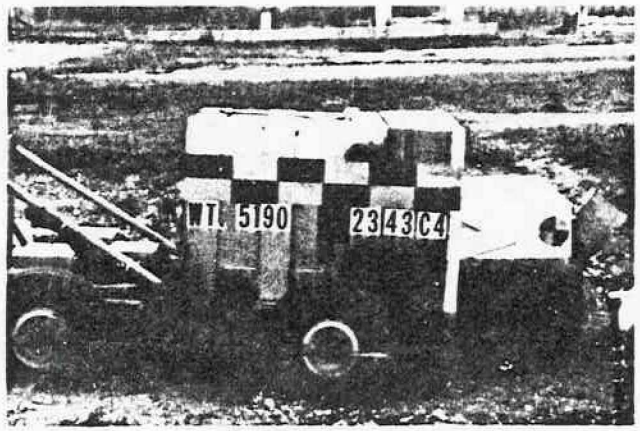

0.124 sec

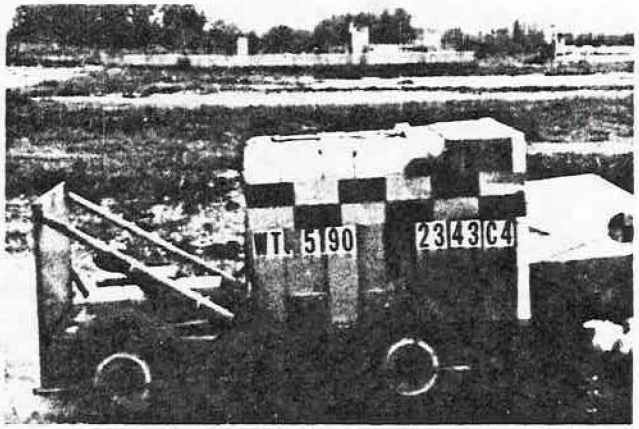

0.174 sec

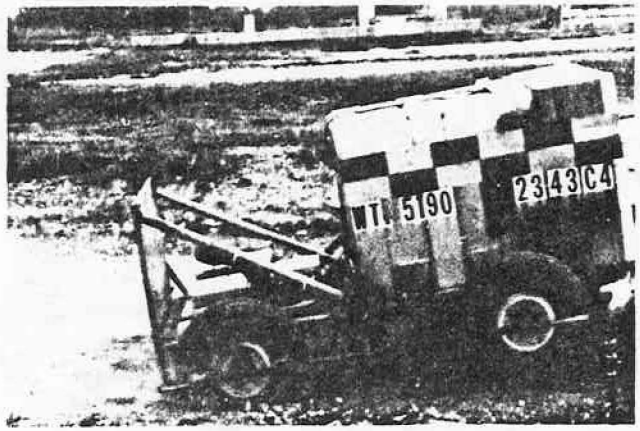

0.224 sec

FIG. 83b.-Sequence Photographs for Test C4